The role of AMPK in the regulation of Nitric Oxide synthesis by Perivascular Adipose Tissue

Abdmajid Saad Hwej

BSc, MSc

Thesis submitted in fulfilment of the requirements for the degree of Doctor of Philosophy

May 2023

School of Cardiovascular and Metabolic Health

College of Medical, Veterinary and Life Sciences

University of Glasgow

Abstract

Nitric oxide (NO) is a key signalling molecule in the cardiovascular, genitourinary, respiratory, nervous, and gastrointestinal systems. NO is released by the endothelium of blood vessels and inhibits vascular smooth muscle cell (VSMC) migration and proliferation, modulates vascular tone and maintains cardiovascular homeostasis. Several clinical studies have shown that a reduction of NO bioavailability has a significant role in the development of endothelial dysfunction and other cardiovascular diseases.

Perivascular adipose tissue (PVAT) is the outer layer of connective tissue that surrounds most systemic blood vessels, adjacent to the adventitia. Adipose tissue provides a protective layer of tissue surrounding most of the body organs and, in the case of PVAT, regulates vascular function by production of many autocrine and paracrine molecules including adiponectin, prostacyclin and angiotensin 1–7. AMP-activated protein kinase (AMPK) plays a major role in sensing cellular energy status and signalling this information back to the mitochondria to modulate their function according to the energy demands of the cell. Previous work in our laboratory has demonstrated that the presence of PVAT enhances vascular relaxation to cromakalim in endothelium-intact thoracic aortic rings from wild type (WT), but not in mice lacking AMPKα1.

Compared to previous studies which examined the role of AMPK in regulation of NO release from the endothelium, the current research has focused on the mechanisms by which AMPK regulates NO production by PVAT and what effect this has on vascular tone.

In this project experiments were conducted using wild type (WT) and global AMPKα1 knockout (KO) mice. Thoracic and abdominal aortic PVAT was utilised to measure the difference in NO production between fat depots. The anti-contractile effect of PVAT from WT and KO aortic rings was studied using wire myography. Furthermore, immunoprecipitation was used to measure the Cav-1/eNOS coupling and immunofluorescence was used to study Cav-1/eNOS colocalization in 3T3-L1 adipocytes.

The results showed that there was a significant decrease in NO production in conditioned media derived from both the thoracic and abdominal PVAT from KO mice compared to WT mice, although the quantities of NO generated by the abdominal aortic PVAT was much lower. Overall, eNOS activity in WT thoracic PVAT was significantly increased compared to WT abdominal PVAT suggesting that changes in eNOS activity could account for the difference in NO production. Furthermore, in abdominal PVAT, considerably more caveolin-1 (Cav-1), a negative regulator of eNOS, was detected in both WT and KO mice compared with thoracic PVAT, which may also limit NO production by abdominal PVAT. Cav-1 was detected in eNOS immunoprecipitates and levels of Cav-1/eNOS association were increased in abdominal PVAT relative to thoracic PVAT of WT mice and the total Cav-1 levels in abdominal PVAT lysates was increased. Intriguingly, Cav-1/eNOS association was significantly increased in thoracic PVAT from KO mice compared with WT mice, which might account for the reduction in NO production in KO thoracic PVAT compared with WT.

In 3T3-L1 adipocyte adipogenesis, eNOS levels and NO production were significantly reduced. Incubation of 3T3-L1 preadipocytes or adipocytes with methyl-ß-cyclodextrin (MßCD), which disrupts Cav-1 and therefore leading to a noticeable reduction in Cav-1/eNOS colocalization and a significant increase in NO production both in preadipocytes and adipocytes compared with non-treated cells. Incubation of 3T3-L1 adipocytes with a mutant cell–permeable scaffolding domain peptide of Cav-1 (CAV-AP) reduced Cav-1/eNOS colocalization compared with control. In functional experiments, CAV-AP reduced PE-induced contraction in both WT and KO thoracic aortic rings lacking endothelium.

Overall, the results presented in this thesis demonstrate that AMPKα1 has an important role in regulating NO production by PVAT, likely through regulating Cav-1/eNOS binding. Manipulating Cav-1/eNOS binding in adipocytes using scaffolding mutant peptides without interfering with the other biological effects of endogenous Cav-1 may have beneficial effects in restoration of NO production under conditions or diseases associated with impaired NO bioavailability.

Table of Contents

Abstract ii

Table of Contents iv

List of Tables xi

List of Figures xii

Acknowledgement xv

Author's Declaration xvi

List of Abbreviations xvii

Chapter 1 - Introduction 1

1.1 Cardiovascular system 2

1.1.1 Endothelium layer 3

1.1.2 Vascular smooth muscle layer 3

1.1.3 Adventitia (Perivascular adipose tissue) 4

1.2 Adipose tissue 4

1.2.1 White adipose tissue 5

1.2.2 Brown adipose tissue 5

1.3 Perivascular adipose tissue (PVAT) 6

1.3.1 Anticontractile action of PVAT 8

1.4 Nitric oxide and regulation of vascular function 10

1.4.1 Nitric oxide 10

1.4.2 Nitric Oxide Synthase: structure and function 10

1.4.2.1 Endothelial nitric oxide synthase 11

1.4.2.2 Inducible nitric oxide synthase 13

1.4.2.3 Neuronal nitric oxide synthase 14

1.4.3 Regulation of eNOS 16

1.4.3.1 Phosphorylation of eNOS 17

1.4.3.2 eNOS activation by different kinases 18

1.4.3.3 Endogenous inhibitors of eNOS activity 20
1.4.3.4 Asymmetric dimethylarginine 20
1.4.3.5 Reactive oxygen species 20
1.4.4 eNOS and protein-protein interactions 22
1.4.4.1 Caveolin-1 22
1.4.4.2 Hsp-90 25
1.5 AMP-activated protein kinase (AMPK) 26
1.5.1 Overview 26
1.5.2 AMPK structure 26
1.5.3 Regulation of AMPK 28
1.5.3.1 Allosteric activation of AMPK 28
1.5.4 AMPK activation by upstream kinases 29
1.5.5 Downstream targets of AMPK 30
1.5.6 Pharmacological AMPK activators 31
1.5.7 AMPK inhibitors 34
1.5.8 AMPK and adipose tissue function 35
1.5.8.1 Role of AMPK in regulation of lipid metabolism 35
1.5.8.2 Role of AMPK on adipogenesis 35
1.5.9 The role of AMPK in regulating blood vessels homeostasis 37
1.5.9.1 Role of AMPK in the vascular endothelium and NO production . 37
1.5.9.2 Role of AMPK in vascular smooth muscle cells 37
1.5.9.3 AMPK and inflammation 39
1.5.9.4 Role of AMPK in perivascular adipose tissue 41
1.6 Objectives and aims 42
Chapter 2 - Materials & Methods 43
2.1 Materials 44
2.1.1 List of materials and suppliers 44
2.1.2 List of special equipment and suppliers 48
2.1.3 List of cells and suppliers 49

2.1.3 Animal model 50
2.1.3.1 Genotyping 51
2.1.3.2 DNA extraction 51
2.1.3.3 Polymerase Chain Reaction for AMPKα1 Wild type (WT) and AMPKα1 Knockout (KO) 51
2.1.4 Standard solutions 54
2.1.5 List of antibodies 56
2.1.5.1 Primary antibodies for Western blotting 56
2.1.5.2 Primary antibodies for immunoprecipitation 58
2.1.5.3 Primary antibodies for immunofluorescence 58
2.1.5.4 Secondary detection agents for immunofluorescence 58
2.1.5.5 Secondary antibodies for Western blotting 59
2.1.6 List of Taqman probes and real-time qPCR reagents 60
2.2 Methods 61
2.2.1 Analysis of NO synthesis by PVAT and other adipose tissue depots . 61
2.2.2 Functional studies (wire myography) 62
2.2.2.1 Vessel preparation 62
2.2.2.2 Cumulative Dose-response curve 62
2.2.3 Preparation of tissue lysates, SDS-PAGE and Western blotting 65
2.2.3.1 Preparation of PVAT tissue lysates 65
2.2.3.2 Protein concentration estimation assays 65
2.2.3.2.1 Bicinchoninic acid method (BCA) 65
2.2.3.3 SDS–polyacrylamide gel electrophoresis and immunoblotting .. 65
2.2.3.4 Stripping of nitrocellulose membranes 66
2.2.4 Cell culture procedures 67
2.2.4.1 Cell culture plastic ware 67
2.2.4.2 Recovery of cryopreserved cell stocks from liquid nitrogen 67
2.2.4.3 3T3-L1 adipocyte culture 67
2.2.4.4 Differentiation of 3T3-L1 preadipocytes 67

2.2.4.5 Passaging of 3T3-L1 cells 68
2.2.4.6 Preparation of 3T3-L1 cell lysates 68
2.2.4.7 Analysis of nitric oxide synthesis by 3T3-L1 adipocytes..... 68
2.2.5 Immunoprecipitation 69
2.2.6 ROS Production and Lipid Peroxidation detection 69
2.2.6.1 Measurement of hydrogen peroxide levels..... 69
2.2.6.2 Determination of Lipid Peroxidation levels 70
2.2.7 NOS activity assay 71
2.2.8 Confocal microscopy and staining..... 72
2.2.9 Caveolin-1 (*Cav-1*) Gene Expression 73
2.2.9.1 Purification of total RNA from PVAT 73
2.2.9.2 cDNA generation by polymerase chain reaction (PCR) 73
2.2.9.3 Real time quantitative PCR (RT-qPCR) 74
2.3 Statistical analysis..... 75

Chapter 3 - The role of AMPK in regulation of nitric oxide production by perivascular adipose tissue (PVAT) 76

3.1 Introduction 77
3.2 Aims of the study 80
3.3 Methods 80
3.3.1 Analysis of NO synthesis by PVAT and other adipose tissue depots . 80
3.3.2 Functional studies (wire myography) 80
3.3.3 Preparation of tissue lysates, SDS-PAGE and Western blotting 81
3.3.4 Immunoprecipitation 82
3.3.4.1 Measurement of hydrogen peroxide levels..... 82
3.3.5 NOS activity assay 83
3.3.6 Caveolin-1 (Cav-1) Gene Expression 83
3.4 Results 85
3.4.1 PVAT enhances vascular relaxation to cromakalim in wild type, but not AMPKα1$^{-/-}$ aortic rings 85

3.4.2 Inhibition of NO synthesis by PVAT suppresses U46619-mediated contraction in thoracic but not abdominal aortic rings from both WT and AMPKα1$^{-/-}$ mice 86

3.4.3 NO synthesis is greater in thoracic PVAT relative to abdominal PVAT and reduced in AMPKα1$^{-/-}$ mice 89

3.4.4 eNOS, iNOS and nNOS levels in WT and AMPKα1$^{-/-}$ abdominal and thoracic aortic PVAT..... 90

3.4.5 eNOS activity in PVAT of WT and AMPKα1$^{-/-}$ mice 91

3.4.6 eNOS phosphorylation in abdominal and thoracic aortic PVAT of WT and AMPKα1$^{-/-}$ mice..... 92

3.4.7 UCP-1 levels in abdominal and thoracic aortic PVAT in WT and AMPKα1$^{-/-}$ mice 93

3.4.8 UCP-1 expression in other fat depots of WT and AMPKα1$^{-/-}$ mice ... 94

3.4.9 Nitric oxide synthesis is decreased in BAT and WAT depots from AMPKα1$^{-/-}$ mice 95

3.4.10 Wild type abdominal PVAT releases less H_2O_2 compared with WT thoracic PVAT..... 96

3.4.11 Superoxide dismutase suppresses U46619-mediated contraction in thoracic aortic rings containing PVAT from both WT and AMPKα1$^{-/-}$ mice... 98

3.4.12 Lower levels of caveolin-1 are associated with eNOS in thoracic PVAT relative to abdominal PVAT and are increased in thoracic PVAT from AMPKα1$^{-/-}$ mice 99

3.4.13 Caveolin-1 gene (*Cav1*) is reduced in WT thoracic aortic PVAT compared with AMPKα1$^{-/-}$ mice 101

3.4.14 Lower levels of Hsp-90 are associated with eNOS in thoracic PVAT relative to abdominal PVAT and are increased in thoracic PVAT from AMPKα1$^{-/-}$ mice 103

3.5 Discussion 105

Chapter 4 - Characterisation of nitric oxide synthesis and Cav-1 /eNOS coupling in 3T3-L1 adipocyte. 112

4.1 Introduction 113

4.2 Aims of the study 116
4.3 Methods 116
4.3.1 Analysis of NO synthesis by 3T3-L1 preadipocytes and adipocytes. 116
4.3.2 3T3-L1 adipocyte culture 116
4.3.3 Confocal microscopy and staining 117
4.4 Results 118
4.4.1 Characterization of NOS levels and NO production during 3T3-L1 cell adipogenesis 118
4.4.2 Effect of IL-1β and TNF- α on NO production in 3T3-L1 preadipocytes and adipocytes 120
4.4.3 Effect of IL-1β and TNF- α on iNOS levels in 3T3-L1 preadipocytes and adipocytes 121
4.4.4 Disruption of caveolae in 3T3-L1 preadipocytes and adipocytes using Methyl-β-cyclodextrin 122
4.4.5 Methyl-β-cyclodextrin increases NO synthesis in 3T3-L1 preadipocytes and adipocytes 125
4.4.6 Effect of geldanamycin on NO production in both preadipocytes and adipocytes 127
4.4.7 Effect of AMPK activation by compound 991 on NO production in 3T3-L1 preadipocytes and adipocytes 128
4.4.8 Effect of AICAR and A769662 on NO production in 3T3-L1 preadipocytes and adipocytes 130
4.4.9 Effect of compound C on NO production in 3T3-L1 preadipocytes and adipocytes 132
4.5 Discussion 134

Chapter 5 - Investigating the role of caveolin-1 in the regulation of nitric oxide synthesis by PVAT 139

5.1 Introduction 140
5.2 Aims of the study 141
5.3 Methods 141

5.3.1 Analysis of NO synthesis by PVAT and other adipose tissue depots 141

5.3.2 Functional studies (wire myography) 141

5.3.3 Immunoprecipitation 141

5.3.4 Confocal microscopy and staining 142

5.4 Results 143

5.4.1 Effect of compound C and SBI-0206965 on the level of phospho-Acetyl-CoA Carboxylase 143

5.4.2 Effect of compound C and SBI-0206965 on Cav-1/eNOS and Hsp-90/eNOS binding in thoracic and abdominal PVAT 145

5.4.3 Effect of compound 991 on Cav-1 and Hsp-90 /eNOS binding in thoracic and abdominal PVAT 147

5.4.4 CAV-AP peptide increases NO synthesis in thoracic PVAT from AMPKα1$^{-/-}$ mice but not in WT mice 149

5.4.5 CAV-AP suppresses phenylephrine-stimulated contraction of thoracic aortic rings from AMPKα1$^{-/-}$ mice 150

5.4.6 Effect of CAV-AP on Cav-1/eNOS colocalization and nitric oxide production in 3T3-L1 preadipocytes and adipocytes 152

5.5 Discussion 155

Chapter 6 - Final discussion and future work 163

6.1 Nitric oxide production by PVAT 164

6.2 Role of AMPK in PVAT function 166

6.3 Role of AMPK in regulation of Cav-1 /eNOS binding in PVAT 168

6.4 Future work 171

6.5 Chemical libraries for protein-protein interaction inhibitors 173

6.6 Conclusion 176

6.7 Appendices 177

Chapter 7 - List of References 190

List of Tables

Table 1-1: Types of adipocytes 6

Table 1-2: Functions of NOS isoforms and phenotypes of NOS knockout mice ... 16

Table 2-1: RT-PCR reaction mixture per sample for genotyping 51

Table 2-2: List of DNA primers for genotyping 53

Table 2-3: Primary antibodies for Western blotting 56

Table 2-4: Primary antibodies used for immunoprecipitation 58

Table 2-5: Primary antibodies used for immunofluorescence 58

Table 2-6: Secondary antibodies for immunofluorescence 59

Table 2-7: Secondary antibodies used for immunoblotting 59

Table 2-8: Forward primer, Reverse primer and Taqman probes 60

Table 3-1: Maximal KPSS contraction 87

Table 3-2: The CT values for WT and KO thoracic. 101

List of Figures

Figure 1-1: Structure of a blood vessel..... 3

Figure 1-2: Nitric oxide and superoxide anion generation by eNOS..... 13

Figure 1-3: Structure and functional domains of NOS isoforms 15

Figure 1-4: A schematic diagram showing eNOS regulation and activation 19

Figure 1-5: A schematic diagram of Cav-1 structure 24

Figure 1-6: Domain structure of AMPK subunit isoforms 28

Figure 1-7: AMPK activation by upstream kinases and metabolic outcomes..... 31

Figure 1-8 Pharmacological activation of AMPK..... 34

Figure 1-9 Schematic presentation of how AMPK regulate the vascular function 39

Figure 2-1: Genotyping of AMPK Kα1 KO mice 53

Figure 2-2: The wire myograph components 64

Figure 2-3: Conversion of Amplex red to Resorufin in the presence of H_2O_2 and horseradish peroxidase (HRP)..... 70

Figure 2-4: Formation of MDA–TBA 2 adduct after reaction between malondialdehyde (MDA) and thiobarbituric acid (TBA) 71

Figure 2-5: NOS catalyses a 5-electron oxidation of a guanidino nitrogen of L-arginine to generate NO and L-citrulline 72

Figure 3-1: Inhibition of PVAT NO synthesis suppresses U46619-mediated contraction in thoracic but not abdominal aortic rings from both WT and AMPKα1$^{-/-}$ mice 88

Figure 3-2: NOx production by thoracic and abdominal aortic PVAT in WT and KO mice 89

Figure 3-3: eNOS, iNOS and nNOS expression and activity in PVAT (WT and KO mice) 90

Figure 3-4: eNOS activity in PVAT of WT and KO mice..... 91

Figure 3-5: Levels of phospho-eNOS (Ser^{1177}, Ser^{615} or Thr^{495}) in thoracic and abdominal PVAT from WT and KO mice 92

Figure 3-6: UCP-1 expression in PVAT from WT and KO mice..... 93

Figure 3-7: UCP-1 levels in other fat depots (WT and KO mice)..... 94

Figure 3-8: NO production is decreased in BAT and WAT depots from KO mice . 95

Figure 3-9: Abdominal PVAT exhibits reduced H_2O_2 levels 97

Figure 3-10: Superoxide dismutase (PEG-SOD) suppresses U46619-mediated contraction in thoracic aortic rings with PVAT from both WT and KO mice 98

Figure 3-11: Lower levels of caveolin-1 are associated with eNOS in thoracic PVAT relative to abdominal PVAT and are increased in thoracic PVAT from KO mice compared with WT PVAT.....100

Figure 3-12: Cav1 mRNA in thoracic PVAT from WT and KO mice.....102

Figure 3-13: Higher levels of Hsp-90 are associated with eNOS in abdominal PVAT relative to thoracic PVAT 104

Figure 4-1: Levels of NOS isoforms and NO production during 3T3-L1 adipogenesis 119

Figure 4-2: Effect of IL-1ß or TNF-α on NOx production in 3T3-L1 preadipocytes and adipocytes.....120

Figure 4-3: Effect of IL-1ß or TNF-α on iNOS levels in 3T3-L1 preadipocytes and adipocytes 121

Figure 4-4: Methyl-ß-cyclodextrin reduces Cav-1/ eNOS co-localisation in 3T3-L1 preadipocytes 123

Figure 4-5: Methyl-ß-cyclodextrin reduces Cav-1/ eNOS co-localisation in 3T3-L1 adipocytes 124

Figure 4-6: Disruption of caveolae with methyl-ß-cyclodextrin increases NO synthesis by preadipocytes and adipocytes.....126

Figure 4-7: Effect of geldanamycin on NOx production in 3T3-L1 preadipocytes and adipocytes.....127

Figure 4-8: Effect of Compound 991 on ACC phosphorylation and NOx production in 3T3-L1 preadipocytes and adipocytes 129

Figure 4-9: Effect of AICAR and A769662 on ACC phosphorylation and NO production in 3T3-L1 preadipocytes and adipocytes 131

Figure 4-10: Effect of compound C on ACC phosphorylation and NO production in 3T3-L1 preadipocytes and adipocytes 133

Figure 5-1: Effect of compound C and SBI-0206965 on ACC phosphorylation in thoracic and abdominal PVAT 144

Figure 5-2: Effect of compound C or SBI-0206965 on Cav-1 and Hsp-90 binding to eNOS in thoracic and abdominal PVAT 146

Figure 5-3: Effect of compound 991 on ACC phosphorylation and association of Cav-1 or Hsp-90 with eNOS in thoracic and abdominal PVAT 148

Figure 5-4: CAV-AP peptide increases NO synthesis by thoracic PVAT from AMPKα1$^{-/-}$ mice but not WT mice 149

Figure 5-5: CAV-AP suppresses phenylephrine-stimulated contraction of thoracic aortic rings 151

Figure 5-6: Effect of CAV-AP on Cav-1/eNOS colocalization and NO synthesis in 3T3-L1 preadipocytes 153

Figure 5-7: CAV-AP reduces Cav-1/eNOS co-localisation in 3T3-L1 adipocytes without altering NO synthesis 154

Figure 5-8: Depicted representation of Cav-1/eNOS binding site 161

Figure 6-1: Vasorelaxation effect of PVAT.....166

Figure 6-2: Regulation of NO production in PVAT mediated by AMPK signalling within adipocytes.....170

Figure 6-3: A proposed mechanism of increased eNOS- NO release by CAV-AP .171

Acknowledgement

In the name of Allah, the Most Gracious and the Most Merciful first and foremost I would like to express my gratitude to Allah (God) for providing me the blessings to complete this work.

Also, I would like to sincerely thank my supervisors, Prof. Simon Kennedy, and Dr. Ian Salt for all their tremendous support, guidance, advice, enthusiasm, and the opportunities I've had over the period of my PhD, also I could not have undertaken this journey without their advice. I would also like to acknowledge the Libyan Ministry of Higher Education and Scientific Research and my University for their support and funding of this project. Special thanks to the members of Kennedy and Salt groups, past and present for helping me with just about everything. Thanks, should also go to the laboratory technicians: John McAbney and others for being good listeners and great advisors.

Lastly, but most importantly, I would like to dedicate this work to my mother, father, brothers, and sisters who have been away from me during my PhD, and all my family especially my lovely wife Malak and my son Anas and my daughters Aseel and Roaa, their belief in me has kept my spirits and motivation high during this process.

Author's Declaration

I declare that this thesis has been written solely by me with the research entirely generated by myself, unless otherwise stated. It is entirely of my own composition and has not, in whole or in part, been submitted for any other degree.

This project was under the supervision of Prof. Simon Kennedy and Dr. Ian Salt.

Abdmajid, S. Hwej

May 2023

List of Abbreviations

3T3-L1	Fibroblast cell line isolated from 3T3 mouse embryo
A769662	6,7-Dihydro-4-hydroxy-3-(2′-hydroxy[1,1′-biphenyl]-4-yl)-6-oxo-thieno[2,3-b]pyridine-5-carbonitrile
ACC	Acetyl-CoA Carboxylase
AdipoR1	Adiponectin Receptor 1
ADMA	Asymmetric Dimethylarginine
ADRF	Adipocyte-Derived Relaxing Factor
AICAR	5-Aminoimidazole-4-Carboxamide 1-ß-D-Ribonucleoside
AIS	Autoinhibitory sequence
AMPK	AMP-Activated Protein Kinase
CTS	C-terminal Sequence
Akt	Protein Kinase B
APS	Ammonium peroxidisulphate
BAT	Brown Adipose Tissue
BH_4	Tetrahydrobiopterin
BSA	Bovine Serum Albumin
C/EBPs	CCAAT/Enhancer-Binding Proteins
CaMKKß	Calcium/Calmodulin-dependent Protein Kinase Kinase ß
Cav-1	Caveolin-1
CBM	Carbohydrate-Binding Module
CBS	Cystathionine-ß-Synthase
CCAAT	Cytosine-cytosine-adenosine-adenosine-thymidine
cGMP	Cyclic Guanosine Monophosphate
CPT1	Carnitine palmitoyl transferase 1
CTD	C-terminal domain
CVD	Cardiovascular Diseases
CXCL10	C-X-C motif chemokine ligand 10
DMEM	Dulbecco's Modified Eagle's Medium
DMSO	Dimethyl Sulfoxide
D-NAME	Nω-Nitro-D-arginine methyl ester hydrochloride
dNTP	Deoxyribonucleotide triphosphate
eNOS	Endothelial NO Synthase
ERK1/2	Extracellular signal–Regulated Kinases 1/2

FA	Fatty acid
FABP4	Fatty acid binding protein 4
FAD	Flavin Adenine Dinucleotide
FAK	Focal adhesion kinase
FAS	Fatty acid synthase
FFAs	Free Fatty Acids
FCS	Foetal calf serum
FMN	Flavin Mononucleotide
GAPDH	Glycerol 3-Phosphate Dehydrogenase 1
GBD	Glycogen-binding domain
GTP	Guanosine Triphosphate
H_2O_2	Hydrogen Peroxide
H_2S	Hydrogen Sulphide
HAECs	Human Aortic Endothelial Cells
HEK293	human embryonic kidney 293
HFD	High Fat Diet
HMG-CoA	Reductase 3-Hydroxy-3-Methyl-Glutaryl-Coenzyme A reductase
HMGR	3-hydroxy-3-methylglutaryl-CoA reductase
Hsp-90	Heat shock protein 90
IκBα	Inhibitor of κB
IBMX	Isobutylmethylxanthine
IFN-γ	Interferon gamma
IGF-1	Insulin-like growth factor-1
IKK	IκB kinase
IL-1	Interleukin-1
IL-6	Interleukin-6
iNOS	Inducible NO synthase
IRAK4	Interleukin-1 receptor associated kinase-4
IR	Insulin Receptor
IRS-1	Insulin Receptor Substrate 1
IP	Immunoprecipitation
IF	Immunofluorescence
KATP	ATP-activated potassium channels
KLF4/5	Kruppel-like factors 4 and 5
LKB1	Liver kinase B1

MARK3/4	Mitogen-activated protein kinases 3/4
MCE	Mitotic clonal expansion
MLK1/3	Mut9p-LIKE KINASE 1/3
MNK1	MAPK interacting-kinase 1
mTORC1	mammalian target for rapamycin complex 1
NADPH	Nicotinamide Adenine Dinucleotide Phosphate
NAMPT	Nicotinamide Phosphoribosyltransferase
NCS	New born calf serum
NFk-B p65	Nuclear Factor-kappa B p65
NMN	Nicotinamide Mononucleotide
nNOS	Neuronal nitric synthase
NUAK1	NUAK Family Kinase 1
$O2^{\cdot-}$	Superoxide
OBB	Odyssey® blocking buffer
OCT1	Organic cation transporter 1
PAGE	Polyacrylamide gel electrophoresis
PAI-1	Plasminogen Activator Inhibitor type-1
PBS	Phosphate Buffered Saline
PBST	PBS + Tween 20
PCR	Polymerase Chain Reaction
PHK	Phosphorylase kinase
PI3K	Phosphatidylinositol-3-kinase
PJS	Peutz-Jeghers Syndrome
PKA	Protein kinase A
PKB	Protein kinase B
PKC	Protein kinase C
PPARγ	Peroxisome Proliferator-Activated Receptor γ
PVAT	Perivascular Adipose Tissue
ROS	Reactive Oxygen Species
SAT	Subcutaneous Adipose Tissue
SDS	Sodium Dodecyl Sulphate
SDS-PAGE	SDS-polyacrylamide gel electrophoresis
siRNA	Small interfering RNA
Src	Sarcoma kinase
SREBP	Sterol regulatory element binding protein

STAT1	Signal transducer and activator of transcription 1
STK11	Serine/threonine kinase 11
T2DM	Type 2 Diabetes Mellitus
TEMED	N, N, N', N'-tetramethylenediamine
TCA	Trichloroacetic acid
TGF-ß	Transforming growth factor beta
TNF-α	Tumour Necrosis Factor α
TZDs	Thiazolidinediones
UCP-1	Uncoupling Protein 1
ULK1/2	Unc-51-like kinase
VEGF-A	Vascular Endothelial Growth Factor A
VSMCs	Vascular Smooth Muscle Cells
VAT	Visceral adipose tissue
WAT	White Adipose Tissue
ZMP	5-aminoimidazole-4-carboxamide-1-β-D-furanosyl 5′-monophosphate

Chapter 1 - Introduction

1.1 Cardiovascular system

The cardiovascular system or the circulatory system is responsible for transport of oxygenated blood from the lungs, hormones from glands of the endocrine system, nutrients from the digestive system and waste materials from cells throughout the body systems and also plays an important role in regulating body temperature. The main components of the circulatory system are the heart, blood and blood vessels including arteries, veins, arterioles, and capillaries. The heart is a muscular structure in the chest cavity which plays an important role in maintaining a sufficient supply of oxygenated blood via the vascular network of the body to end organs and tissues. The role of the blood vessels is to transport oxygenated blood and nutrients from the heart via the systemic circulation to the rest of the body, before returning the blood back to heart and delivering it to the lungs via the pulmonary circulation (Matienzo and Bordoni, 2023).

The wall of blood vessels consists of three layers: tunica intima, tunica media and tunica adventitia. The innermost layer of the blood vessel, the tunica intima consists of a single layer of endothelial cells (ECs) supported by an elastic lamina while the tunica media beneath is composed of vascular smooth muscle cells (VSMCs) and elastic fibres responsible for regulating vascular tone. The tunica adventitia is the outer layer of the vascular wall and contains two layers: 1) adventitia compacta which is a collagen and fibroblast layer and 2) perivascular adipose tissue (PVAT) which is present in most blood vessels (Figure 1-1).

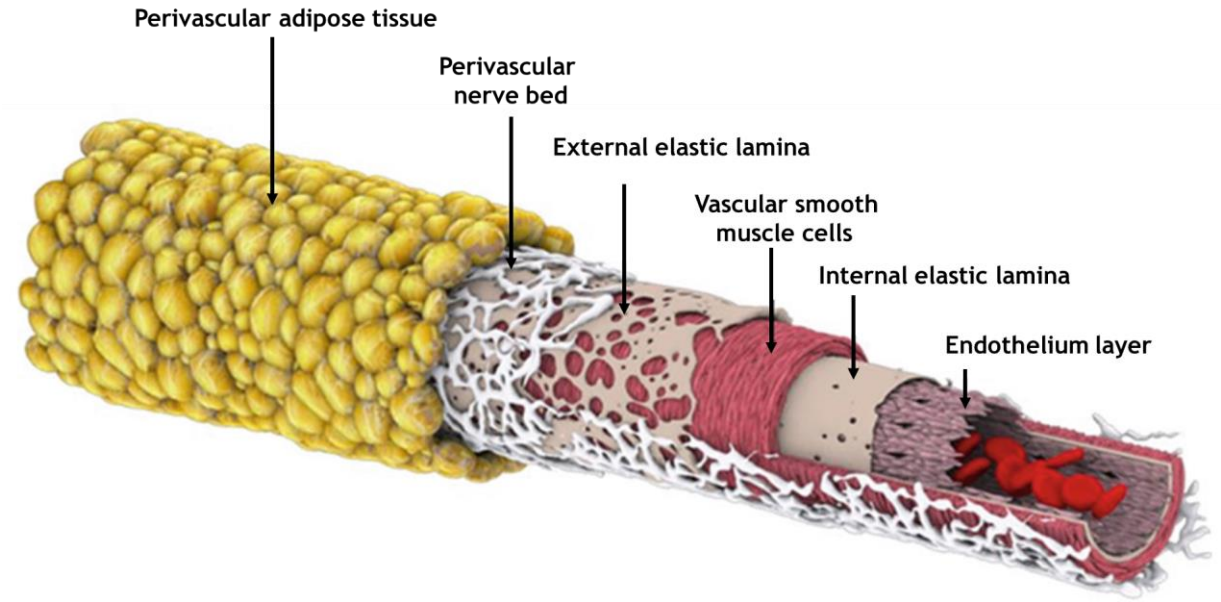

Figure 1-1: Structure of a blood vessel

The wall of the blood vessel consists of three layers: tunica intima composed of endothelial cells surrounded by an internal elastic lamina, tunica media composed of vascular smooth muscle cells surrounded by an external elastic lamina and an external layer, the tunica adventitia which contains fibroblasts, nerves, blood vessels and PVAT (Daly, 2019).

1.1.1 Endothelium layer

The vascular endothelium refers to a monolayer of cells that line the interior surface of all vascular beds and lymphatic vessels. ECs separate, metabolically and mechanically, the inner layer of the vascular wall from the circulating blood components, forming an interface between circulating blood or lymph in the lumen and the rest of the vessel wall. ECs are not only a barrier between the circulation and peripheral tissues, but also actively regulate vascular tone, blood flow and platelet function (Lerman and Zeiher, 2005, Pi *et al.*, 2018). It is well defined that the endothelium releases a wide variety of vasoactive molecules involved in regulating vascular function and tone, cellular adhesion, platelet aggregation and cell proliferation and angiogenesis. These cells also act as an active signal transducer that can modify the vessel wall phenotype (Vita and Keaney, 2002, Deanfield *et al.*, 2007).

1.1.2 Vascular smooth muscle layer

VSMCs and elastic fibres are the major component of the tunica media. This layer plays an important role in maintaining the integrity of the arterial wall and

controlling vascular tone and vascular remodelling (Hu *et al.*, 2019). In response to inflammation, vascular injury, and accumulation of different lipoproteins during disease progression, VSMCs show noticeable plasticity via a shift in gene expression to a pro-migratory, pro-proliferative phenotype. Additionally, they can be involved in helping repair vascular injury (Owens *et al.*, 2004, Cao *et al.*, 2022). Furthermore, it is well established that Ca^{2+} is the main regulator of VSMC contraction and the source of this Ca^{2+} can be from outside the cell or via stimulation of inositol 1,4,5-trisphosphate (IP3) receptors to release intracellular stores from the sarcoplasmic reticulum. The increase in $[Ca^{2+}]_i$ activates Ca^{2+}-dependent myosin light chain (MLC) phosphorylation that stimulates actin–myosin interaction, and initiates VSM contraction (Khalil, 2010).

1.1.3 Adventitia (Perivascular adipose tissue)

PVAT is the outer layer of connective tissue that surrounds most of the vasculature, also called the tunica adventitia. Its role is complementary to that of the serosa, which also provides a protective layer of tissue surrounding most of the body organs. PVAT structure and function will be reviewed in more detail in (section 1.3).

1.2 Adipose tissue

Adipose tissue is widely distributed in mammals and contains either white or brown adipocytes or a mixture of the two. Although adipocytes are most abundant in adipose depots, adipose tissue also contains pre-adipocytes, macrophages, leukocytes, fibroblasts, blood vessels and nerves. Adipose tissue plays an important role in regulating energy homeostasis and can be classified into three categories according to the size of the lipid droplet and number of mitochondria: white adipose tissue (WAT) brown adipose tissue (BAT) and beige adipose tissue (BeAT) (Lasar *et al.*, 2013, Frontini *et al.*, 2013), (Table 1-1). BAT is found principally in neonates, although growing evidence suggests that BAT is also found in adults. BAT can take up lipids to generate heat by uncoupling oxidation of the mitochondrial electron transportation chain, which promotes the clearance of plasma lipids and prevents storage of lipids in WAT and other organs (Cannon and Nedergaard, 2004) . Excess lipid accumulation and dysfunctional WAT can lead to adipocyte hypertrophy and increased risk of atherosclerosis, while activation of

BAT may protect against atherosclerosis (Berbée *et al.*, 2015). In addition to the categorization of adipose tissues by their colour, adipose tissues can be categorized according to their anatomical locations (Richard *et al.*, 2020) .

1.2.1 White adipose tissue

WAT is the most abundant type of adipose tissue, a primary site for energy storage and is composed of large adipocytes with more than 90% of their volume occupied by a single large lipid droplet of triglyceride and a few mitochondria. WAT stores excess calories as triglyceride in the fed state which undergo lipolysis in the fasted state to liberate FA and glycerol for ATP production by other tissues and gluconeogenesis in the liver respectively. WAT plays an important role in secreting several biologically active proteins including adipokines which have autocrine, paracrine, and endocrine effects. The paracrine effect adipokines control energy homeostasis via liberation of fatty acids which can be utilised as fuel for the brain, muscle, and other tissues during starvation. WAT is the predominant component of subcutaneous (sWAT) and visceral (vWAT) depots, and gluteofemoral areas in females (Cinti, 2011). vWAT or abdominal fat located inside the peritoneal cavity provides a protective lining for some organs such as the stomach, liver, intestines and kidneys and also has an insulation function to prevent loss of heat through the skin (Choe *et al.*, 2016, Victorio *et al.*, 2016, Richard *et al.*, 2020).

1.2.2 Brown adipose tissue

BAT is composed of adipocytes that have multiple small lipid droplets and a larger number of mitochondria than WAT and express a characteristic browning marker, uncoupling protein 1 (UCP-1), that is responsible for the thermogenic activity of BAT (Machado *et al.*, 2022). The brown colour of BAT is mainly due to the presence of the cytochromes in the larger number of mitochondria. BAT has a vital role in dissipating energy in the form of heat during cold exposure (non-shivering thermogenesis). BAT is located primarily in perirenal, periovarian, supraclavicular, neck, and mediastinal regions and surrounds some blood vessels such as the thoracic aorta (Cinti, 2011, Gil-Ortega *et al.*, 2015, Hildebrand *et al.*, 2018).

In addition, “brown-like” adipocytes are another type of WAT which express UCP-1 and have thermogenic capabilities with a similar phenotype to brown adipocytes. They are sometimes referred to as: “beige” or “brite’’ adipocytes, with the only difference distinguishing beige from classical brown adipocytes being that they are not derived from the same embryonic precursors (Wu *et al.*, 2012, Park *et al.*, 2014). It is not well understood whether beige adipocytes develop from white adipocytes through *de novo* maturation and differentiation of preadipocytes (Wang *et al.*, 2013), or in response to different endogenous stimuli (Vitali *et al.*, 2012, Frontini *et al.*, 2013), (Table 1-1).

Table 1-1: Types of adipocytes

Epithelial like antigen-1 (Eva1), transmembrane protein 26 (TMEM26), pyruvate dehydrogenase kinase 4 (Pdk4), early B-cell factor 3 (Ebf3), lipoprotein lipase (LPL), glycerol-3-phosphate dehydrogenase (G3PDH), developmental transcription factor (Tbx1) and short stature homeobox 2 (Shox2).

	Brown	White	Beige (Brown-like)
Location	Thoracic PVAT, Interscapular, perirenal, paravertebral axillary	Abdominal PVAT, Inguinal (sWAT), mesenteric, retroperitoneal, perigonadal, omental (vWAT)	Within inguinal WAT, other sWAT?
Function	Heat production (thermogenic)	Storage of energy as triglycerides Autocrine and paracrine activity	Adaptive thermogenesis
Morphology	Multilocular/small lipid droplets	Single large lipid droplets	Unilocular large/multiple small lipid droplets
Mitochondria	(+++)	(+)	Upon stimulation (++)
Markers	UCP1, Eva1, Pdk4, Ebf3	Resistin, LPL, G3PDH	Tmem26, Tbx1, Shox2

1.3 Perivascular adipose tissue (PVAT)

PVAT surrounds most systemic blood vessels, with the exception of cerebral blood vessels and capillaries, and regulates vascular function by the production of many autocrine and paracrine molecules. Many of these molecules are vasoactive and include: adiponectin (Boateng *et al.*, 2021), PVAT-derived relaxing factors (PDRF)

(Lynch *et al.*, 2013), prostacyclin (Chang *et al.*, 2012), gaseous molecules (NO and H_2S) (Szasz and Webb, 2012), and angiotensin 1–7 (Lee *et al.*, 2009).

Previous studies have demonstrated that PVAT attenuates vascular contraction in multiple vascular beds including coronary vessels (Aghamohammadzadeh *et al.*, 2012) and rat mesenteric arteries (Verlohren *et al.*, 2004). PVAT is composed of white or brown adipocytes, or a mixture of both depending on the vascular bed (Gao *et al.*, 2007, Cinti, 2011, Fitzgibbons *et al.*, 2011). The vasoregulatory function of PVAT is adversely affected in cases of obesity and atherosclerotic disease (Szasz and Webb, 2012, Chang *et al.*, 2020). It has been shown that the secretory profile of PVAT is changed by hypertension, obesity and other cardiovascular diseases, leading to dysregulation between its anti-contractile and pro-contractile effects (Ramirez *et al.*, 2017). Heterogeneity of PVAT has been reported even within the same blood vessel; PVAT around the abdominal aorta is predominantly white with a small amount of brown adipocytes while PVAT around the thoracic aorta is mainly composed of brown adipocytes (Padilla *et al.*, 2013, Brown *et al.*, 2014, Kong *et al.*, 2018).

In 1994 leptin was the first adipokine discovered, and since then more than 600 adipokines have been identified (Taylor, 2021). Adipokines can be categorised according to their physiological effect as either anti-inflammatory such as adiponectin and adrenomedullin (Fésüs *et al.*, 2007, Zhu *et al.*, 2008) or pro-inflammatory such as leptin (Nakagawa *et al.*, 2000, Şahin and Bariskaner, 2007). Some adipokines including vaspin (Phalitakul *et al.*, 2012) and chemerin have been suggested to play a positive role in modulating vascular function of the cardiac circulation (Yamawaki *et al.*, 2012). With some adipocytokines such as visfatin, which is produced in large quantities within PVAT, the source seems to be the stromal vascular cells rather than the adipocytes (Stastny *et al.*, 2012). Moreover, PVAT can also generate cytokines such as interleukin (IL-6), (IL-8), the chemokine monocyte chemoattractant protein-1 (MCP-1) and plasminogen-activator inhibitor-1 (Thalmann and Meier, 2007) from cells such as fibroblasts, macrophages, capillary endothelial cells and T lymphocytes residing in PVAT or attracted to PVAT in response to inflammatory chemokines released by adipocytes (Szasz and Webb, 2012).

1.3.1 Anticontractile action of PVAT

PVAT was previously considered to be a supporting structure with only a role in the mechanical protection of the underlying blood vessels. It was routinely removed during blood vessel reactivity studies as it was thought that its existence might affect vascular reactivity either by metabolising and changing the chemical properties of some pharmacological agents or obscuring diffusion of the these agents to the adventitia layer (Oriowo, 2015). In 1991 Soltis and Cassis reported that thoracic PVAT from male Sprague-Dawley rats significantly attenuated the contractile response to noradrenaline (Soltis and Cassis, 1991) and since then many other studies have reported that PVAT is not only a connective tissue supporting blood vessels but also an endocrine, paracrine and autocrine organ which releases a wide variety of bioactive and vasoactive molecules. As noted above, these can regulate metabolic and vascular functions and examples include: leptin, vascular endothelial growth factor, insulin-like growth factor, tumour necrosis factor-alpha (TNF-α), resistin, adiponectin, plasminogen activator substance, angiotensinogen and IL-6 (Szasz and Webb, 2012).

So-called adipocyte-derived relaxing factors (ADRFs) were the first identified vasoactive molecules released from PVAT which diffuse into the adventitia to induce a vascular relaxation (Löhn *et al.*, 2002). Lohn and co-workers demonstrated that transferring bath solution from an artery segment with intact PVAT into a bath containing a precontracted artery segment lacking PVAT resulted in a rapid relaxation, suggesting that PVAT releases transferable PVAT-derived vasorelaxant factor(s). These early findings were subsequently confirmed by other studies (Verlohren *et al.*, 2004, Malinowski *et al.*, 2008, Greenstein *et al.*, 2009, Almabrouk *et al.*, 2017).

The anticontractile action of PVAT has been reported to modulate vascular function either by an endothelium-dependent or endothelium-independent mechanism. A growing body of evidence indicates that PVAT exerts its relaxant effects via release of a wide variety of molecules such as NO that have a direct effect on VSM cells (Orshal and Khalil, 2004, Virdis *et al.*, 2015).

In terms of endothelium-dependent effects, Gao and co-workers demonstrated that transfer of conditioned medium from intact aortic rings with PVAT attached

(donor) to a bath containing aortic rings with denuded endothelium did not enhance the relaxation response of the vessels. They proposed that PVAT exerts its anti-contractile effects via PVAT releasing a transferable relaxing factor which induces endothelium-dependent relaxation through NO release and following activation of K^+ channels in VSMCs (Gao *et al.*, 2007, Gao, 2007). Adiponectin is another adipokine that is secreted by PVAT and reported to induce vascular relaxation through endothelium-dependent mechanisms via enhancing eNOS phosphorylation at Ser^{1177} via phosphoinositide-3-kinase–protein kinase B (PI3K-Akt) and AMPK signalling and increasing NO production (Chen *et al.*, 2003, Antoniades *et al.*, 2009, Almabrouk *et al.*, 2017). The role of AMPK in PVAT-mediated effects will be discussed later in (section 1.5).

Another mechanism underlying the anticontractile effect of PVAT is mediated through the activation of voltage-dependent potassium channels (Kv channels), which modulate basal vascular smooth muscle tone (Verlohren *et al.*, 2004). Verlohren and co-workers reported that the resting membrane potential was hyperpolarized in vessels with intact PVAT compared to vessels with the PVAT removed, indicating that PVAT plays an important role in regulating vascular smooth muscle tone (Verlohren *et al.*, 2004). Supporting that, a different study reported that XE 991, a selective inhibitor of non-inactivating voltage-gated potassium channels (Kv7) reduced the hyperpolarized resting membrane potential in the rat gracilis artery with intact PVAT (Zavaritskaya *et al.*, 2013), confirming a role for Kv channels in PVAT-induced regulation of membrane potential and resting tone of the rat aorta.

On the other hand, under certain pathological conditions, PVAT releases a different profile of contractile factors which impair its anticontractile effect. These were initially termed PVAT-derived contracting factors (PVCFs) (Gao *et al.*, 2007, Meyer *et al.*, 2013) and include resistin, IL-6, leptin, TNF-α and angiotensin II (Ramirez *et al.*, 2017).

1.4 Nitric oxide and regulation of vascular function

1.4.1 Nitric oxide

Nitric oxide is an inorganic free radical gas that was identified as an endogenous vasodilator in 1987. It is synthesised by vascular endothelial cells from L-arginine and acts as a transcellular signalling molecule and cell communication enhancer. The enzymes responsible for the synthesis of NO from L-arginine in mammalian tissues are known as NO synthases (NOS) (Knowles and Moncada, 1994, Maiuolo *et al.*, 2019). NO is a key physiological mediator involved in signal transduction in the cardiovascular, genitourinary, respiratory, nervous, and gastrointestinal systems and plays a significant role in control of vascular tone. As such, dysregulation of NO generation and signalling has been implicated in a wide range of diseases (Spiers *et al.*, 2019, Król and Kepinska, 2020).

NO rapidly reacts with various cellular targets that contribute to its short biological half-life, which in most circumstances is less than 2 seconds (Thomas *et al.*, 2001). This represents an extremely short half-life in comparison with other signalling molecules but more than other free radicals, whose lifespan is often of the order of milliseconds. As NO contains an unpaired electron but does not possess an electrical charge, NO can cross biological membranes by passive diffusion and has several effects including: inhibition of adhesion and aggregation of blood platelets to the vascular endothelium, prevention of leukocyte migration and adhesion onto vascular wall, inhibition of vascular smooth muscle cell proliferation and inhibition of low-density lipoprotein oxidation (Garg and Hassid, 1989, Lefer *et al.*, 1999, Freedman *et al.*, 1999, Förstermann and Sessa, 2012, Förstermann *et al.*, 2017). Furthermore, NO is soluble in both hydrophilic and hydrophobic environments although it is more soluble in hydrophobic environments by a factor of about 10; a property important for its ability to cross cell membranes (Liu *et al.*, 1998).

1.4.2 Nitric Oxide Synthase: structure and function

NO is synthesised via one of three isoforms of nitric oxide synthase: neuronal nNOS (NOS1), inducible iNOS (NOS2) or endothelial eNOS (NOS3). Each NOS isoform has

different tissue distributions, differential regulation and subcellular localization (Villanueva and Giulivi, 2010, Costa *et al.*, 2016).

eNOS and nNOS generally produce low (nM) concentrations of NO, whereas iNOS is overexpressed and upregulated during inflammation in response to different stimuli including cytokines and bacterial infection, and able to produce far higher concentrations of NO for relatively prolonged periods (Thomas, 2015). Circulating blood elements such as macrophages and neutrophils express iNOS when activated, whereas the vasculature and nerve fibres in other tissues express eNOS and nNOS (Sproston *et al.*, 2018, Tejero *et al.*, 2019b).

1.4.2.1 Endothelial nitric oxide synthase

eNOS contains a N-terminal oxygenase domain which carries a haem group. This domain binds to the cofactor (6R-)5,6,7,8-tetrahydrobiopterin (BH_4) and the substrates O_2 and L-arginine. This domain is linked to the C-terminal reductase domain which binds the other substrate, reduced nicotinamide adenine dinucleotide phosphate (NADPH), and the cofactors flavin mononucleotide (FMN) and flavin adenine dinucleotide (FAD) (Förstermann *et al.*, 1994) (Figure 1-2). Endothelial NOS is encoded by the *NOS3* gene and is mainly expressed in vascular endothelial cells which are responsible for most NO produced in the vasculature (Förstermann and Sessa, 2012, Oliveira-Paula *et al.*, 2017). eNOS is activated by endogenous agonists such as acetylcholine, bradykinin, histamine, vascular endothelial growth factor and also by shear stress generated by the laminar flow of blood (Konukoglu and Uzun, 2017, Suvorava *et al.*, 2022). Different agonists stimulate eNOS by diverse mechanisms including protein phosphorylation, increased intracellular Ca^{2+} and altering the interaction with substrate and co-factors (Fleming and Busse, 2003, Heiss and Dirsch, 2014a).

Early studies reported that mice lacking eNOS ($eNOS^{-/-}$) exhibited abnormalities in vascular relaxation, cardiac contractility and the experimental induction of stroke resulted in more severe brain injury (Liu and Huang, 2008). Furthermore, eNOS knockout mice exhibit hyperinsulinaemia, insulin resistance and hypertension (Duplain *et al.*, 2001), indicating that eNOS is important for the regulation not only of blood pressure but also has a role in lipid and glucose homeostasis. In addition, it has been suggested that eNOS-derived NO may contribute to the

antiaging effects of calorie restriction and enhance mitochondrial biogenesis (Nisoli *et al.*, 2005, Csiszar *et al.*, 2009).

Even though eNOS is primarily expressed in the endothelium, a growing body of evidence using bone marrow transplant mouse models and flow cytometry reported that functional eNOS is also expressed by red blood cells that it contributes partially to systemic blood pressure regulation and reduces risk of myocardial injury (Cortese-Krott *et al.*, 2012, Wood *et al.*, 2013, Yang *et al.*, 2013, Kuhn *et al.*, 2017). Given that, Cortese-Krott and co-workers demonstrated that under normoxic conditions human red blood cells constitutively generate NO via eNOS. Furthermore, the activity of eNOS was compromised in red blood cells from patients with coronary artery disease compared with age-matched healthy individuals (Bhattacharya *et al.*, 2001, Kleinbongard *et al.*, 2006, Cortese-Krott *et al.*, 2012, Cortese-Krott and Kelm, 2014).

The activity of eNOS is regulated by a variety of factors, including its dimerization status and when eNOS becomes uncoupled it becomes a source of oxidative stress. However, it is essential to note that while eNOS coupling is a significant source of oxidative stress, it is not the sole contributor in this context. Other sources, such as Nox-NADPH oxidases, also play a crucial role in generating oxidative stress within the vascular system. This broader perspective underscores the multifactorial nature of oxidative stress mechanisms and their potential implications for vascular health (Tran *et al.*, 2022).

Also, eNOS exists in both monomeric and dimeric forms but under normal physiological condition eNOS exists as a dimer and produces NO. Under some physiopathological conditions eNOS is uncoupled to monomeric forms, generating superoxide anions and this is thought to be a predisposing factor for endothelial dysfunction in several cardiovascular diseases (Chang *et al.*, 2019). Several lines of evidence have demonstrated that eNOS dimerization is regulated by post-translational modifications, including eNOS phosphorylation at Ser^{1177} (Heiss and Dirsch, 2014b, Mazrouei *et al.*, 2019). It has also been reported that statins and angiotensin-converting enzyme (ACE) inhibitors promote eNOS dimerization, leading to improved endothelial function and decreased cardiovascular risk (Chang *et al.*, 2019).

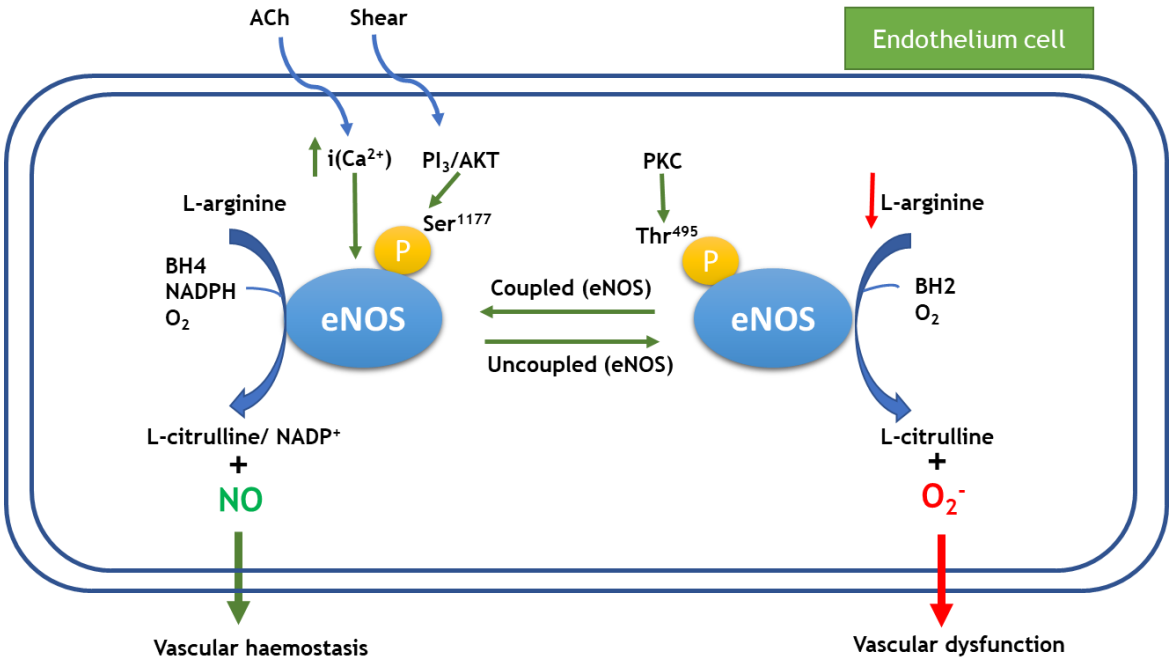

Figure 1-2: Nitric oxide and superoxide anion generation by eNOS

In the coupled state eNOS dimers produce NO, L-citrulline and NADP+ from L-arginine (Left panel), which requires the presence of tetrahydrobiopterin (BH_4), NADPH, and oxygen, while in the uncoupled state eNOS generates superoxide anions and other ROS instead of NO, leading to vascular dysfunction (right panel). Uncoupling can be due to oxidation of BH_4 to dihydrobiopterin (BH_2). Acetylcholine (ACh) increases calcium concentrations to mediate calcium-calmodulin (CaM)-dependent activation of eNOS and protein kinase A (PKA)-dependent phosphorylation of eNOS at Ser^{1177} and Ser^{633} residues which also increases eNOS activity. Protein kinase C (PKC) increases eNOS phosphorylation at Thr^{495} which downregulates eNOS activity and reduce NO synthesis.

1.4.2.2 Inducible nitric oxide synthase

Inducible NOS (iNOS or NOSII) was initially identified in cytokine-induced macrophages. In human physiology the primary function of iNOS derived NO is the destruction of invading pathogens thereby having antiparasitic, microbicidal and antiviral effects (Chakravortty and Hensel, 2003, Pautz *et al.*, 2010). In the vascular system iNOS is mainly synthesised or expressed in response to inflammatory mediators (Förstermann and Sessa, 2012, Zhao *et al.*, 2021).

Excessive iNOS activity has been associated with several pathological conditions including septic shock, cardiac dysfunction and neurodegeneration (Cinelli *et al.*, 2020).

BH_4 also plays an important role in regulating iNOS dimerization and activity, as The embryonic mouse fibroblast cells (NIH 3T3) deficient in *de novo* BH_4 biosynthesis expressed monomeric inactive iNOS, but supplementation with BH_4 or it is precursor sepiapterin increased iNOS dimerization and coupling (Tzeng *et al.*, 1995, Ghosh *et al.*, 1999, Cinelli *et al.*, 2020). The structure of iNOS is shown in (Figure 1-3).

1.4.2.3 Neuronal nitric oxide synthase

Neuronal NOS (nNOS) was originally discovered in rat neurons (Bredt, 1990) and is predominantly expressed in certain neurons but is also found in skeletal muscle, perivascular nerve fibres, in the vascular wall, cardiomyocytes and endothelial cells (Schwarz *et al.*, 1999, Tsutsui, 2004, Xu *et al.*, 1999, Lührs, 2002). The structure of nNOS is shown in (Figure 1-3).

Like eNOS, nNOS activity is principally regulated by intracellular Ca^{2+}/calmodulin levels, binding to cofactors such as BH_4 and dimerization (Alderton *et al.*, 2001). In the vascular bed, NO derived from nNOS contributes to vasodilation (Seddon *et al.*, 2009, Capettini *et al.*, 2011). In addition, the expression of nNOS in endothelial cells and vascular smooth muscle has been associated with the control of brain blood flow (Kitaura *et al.*, 2007). Interestingly, two studies have demonstrated that nNOS generates NO and H_2O_2 under normal physiological conditions. Studies simultaneously measuring NO, H_2O_2 and vascular function using antisense nNOS knockdown and pharmacological inhibitors indicated that nNOS-derived H_2O_2 is the main endothelium-dependent relaxing factor (EDRF) in the mouse aorta and contributes importantly to endothelium-dependent vasodilatation (Rabelo *et al.*, 2003, Capettini *et al.*, 2011) (Table 1-2).

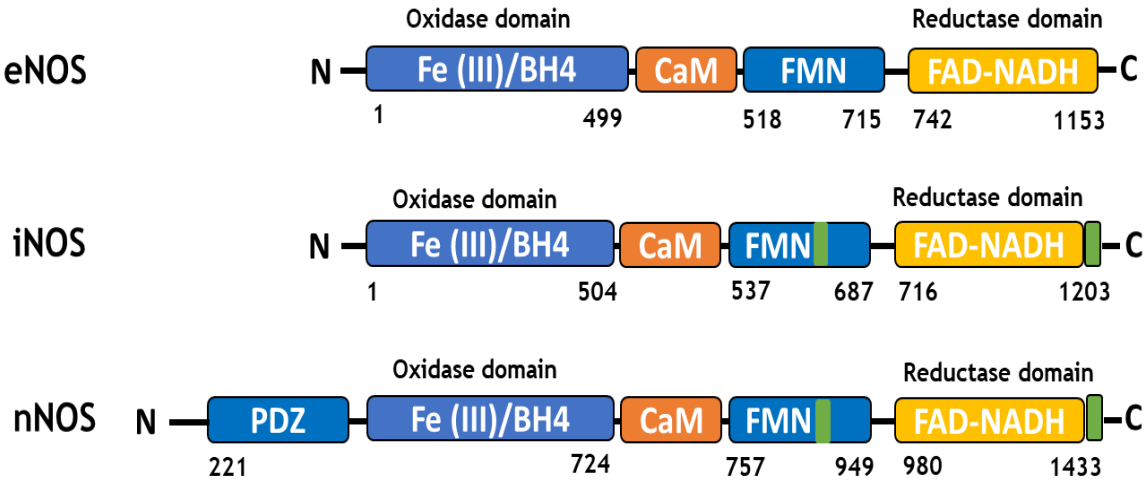

Figure 1-3: Structure and functional domains of NOS isoforms

Each NOS isoform is comprised of an N-terminal oxidase domain, CaM-binding and FMN-binding domains and a C-terminal reductase domain. There are three nitric oxide synthase (NOS) isoforms: Ca^{2+}-dependent endothelial NOS (eNOS) and neuronal NOS (nNOS) and Ca^{2+}-independent inducible NOS (iNOS). The oxidase domain contains the L-arginine, haem, and tetrahydrobiopterin (BH_4)-binding sites. Flavin mononucleotide (FMN) binds to the reductase domain. Flavin adenine dinucleotide (FAD), and nicotinamide adenine dinucleotide phosphate (NADPH)-binding sites are within the reductase domain which also binds L-arginine. An additional postsynaptic Drosophila zonula occludens-1 protein (PDZ) domain is found only in the N-terminal of the nNOS and allows the enzyme to bind other proteins with a similar structure.

Table 1-2: Functions of NOS isoforms and phenotypes of NOS knockout mice

isoform	function	Phenotype of KO mice
eNOS	Vasodilation Modulation of leukocyte–endothelial Interaction Modulation of platelet aggregation	Elevated mean arterial blood pressure Absence of EDRF activity in aorta Increased vascular response to injury Enhanced cardiac contractile response to β-adrenergic stimulation Increased susceptibility to global ischemia
nNOS	Signal transduction Neurotransmission	Enlarged stomach, pyloric stenosis Aggressive behaviour Reduced cardiac contractile response to β-adrenergic stimulation Increased diet-induced atherosclerosis No protection from cerebral ischaemic preconditioning
iNOS	Defence against pathogens Inflammation	Susceptible to tuberculosis & other infections Resistance to sepsis-induced hypotension Decreased neuronal injury after stroke (delayed) Decreased diet-induced atherosclerosis

1.4.3 Regulation of eNOS

Studies to understand the mechanism of eNOS regulation have been crucial in understanding how the blood vessels are regulated by the vascular endothelium and smooth muscle cells (Siragusa and Fleming, 2016, Garcia and Sessa, 2019). In addition, experiments using eNOS mutated mice have revealed that eNOS has antithrombotic, antiatherosclerotic and antihypertensive effects (Xia *et al.*, 2017). eNOS activity is tightly regulated by a number of mechanisms including allosteric modulation, posttranslational modification, protein-protein interactions and also subcellular localisation (Siragusa and Fleming, 2016, Meza *et al.*, 2019, Garcia and Sessa, 2019, Garcia *et al.*, 2020b). Posttranslational modifications include phosphorylation, as well as lipid modifications such as myristoylation and palmitoylation which play an important role in eNOS subcellular localisation (Gonzalez *et al.*, 2002). It has also been demonstrated eNOS is modified by O-GlcNAcylation as a consequence of hyperglycaemia leading to reduced eNOS phosphorylation at Ser^{1177} and therefore reducing eNOS activity (He *et al.*, 2020).

1.4.3.1 Phosphorylation of eNOS

It has been reported that eNOS phosphorylation at tyrosine, serine and threonine residues plays an important role in the regulation of activity and sensitivity of eNOS to calcium and there are at least 8 defined sites of eNOS phosphorylation. Initial studies to identify the sites of eNOS phosphorylation were performed in bovine aortic endothelial cells (BAECs) (Gallis *et al.*, 1999). eNOS activity is stimulated by phosphorylation at Ser^{1177} in response to several stimuli such as shear stress and adiponectin. Phosphorylation of eNOS at Ser^{633} also activates eNOS, whereas phosphorylation of Thr^{495} inhibits eNOS activity (Chen *et al.*, 2009, Gaynullina *et al.*, 2022).

Phosphorylation of eNOS at Ser^{1177} close to the carboxy-terminal by Akt results in a conformational change of eNOS, allowing allosteric binding of CaM at suboptimal Ca^{2+} concentrations, resulting in an increase in eNOS activity and an increase in NO production (Michell *et al.*, 1999, Musicki *et al.*, 2005).

Mutation of Ser^{1177} with alanine reduces both basal and stimulated NO synthesis (Bauer *et al.*, 2003), indicating the importance of the Ser^{1177} residue in regulating eNOS activity and NO production. Indeed, phosphorylation of eNOS at Ser^{1177} seems to be the most important for regulating eNOS phosphorylation in response to any internal and external stimuli that promote eNOS activation (Rafikov *et al.*, 2011).

A growing body of evidence has reported that phosphorylation of eNOS at Ser^{633} in the flavin mononucleotide binding domain (FMN) is also important for eNOS activation to maintain NO production in blood vessels. Indeed, phosphorylation at this site has been linked with eNOS activation in response to a wide variety of stimuli including mechanical factors such as shear stress (Boo *et al.*, 2002). Conversely, phosphorylation of eNOS at Thr^{495} interferes with the binding of calmodulin to the eNOS calmodulin-binding domain, thereby inhibiting NO synthesis (Fleming *et al.*, 2001, Kang *et al.*, 2012).

An early finding reported that incubation of human aortic endothelial cells with insulin rapidly increases eNOS phosphorylation at Ser^{1177} and Ser^{615} in response to

Akt activation and influence Ca^{2+} sensitivity, however, phosphorylation of Ser^{633} Thr^{495} Ser^{114}, was unaltered (Ritchie *et al.*, 2010).

1.4.3.2 eNOS activation by different kinases

Several kinases have been reported to phosphorylate eNOS, including: Akt (also termed protein kinase B), AMPK, PKA, PKG, PYK2, CaMKK2 and PKC. Some earlier studies demonstrated AMPK activation in rat skeletal and cardiac muscle under vigorous exercise and ischaemic stress which would then induce eNOS phosphorylation and NO generation (Chen *et al.*, 1999).

eNOS is also regulated by several upstream kinases, including protein kinase A (PKA) and protein kinase B (PKB) (Chen *et al.*, 2009, Zhu *et al.*, 2016, Gaynullina *et al.*, 2022). Phosphorylation of eNOS by Akt represents a novel Ca^{2+} -independent regulatory mechanism for activation of eNOS (Dimmeler *et al.*, 1999), and activation of cAMP-dependent protein kinase A (PKA) causes Ser^{635} phosphorylation (Boo *et al.*, 2002, Michell *et al.*, 2002), while protein kinase G (PKG) (Butt *et al.*, 2000), calmodulin/Ca^{2+} -dependant protein kinase (CaMK2), increases phosphorylation of eNOS at Ser^{1177} (Fleming *et al.*, 2001).

The other kinase that is thought to regulate eNOS activity is PKC which downregulates eNOS activity through Thr^{495} phosphorylation and eNOS uncoupling in response to Ach, bradykinin, VEGF and ATP (Sessa, 2004) (Figure 1-4).

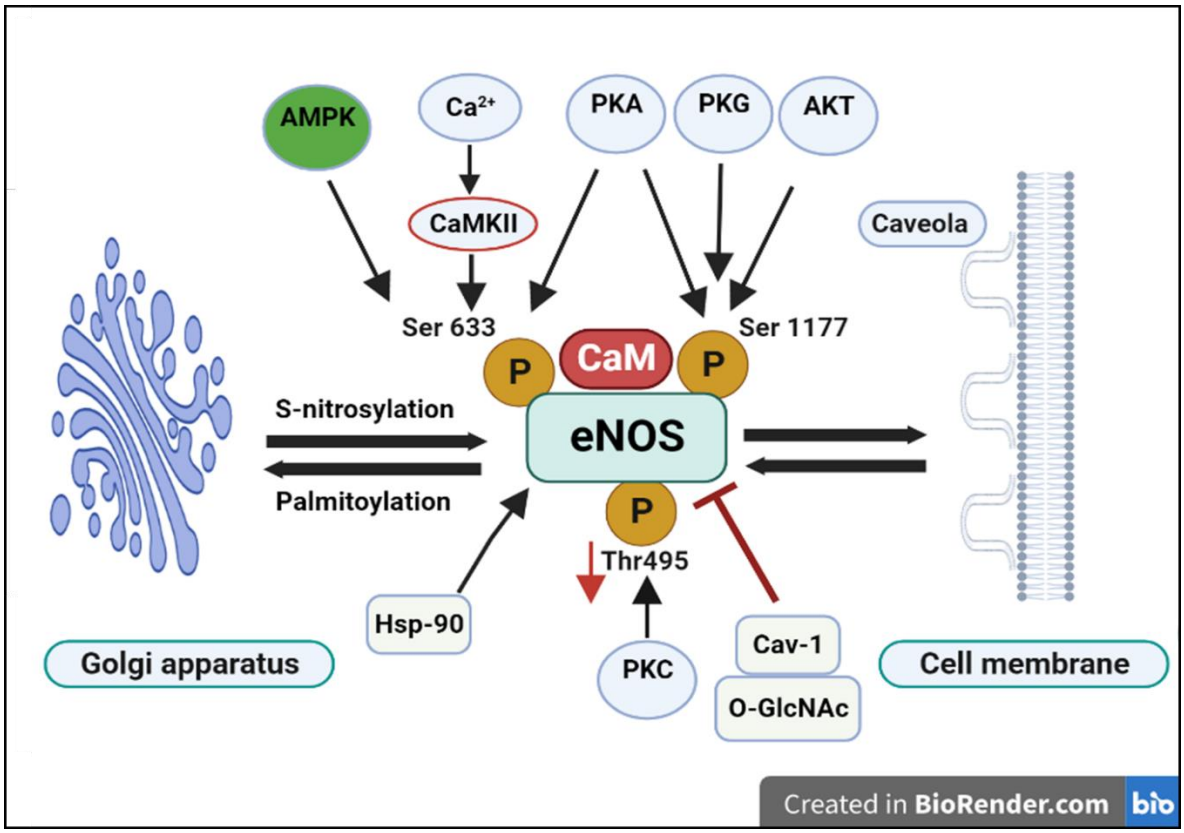

Figure 1-4: A schematic diagram showing eNOS regulation and activation

eNOS is positively modulated by phosphorylation of Ser^{1177} and Ser^{633} and negatively regulated by phosphorylation of Thr^{495}. Ser^{1177} is reported to be phosphorylated by several upstream kinases including Akt, protein kinase G (PKG) and protein kinase A (PKA). Ca^{2+} /CaM dependent kinase II (CaMKII), PKA and AMP-activated protein kinase (AMPK) have been reported to phosphorylate Ser^{633}. Protein kinase C (PKC) phosphorylates the inhibitory Thr^{495} site. In addition, eNOS activity is inhibited by its interaction with caveolin-1 and by O-GlcNAc modification inhibiting NO production, while eNOS association with heat shock protein 90 (Hsp-90) favours its activation. S- nitrosylation and palmitoylation stimulates eNOS trafficking from Golgi apparatus and the cell membrane. Created with BioRender.com.

1.4.3.3 Endogenous inhibitors of eNOS activity

1.4.3.4 Asymmetric dimethylarginine

Regulation of eNOS activity by endogenous inhibitors is of great interest as pharmacological targets for treatment of cardiovascular diseases. A potent endogenous inhibitor of eNOS is asymmetric dimethylarginine (ADMA), a homologue of L-arginine which competes with L-arginine for NOS, leading to a reduction of NO generation. ADMA is generated from hydrolysis and degradation of proteins containing arginine residues methylated by protein arginine methyltransferases (PRMT), and the resulting ADMA competitively antagonises eNOS and reduces NO production (Cooke, 2010, Alpoim *et al.*, 2015). Furthermore, ADMA is degraded by two enzymes: dimethylarginine dimethyl amino hydrolase 1 and 2 (DDAH1 and DDAH2) (Vallance *et al.*, 1992, Tran *et al.*, 2003, Böger, 2003). Several lines of evidence suggest that DDAH1 but not DDAH2 is the isoform responsible for ADMA degradation. For example, in cultured vascular endothelial cells, silencing of DDAH1 results in a decrease in NO production and ADMA accumulation, whilst silencing of DDAH2 has no effect on ADMA levels (Hulin *et al.*, 2020).

An increase in ADMA levels has been considered as a risk factor for the pathogenesis of cardiovascular diseases (Vallianou *et al.*, 2019). Furthermore, drugs that influence cardiovascular disease risk may influence ADMA levels, as it has been reported that the lipid lowering drug simvastatin increased DDAH1 expression levels and decreased ADMA concentrations in cultured endothelial cells, leading to eNOS activation and enhanced NO production (Hsu *et al.*, 2016). Another study reported that in hyperlipidaemic rabbits the angiotensin converting enzyme inhibitor (ACEI) captopril significantly lowered ADMA serum levels and enhanced endothelial function via increased DDAH1 activity (Lin *et al.*, 2017).

1.4.3.5 Reactive oxygen species

Oxidative stress is generated during inflammation and endothelial dysfunction and can modulate vascular function and structure. Oxidative stress is defined as an imbalance between the production of free radical reactive oxygen species (ROS) and antioxidant defences. In the vascular system, ROS are produced by many cells including: vascular smooth muscle cells, endothelial cells and inflammatory cells

infiltrating the perivascular adipose tissue (Man *et al.*, 2020). ROS include hydrogen peroxide and superoxide, which can act in the vascular system as signalling molecules, as effectors of the immune response, or as by-products of cellular metabolism (Schieber and Chandel, 2014, Wang *et al.*, 2018). ROS levels can be increased by activation of NADPH oxidase in endothelial cells and lead to the oxidation of BH_4 to the $BH_3^{\bullet}$ radical, with eNOS uncoupling and a reduction in activity (Kuzkaya *et al.*, 2003). There are many proposed pathways by which ROS reduce NO availability, for example, during inflammation or oxidative stress, NO reacts with superoxide resulting in peroxynitrite formation. Peroxynitrite can damage a wide range of cells and tissues via direct oxidative reactions or indirect radical-mediated mechanisms leading to oxidative injury, committing cells to necrosis or apoptotic cellular DNA damage (Cassuto *et al.*, 2014, Ahmad *et al.*, 2019). As a result, the accumulation of ROS leads to a drop in NO bioavailability and tissue damage (Chrissobolis *et al.*, 2011, Förstermann and Li, 2011, Dix, 2017).

As mentioned in section (1.4.2.1), eNOS normally exists as a dimer and produces NO but under conditions such as oxidative stress and/or decreased BH_4 levels, eNOS uncouples and generates free radicals such as superoxide anions ($O_2^{\bullet -}$) instead of NO. This leads to generation of other free radicals including reactive nitrogen species (RNS) such as nitroxyl anions and nitrosonium cations, that leads to endothelial dysfunction, decreased NO bioavailability, vasoconstriction, enhanced systemic vascular resistance and increased blood pressure (Schiffrin, 2008, Yang *et al.*, 2009). Oxidation of eNOS, at the zinc-sulphur-complex, or S-glutathiolation of cysteine residues in the reductase domain, causes an oxidative disruption of the dimeric eNOS complex (Loot *et al.*, 2009). It has been reported that eNOS phosphorylation at Thr^{495} is mediated by protein kinase C (PKC) and increasing ROS levels leads to increases in levels of ADMA, thereby reducing eNOS activity (Schulz *et al.*, 2014, Laher, 2014, Daiber *et al.*, 2019).

Hyperlipidaemic mice have been reported to exhibit BH_4 deficiency in macrophages and endothelial cells, this leads to atherosclerosis and triggers endothelial dysfunction associated with mildly increased blood pressure, and increased plaque macrophage content due to eNOS uncoupling as well as increased superoxide generation (Douglas *et al.*, 2018, Münzel and Daiber, 2018). In line with this, a combination of antioxidant therapy and BH_4 supplementation was

reported to have a reparative effect on endothelial function and to improve vascular function in pre-clinical and clinical studies, reducing the incidence of cardiovascular events in patients with cardiovascular disease and improving endothelium integrity in hypoxia-induced neonatal retinopathy in mice (Münzel *et al.*, 2010, Edgar *et al.*, 2017). The BH_4 precursor sepiapterin and polyethylene glycolated-superoxide dismutase also improve endothelial function *ex vivo* and *in vivo* (Daiber *et al.*, 2019). These data suggest that eNOS uncoupling could be largely due to BH_4 deficiency.

1.4.4 eNOS and protein-protein interactions

Direct and indirect protein–protein interactions have been shown to modulate eNOS activity. The best characterised example of this is where eNOS function is negatively regulated via caveolin-1 (Cav-1) binding to plasmalemmal anchored eNOS (Garcia-Cardena *et al.*, 1997). Early studies also reported that eNOS activity increases via interaction with heat shock protein-90 (Hsp-90) (Gupta *et al.*, 2017), which promotes conformational changes and stabilises the haem moiety in eNOS (Czekay *et al.*, 2011). Furthermore, Hsp-90 has been reported to interact and regulate eNOS activity by recruiting kinases such as AMPK and Akt to phosphorylate eNOS at multiple sites including Ser^{1177}, Ser^{615} and Ser^{633} and promote NO synthesis (Fulton *et al.*, 2004).

1.4.4.1 Caveolin-1

Caveolins are small transmembrane proteins forming cave-like membrane structures with a diameter of 50 to 100 nm called caveolae. Three caveolin proteins have been characterised consisting of six known and distinct caveolin subtypes that are highly homologous. However, they differ in their tissue distribution and localisation and possibly their physiological roles in signal transduction. Caveolin-1 (Cav-1 α/ß) and caveolin-2 (Cav-2 α/ß/γ) are co-expressed and co-localize in many tissues, while caveolin-3 (Cav-3) is specifically expressed in muscle tissue, including cardiomyocytes and skeletal muscle. Cav-3 has less protein-sequence similarity to Cav-2 compared with Cav-1 (Kawabe *et al.*, 2001, Williams and Lisanti, 2004, Fridolfsson *et al.*, 2014, Zipes *et al.*, 2018).

Full-length Cav-1 is a 178 amino acid membrane protein and the major structural protein of caveolae in the plasma membrane. It acts as a scaffolding protein which binds to other proteins and is involved in cell signalling and membrane trafficking (Campos *et al.*, 2019). Cav-1 is associated with cholesterol distribution, extracellular matrix organisation, endocytosis, exocytosis, cell migration as well as integration and compartmentalization of signal transduction intermediates in adipocytes but also has an important role in eNOS function (Parton and Simons, 2007, Nwosu *et al.*, 2016). Most cell types contain caveolae but they are particularly abundant in adipocytes, where they account for 30% of the PM surface area (Fan *et al.*, 1983). In adipocytes, Cav-1 is the most abundant isoform of caveolin which is responsible for caveolae formation (Scherer *et al.*, 1994). It has been shown that Cav-1 expression is considerably enhanced by DNA demethylation during adipocyte differentiation, and it has been proposed to be an important mediator of the insulin signalling pathway (Palacios-Ortega *et al.*, 2014).

Cav-1 comprises a number of domains: an N-terminal domain (residues 1–81), a scaffolding domain (CSD, residues 82–101), intermembrane domain (residues 102–134), and a C-terminal domain (residues 135–178) (Rui *et al.*, 2014, Root *et al.*, 2015). Cav-1 is post-translationally modified by phosphorylation in the N-terminal domain at tyrosine 14 (Tyr^{14}) and serine 80 (Ser^{80}). These modifications are implicated in regulating signalling and assembly of the caveolae structure (Campos *et al.*, 2019), and palmitoylation on three cysteine residues located near or at the C-terminal domain (C133, C143, and C156) (Krishna and Sengupta, 2019). Early studies reported that in human embryonic kidney 293 (HEK293) cells Cav-1 is ubiquitinated, and ubiquitination is required for Cav-1 degradation and in particular, ubiquitination at specific N-terminal lysine residues (Hayer *et al.*, 2010) (Figure 1-5).

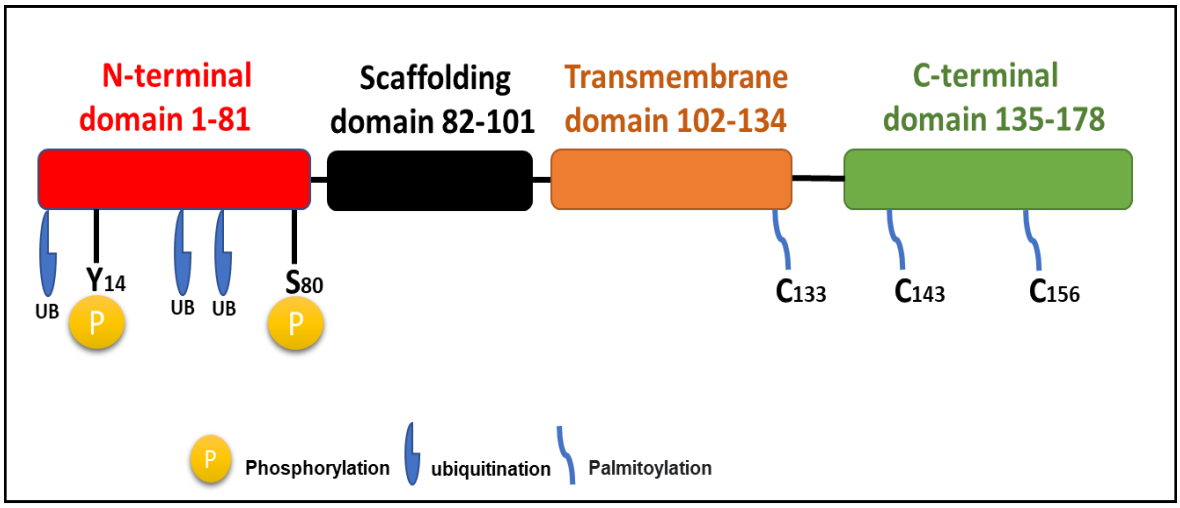

Figure 1-5: A schematic diagram of Cav-1 structure

Cav-1 is a 178 amino acid (aa) membrane protein consisting of an N-terminal domain (Red), scaffolding domain from 82 to 101 (black), a hydrophobic hairpin-transmembrane domain from 102 to 134 (orange) and a C-terminal domain from 135 to 178. Posttranslational modification of Cav-1 occurs, including phosphorylation on Tyr^{14} and Ser^{80}, ubiquitination of N-terminal residues and palmitoylation of sites at the C-terminus.

It has been shown that eNOS localisation Influences the enzyme's activity and NO production in endothelial cells (Chakraborty and Ain, 2017). eNOS translocation to the plasma membrane leads to its association with Cav-1 which contributes to reduced enzymatic activity and NO production (Wang *et al.*, 2009). Evidence suggests that Cav-1 binds eNOS and inhibits NO production by interfering with the interaction of the enzyme with Ca^{2+}/CaM via the scaffolding domain of Cav-1 (amino acids 82–101; DGIWKASFTTFTVTKYWFY). Within that sequence, amino acids 89–95 (FTTFTVT) and specifically F92 mediates eNOS inhibition by Cav-1, thereby reducing NO production (Li *et al.*, 1996, Garcia-Cardena *et al.*, 1997, Razani *et al.*, 2001, Cohen *et al.*, 2003).

A cell-permeable mutant scaffolding domain peptide of Cav-1 has previously been reported to disrupt the inhibitory action of Cav-1 on eNOS, thereby alleviating inhibition of NO production (Bernatchez *et al.*, 2011). It has been recently reported that in endothelial cells from rat vagina, oestrogen, and VEGF increase eNOS phosphorylation at Ser^{1177} mediated by phosphorylation of Akt and limiting eNOS interaction with Cav-1 (Musicki *et al.*, 2010).

In addition to direct effects on eNOS, Cav-1 has been reported to negatively regulate the small GTPase -Ras-related C3 botulinum toxin substrate 1 (Rac1) which regulates cell motility, cell growth, control cytoskeleton organization, transcription, and cell proliferation (Kinsella *et al.*, 1991, Burridge and Wennerberg, 2004, Ramadoss *et al.*, 2013). Rac1 in turn modifies the PI3K/Akt/eNOS pathway in endothelial cells (Gonzalez *et al.*, 2004, Gonzalez *et al.*, 2006). Another study reported that siRNA-mediated Cav-1 knockdown in BAECs enhances AMPK phosphorylation which in turn upregulates eNOS activity (Levine *et al.*, 2007).

1.4.4.2 Hsp-90

Heat shock protein 90 (Hsp-90) is an eukaryotic chaperone protein, responsible for the folding and functional activation of various client proteins (Chatterjee *et al.*, 2019). Under physiological conditions Hsp-90 modulates diverse cellular activities, acting to reduce cell apoptosis and degradation of non-functional proteins via the ubiquitin-proteasome pathway (Bagatell and Whitesell, 2004, Taipale *et al.*, 2010). In basal conditions in BAECs, Hsp-90 binds the non-caveolar fraction of eNOS thereby stabilizing activated eNOS and increases NO production (Takahashi and Mendelsohn, 2003, Ramadoss *et al.*, 2013).

It has been reported that eNOS activity increases via interaction of eNOS with Hsp-90 (Gupta *et al.*, 2017), which promotes conformational changes that stabilise the haem moity in NOS. Hsp-90 has also been reported to recruit kinases such as AMPK and Akt that phosphorylate eNOS via multiple sites including Ser^{1177}, Ser^{615} and Ser^{633} and promote NO synthesis (Gratton *et al.*, 2000, Fulton *et al.*, 2004, Fernández-Hernando *et al.*, 2006, Czekay *et al.*, 2011).

1.5 AMP-activated protein kinase (AMPK)

1.5.1 Overview

AMPK activity was first described in 1973 when two independent groups showed that ATP caused inhibition of acetyl CoA carboxylase (ACC) or 3-hydroxy-3-methylglutaryl coenzyme A HMG-CoA reductase (HMGR) (Carlson and Kim, 1973, Beg *et al.*, 1978). Several years later another group reported that this effect was due to a protein kinase that was responsible for the inactivation and phosphorylation of ACC and HMGR that they named AMP-activated protein kinase (AMPK) after its allosteric activator 5'-AMP (Munday *et al.*, 1988, Carling *et al.*, 1987). AMPK is a metabolic stress-sensing protein kinase which is the downstream component of a protein kinase cascade that plays an important role in the regulation of cell metabolism and energy balance at both the cellular and organ level.

1.5.2 AMPK structure

AMPK is a serine/threonine protein kinase that exists as heterotrimeric complexes consisting of a catalytic α subunit and regulatory ß and γ subunits (α1, α2, ß1, ß2, γ1, γ2 and γ3) in mammals. These isoforms are encoded by seven genes (α1-PRKAA1, α2-PRKAA2, ß1-PRKAB1, ß2-PRKAB2, γ1-PRKAG1, γ2-PRKAG2 and γ3-PRKAG3) and these together can form 12 different heterotrimeric complexes (Kahn *et al.*, 2005). The expression of some of these isoforms is tissue specific and they exhibit differences in sensitivity to stimulation by AMP, subcellular localisation and sensitivity to pharmacological stimuli (Mihaylova and Shaw, 2011, Salt *et al.*, 1998, Karabiyik, 2021).

The catalytic α subunit of AMPK consists of a C-terminal regulatory domain and an N-terminal catalytic serine/threonine kinase domain which has significant activity when phosphorylated at a conserved threonine residue at position 172 within the activation loop which is essential for AMPK activity (Hawley *et al.*, 1996). The α subunit also consists of an autoinhibitory sequence (AIS) which negatively regulates AMPK through interaction with the kinase domain while the C-terminal domain is responsible for interaction with ß and γ subunits and AMPK complex formation (Pang *et al.*, 2007, Li and Chen, 2019, Wang *et al.*, 2022) (Figure 1-6).

The β subunits consist of an N-terminal region (~70 residues) which acts as a targeting scaffold domain that plays an important role in the assembly of the AMPK complex and regulates subcellular localization (Iseli *et al.*, 2005, Xiao *et al.*, 2013), and an internal carbohydrate binding module (CBM) which has been reported to bind glycogen and inhibit AMPK activity (McBride *et al.*, 2009).

The γ subunits consist of four cystathione-β-synthase motifs (CBS) which are required for binding the regulatory nucleotides that allosterically regulate the AMPK complex. A reduction in intracellular ATP levels leads to increased concentrations of AMP (and ADP) which can directly bind to the CBS motifs and allosterically activate AMPK and increase AMPK phosphorylation (Steinberg and Carling, 2019) (Figure 1-6).

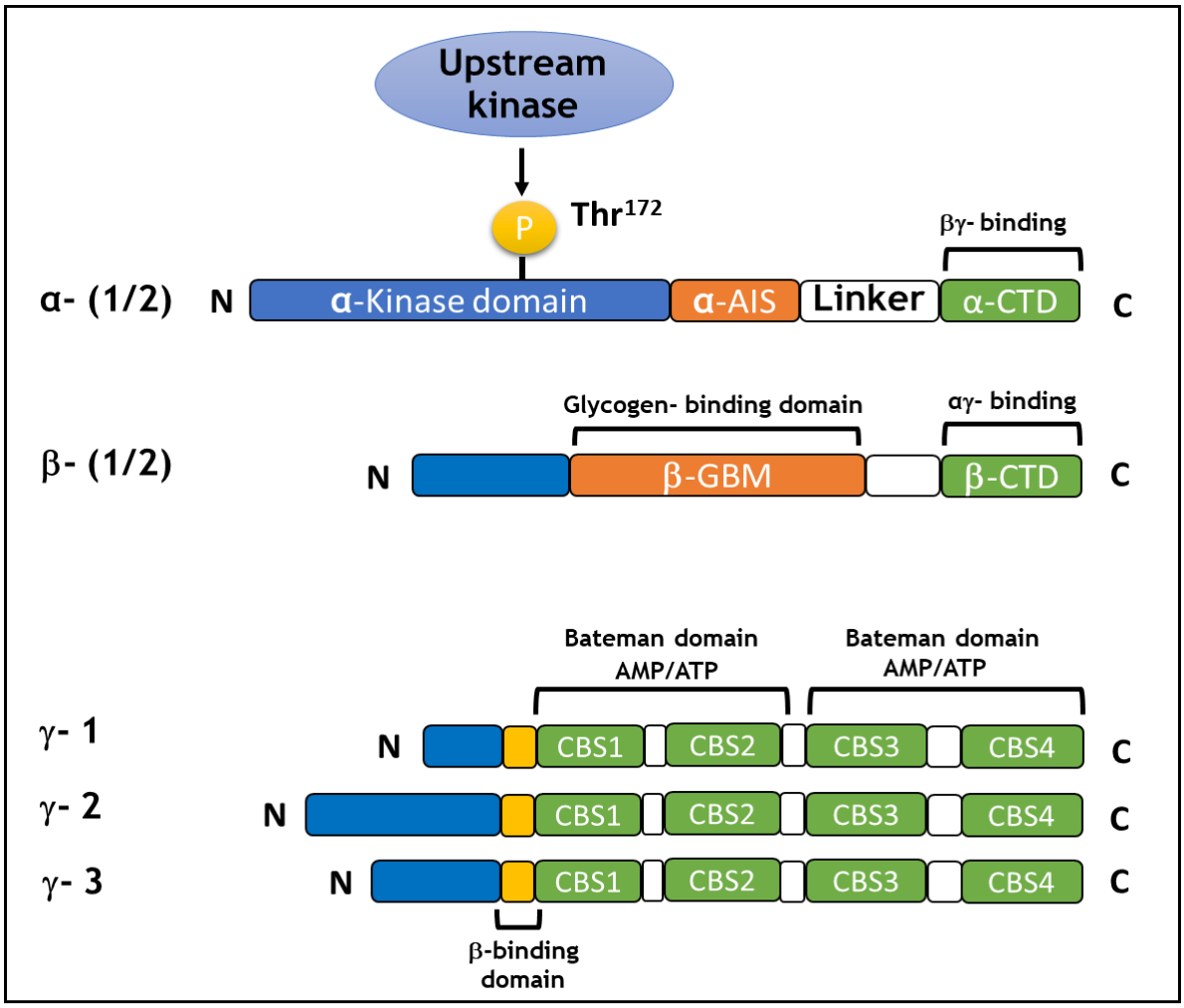

Figure 1-6: Domain structure of AMPK subunit isoforms

AMPK exists as a trimeric complex consisting of a catalytic subunit (α) and two regulatory subunits (β and γ). The catalytic α subunit contains a kinase domain with a conserved phosphorylation (P) site at Thr^{172} which is phosphorylated by upstream kinases and a central auto-inhibitory sequence (AIS). The β-subunit contains a glycogen-binding domain (GBD) and C-terminal domain (CTD) required for AMPK complex formation with α and γ. The γ subunits consist of four conserved cystathionine-β-synthase (CBS) motifs arranged in two tandem Bateman domains capable of co-operatively binding to AMP, ADP and ATP.

1.5.3 Regulation of AMPK

1.5.3.1 Allosteric activation of AMPK

AMPK plays an important role in sensing cellular energy changes under many physiological conditions where there is a reduction in ATP or an increase in AMP or ADP levels, such as during starvation or hypoxia. AMP or ADP binds to the CBS domains on the AMPKγ subunit, increasing its activity allosterically and increasing

the phosphorylation of AMPKα at Thr^{172} (Hawley *et al.*, 1996, Carling *et al.*, 2012, Ignoul and Eggermont, 2005, Xiao *et al.*, 2007, Xiao *et al.*, 2013).

Allosteric activation protects AMPK from dephosphorylation at Thr^{172} and this is antagonized by high ATP levels (Gowans and Hardie, 2014, Qi and Young, 2015). A previous study has revealed that ADP and AMP activate AMPK via phosphorylation of AMPK at Thr^{172} and by inhibiting dephosphorylation by Ca^{2+}/calmodulin-dependent protein kinase kinase-ß (CaMKK2) or liver kinase B1 (LKB1) (Oakhill *et al.*, 2011, Rodríguez *et al.*, 2021). In contrast, binding of ATP to the AMPKγ subunit competitively antagonises AMP- or ADP-mediated AMPK Thr^{172} phosphorylation and activation (Carling *et al.*, 2012, Hardie and Lin, 2017) (Figure 1-7).

1.5.4 AMPK activation by upstream kinases

Phosphorylation of AMPK at Thr^{172} is fundamental for kinase function and activity, as mutation of Thr^{172} to alanine results in an inactive catalytic subunit and revokes AMPK activity (Crute *et al.*, 1998, Willows *et al.*, 2017b). AMPK can be phosphorylated at Thr^{172} on the catalytic α subunit by upstream kinases LKB1 and CaMKK2 (Ovens *et al.*, 2021).

LKB1, also known as serine/threonine kinase 11 (STK11), was originally identified as a tumour suppressor gene mutated in Peutz-Jeghers Syndrome (PJS) (Hemminki *et al.*, 1998, Altamish *et al.*, 2020) and is ubiquitously expressed and not stimulated directly by AMP (Woods *et al.*, 2003, Hawley *et al.*, 2003). LKB1 is inactivated in many cancers, including the HeLa cancer cell line, in addition, AMPK phosphorylation by LKB1 at Thr^{172} results in at least a 100-fold increase in AMPK activity (Hawley *et al.*, 2003).

Even though LKB1 initially was identified as the major AMPK upstream kinase, previous studies demonstrated that significant basal Thr^{172} phosphorylation remained in LKB1-deficient cells that could be stimulated by Ca^{2+} ionophores. Therefore, another AMPK upstream kinase was proposed to exist, later identified as CaMKK2 (Hawley *et al.*, 2005).

LKB1 also phosphorylates 12 other kinases (termed AMPK-related kinases) that share a highly conserved sequence around Thr^{172} in the two catalytic subunit

isoforms of AMPK. None of the 12 AMPK-related kinases have been found to be activated by CaMKK2 in intact cells or cell-free assays (Fogarty *et al.*, 2010, Steinberg and Carling, 2019).

1.5.5 Downstream targets of AMPK

Upon AMPK activation, AMPK directly activates several downstream targets that switch off many anabolic processes that require ATP such as fatty acid synthesis, protein synthesis, glycogen synthesis, cholesterol, triglyceride and gluconeogenesis to reverse the energy imbalance (Hardie, 2011, Salt and Hardie, 2017). To date, at least 100 downstream targets of AMPK have been identified, the first of which was acetyl-CoA carboxylase (ACC) which catalyses the formation of malonyl CoA from acetyl CoA, and is a key enzyme in lipid synthesis (Hardie, 2022). AMPK also phosphorylates 3-hydroxy-3-methylglutaryl-CoA reductase (HMGR), the rate-limiting step in sterol and isoprenoid synthesis during FA synthesis in a wide-variety of eukaryotic muscle and adipose tissue (Mihaylova and Shaw, 2011, Garcia *et al.*, 2020a).

In addition, AMPK activation stimulates catabolic processes that generate ATP e.g glucose uptake in muscle, fatty acid oxidation, glycolysis and autophagy. AMPK also has another role in maintaining the capacity of the cell for oxidative metabolism by enhancing the production of new mitochondria and discarding of dysfunctional ones (Hardie, 2011, Packer, 2020). AMPK also phosphorylates and activates unc-51-like autophagy-activating kinase 1 (ULK1) which initiates autophagy and negatively regulates mammalian target of rapamycin complex 1 (mTORC1), reducing protein translation and further activating autophagy since mTORC1 ordinarily suppresses autophagy (Egan *et al.*, 2011, Kim *et al.*, 2011, Mack *et al.*, 2012, Kim *et al.*, 2013). Together these processes control energy metabolism and growth, or induce changes in gene expression that result in long-term effects on metabolic function (Mihaylova and Shaw, 2011, Hardie, 2011) (Figure 1-7).

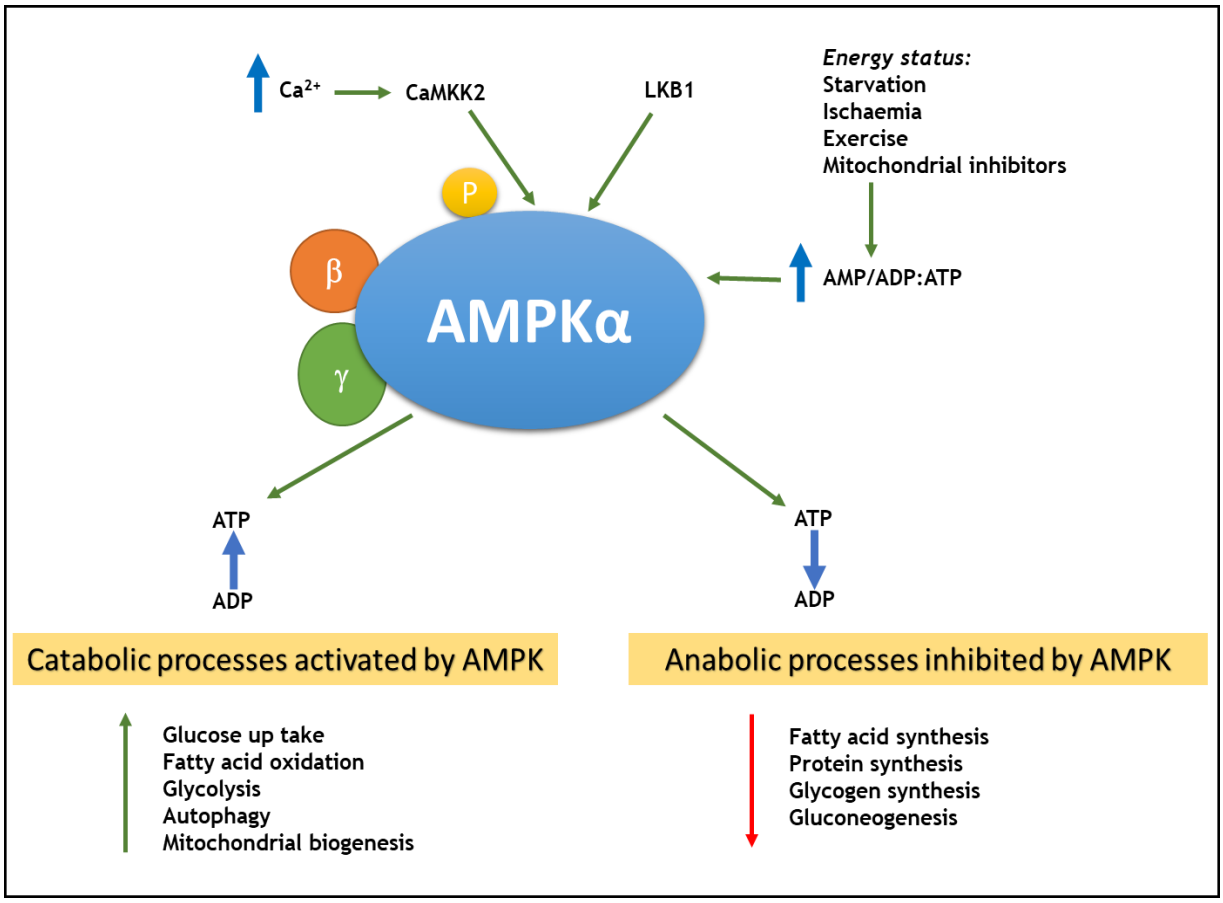

Figure 1-7: AMPK activation by upstream kinases and metabolic outcomes

AMPK is phosphorylated by different upstream kinases such as CaMKK2 and LKB1. AMPK phosphorylation can be activated in a nucleotide-dependent manner resulting from increases in the ADP:ATP or AMP:ATP ratios, due to a variety of energy stresses such as starvation, ischaemia, exercise or mitochondrial inhibition. AMPK can also be regulated in a nucleotide-independent manner, via phosphorylation of Thr^{172} by CaMKK2 in response to increases in intracellular Ca^{2+} levels. AMPK restores ATP levels by activating catabolic processes through the breakdown of nutrients such as glucose and lipid or reducing anabolic processes such as fatty acid, protein and glycogen synthesis and gluconeogenesis.

1.5.6 Pharmacological AMPK activators

It is well defined that AMPK regulates energy balance at both the cellular and whole-body levels, including increasing glucose uptake into muscle and other tissues, reducing synthesis and increasing oxidation of FFAs as well as regulation of cell growth, proliferation and vascular function (Almabrouk *et al.*, 2014, Salt and Hardie, 2017, Garcia and Shaw, 2017).

Since the discovery of AMPK, many pharmacological AMPK activators have been developed, and some other drugs used therapeutically have been found to indirectly activate AMPK including metformin, which is a hypoglycaemic drug widely used for treatment of type 2 diabetes mellitus (Zhou *et al.*, 2001). Another class of anti-hyperglycaemic drugs, the thiazolidinediones (TZDs) (Fryer *et al.*, 2002) including troglitazone, pioglitazone and rosiglitazone which primarily target peroxisome proliferator-activated receptor-γ (PPARγ) and improve insulin sensitivity in the peripheral tissues also activate AMPK (Soccio *et al.*, 2014). Both metformin and the TZDs inhibit NADH dehydrogenase (Complex I) of the mitochondrial respiratory chain, increasing the cellular AMP/ATP ratio, thereby activating AMPK (Zhou *et al.*, 2001, Hawley *et al.*, 2010). It has been shown previously that TZDs increase AMPK activity in adipose tissue, liver and skeletal muscle (LeBrasseur *et al.*, 2006). However, whether the therapeutic effects of TZDs are AMPK-dependent has not been determined. TZDs indirectly increase phosphorylation and activity of AMPK by stimulating adiponectin expression in adipose tissue, which activates AMPK in target tissues (Yamauchi *et al.*, 2002, Boyle *et al.*, 2008, Mohseni *et al.*, 2023).

AICAR (5'-aminoimidazole-4-carboxamide ribonucleoside) is an another commonly used AMPK activator. AICAR is an adenosine analogue, transported into cells via adenosine transporters where it is phosphorylated to the AMP mimetic ZMP (5-aminoimidazole-4-carboxamide-1-ß-D-furanosyl 5′-monophosphate) by adenosine kinase (Merrill *et al.*, 1997, Gao *et al.*, 2018), therefore activating AMPK without changing adenine nucleotide ratios (ADP/ATP or AMP/ATP ratios). ZMP also influences other metabolic enzymes such as phosphofructokinase and fructose 1,6-bisphosphatase that are allosterically regulated by AMP, therefore AICAR could have off-target effects (Rena *et al.*, 2017).

A769662 (6,7-Dihydro-4-hydroxy-3-(2′-hydroxy[1,1′-biphenyl]-4-yl) - 6-oxo-thieno [2,3-b] pyridine-5-carbonitrile, a member of the thienopyridone family, is a direct allosteric activator of AMPK. Activation involves the CBM of the AMPKß1 subunit isoform which interacts with γ subunit residues distinct from those involved in AMP binding (termed the ADaM site) and inhibits dephosphorylation of Thr^{172} by protein phosphatases (Cool *et al.*, 2006, Scott *et al.*, 2008). A769662 is selective

for complexes containing the ß1 regulatory subunit (Scott *et al.*, 2008, Hardie *et al.*, 2012, Aledavood *et al.*, 2021).

Compound 991 (C991) is an another direct allosteric AMPK activator (Willows *et al.*, 2017a), that binds at the ADaM site, the same allosteric site as A769662, yet stimulates both AMPKß1- and AMPKß2-containing complexes, with a preference toward ß1 (Xiao *et al.*, 2013). C991 increases LKB1-mediated phosphorylation of Thr^{172} and suppresses dephosphorylation of Thr^{172}. Furthermore, C991 stabilises the interaction between the kinase domain and the CBM of the ß subunit thereby activating AMPK (Gwinn, 2008, Willows *et al.*, 2017a, Kopietz *et al.*, 2018)

Aspirin (acetyl salicylate) is derived from the natural plant extract salicylate, which has been demonstrated to directly activate AMPK. Salicylate also binds to the ADaM site on the ß1 subunit and, like A769662 and C991, causes allosteric activation of AMPK via inhibition of AMPK dephosphorylation at Thr^{172} by an AMP-independent mechanism (Johanns *et al.*, 2023). *In vitro*, the capability of salsalate, which is metabolised to salicylate, to lower plasma fatty acids and increase fat utilization were lost in AMPK KO mice, suggesting that AMPK may play an important role in the beneficial effects of salsalate in humans (Hawley *et al.*, 2012) (Figure 1-8).

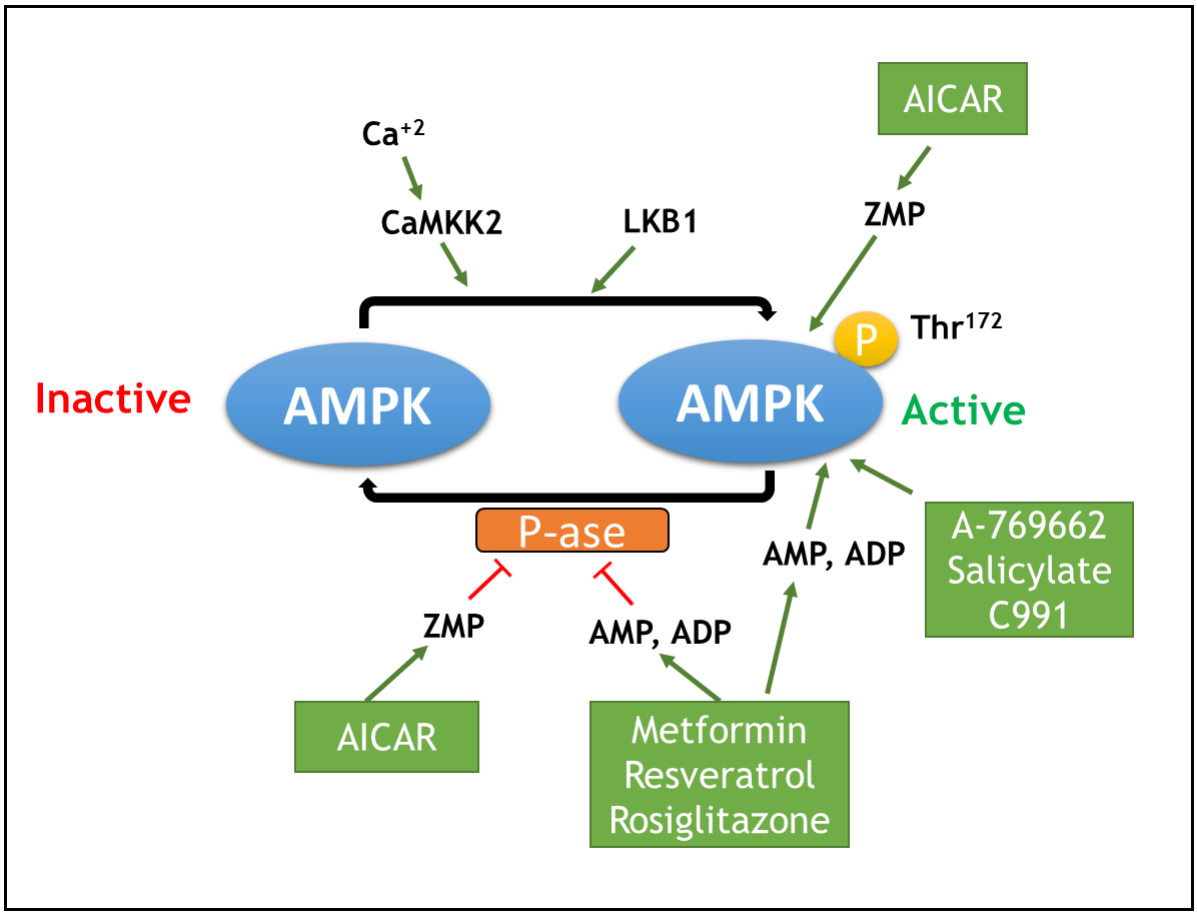

Figure 1-8 Pharmacological activation of AMPK

Increased intracellular Ca^{2+} stimulates CaMKK2 which triggers AMPK activation by phosphorylation of the α catalytic subunit at Thr^{172}. Increased ADP or AMP concentration activates AMPK and also inhibits dephosphorylation of Thr^{172} by protein phosphatases (P-ase) and makes AMPK a better substrate for phosphorylation by LKB1. AMP also promotes phosphorylation of AMPK at Thr^{172}. by the constitutive kinase, LKB1. AICAR is metabolised to the nucleotide ZMP which mimics AMP thereby activating AMPK. A769662, salicylate and compound 991 activate AMPK complexes containing the β1 subunit by binding a different allosteric site to the CBS motifs that bind AMP. A number of antidiabetic agents such as metformin and the thiazolidinedione rosiglitazone in addition to plant derived compounds such as resveratrol inhibit mitochondrial ATP synthesis, thereby increasing the AMP/ATP or ADP/ATP ratio and thus activate AMPK.

1.5.7 AMPK inhibitors

Compound C (CC or dorsomorphin) is an AMPK inhibitor that has been widely used as an experimental tool to block the effects of AMPK activators such as AICAR in cell-based, biochemical and *in vivo* assays which used to study cellular function of AMPK (Zhou *et al.*, 2001, Liu *et al.*, 2014). In addition, it inhibits AMPK via binding to the ATP-binding site of the AMPK kinase domain. However, CC is poorly

selective and also inhibits other protein kinases including phosphorylase kinase (PHK), MAPK interacting-kinase 1 (MNK1), ERK 8, sarcoma kinase (Src) and NUAK Family Kinase 1 (NUAK1) (Bain *et al.*, 2007, Banerjee *et al.*, 2014).

More recently the ULK1 inhibitor SBI-0206965 has been reported to show greater selectivity for AMPK than CC, inhibiting AMPK and ULK1 at similar concentrations but it also inhibits other kinases including focal adhesion kinase (FAK), NUAK1, mitogen-activated protein kinases 3/4 (MARK3/4) and Mut9p-LIKE KINASE 1/3 (MLK1/3) , all of which contain a methionine in their gatekeeper position (Dite *et al.*, 2018, Ahwazi *et al.*, 2021).

1.5.8 AMPK and adipose tissue function

1.5.8.1 Role of AMPK in regulation of lipid metabolism

Upon a reduction of cellular energy, AMPK restores energy balance by inhibition and activation of different metabolic pathways, including stimulation of FA oxidation and inhibition of FA synthesis. AMPK phosphorylates and inhibits ACC, responsible for conversion of acetyl CoA to malonyl CoA in the biosynthesis of FAs. As malonyl CoA is an inhibitor of FA oxidation via the allosteric inhibition of carnitine palmitoyl transferase 1 (CPT1), AMPK inhibition of ACC also leads to a reduction in malonyl-CoA levels and increases transport of fatty acyl-CoA into mitochondria and the subsequent oxidation to produce ATP (McGarry, 1995, Boudaba *et al.*, 2018, Fadó *et al.*, 2021).

1.5.8.2 Role of AMPK on adipogenesis

Adipogenesis is a complex biological process in which fibroblast-like preadipocytes differentiate into mature, lipid-laden and insulin-responsive adipocytes (Ruiz-Ojeda *et al.*, 2016). Adipogenesis is controlled by a highly regulated gene expression program; in mammalian cells PPAR-γ, cytosine-cytosine-adenosine-adenosine-thymidine (CCAAT)/enhancer-binding proteins (C/EBPs) such as C/EBPα, β and δ, and sterol regulatory element binding protein (SREBP) transcription factors are considered the key early regulators of adipogenesis (Chen and Liu, 2016). Fatty acid synthase (FAS) and perilipin are responsible for the formation of a mature adipocyte, while fatty acid binding protein 4 (FABP4) and

adiponectin are markers for the formation of mature adipocytes (Ali *et al.*, 2013, Moseti *et al.*, 2016).

Adipogenesis is achieved experimentally using a hormonal differentiation cocktail (HDC) containing a phosphodiesterase inhibitor, 3-isobutylmethylxanthine (IBMX), insulin and dexamethasone. Adding this cocktail triggers the preadipocytes to undergo growth arrest in the G1 phase followed by mitotic clonal expansion (MCE) (Tang *et al.*, 2003). At this point, transcription factors, including C/EBPδ and C/EBPß are expressed, and early adipogenic transcription factors, including C/EBP-δ, Kruppel-like factors 4 and 5 (KLF4/5) and CCAAT/enhancer-binding protein (C/EBP)-ß, are gradually expressed (Wu and Wang, 2013). In addition, C/EBP-ß and C/EBP-δ stimulate expression of adipocyte-specific transcription factors, such as C/EBP-α and PPAR-γ. These factors play an essential role in the control of adipocyte differentiation by controlling downstream gene expression, FAS, perilipin, adipocyte fatty acid binding protein 2 (aP2) and ACC, which subsequently promotes lipid droplet formation in mature adipocytes (Rosen *et al.*, 2000, Rosen and MacDougald, 2006).

Previous studies have shown that the effect of AMPK inhibitors such as CC on adipogenesis is via inhibition of hormone-induced preadipocyte differentiation and inhibition of mitotic clonal expansion (Nam *et al.*, 2008).

In addition, an early study reported that in 3T3-L1 the expression of C/EBPα, C/EBPβ, and PPARγ was reduced upon incubation with A769662, leading to a reduction of lipid droplet accumulation (Zhou *et al.*, 2009). Likewise Moreno-Navarrete and co-workers reported that activation of AMPK by metformin in human white preadipocytes caused a reduction in expression of key adipogenic factors such as PPARγ, ACC and fatty acid synthase (FASN) (Moreno-Navarrete *et al.*, 2011) via increased expression of organic cation transporter 1 (OCT1) gene (He *et al.*, 2013).

1.5.9 The role of AMPK in regulating blood vessels homeostasis

1.5.9.1 Role of AMPK in the vascular endothelium and NO production

AMPK plays an important role within the endothelium and can modulate vascular function. Both α subunit isoforms of AMPK are expressed in endothelial cells with the activity of AMPK complexes containing α1 accounting for the majority of total cellular AMPK activity (Morrow *et al.*, 2003, Fisslthaler and Fleming, 2009). However, Wang and co-workers have reported that AMPK α2 preserves endothelial cells in a normal, non-inflammatory and non-atherogenic phenotype, since it inhibits NADPH oxidase and ROS generation in a mechanism involving reduction of the expression of NOX subunits and inhibition of NADPH assembly (Wang *et al.*, 2010). Furthermore, in ECs AMPK activation by salicylate and metformin phosphorylates eNOS, thereby increasing NO production and suppressing IL-6-stimulated Janus kinase (JAK) mediated STAT signalling via an AMPK-dependent mechanism (Siragusa and Fleming, 2016, Rutherford *et al.*, 2016). In addition, it has been shown that in human endothelial cells, rosiglitazone stimulated an increase in the ADP/ATP ratio resulting in increased NO synthesis via AMPK-mediated eNOS Ser^{1177} phosphorylation (Boyle *et al.*, 2008).

1.5.9.2 Role of AMPK in vascular smooth muscle cells

Since AMPK is a highly conserved protein, a growing body of evidence has also reported that AMPK is a key regulatory kinase for vascular smooth muscle function. For example, it has been shown that AMPK regulates VSMCs contraction and relaxation by modulating the activity of ion channels and transporters, such as by increasing the activity of the large-conductance calcium-activated potassium (BKCa) channels, leading to hyperpolarization and relaxation of the VSM (Schneider *et al.*, 2015, Chen *et al.*, 2020).

In VSMCs, both catalytic (α1& α2) AMPK subunits are expressed with α1 being the predominant subunit (Rubin *et al.*, 2005). It has been reported that activation of AMPK using metformin in VSMCs reduces inflammatory signalling, including that induced by angiotensin II and also inhibits TNF-α induced inflammatory response and ROS generation (Kim and Choi, 2012).

Potassium channels in the endothelium, when opened, allow release of potassium ions, leading to activation of Na^+/K^+-ATPase and inwardly rectifying potassium (K_{IR}) channels in the underlying SMCs, causing hyperpolarization of VSMCs and vessel relaxation (Jackson, 2017). A recent study reported that activation of AMPK by either A769662 or AICAR inhibited ACh-induced relaxation in rat mesenteric arteries, a response which was inhibited by the AMPK inhibitor CC (Chen *et al.*, 2019).

Horman and co-workers reported that in aortic rings from mice, phenylephrine (PE) or KCl-induced contraction was increased in AMPK α1 KO mice suggesting that AMPK may attenuate VSMCs contraction via phosphorylating and inactivating myosin light chain kinase (MLCK) (Horman *et al.*, 2008).

A number of studies have reported that high glucose inhibits AMPK in VSMCs, likely due to Akt-mediated inhibition of AMPKα1 phosphorylation reviewed in (Salt and Hardie, 2017). In addition, AMPK plays an important role in inhibition of VSMCs proliferation (Figure 1-9), via regulating various cell signalling pathways including inhibition of protein synthesis and regulation of the cell cycle in a mechanism involving inhibition of Insulin-like growth factor-1 (IGF-1) and stimulation of insulin receptor substrate 1 phosphorylation at Ser^{794} and tuberous sclerosis 2 phosphorylation at Ser^{1345} (Ning and Clemmons, 2010). Recent data from our laboratory reported that conditioned medium from PVAT of AMPKα1 KO mice or conditioned medium from PVAT incubated with U46619 caused a significant increase in MLC phosphorylation at Ser^{19} or Thr^{18} in HAoVSMCs (Katwan *et al.*, 2019).

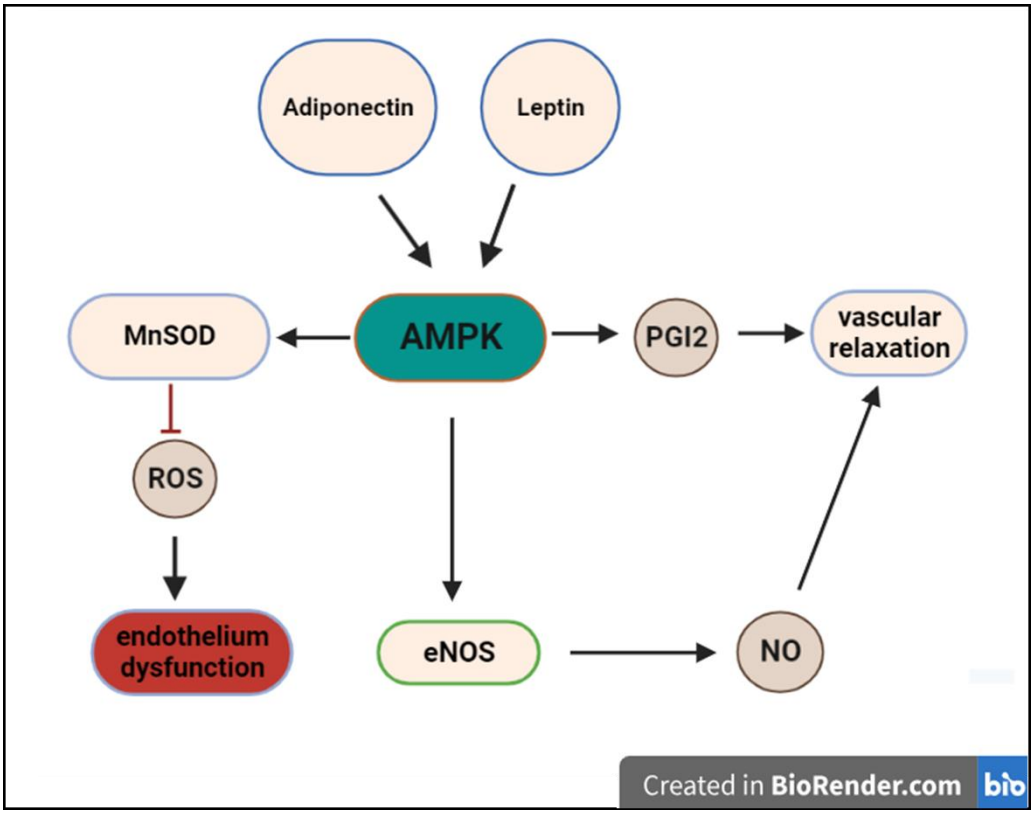

Figure 1-9 Schematic presentation of how AMPK regulate the vascular function.

Schematic illustrating the regulatory role of AMP-activated protein kinase (AMPK) in vascular function. AMPK activation enhances endothelial nitric oxide synthase (eNOS) activity, leading to increased production of nitric oxide (NO) and subsequent vasodilation. AMPK activation also promotes the activity of antioxidant enzymes, such as manganese superoxide dismutase (MnSOD), resulting in the reduction of reactive oxygen species (ROS) levels and mitigation of oxidative stress. Moreover, AMPK negatively regulates mammalian target of rapamycin (mTOR) activity, attenuating pro-inflammatory responses and vascular remodeling. Additionally, AMPK activation positively influences prostacyclin (PGI2) production, contributing to vasodilation and inhibition of platelet aggregation. The liver kinase B (LKB) serves as an upstream activator of AMPK, playing a pivotal role in regulating its activity. Overall, AMPK acts as a key modulator of vascular function, orchestrating a network of signaling pathways to maintain vascular homeostasis and health. Key: eNOS - Endothelial NOS; NO - Nitric oxide; LKB - Liver kinase B; MnSOD - Manganese superoxide dismutase; mTOR - Mammalian target of rapamycin; PGI2 - Prostacyclin; ROS - Reactive oxygen species. Created with Biorender.com.

1.5.9.3 AMPK and inflammation

Inflammation is a key driver of the development and progression of cardiovascular disease. Given that, AMPK has been reported to play a role in regulating vascular inflammation. It has been reported that AMPK activation increased phosphatase

and tensin homologue (PTEN) expression by metformin reduced proinflammatory nuclear factor-kappa B (NF-κB) activity through the inhibition of PI3K and Akt, an effect reversed upon AMPK inhibition using compound C (Isoda *et al.*, 2006, Kim and Choi, 2012). In endothelial cells and VSMCs, activation of AMPK inhibits production of pro-inflammatory cytokines such as TNF-α, interleukin-6 (IL-6) and transforming growth factor beta (TGF-ß) (Hsu *et al.*, 2014, Noor *et al.*, 2020). This effect is proposed to be mediated by AMPK-dependent inhibition of the NF-κB.

AMPK has been shown to modulate the function of immune cells where AMPK activation by metformin enhances macrophage polarization from a pro-inflammatory M1 phenotype to an anti-inflammatory M2 phenotype, leading to decreased inflammation in the vasculature, this has been proposed to be mediated via inhibition of mTORC1 (Sag *et al.*, 2008, Hasanvand, 2022). Moreover, in human endothelial cells IL-1ß-stimulated chemokine and cytokine secretion of MCP-1 and IL-6 was demonstrated to be inhibited by the hypoglycaemic drug canagliflozin in an AMPK-dependent manner (Mancini *et al.*, 2018). Furthermore, IL-1ß-stimulated C-X-C motif chemokine ligand 10 (CXCL10) secretion was inhibited by AMPK activation, an effect associated with downregulation of MKK4/JNK, and reduced phosphorylation of interleukin-1 receptor associated kinase-4 (IRAK4) in adipocytes. In the same study, JNK and STAT3 phosphorylation was increased in adipose tissue of mice lacking AMPKα1 (Mancini *et al.*, 2017).

A study demonstrated that pharmacological activation of AMPK in cultured human aortic smooth muscle cells reduced the activation of signal transducer and activator of transcription 1 (STAT1), whereas, the deletion of AMPKα1 or AMPKα2 leads to activation of STAT1 and an increase in proinflammatory mediators, the same study demonstrated that incubation of AMPKα2 KO mouse aorta with angiotensin II (AngII) exacerbated vascular inflammation relative to wild type animals, and AICAR treatment reduced AngII-induced production of proinflammatory cytokines (He *et al.*, 2015).

1.5.9.4 Role of AMPK in perivascular adipose tissue

AMPK regulates adipocyte metabolism, haemostasis and vascular function, and is expressed throughout the vessel wall as well as in PVAT. However, its role in regulating PVAT function compared with other vascular cells and tissues has not yet been fully investigated. Some studies have shown that AMPK exerts anti-inflammatory effects in several tissues, including endothelial cells (Costa *et al.*, 2018). However, AMPK can also regulate secretion of vascular modulatory mediators secreted by PVAT, suggesting that AMPK may also regulate PVAT function via regulation of adiponectin (and possibly other adipokines) production and secretion (Giri *et al.*, 2006, Almabrouk *et al.*, 2017).

An early study reported that stimulation of rat PVAT with palmitic acid (PA) reduced AMPK activity, accompanied by PVAT dysfunction, reduction of adipocytokine expression and upregulation of inflammatory markers such as TNF-α, IL-6, MCP-1 and iNOS, in addition PA caused downregulation of adiponectin, PPARγ and arginase-1 and reduced NF-κB p65 phosphorylation (Sun *et al.*, 2014, Wu *et al.*, 2020). These effects were antagonised when the PVAT was pre-treated with AICAR and metformin which both reversed PA-stimulated NF-κB p65 phosphorylation (Sun *et al.*, 2014), indicating that AMPK activation restored normal function of dysfunctional PVAT and positively regulates vascular function. In line with that study, previous data from our group reported that PVAT from AMPKα1 KO mice exhibited dysregulation of adipocytokine levels and secretion, including reduced adiponectin release (Almabrouk *et al.*, 2017), suggesting that AMPK might have a beneficial role in regulating PVAT function. In addition, the presence of PVAT enhanced vascular relaxation to cromakalim in endothelium-denuded thoracic aortic rings from wild type, but not AMPKα1 KO mice (Almabrouk *et al.*, 2017).

Other studies have indicated a key role for AMPK within PVAT in modulating vascular function, in which male offspring of female rats fed a high fat diet (HFD) during pregnancy and lactation showed dysfunctional mesenteric PVAT which was associated with a reduction in AMPK activity and reduced NO bioavailability (Zaborska *et al.*, 2016).

1.6 Objectives and aims

The involvement of eNOS-derived NO in the anticontractile effect of PVAT has not been well defined. However, it has been demonstrated that PVAT can induce vascular relaxation through release of various PVAT-derived mediators such as adiponectin. Also, it is well established that AMPK has modulatory effects on vascular smooth muscle and endothelium function.

Previous studies in our laboratory investigated the role of AMPK in PVAT and demonstrated that thoracic PVAT lacking AMPKα1 had impaired anticontractile effects, at least in part via reduction and dysregulation of adipocytokine secretion including adiponectin (Almabrouk *et al.*, 2017). The experiments described in this thesis will extend these observations, investigating the effect of AMPKα1 KO on eNOS expression and activity in PVAT and will aim to define the role of AMPK in the NO-dependent anticontractile effect of PVAT. The principal aims of this study were therefore:

1-To investigate the effects of PVAT-derived NO on vascular smooth muscle relaxation in both thoracic and abdominal aortic rings and potential mechanisms underlying this.

2-To identify the role of AMPKα1 in the regulation of PVAT-mediated NO release.

3-To study the role of caveolin-1 in eNOS activity and nitric oxide production.

Chapter 2 - Materials & Methods

2.1 Materials

2.1.1 List of materials and suppliers

Abcam, Cambridge, UK

A769662 (6,7-Dihydro-4-hydroxy-3-(2'-hydroxy[1,1'-biphenyl]-4-yl)-6-oxothieno[2,3-b] pyridine-5-carbonitrile) (#ab120335).

Anachem, Luton, UK

DNAreleasy.

AOBIOUS Inc., Gloucester, MA, USA

Compound 991 (#AOB8150).

BDH Laboratory Supplies, Poole, UK

Coomassie brilliant blue G-250.

Fisher Scientific UK Ltd, Loughborough, Leicestershire, UK

Corning tissue culture T75 flasks, 10 cm diameter dishes and 6 well plates.

GenScript

Peptides, corresponding to the full-length (amino acids 82-101) or scaffolding domain of Cav-1 as a fusion peptide to the C terminus of the Antennapedia internalization sequence (RQIKIWFQNRRMKWKKDGIWKASFAAATVTKWYFYR) (CAV-AP), were synthesised by GenScript (#SC1208).

Invitrogen (GIBCO Life Technologies Ltd), Paisley, UK

Dulbecco's modified Eagles medium (DMEM, high glucose), foetal calf serum (FCS) (USA origin), foetal calf serum (FCS) (EU origin), L-glutamine, Medium 199, new-born calf serum (NCS), penicillin (100 U/ml)/streptomycin (100 µg/ml), sodium pyruvate, Trypsin-EDTA (0.05 % (v/v), SYBR™ Safe - DNA Gel Stain (#S33102).

Melford Laboratories Ltd, Chelsworth, Ipswich, Suffolk, UK

Dithiothreitol (DTT).

New England Biolabs, Hertfordshire, UK.

Gel loading dye (6x), low molecular weight DNA marker (100 bp).

Blue prestained protein standard, broad range (11-250 kDa) (#P7706).

PALL Life Sciences, Pensacola, FL, USA

Nitrocellulose transfer membrane, 0.45 μM pore size.

Premier International Foods, Cheshire, UK

Dried skimmed milk.

Severn Biotech Ltd, Kidderminster, Hereford, UK

Acrylamide: bisacrylamide (37.5:1; 30% (*w*/*v*) acrylamide).

Sigma-Aldrich Ltd, Gillingham, Dorset, UK

Bovine serum albumin (BSA), benzamidine, dexamethasone, D-mannitol, isobutylmethylxanthine (IBMX) (I5879), $MgCl_2$, Nω-nitro-L-arginine methyl ester hydrochloride (L-NAME), paraformaldehyde, phenylmethylsulphonyl fluoride (PMSF), Ponceau stain, porcine insulin, sodium deoxycholate, soyabean trypsin inhibitor (SBTI), N,N,N',N'-tetramethylethylenediamine (TEMED), Triton X-100, Tween-20, U46619, Methyl-ß-cyclodextrin (MßCD).

Tocris Bioscience, Bristol, UK

Troglitazone (#3114).

VECTOR Laboratory (2BScientific)

VECTASHIELD® Antifade Mounting Medium with DAPI #H-1200

VWR International Ltd., Lutterworth, Leicestershire, UK

Falcon tissue culture 10 cm diameter dishes.

6/12/24 well plates.

Thermo Fisher Scientific UK Ltd, Loughborough, Leicestershire, UK

High-Capacity cDNA Reverse Transcription kit (# 4368814), Reverse Transcription kit (#4368813), BCA™ Protein Assay kit (#23235), Amplex red kit (#A22188).

Cayman chemical

TBARS assay kit (#700870).

NOS activity assay kit (#781001).

QIAGEN Ltd., Manchester, UK

RNeasy mini mRNA extraction kit (#74104), DNase kit (#79254).

LI-COR BioSciences, Lincoln, NE, USA

REVERT Total protein staining (#926-11010).

Merck Chemicals Ltd, Nottingham, UK

Dorsomorphin (Compound C) (#P5499), SBI-0206965 (#SML1546).

MRC Technology (London, U.K.)

Compound 991.

Roche Diagnostic Ltd, Burgess Hill, UK

Agarose MP.

Toronto Research Chemicals Inc, Ontario, Canada

AICAR (5-aminoimidazole-4-carboxamide-1-beta-4-ribofuranoside) (#A611700).

GE Healthcare, Little Chalfont, Buckinghamshire, UK

3MM Whatman filter paper.

2.1.2 List of special equipment and suppliers

Beckman Coulter™, High Wycombe, UK

SW40 rotor and LS 6500 multi-purpose scintillation counter, Optima™ XL-80K ultracentrifuge, Allegra® X-12 centrifuge.

Bio-Rad Laboratories, Hemel Hempstead, UK

Protein gel casting and Western blotting equipment (Mini Protean III), agarose gel casting equipment (Mini-Sub/Wide Mini-Sub Cell GT gel system).

BMG Labtech, Ortenberg, Germany

FLUOstar OPTIMA Microplate Reader.

Bibby Scientific, Essex, UK

Jenway Genova spectrophotometer.

Carl Ziess Ltd, Cambridge, UK

LSM Exciter laser scanning microscope and Axiovision light microscope.

Fisher Scientific, Loughborough, UK

Polycarbonate freezing container.

GE Analytical Instruments, Colorado, USA

Sievers 280 NO Analyser.

Invitrogen (by Thermo Fisher Scietific), Life Technologies Ltd, Paisley, UK

EVOS™ M7000 Imaging System (#AMF7000).

LI-COR BioSciences, Lincoln, NE, USA

LI-COR Odyssey® Sa infrared imaging system, XDS-1B light microscope.

Techne, Bibby Scientific Ltd, Staffordshire, UK

Progeny FPR0G050 Thermocycler.

Thermo Scientific, Waltham, MA, USA

Nanodrop spectrophotometer.

WPA, Cambridge, UK

S2000 spectrophotometer.

2.1.3 List of cells and suppliers

3T3-L1 preadipocytes originally purchased from (American Type Culture Collection, Manassas, VI, USA) were kindly provided by Prof. G. W. Gould (University of Strathclyde, Glasgow, UK).

2.1.3 Animal model

Generation of α1-AMPK Knockout Mice

AMPK α1 KO mice were generated by Dr Benoit Viollet using a library containing the genomic material from the 129-strain mouse was subjected to screening using a specific 500-base pair fragment of the mouse AMPK catalytic α1-subunit made by reverse transcription-polymerase chain reaction on liver messenger RNA using the forward 5′-AGGGCCCGACACACCCTAGA-3′ and the reverse 5′-TGTGACTTCCTGGTCTTGGA-3′ primers. A genomic clone containing a 14.5-kilobase fragment was selected to create the targeting construct. This fragment contained exons that encode the N-terminal catalytic domain of the α1-AMPK subunit, specifically corresponding to amino acids 31–239. To construct the targeting vector, a 4-kilobase 5′ homologous genomic fragment was treated, modified, and inserted into the IRES-βgeo plasmid.

The targeting construct was linearized and introduced into 1×10^7 embryonic stem cells (ES cells). These ES cells were cultured on mitomycin-treated embryonic fibroblasts. Finally, the positive ES cells were injected into blastocysts obtained from C57BL/6J mice. Chimeric males resulting from this process were bred with wild type C57BL/6J females to achieve germ line transmission. Mice carrying the heterozygous gene targeting event were used to produce homozygous α1-AMPK mutant mice, thereby creating the desired knockout model. (Jørgensen *et al.*, 2004). These mice were normotensive (Almabrouk *et al.*, 2018).

Wild type (Sv129) mice (12-20 weeks old) were originally purchased from Harlan Laboratories (Oxon, UK), and AMPKα1 knockout mice (KO) were kindly supplied by Dr. Benoit Viollet (Institute Cochin, Paris, France). All mice were housed in the Central Research Facility at the University of Glasgow and maintained on 12 hours cycles of light and dark and were fed a standard chow diet. Animals were humanely euthanised by a rising concentration of CO_2. All experiments were performed in accordance with the United Kingdom Home Office Legislation under the Animals (Scientific Procedure) Act 1986 (project licenses 60/4114 and 70/8572) which were approved by the Glasgow University Animal Welfare and

Ethical Review Board) and guidelines from Directive 2010/63/EU of the European Parliament on the protection of animals used for scientific purposes.

2.1.3.1 Genotyping

In all experiments, the genotype of mice (HT, WT and KO) was confirmed prior to experimental involvement as follows:

2.1.3.2 DNA extraction

Ear notches from mice were obtained by staff from the Central Research Facility at 4 weeks of age when animals were weaned. Samples were stored at -20^{o}C until DNA was ready to be extracted using DNAreleasy. 10 µL of DNAreleasy was added to each ear notch and PCR was performed as follows: 75^{o}C for 5min, 96^{o}C for 2 min, then 90µL of nuclease free dH_2O was added to the samples. Genotyping was performed by RT-PCR using the Go Taq amplification system (Promega, Southampton, U.K.) as per the manufacturer's instructions, with reaction mixture details given in (Table 2-1).

Table 2-1: RT-PCR reaction mixture per sample for genotyping

Reaction mixture
1- 13.75 µL TAQ (GO) HOT START GREEN MASTERMIX which contains Taq DNA polymerase, dNTPs, $MgCl_2$ and load dye.
2- 0.55 µL FORWARD primer from either wild type or knockout sequence
3- 0.55 µL REVERSE primer from either wild type or knockout sequence
4- 0.2 µL Extracted DNA sample

2.1.3.3 Polymerase Chain Reaction for AMPKα1 Wild type (WT) and AMPKα1 Knockout (KO)

Details of the primers and their sequences, annealing temperatures and electrophoresis bands are shown in (Table 2-2). All PCR cycles were subject to a hot start at 95^{o}C for 5min (enzyme activation), followed by 40 cycles of 95^{o}C for

30 seconds (DNA denaturation), 58^{0}C for 40 seconds and 72^{0}C for 1 min (primer binding). Samples were further subjected to 72^{o}C for 10 min and then 4^{0}C where they were stored until used. Samples were electrophoresed on a 2% (*w*/*v*) agarose/TAE gel and visualized with SYBR Safe DNA gel stain (invitrogen # s33102) using a Bio-Rad imaging system. The wild type and knockout animals were identified by the presence or absence of a targeted sequence in comparison with a 100 bp ladder (Promega, UK) run at the same time and as shown in (Figure 2-1).

Table 2-2: List of DNA primers for genotyping

All primers were purchased from ThermoFisher.

Primer	Type	Sequence (5'-3')	Annealing temp.	Product size (bp)
Wild Type	Forward primer	AGCCGACTTTGGTAAAGGATG	64.0	Approx 500
	Reverse primer	CCCACTTTCCATTTTCTCCA	63.7	
Knockout	Forward primer	GGGCTGCAGGAATTCGATATCAA	69.8	Approx 500
	Reverse primer	CCTTCCTGAAATGACTTCTA	58.9	

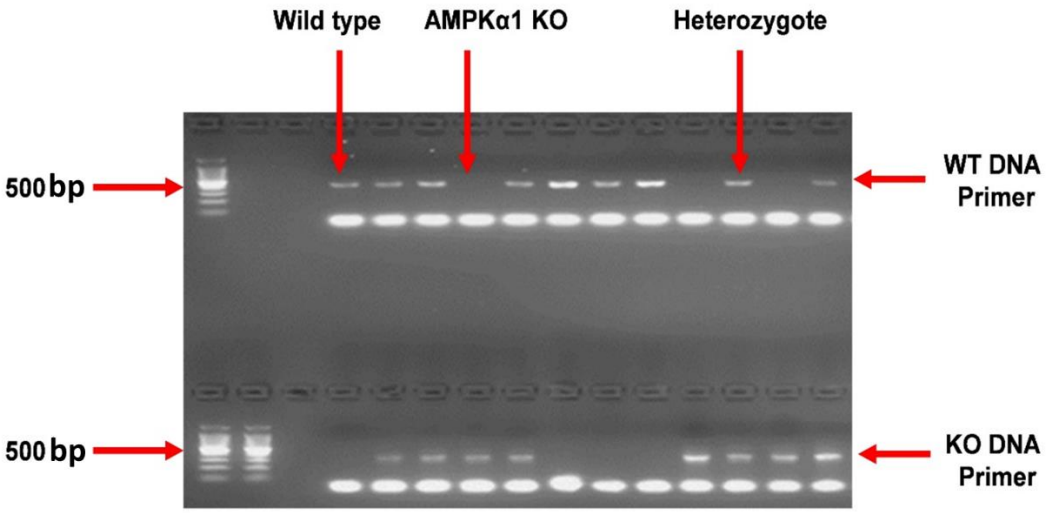

Figure 2-1: Genotyping of AMPK Kα1 KO mice

Gel electrophoresis of amplified PCR products from ear notches taken from mice. A 100 bp DNA ladder is shown on the left. The upper half of the agarose gel shows DNA products from PCR reactions using primers specific to WT alleles. The lower half of the agarose gel shows DNA products from PCR reactions using primers specific to KO alleles. Examples of wild type (WT), AMPK Kα1 knockout (KO) and heterozygotes (Het) genotypes are indicated.

2.1.4 Standard solutions

Unless otherwise stated, all buffers and reagents were made up with distilled water (dH_2O).

Bradford's reagent

35.0 mg/L Coomassie brilliant blue, 5.0% (*v*/*v*) ethanol, 5.1% (*v*/*v*) orthophosphoric acid. Bradford's reagent was filtered and stored in the dark.

Immunoprecipitation (IP) buffer

50 mM Tris-HCl (pH 7.4 at 4˚C), 150 mM NaCl, 50 mM NaF, 5 mM $Na_4P_2O_7$, 1 mM EDTA, 1 mM EGTA, 1% (*v*/*v*) Triton-X-100, 1% (*v*/*v*) glycerol, 1 mM DTT, 0.1 mM benzamidine, 1 mM PMSF, 5 µg/mL SBTI, 1 mM Na_3VO_4.

Krebs-Ringer phosphate (KRP) buffer

119 mM NaCl, 5 mM $NaHCO_3$, 4.7 mM KCl, 1.3 mM $CaCl_2$, 1.2 mM $MgSO_4$, 1.2 mM NaH_2PO_4, 5 mM glucose and 0.1% (*w*/*v*) bovine serum albumin (pH 7.4).

Krebs-Ringer HEPES (KRH) buffer

119 mM NaCl, 20 mM HEPES-NaOH (pH 7.4), 5 mM $NaHCO_3$, 10 mM glucose, 4.8 Mm KCl, 2.5 mM $CaCl_2$, 1.2 mM $MgSO_4$, 1.2 mM NaH_2PO_4.

Lysis buffer

50 mM Tris-HCl (pH 7.4 at 4ºC), 50 mM NaF, 1 mM $Na_4P_2O_7$, 1 mM EDTA, 1 mM EGTA, 1% (*v*/*v*) Triton-X-100, 250 mM mannitol, 1 mM DTT, 1 mM Na_3VO_4, 0.1 mM benzamidine, 0.1 mM PMSF, 5 µg/mL SBTI.

Phosphate-buffered saline (PBS)

85 mM NaCl, 1.7 mM KCl, 5 mM Na_2HPO_4, 0.9 mM KH_2PO_4.

Phosphate-buffered saline-Tween 20 (PBS-T)

85 mM NaCl, 1.7 mM KCl, 5 mM Na_2HPO_4, 0.9 mM KH_2PO_4, 0.1% (*v*/*v*) Tween 20.

Ponceau S stain

0.2% (*w*/*v*) Ponceau S, 1% (*v*/*v*) acetic acid.

SDS-PAGE resolving gel

8-15% (*v*/*v*) acrylamide/0.163-0.408% (*v*/*v*) bisacrylamide in 125 mM Tris-HCl (pH 8.8), 0.1% (*w*/*v*) SDS, 0.1% (*w*/*v*) ammonium persulphate, 0.05% (*v*/*v*) TEMED.

SDS-polyacrylamide gel electrophoresis (SDS-PAGE) Running buffer

190 mM glycine, 62 mM Tris base, 0.1% (*w*/*v*) SDS.

SDS-PAGE sample buffer (4X)

200 mM Tris-HCl (pH 6.8), 8% (*w*/*v*) SDS, 40% (*v*/*v*) glycerol, 0.4% (*w*/*v*) bromophenol blue. 200 mM DTT was added fresh on the day of use.

SDS-PAGE stacking gel

5% (*v*/*v*) acrylamide/0.136% (*v*/*v*) bisacrylamide in 125 mM Tris-HCl (pH 6.8), 0.1% (*w*/*v*) SDS, 0.1% (*w*/*v*) ammonium persulphate, 0.05% (*v*/*v*) TEMED.

TAE buffer

40 mM Tris-acetate (pH 8.2), 1 mM EDTA.

Transfer buffer

25 mM Tris base, 192 mM glycine, 20% (*v*/*v*) ethanol.

Tris-buffered saline (TBS)

20 mM Tris-HCl (pH 7.5), 137 mM NaCl.

Tris-buffered saline - Tween 20 (TBST)

20 mM Tris-HCl pH (7.5), 137 mM NaCl, 0.1% (*v*/*v*) Tween 20.

2.1.5 List of antibodies

2.1.5.1 Primary antibodies for Western blotting

The primary antibodies shown in (Table 2-3). Unless stated otherwise, all antibodies for immunoblotting were prepared in TBST supplemented with 5% (*w*/*v*) BSA and used on nitrocellulose membranes blocked with TBS supplemented with 5% (*w*/*v*) milk powder and incubated 4ºC overnight.

Table 2-3: Primary antibodies for Western blotting

Epitope (Clone)	Host species	Dilution	Molecular weight	Source Cat#
ACC	Rabbit	1:1000	280 kDa	Cell Signalling Technology #3676
Adiponectin	Rabbit	1:1000	27 kDa	Cell Signalling Technology #2789
AKt	mouse	1:1000	60 kDa	Cell Signalling Technology #2920
AMPK α1	Rabbit	1:1000	60 kDa	Cell Signalling Technology #2532
Caveolin -1	Mouse	1:1000	21 kDa	R&D Systems: MAB7418
eNOS	Rabbit	1:1000	140 kDa	Cell Signalling Technology #9572
eNOS	Rabbit	1:4000	140 kDa	Sigma-Aldrich, Gillingham, Dorset, UK, #N2643
GAPDH	Rabbit	1:1000	36 kDa	Thermo scientific #PA1-988
Hsp-90	Mouse	1:1000	90 kDa	BD Transduction Laboratories™ #612392
Hsp-90	Rat	1:1000	90 kDa	Abcam, Cambridge, UK, (ab52174).
iNOS	Rabbit	1:1000	140 kDa	Cell Signalling Technology #13120
nNOS	Rabbit	1:1000	140 kDa	Cell Signalling Technology #4234

Phospho-ACC (Ser^{79})	Rabbit	1:1000	280 kDa	Cell Signalling Technology #3661
Phospho-AKt (Ser^{473})	Rabbit	1:1000	60 kDa	Cell Signalling Technology #4060
Phospho-AMPK (Thr^{172})	Rabbit	1:1000	60 kDa	Cell Signalling Technology #2535
Phospho-caveolin-1 (Tyr^{14})	Rabbit	1:1000	21 kDa	Cell Signalling Technology #3251
Phospho-eNOS (Ser^{1177})	Rabbit	1:1000	140 kDa	Cell Signalling Technology #2603
Phospho-eNOS (Ser^{1177})	Mouse	1:1000	140 kDa	BD Transduction Laboratories™ #612392
Phospho-eNOS (Thr^{495})	Rabbit	1:1000	140 kDa	Cell Signalling Technology #9547
Phospho-eNOS (Ser^{635})	Rabbit	1:2000	140 kDa	Millipore, Hertfordshire, UK, #07-562
SIRT-1	Rabbit	1:1000	120 kDa	Cell Signalling Technology #2496
SOD-1	Rabbit	1:000	19 kDa	Sigma-Aldrich, Gillingham, Dorset, UK, (SAB5200083).
UCP-1	Rabbit	1:1000	30 kDa	Cell Signalling Technology #14670
ß-actin	Rabbit	1:1000	45 kDa	Cell Signalling Technology #4970

2.1.5.2 Primary antibodies for immunoprecipitation

All antibodies for immunoprecipitation experiments were added directly to cell lysates in IP buffer.

Table 2-4: Primary antibodies used for immunoprecipitation

Epitope (Clone)	Host species	Dilution	Molecular weight	Source Cat#
Caveolin-1	Mouse	1:50	21 kDa	R&D Systems: MAB7418
eNOS	Rabbit	1:50	140 kDa	Cell Signalling Technology #2603
eNOS	Rabbit	N/A (agarose-conjugated)	140 kDa	Santa Cruz Biotechnology sc-654-AC
Hsp-90	Mouse	1:50	90 kDa	BD Transduction Laboratories™ #612392

2.1.5.3 Primary antibodies for immunofluorescence

All coverslips were incubated overnight with primary antibodies in 2% (*w*/*v*) BSA and 20 mM glycine.

Table 2-5: Primary antibodies used for immunofluorescence

Epitope (Clone)	Host species	Dilution	Source (Cat #)
eNOS	Rabbit	1:100	Cell Signalling Technology #32027
Caveolin -1	Mouse	1:100	R&D Systems: MAB5736

2.1.5.4 Secondary detection agents for immunofluorescence

All secondary antibodies (Invitrogen) prepared in IF buffer (1:100) was added and incubated for 1 h in the dark.

Table 2-6: Secondary antibodies for immunofluorescence

Conjugate	Epitope	Host species	Dilution	Source (Cat #)
Alexa Flour® 488 (green)	Rabbit IgG	Donkey	1:100	Invitrogen life Technologies Ltd, Paisley, UK #A32790TR
Alexa Flour® 594 (red)	Mouse IgG	Donkey	1:100	Invitrogen life Technologies Ltd, Paisley, UK #A32744

2.1.5.5 Secondary antibodies for Western blotting

All blots were incubated with secondary antibodies for 1 h at room temperature.

Table 2-7: Secondary antibodies used for immunoblotting

Conjugate	Epitope (Clone)	Host species	Dilution	Reference/design
IRDye® 680CW	Mouse IgG	Donkey	1:5000	LI-COR Biosciences, Lincoln, NE, USA (#925-68072).
IRDye® 680CW	Rabbit IgG	Donkey	1:5000	LI-COR Biosciences, Lincoln, NE, USA (#926-68073).
IRDye® 800CW	Mouse IgG	Donkey	1:5000	LI-COR Biosciences, Lincoln, NE, USA (#926-32210).
IRDye® 800CW	Rabbit IgG	Donkey	1:5000	LI-COR Biosciences, Lincoln, NE, USA (#926-32213).

2.1.6 List of Taqman probes and real-time qPCR reagents

Taqman probes were obtained from ThermoFisher Scientific.

Table 2-8: Forward primer, Reverse primer and Taqman probes

Gene (mRNA)	**TAQMAN probes (Catalogue number)**
Caveolin -1	(Mm 00483057_m1) cat #4453320 Mouse

2.2 Methods

2.2.1 Analysis of NO synthesis by PVAT and other adipose tissue depots

Adipose tissue from WT and KO mice was collected, weighed, and incubated for 30 min in 1 mL oxygenated physiological buffer solution (1.2 mM $MgSO_4$, 25 mM $NaHCO_3$, 1.03 mM KH_2PO_4, 118 mM NaCl, 11 mM glucose, 2.5 mM $CaCl_2$, pH 7.4 and 4.7 mM KCl) at 37ºC, in the myograph chamber. From this, 100 µL of conditioned media was collected and 400 µL methanol was added and the sample centrifuged (21,910 x g, 4˚C, 20 min). The supernatant was collected and assayed for NO + NO_2^- content using a Sievers 280 NO Analyser. The NO analyser calculates the amount of NO produced by the PVAT from the amount of NO_2^- present in the conditioned medium. To set up the NO analyser for NO_2^- reduction, a reducing agent (composed of 5 mL glacial acetic acid and 50 mg NaI dissolved in 1.5 mL of dH_2O) was added to the purge vessel and flushed with N_2 to purge any NO_2^- from the vessel. After 30 min of purging, the purge vessel was sealed with a septum and the reducing agent was refluxed under N_2 gas. Prior to each experiment, a NO_2^- standard curve was constructed: from a standard solution of 100 mM $NaNO_2$, serial dilutions of 50 µM, 10 µM, 1 µM, 100 nM and 500 nM were prepared and injected into the purge vessel using a micro syringe. Under the NO_2^- reducing conditions used, NO_2^- present in the standards was reduced to NO. The NO analyser calculates the amount of NO in the conditioned media supernatant as shown in the following equation.

$$I^- + NO_2^- + 2H^+ \rightarrow NO + \tfrac{1}{2}I_2 + H_2O$$

The NO produced was then detected by the NO analyser and reacted with O_2 to produce O_3, which was detected by chemiluminescence. The chemiluminescence signal was converted to an electrical potential and displayed as mV by the NO analyser. The amount of NO produced by duplicates of each NO_2^- standard was recorded by the analyser and used to produce a calibration curve. After generating the standard curve, conditioned medium from PVAT was injected into the purge vessel using a micro syringe. Samples were injected at 2 min intervals to allow the output curve to return to baseline.

2.2.2 Functional studies (wire myography)

2.2.2.1 Vessel preparation

WT and KO mice were euthanised by a rising concentration of CO_2. Thoracic and abdominal aortae were dissected and kept in a cold oxygenated physiological buffer solution (118 mM NaCl, 4.7 mM KCl, 1.2 mM $MgSO_4$, 25 mM $NaHCO_3$, 1.03 mM KH_2PO_4, 11 mM glucose and 2.5 mM $CaCl_2$, pH 7.4). Aortic rings (approximately 1-2 mm long) with intact PVAT were prepared from each artery. The intimal layer (endothelium) of the artery was denuded by gently rubbing the vessel with the back of a pair of forceps and its absence was confirmed by lack of vasodilation (<10%) in response to 10^{-5} M acetylcholine. The vessels were mounted in a four-channel small vessel wire myograph (Danish Myo Technology, Aarhus, Denmark) as shown in (Figure 2-2), with one of the wires connected to a force transducer and the other to an adjustable arm. Vessels were incubated at 37ºC in Krebs-Henseleit buffer and gassed continuously with 95% O_2, 5% CO_2. The artery segments were equilibrated for at least 30 min at resting tension. A predetermined optimum tension was then applied by increasing tension every 5 min up to 9.8 mN for a further 30 minutes. Chart™ 5 Pro software (ADInstruments, Chalgrove, U.K.) was used to record and measure vessel responses to different reagents.

In order to make sure that a comparable amount of PVAT were present across experiments a standardised dissection technique was followed for all vessels to minimize variations in the amount of PVAT removed. This included removing the surrounding connective tissue and fat while preserving a similar thickness of PVAT around the vessel to ensure the PVAT is comparable across the samples, In addition, visual inspection of the dissected vessels can provide a rough estimation of the relative amount of PVAT present. Careful examination was helpful to identify and exclude vessels with excessively low or high amounts of PVAT compared to others.

2.2.2.2 Cumulative Dose-response curve

In all experiments the rings were pre-sensitised before other pharmacological agents were added. The vessels were first challenged twice by adding 5 ml of 62.5

mM high potassium physiological salt solution (KPSS, 1.2 mM $MgSO_4$, 62.5 mM KCl, 24.9 mM $NaHCO_3$, 1.2 mM KH_2PO_4, 2.5 mM $CaCl_2$ and 11.1 mM glucose). All vessels were then constricted with the thromboxane mimetic U46619 (9,11-Dideoxy-11α,9α-epoxymethanoprostaglandin F2α) at a concentration of $3x10^{-8}$ M, until a steady state of contraction was reached. In some experiments, one ring (treated) was incubated with the NOS inhibitor L-NAME (200 μM) for 15 min and the other served as a control (treated with an identical volume of solvent). Cumulative dose-response curves to U46619 were then created at concentrations ranging from $1x10^{-9}$ M to $1x10^{-6}$ M at 10 min intervals. The maximal contraction (mN) induced by each concentration of U46619 was measured. In addition, the effect of the CAV-AP mutant peptide on vascular reactivity was studied in endothelium denuded rings incubated (10 μM for 6 h) with CAV-AP or antennapedia (control). The concentration of CAV-AP was optimized by performing a dose-response experiment. Various concentrations of CAV-AP were tested, ranging from lower (1-5 μM) to higher concentrations (10 μM), also the incubation time was optimised by testing incubating periods from 6h to 24h. The response to the peptide, such as activation of the target pathway or functional changes, was measured at each concentration. Based on the dose-response experiment, the concentration of 10 μM was identified as the optimal concentration that effectively induced the desired response without causing significant cytotoxicity or off-target effects.

Endothelium was denuded to remove that source of NO during the experiments. Vascular responses to KPPS and phenylephrine (PE) were examined, and vascular function was directly assessed by myography.

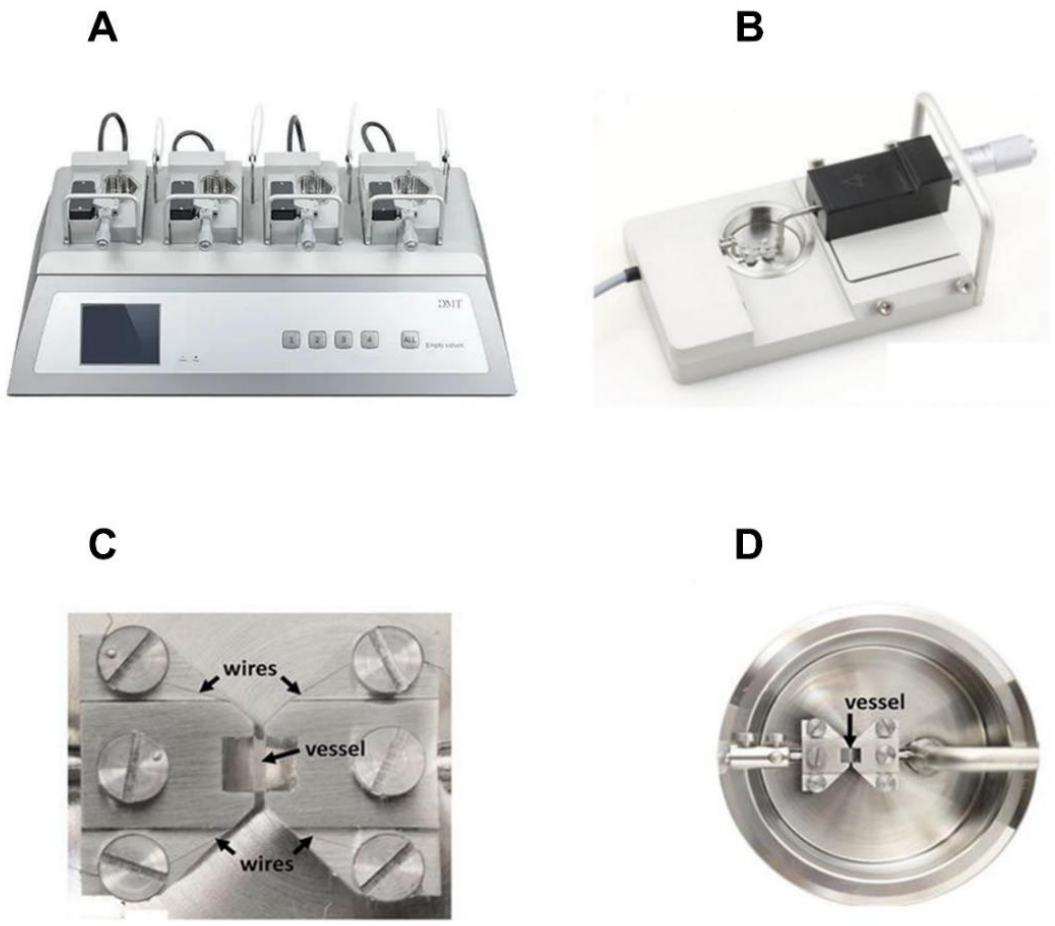

Figure 2-2: The wire myograph components

(A) DMT multi-chamber 620M Wire Myograph, (B) Myograph unit which has a force transducer (left) and a micrometre (right). (C) the jaws, screws, wires, and a mounted vessel segment, (D) Organ bath unit with the jaws and a mounted vessel segment adapted from Danish Myo Technology, (Aarhus, Denmark).

2.2.3 Preparation of tissue lysates, SDS-PAGE and Western blotting

2.2.3.1 Preparation of PVAT tissue lysates

PVAT and other adipose tissues were carefully dissected, weighed, snap-frozen in liquid nitrogen and stored at –80^{0}C. Tissues were then homogenized in 200 µL cold lysis buffer (50 mM Tris-HCl (pH 7.4 at 4^{0}C), 50 mM NaF, 1 mM $Na_4P_2O_7$, 1 mM EDTA, 1 mM EGTA, 1% (v/v) Triton-X-100, 250 mM mannitol, 1 mM DTT, 1 mM Na3VO4, 0.1 mM benzamidine, 0.1 mM PMSF, 5 µg/mL SBTI . Adipose tissue was homogenised on ice using a battery-operated pestle motor mixer (Sigma-Aldrich. UK). Lysates were transferred into ice-cold microcentrifuge tubes and centrifuged (18000 x g, 10 min, 4^{0}C). The infranatants were carefully collected and kept in fresh pre-chilled microcentrifuge tubes and stored at -20^{0}C.

2.2.3.2 Protein concentration estimation assays

2.2.3.2.1 Bicinchoninic acid method (BCA)

The bicinchoninic acid (BCA) method was also used to evaluate the protein concentration. In 96 well plates, standard dilutions of bovine serum albumin (BSA) ranging from 0.2-2 mg/mL were used to generate a standard protein curve with distilled water as a blank. A working reagent (WR) was prepared by mixing BCA Reagent A with BCA Reagent B (50:1, Reagent A: B) (Pierce™ BCA Protein Assay Kit, Thermo Scientific™, UK). Lysates (2 µL, in duplicate) were added and then made up to 10 µL with dH_2O. 200 µL of working reagent was added to all samples and reference standards. The plate was covered and incubated at 37°C for 30 min. Absorbance was measured at 595 nm using a FLUOstar OPTIMA microplate reader (BMG Labtech, Germany). The mean absorbance from each sample was generated in duplicate and the protein concentration was determined by comparison with the BSA standard curve.

2.2.3.3 SDS–polyacrylamide gel electrophoresis and immunoblotting

Equal amount of cell lysate protein, as determined by BCA, were loaded according to the molecular wight of the target protein on an 8, 10, 12 or 15 % acrylamide

gel and resolved for approximately 20 min at 80 V until the dye reached the running gel, then the voltage was increased to 140 V for 1 h until the dye reached the bottom of the gel. At this stage the current was stopped, and proteins were transferred onto a nitrocellulose membrane (Thermo scientific, Germany) for 135 min at 60 V in transfer buffer containing 10 % (*v*/*v*) ethanol. Then the membranes were blocked for 30 min in TBS supplemented with 5% (*w*/*v*) milk powder at room temperature with continuous shaking. Membranes were washed with TBST (3 x 5 min) with continuous shaking and incubated with primary antibodies overnight at 4ºC in TBST (Table 2-3) Membranes were then washed in TBST (3 x 5 min) and incubated for 1 hour at room temperature with IRDye®-labelled secondary antibodies (Table 2-7) in TBST supplemented with 5 % BSA with continuous shaking. Ponceau stain was used to confirm protein transfer. Finally, immunolabelled bands were visualised using an Odyssey Sa Infrared Imaging System (LI-COR, USA). Western blots were quantified using Empiria Studio® Software 1.1 (LI-COR, USA).

2.2.3.4 Stripping of nitrocellulose membranes

To strip and re-probe immunoblots, nitrocellulose membranes were incubated in Restore Plus Western Blot Stripping Buffer (Thermo-scientific, UK) for 15 min at room temperature. Membranes were then rinsed with TSBT (3 x 5 min) and TBS (1 x 5 min) and re-probed with indicted antibodies as previously described.

2.2.4 Cell culture procedures

2.2.4.1 Cell culture plastic ware

3T3-L1 preadipocytes were maintained in Corning T75 flasks. To prepare cells for experiments, 3T3-L1 preadipocytes were sub-cultured in Falcon 6- and 12- well plates, or 10 cm diameter dishes.

2.2.4.2 Recovery of cryopreserved cell stocks from liquid nitrogen

Cryogenic vials containing frozen cell stocks were removed from liquid nitrogen and rapidly thawed by incubating in a water bath at 37ºC. Vials were then transferred to a sterile cell culture flow hood where cells were transferred to a T75 flask containing pre-warmed medium equilibrated to 37ºC in 5 or 10% (*v*/*v*) CO_2. Cells were then incubated overnight at 37ºC in an atmosphere of 5 or 10% (*v*/*v*) CO_2. Thereafter, the medium was aspirated to remove cryoprotective agents and cell debris and replaced with fresh medium.

2.2.4.3 3T3-L1 adipocyte culture

Preadipocytes (American Type Culture Collection, Manassas, USA) (passage 2-12) were maintained in Corning T75 flasks in Dulbecco's modified Eagles medium (DMEM) supplemented with 10% (*v*/*v*) new-born calf serum (NCS) and 100 U/ml (*w*/*v*) penicillin and streptomycin. Cells were incubated at 37ºC in a humidified atmosphere of 10% (*v*/*v*) CO_2 and the media was replaced every 48 h.

2.2.4.4 Differentiation of 3T3-L1 preadipocytes

For differentiation of 3T3-L1 preadipocytes into adipocytes, preadipocytes were grown to 100% confluence in DMEM containing 10% (*v*/*v*) NCS. At 48 h post-confluence, cell medium was aspirated and replaced with differentiation medium consisting of DMEM containing 10% (*v*/*v*) FCS, 0.5 mM 3-isobutyl-1-methylxanthine (IBMX), 0.25 µM dexamethasone, 5 µM troglitazone and 1 µg/mL insulin. The medium was then filter-sterilised (0.2 µm) prior to use. The cells were incubated in this medium for further 3 days before medium was aspirated and replaced with DMEM supplemented with 10% (*v*/*v*) FCS alone. Adipocytes were used for

experimentation 8–12 days post-induction of differentiation in experiments investigating the effect of different substances on NO production.

During all procedures, cells were cultured in a humidified environment at 37°C in an atmosphere of 10% (*v*/*v*) CO2.

2.2.4.5 Passaging of 3T3-L1 cells

When 3T3-L1 cells in T75 flasks were 70-80% confluent, cell growth medium was aspirated, and the cells washed with pre-warmed sterile PBS before 3 mL of sterile trypsin-EDTA 0.05% (*v*/*v*) was added to each T75 flask. Flasks were then incubated at 37ºC in 10% (*v*/*v*) CO_2 until the cells fully detached. Trypsin was then neutralised by adding an appropriate volume of DMEM/NCS growth medium and the cell suspension was then divided as required. For experimental conditions, 3T3-L1 preadipocytes were cultured in Falcon 6-well plates, 12-well plates, or 10cm-diameter dishes.

2.2.4.6 Preparation of 3T3-L1 cell lysates

Cells grown in 6-well plates were first washed and then incubated for 2 h in serum-free DMEM at 37ºC in 10% (*v*/*v*) CO_2, followed by a 1 hr incubation at 37°C in 1 ml Krebs-Ringer Phosphate (KRP) buffer (119 mM NaCl, 5 mM $NaHCO_3$, 4.7 mM KCl, 1.3 mM $CaCl_2$, 1.2 mM $MgSO_4$, 1.2 mM NaH_2PO_4, 5 mM glucose and 0.1% (*w*/*v*) bovine serum albumin). The medium was aspirated, and cells washed once with pre-cooled PBS prior to addition of 200 µL/well of ice-cold cell lysis buffer. The cell extract was scraped off using a cell lifter and transferred into pre-cooled 1.5 mL microcentrifuge tubes. The extracts were mixed and incubated on ice for 30 min prior to centrifugation (21,910 x g, 10 min, 4ºC) in a bench top centrifuge. The supernatants were transferred to fresh, prechilled microcentrifuge tubes and stored at -20ºC.

2.2.4.7 Analysis of nitric oxide synthesis by 3T3-L1 adipocytes

3T3-L1 adipocytes were washed with and incubated for 2 h in serum-free DMEM at 37ºC and 10% (*v*/*v*) CO_2. The medium was removed and replaced with serum-free DMEM containing test substances or vehicle for the indicated times. Aliquots of the medium were collected after various incubation times, 4 volumes (1:4) of

methanol added and samples were then centrifuged (21,910 x g, 4ºC, 20 min). In addition, 3T3-L1 cells were cultured and incubated (10 µM for 6 h) with CAV-AP or antennapedia (control). Supernatant was collected and assayed for NOx content using a Sievers 280 NO Analyser.

2.2.5 Immunoprecipitation

Protein A-conjugated magnetic beads (Bio-Rad) were resuspended in PBS and 100 µL (1 mg) transferred to 1.5 mL tubes. Beads were magnetized and supernatant was discarded, beads were then washed and further magnetized 3 times with 1 mL PBS-T (PBS + 0.1% Tween 20). 1 µg of anti-eNOS antibody was added to each 1 mg of beads and incubated for 1 h at room temperature (Table 2-4). Beads were washed 3 times with 300 µL IP buffer. Cell lysate (100-200 µg) was added to the beads/antibodies complex and incubated overnight at 4ºC on a rotating mixer. Beads were magnetized and supernatants (immunodepletes) were collected. Beads were washed 3 times with 300 µL IP buffer, then eluted using 40 µL sample buffer, incubated for 10 min at 70ºC and samples were resolved by SDS-PAGE to detect target proteins.

2.2.6 ROS Production and Lipid Peroxidation detection

2.2.6.1 Measurement of hydrogen peroxide levels

H_2O_2 levels were evaluated in PVAT lysates using the Amplex red H_2O_2/peroxidase assay kit according to the manufacturer's instructions. The Amplex Red assay is a widely used method for quantifying H_2O_2 released from various sources such as mitochondria, cells, vessels, and cell-free systems. In tissue samples, the assay product (resorufin) has the potential to undergo non-specific oxidation due to its interactions with various oxidants and radicals. To address this issue and ensure accurate measurements, it is essential to include control experiments with the addition of superoxide dismutase (SOD) and catalase to correct for any fluorescent background caused by non-specific reactions (Griendling *et al.*, 2016).

Briefly, Amplex red reagent in combination with horseradish peroxidase (HRP) react in the presence of H_2O_2 producing a red fluorescent oxidation product, resorufin (Figure 2-3). PVAT lysates (50 µL) were added to 50 µL Amplex red and HRP working solution in a 96-well plate. The plate was incubated in the dark for 30 min at room temperature and absorbance at 560 nm assessed using a FLUOstar OPTIMA microplate reader. The results were analysed relative to a H_2O_2 standard curve and normalised to the protein concentration.

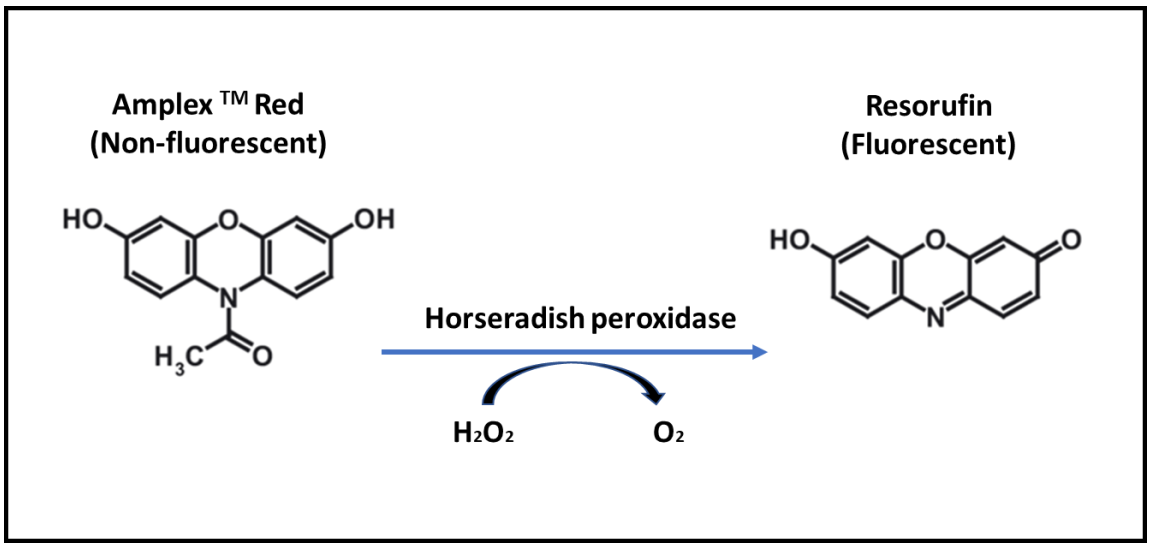

Figure 2-3: Conversion of Amplex red to Resorufin in the presence of H_2O_2 and horseradish peroxidase (HRP)

2.2.6.2 Determination of Lipid Peroxidation levels

Lipid Peroxidation was evaluated using a Thiobarbituric Acid Reactive Substances (TBARS) assay kit according to the manufacturer's instructions. PVAT lysate or standard (100 µL) were added to 100 µL TBA assay reagent and 800 µL colour reagent and the mixture was vortex mixed. Samples were boiled for 1 h, placed on ice for 10 min to stop the reaction and centrifuged (1600 x g, 4ºC, 10 min). Samples (200 µL) were added in duplicate to a 96-well plate. The reaction produces a pink colour measured at 540 nm. The reaction between thiobarbituric acid (TBA) mix and malondialdehyde (MDA) from samples forms an MDA-TBA adduct under high temperature and acidic conditions (Figure 2-4). The intensity of the colour is directly proportional to the amount of MDA in the sample. The

levels of MDA in the samples were assessed using the linear MDA standard curve and data was normalised to the protein concentration of each sample.

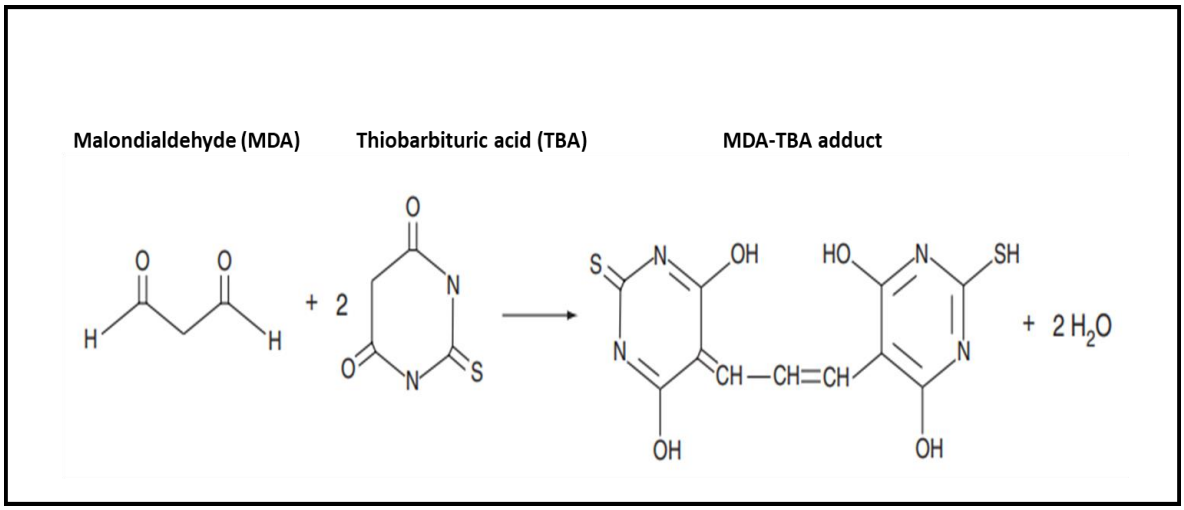

Figure 2-4: Formation of MDA–TBA 2 adduct after reaction between malondialdehyde (MDA) and thiobarbituric acid (TBA)

2.2.7 NOS activity assay

NOS activity was assessed by measuring the conversion of [^{14}C]-L-arginine to [^{14}C]-L-citrulline using a NOS activity kit (Figure 2-5). PVAT was harvested and 200 µL of ice-cold homogenization buffer (250 mM Tris-HCl (pH 7.4) buffer containing 10 mM EDTA and 10 mM EGTA) added to each sample. Tissue was homogenized using a tissue grinder on ice, homogenates centrifuged at (10,000 x g for 15 min at 4ºC) and the pellet resuspended in homogenization buffer. The supernatant was transferred to fresh microcentrifuge tubes and kept on ice until use. Protein concentration was adjusted to 1.7 mg/mL and 60 µL was mixed with 40 µL of reaction mixture (2.5 µCi/mL [^{14}C]-L-arginine, 100 µM L-arginine, 2 µM calcium, 200 nM calmodulin, 250 µM NADPH and 250 µM Tris-HCl, pH 7.4) and incubated for 30 min at 30ºC in a microcentrifuge tube. After incubation, 400 µL of stop buffer was added to each tube to terminate the reaction and 100 µL of equilibrated resin added to each reaction tube. Samples were transferred to spin columns and centrifuged at 20,000 x *g* for 30 s. Spin columns were removed and the eluate was transferred to scintillation fluid and [^{14}C]-L-citrulline production quantified by scintillation spectroscopy.

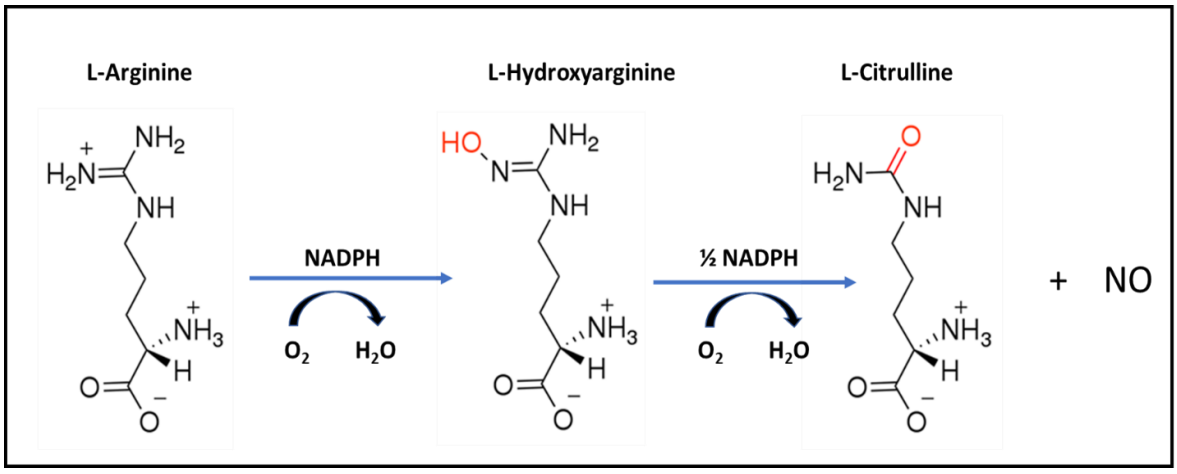

Figure 2-5: NOS catalyses a 5-electron oxidation of a guanidino nitrogen of L-arginine to generate NO and L-citrulline

L-Hydroxyarginine is formed as an intermediate that is tightly bound to the enzyme. Both steps in the reaction are dependent on calcium and calmodulin.

2.2.8 Confocal microscopy and staining

3T3-L-1 preadipocytes and adipocytes were grown on 6 well plates containing sterilised 13 mm diameter glass coverslips and incubated with either CAV-AP or MβCD for 6 h. Cells were then washed 3 times in PBS and fixed in 4% (*w*/*v*) paraformaldehyde at RT for 30 min, and then washed three times in PBS and incubated in quenching buffer (50 mM NH_4Cl in PBS) for 10 min. Coverslips were then washed three times in PBS before incubating them in permeabilization buffer (0.1% (*w*/*v*) Triton X-100 in PBS) for 20 min. Coverslips were then washed three times in PBS before blocking in immunofluorescence (IF) buffer (PBS containing 10% (*v*/*v*) donkey serum) for 30 min. Coverslips were then washed three times in PBS and cells were incubated overnight with primary antibodies (anti-eNOS and anti-Cav-1), prepared in IF buffer (1:100) (Table 2-5). Coverslips were then washed three times in IF buffer and Alexa Fluor® 488-conjugated anti-rabbit and Alexa Fluor® 594-conjugated anti-mouse IgG secondary antibodies (Invitrogen) prepared in IF buffer (1:100) was added and incubated for 1 h in the dark (Table 2-6). Coverslips were then washed 3 times in IF buffer before being mounted on microscope glass slides, using one drop of VECTASHIELD® Antifade Mounting Medium with DAPI (VECTOR Laboratories # H-1200). Slides were stored overnight

in the dark to dry. Immunolabelled samples were analysed using a Zeiss LSM 5 exciter laser scanning microscope with a Plan Apochromat X63/1.4 Oil DIC objective and LSM 510 software (Zeiss, Feldbach, Switzerland). The co-localization of eNOS with other proteins was analysed using ImageJ, BIOP/JACoP plug-in software, calculating Pearson's correlation coefficient. For each biological replicate, an average of 50 cells per condition was analysed.

2.2.9 Caveolin-1 (*Cav-1*) Gene Expression

2.2.9.1 Purification of total RNA from PVAT

Expression of *Cav-1* mRNAs in the PVAT (WT and KO) was evaluated using real-time PCR. Total RNA was obtained from PVAT samples using a RNeasy Lipid Tissue Mini Kit. Briefly, tissue was lysed using 700 µL of (QIAzol Lysis Reagent #79306) per 250 mg PVAT. Lysates were homogenised using a TissuRuptor® for 2 min. The homogenate was incubated for 5 min and transferred to a microcentrifuge tube, 200 µL of chloroform was added with shaking for 15 s and incubated for a further 3 min. The homogenate was centrifuged (12,000 x g for 15 s at 4ºC), and the upper aqueous layer transferred to a microcentrifuge tube and mixed with 350 µL 70% (*v*/*v*) ethanol. Samples were transferred to a RNeasy Mini spin column and centrifuged at 8000 x g for 15 min at 4ºC. DNA digestion was performed by adding 350 µL RW1 buffer to each column, centrifuging at 21,000 x g for 15 s and adding 80 µL DNase I solution (10 µL DNase I mixed with 70 µL of RDD buffer). Columns were incubated for 15 min and washed again with 350 µL of RW1 buffer. Then columns were washed twice with RDE buffer and mRNA eluted by adding 30 µL of RNase-free dH_2O and centrifuging columns for 2 min at 8,000 x g. mRNA content was quantified by measuring absorbance at 260 nm using a Nano-Drop. Samples were stored at -20ºC for up to two weeks and at -80˚C for long-term storage.

2.2.9.2 cDNA generation by polymerase chain reaction (PCR)

cDNA was synthesised using a High-Capacity cDNA reverse transcription kit (Applied Biosystems). Briefly, 1 µg of DNase I-treated RNA was diluted up to 10 µL with RNase-free H_2O and added to 2 µL 10X RT buffer, 0.8 µL 25X dNTP Mix (100

mM), 2 µL 10X RT random primers used, 1 µL MultiScribe™ Reverse Transcriptase, 1 µl of RNase inhibitor and 4.2 µL of RNase-free dH_2O were added to each reaction tube. Mixtures were vortex-mixed and centrifuged for 15 s at 21,000 x g. Tubes were loaded in a thermal cycler and cDNA generated with the following steps (step 1- 25ºC, 10 min; step 2- 37ºC, 120 min; step 3- 85ºC, 5 min; and step 4- 4ºC until taken for storage). Samples of the PCR product was stored at -20°C for up to two weeks and at -80°C for long-term storage.

2.2.9.3 Real time quantitative PCR (RT-qPCR)

mRNA expression of *Cav-1* in PVAT was analysed using TaqMan R probes and TaqMan R Real-Time PCR Master Mix (Thermo Fisher Scientific), in 384-Well PCR plates (Applied Biosystems™ Applied, Life Technologies). TaqMan probes (1 µL per sample) were added to 2 µL cDNA, 2 µL nuclease-free dH_2O and 5 µL TaqMan™ Universal PCR standard Master Mix (Applied Biosystems) per well. All samples were performed in triplicate. The PCR plate was sealed using qPCR transparent plastic adhesive and centrifuged (2000 x g for 40 s). Expression of *Cav-1* was analysed relative to TATA binding protein (*Tbp* 4333769F#). Reactions were run on a QuantStudio™ 12K Flex Real-Time PCR System using Standard Taqman protocol (Step 1 – 6995°C, 10 min, performed once; Step 2 - 95°C, 15 s followed by 60°C, 1 min, repeated for 40 cycles; Step 3 – 55°C, 80 cycles), and mRNA expression was analysed using Quant-Studio ™ 7 Time PCR Software. All data were normalized to levels of TATA box mRNA and relative quantification was calculated as $2\Delta^{-Ct}$. Details of the probes and primers used are listed in (Table 2-8).

2.3 Statistical analysis

GraphPad Prism software, (version 8.0) was used to perform student t-tests and one or two-way ANOVA (with Tukey's multiple comparison test), was used where appropriate. The *n* number represents the number of biological replicates. All data are presented as a relative change (mean ± standard error of the mean (SEM) from control baseline or normalized to group of reference for each experiment as indicated. In all cases, a *P* value of less than 0.05 was considered statistically significant.

Chapter 3 - The role of AMPK in regulation of nitric oxide production by perivascular adipose tissue (PVAT)

3.1 Introduction

Nitric oxide (NO) is a key physiological mediator involved in signalling transduction in the cardiovascular, genitourinary, respiratory, nervous, and gastrointestinal systems. Perturbations in NO generation have been implicated in a wide range of diseases including hypertension and atherosclerosis (Hanafy *et al.*, 2001). Endothelium-derived NO is a vasodilator that is essential for the maintenance of vascular tone and its deficiency contributes to vascular dysfunction (Chrissobolis *et al.*, 2011). Release of NO by the endothelium of blood vessels reduces vascular tone, inhibits vascular smooth muscle cell (VSMC) migration and proliferation, platelet activation and aggregation, maintaining cardiovascular homeostasis (Yang *et al.*, 2015). The enzymes responsible for the synthesis of NO from L-arginine in mammalian tissues are known as NO synthases (NOS) (Knowles and Moncada, 1994).

Adipose tissue is distributed throughout the body and classified into three main categories: white adipose tissue (WAT) brown adipose tissue (BAT) and beige adipose tissue (BeAT) (Lasar *et al.*, 2013, Frontini *et al.*, 2013). WAT stores excess calories as triglycerides, whereas BAT can oxidise lipids to generate heat by uncoupling oxidation of the mitochondrial electron transport chain, which promotes the clearance of plasma lipids and prevents storage of lipids in WAT and other organs (Cannon and Nedergaard, 2004). Excess lipid accumulation and dysfunctional WAT leads to adipocyte hypertrophy which is associated with atherosclerosis development, while activation of BAT may protect the vessel against atherosclerosis development (Berbée *et al.*, 2015). In addition to the categorization of adipose tissues as WAT/BAT, adipose tissues can be categorized according to their anatomical location. One depot, perivascular adipose tissue (PVAT) surrounds blood vessels and is composed of either white adipocytes or brown adipocytes, or a mixture of both depending on the vascular bed (Gao *et al.*, 2007). Earlier reports showed that PVAT in the thoracic aorta is composed of brown adipocytes, while PVAT in the abdominal aorta has predominantly white adipocyte phenotype (Brown *et al.*, 2014). PVAT surrounds most of the vasculature and regulates vascular homeostasis by producing a wide range of autocrine and paracrine factors, many of which are vasoactive, including: PVAT-derived relaxing

factors (PDRF) (Lynch *et al.*, 2013), prostacyclin (Chang *et al.*, 2012), gaseous molecules (NO and H_2S) (Szasz *et al.*, 2012) and angiotensin 1–7 (Lee *et al.*, 2009). Previous studies have demonstrated that PVAT attenuates vascular contraction in multiple vascular beds including coronary vessels (Aghamohammadzadeh *et al.*, 2012), rat mesenteric arteries (Verlohren *et al.*, 2004), and thoracic aorta from WT but not AMPK KO mice (Almabrouk *et al.*, 2017). The anti-contractile effect of PVAT is suggested to be due to the release of PVAT-derived relaxing factor(s) which act via multiple pathways, including voltage-gated potassium channels (K_V) (Verlohren *et al.*, 2004), ATP-activated potassium channels (K_{ATP}) (Dubrovska *et al.*, 2004) and large conductance calcium-activated potassium channels (BK_{Ca}) (Lynch *et al.*, 2013). In addition, PVAT secretes bioactive molecules such as adiponectin that maintain vascular homeostasis (Szasz *et al.*, 2012). Conversely, recent studies have demonstrated that PVAT-derived inflammatory mediators may enhance atherosclerotic plaque formation and stability and increase the progression of atherosclerosis (Quesada *et al.*, 2018).

AMPK is a serine/threonine-protein kinase that exists as heterotrimeric complexes containing a catalytic α subunit with regulatory ß and γ subunits. In mammals, the α subunit of AMPK consists of a C-terminal regulatory domain and an N-terminal catalytic kinase domain and this has significant activity when phosphorylated at a conserved threonine residue within the activation loop (Thr^{172} in human α1) (Hawley *et al.*, 1996). Several studies have demonstrated that activated endothelial AMPK increases phosphorylation and activation of endothelial NOS (eNOS) at Ser^{1177} (Chen *et al.*, 2003, Morrow *et al.*, 2003, Davis *et al.*, 2006) and Ser^{633} (Chen *et al.*, 2009) to increase NO availability and vascular relaxation. AMPK is expressed in the three layers of the blood vessel: the endothelium, smooth muscle (VSM), and PVAT (Ewart and Kennedy, 2011).

PVAT has been recently considered as a putative target for intervention in cardiovascular diseases. However, although the evidence points to a role in vascular haemostasis, there is still much more research required until the role of PVAT in physiology and pathology is completely understood. The general concept that the anti-contractile effect of PVAT is beneficial, and its pro-contractile effect is harmful is being questioned by several reports. The role of some important PVAT-derived products or systems such as reactive oxygen species (ROS), and

reactive nitrogen species (RNS) may be dependent on whether the PVAT is in a physiological or pathophysiological state and therefore, the role of mediators produced by PVAT requires more investigation (Barp *et al.*, 2021). PVAT produces ROS such as H_2O_2 and superoxide and these may have a signalling role in the vascular system, as effectors of the immune response. They may also be formed as by-products of cellular metabolism. NO and ROS can be generated by distinct enzymes or by the same enzyme through alternate reduction and oxidation processes (Tejero *et al.*, 2019a). Consequently, PVAT could be a potential therapeutic target for the prevention and treatment of cardiovascular diseases.

Even though it is well-known that AMPK can modulate vascular function, its effect on the anti-contractile effect of PVAT and NO production remain incompletely understood. Recent studies have shown that eNOS is expressed not only in endothelial cells but also in PVAT. However, how AMPK influences the expression or activity of eNOS in the PVAT has been poorly characterized.

3.2 Aims of the study

The hypothesis of the current study is that AMPK modulates NO release by PVAT to influence vascular contractility.

The aim of this chapter was to study in more detail the effects of PVAT-derived NO on vascular smooth muscle relaxation in both thoracic and abdominal aortic rings and potential mechanisms underlying this. Secondly the role of AMPKα1 in the regulation of PVAT-mediated NO release was investigated.

3.3 Methods

In this study, adipose tissue from both wild-type (WT) and AMPK knockout (KO) mice was collected and processed for various analyses.

3.3.1 Analysis of NO synthesis by PVAT and other adipose tissue depots

Adipose tissue from both wild-type (WT) and AMPK knockout (KO) mice was incubated in oxygenated physiological buffer solution at 37ºC for 30 minutes. The buffer solution incubated within a myograph chamber. After incubation, 100 µL of conditioned media was collected, and 400 µL of methanol was added. The sample was centrifuged, and the supernatant was assayed for NO + NO_2^- content using a Sievers 280 NO Analyser. The NO analyser determined the amount of NO produced by the perivascular adipose tissue (PVAT) based on the NO_2^- present in the conditioned medium. To prepare the NO analyser for NO_2^- reduction, a reducing agent consisting of 5 mL glacial acetic acid and 50 mg NaI dissolved in 1.5 mL of dH_2O was added to the purge vessel. The vessel was flushed with N2 to eliminate any NO_2^- . After 30 minutes of purging, the vessel was sealed, and the reducing agent was refluxed under N2 gas.

3.3.2 Functional studies (wire myography)

Wild-type (WT) and AMPK knockout (KO) mice were euthanized by a rising concentration of CO_2. Thoracic and abdominal aortae were dissected and placed in a cold oxygenated physiological buffer solution. Aortic rings, approximately 1-

2 mm long, including intact perivascular adipose tissue (PVAT), were prepared. The endothelium (intimal layer) was denuded, confirmed by limited vasodilation to Ach. The vessels were mounted in a four-channel small vessel wire myograph, with one wire connected to a force transducer and the other to an adjustable arm. Incubation at 37^{0}C in Krebs-Henseleit buffer, followed by equilibration for at least 30 minutes at resting tension. Optimal tension was then applied, increasing every 5 minutes up to 9.8 mN for an additional 30 minutes. Chart™ 5 Pro software recorded and measured vessel responses to various stimuli.

The rings were pre-sensitized before the introduction of other pharmacological agents. Initially, the vessels were incubated with 5 ml of 62.5 mM high potassium physiological salt solution (KPSS). Subsequently, all vessels were constricted using the thromboxane mimetic U46619 until reaching a stable contraction state. One ring (treated) was exposed to the NOS inhibitor L-NAME (200 μM) for 15 minutes, while the other served as a control. Cumulative dose-response curves to U46619 were then generated.

3.3.3 Preparation of tissue lysates, SDS-PAGE and Western blotting

Perivascular adipose tissue (PVAT) was dissected, weighed, rapidly frozen in liquid nitrogen, and stored at –80^{0}C. Upon thawing, the tissues were homogenized in 200 μL of cold lysis buffer. Homogenization was performed on ice using a battery-operated pestle motor mixer. The resulting lysates were then transferred to ice-cold microcentrifuge tubes and centrifuged (18000 x g, 10 min, 4^{0}C). The infranatants, were collected and stored in fresh pre-chilled microcentrifuge tubes at -20^{0}C for further analysis.

The protein concentration was assessed using the bicinchoninic acid (BCA) method. Standard dilutions of bovine serum albumin (BSA) were utilized to create a protein standard curve in 96-well plates. A working reagent (WR) was prepared by combining BCA Reagent A with BCA Reagent B from the Pierce™ BCA Protein Assay Kit. Lysates (2 μL, in duplicate) were added and adjusted to 10 μL with dH_2O. Subsequently, 200 μL of the working reagent was added to all samples. The plate was incubated at 37°C for 30 minutes. Absorbance was measured at 595 nm. Mean absorbance values from each sample were generated in duplicate, and

protein concentration was determined by comparing the results to the BSA standard curve.

Electrophoresis was performed at 80 V for approximately 20 minutes until the dye reached the running gel, followed by an increase in voltage to 140 V for 1 hour until the dye reached the bottom of the gel. Subsequently, proteins were transferred onto a nitrocellulose membrane. After transfer, membranes were blocked at room temperature in TBS supplemented. Following this, membranes were washed and incubated overnight at 4ºC with primary antibodies. After washing again membranes were incubated for 1 hour at room temperature with IRDye®-labelled secondary antibodies. Ponceau stain was used to confirm protein transfer. Finally, immunolabeled bands were visualized using an Odyssey Sa Infrared Imaging System.

3.3.4 Immunoprecipitation

Magnetic beads were suspended in PBS, and 100 µL (1 mg) was transferred to 1.5 mL tubes. After magnetization, the supernatant was discarded, and the beads were washed three times. Subsequently, 1 µg of anti-eNOS antibody was added to each 1 mg of beads, and the mixture was incubated for 1 hour at room temperature. Following incubation, beads were washed three times with IP buffer. Cell lysate was introduced to the beads/antibodies complex and incubated overnight at 4ºC. After magnetization, supernatants (immunodepletes) were collected. Beads washes with IP buffer. The elution step involved the addition of 40 µL sample buffer, followed by a 10-minute incubation at 70ºC. The eluted samples were then resolved by SDS-PAGE to detect the target proteins.

3.3.4.1 Measurement of hydrogen peroxide levels

PVAT lysates were combined with 50 µL of Amplex red and horseradish peroxidase (HRP) working solution in a 96-well plate. The plate was then incubated in the dark for 30 minutes at room temperature, and absorbance at 560 nm was measured using a FLUOstar OPTIMA microplate reader. The obtained results were analyzed relative to an H_2O_2 standard curve and normalized to the protein concentration.

3.3.5 NOS activity assay

Perivascular adipose tissue (PVAT) was collected, and each sample was treated with 200 µL of ice-cold homogenization buffer. Tissue homogenization was performed on ice, followed by centrifugation and the resulting pellet was resuspended in homogenization buffer. The supernatant, containing the homogenate, was transferred to fresh microcentrifuge tubes. Protein concentration was adjusted to 1.7 mg/mL, and 60 µL of this solution was mixed with 40 µL of the reaction mixture. This mixture was incubated for 30 minutes at 30^{0}C. Following incubation stop buffer was added to each tube to halt the reaction, and 100 µL of equilibrated resin was introduced. The samples were then transferred to spin columns and centrifuged. After removing the spin columns, the eluate was transferred to scintillation fluid, and the production of [14C]-L-citrulline was quantified using scintillation spectroscopy.

3.3.6 Caveolin-1 (Cav-1) Gene Expression

Purification of Total RNA from PVAT:

For the assessment of Cav-1 mRNA expression in PVAT (WT and KO), total RNA was extracted using the RNeasy Lipid Tissue Mini Kit. The PVAT tissue was lysed in QIAzol Lysis Reagent, homogenized, and subjected to chloroform extraction. After centrifugation, the aqueous layer was mixed with ethanol and processed using a RNeasy Mini spin column. DNA digestion was performed, and mRNA was eluted for subsequent quantification by measuring absorbance at 260 nm.

cDNA Generation by Polymerase Chain Reaction (PCR):

cDNA was synthesized from 1 µg of DNase I-treated RNA using the High-Capacity cDNA reverse transcription kit. The reaction mixture included RT buffer, dNTP mix, RT random primers, MultiScribe™ Reverse Transcriptase, RNase inhibitor, and RNase-free water. The cDNA was generated through a thermal cycling process.

Real-Time Quantitative PCR (RT-qPCR):

mRNA expression of Cav-1 in PVAT was analyzed using TaqMan probes and TaqMan Real-Time PCR Master Mix. TaqMan probes were added to cDNA, and the reactions were performed in triplicate in 384-Well PCR plates. The PCR plate was sealed, centrifuged, and then subjected to real-time PCR using a QuantStudio™ 12K Flex Real-Time PCR System. The mRNA expression levels were normalized to TATA binding protein (Tbp). Probes and primers used are detailed in Table 8. Samples were stored at -20°C and -80°C for short-term and long-term storage, respectively.

3.4 Results

3.4.1 PVAT enhances vascular relaxation to cromakalim in wild type, but not AMPKα1$^{-/-}$ aortic rings

A previous study in our laboratory demonstrated that PVAT enhances vascular relaxation to cromakalim in wild type (WT), but not AMPKα1$^{-/-}$ (KO) thoracic aortic rings with denuded endothelium (Almabrouk *et al.*, 2017). The data reported that PVAT augmenting the relaxation to cromakalim, a K^+ channel opener which induces vascular relaxation via hyperpolarisation of the vascular smooth muscle membrane. AMPKα1 is required for this augmentation since it was not observed in thoracic aortic rings from KO mice.

.

3.4.2 Inhibition of NO synthesis by PVAT suppresses U46619-mediated contraction in thoracic but not abdominal aortic rings from both WT and AMPKα1$^{-/-}$ mice

To determine the influence of PVAT-derived NO and AMPKα1 in the regulation of NO release by PVAT and the effect on contraction of aortic rings, dose-response curves to U46619 were constructed in thoracic and abdominal aortic rings with intact PVAT in the presence or absence of the NOS inhibitor, L-NAME. Rings were endothelium-denuded to ensure the effects of L-NAME were not mediated by inhibition of endothelial NOS. Incubation of WT thoracic aortic rings with L-NAME significantly augmented the contraction to U46619 ($LogEC_{50}$ =0.786 nM vs. 1.17 nM in control rings) without affecting the maximal contraction (E_{max} =13.78 ± 0.99 mN vs.13.35 ± 1.75 mN in control rings) (Figure 3-1 A). In WT abdominal aortic rings there was no significant effect of L-NAME on contraction to U46619 (Figure 3-1 B). A similar effect was seen in KO thoracic aortic rings where L-NAME significantly augmented the contraction to U46619 ($LogEC_{50}$ = 0.69 nM vs. 1.16 nM in control vessels) but had no effect on maximal contraction (E_{max} 16.73 ± 1.49 mN vs.17.03 ± 1.16 mN in control vessels (Figure 3-1 C). Similar to WT abdominal aortic rings, there was no effect of L-NAME on contraction to U46619 in KO abdominal aortic rings (Figure 3-1 D).

The table below (Table **3-1**) indicates that there were no significant differences in the maximal KPSS contraction between groups. This suggests that the contractile response of the vessels was similar across the different experimental groups. Since this study utilised endothelium denuded vessels, the endothelial layer lining the vessel walls was intentionally removed to isolate the effects of perivascular adipose tissue (PVAT) on vascular function.

Table 3-1: Maximal KPSS contraction difference between control and treated vessels, statistical significance was determined by t-test.

	Control	**L-NAME**	**± SEM (C)**	**± SEM (L-NAME)**	*pv*
WT thoracic	8.33 **mN**	8.00 **mN**	± 0.50	± 0.33	0.52
KO thoracic	9.56 **mN**	9.18 **mN**	± 0.85	± 0.38	0.66
WT abdominal	7.96 **mN**	6.85 **mN**	± 0.95	± 0.11	0.26
KO abdominal	6.05 **mN**	6.30 **mN**	± 0.87	± 0.24	0.78

However, it is important to recognize that achieving complete denudation of vessels is a challenging task. The endothelium is a delicate layer that may not be entirely removed in all cases, and the possibility of some vessels retaining residual endothelial function introduces a potential caveat in the study's interpretation. This caveat arises from the difficulty in definitively attributing the observed effects solely to PVAT-derived nitric oxide (NO) and not endothelial-derived NO given that since KPSS contractions are the same therefore, any residual NO form the endothelium may not influencing contraction.

To address the potential limitations associated with incomplete denudation and the modest effect of L-NAME, future studies could consider incorporating additional controls. For instance, including intact vessels with an intact endothelium as a reference group would allow for a direct comparison of responses between intact and denuded vessels.

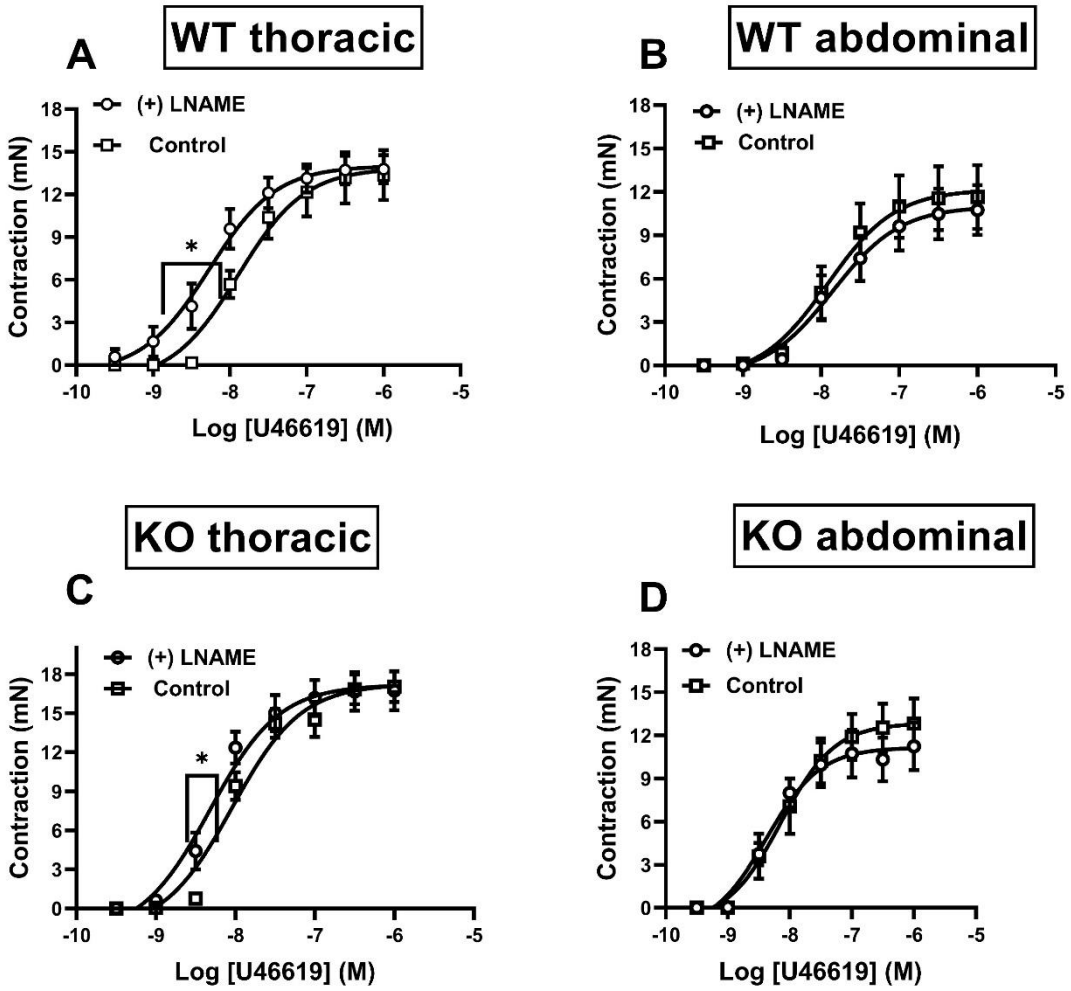

Figure 3-1: Inhibition of PVAT NO synthesis suppresses U46619-mediated contraction in thoracic but not abdominal aortic rings from both WT and AMPKα1$^{-/-}$ mice

Aortic rings from endothelium-denuded thoracic (A & C) or abdominal (B & D) aorta with intact PVAT were isolated from WT (A & B) or AMPKα1$^{-/-}$ (C & D) mice. Dose-response curves to U46619 were constructed using wire myography in the presence or absence of 200 μM L-NAME. *$p < 0.05$, $n = 6$ per group. Statistical significance was determined by two-way ANOVA analysis (with Tukey's test).

3.4.3 NO synthesis is greater in thoracic PVAT relative to abdominal PVAT and reduced in AMPKα1$^{-/-}$ mice

To determine if there were differences in NO production between thoracic and abdominal aortic PVAT which could underlie the data in (Figure 3-1), NO production by PVAT was measured in conditioned media from WT and KO PVAT using a Sievers 280 NO analyser. There was a significant increase in NO production in thoracic PVAT from WT mice compared to KO mice (300.2 nmol NOx/mg/hr (n=8) vs 139 nmol NOx/mg/hr respectively, n=7; $p<0.05$) (Figure 3-2 A). Interestingly, abdominal PVAT from WT mice produced significantly less NOx (43.2 nmol/mg/hr; n=7, p=0.0002) compared with WT thoracic PVAT (Figure 3-2 B), while there was no difference in NOx production between KO abdominal PVAT (40.18 nmol/mg/hr; *n* =7) and KO thoracic PVAT (Figure 3-2 C).

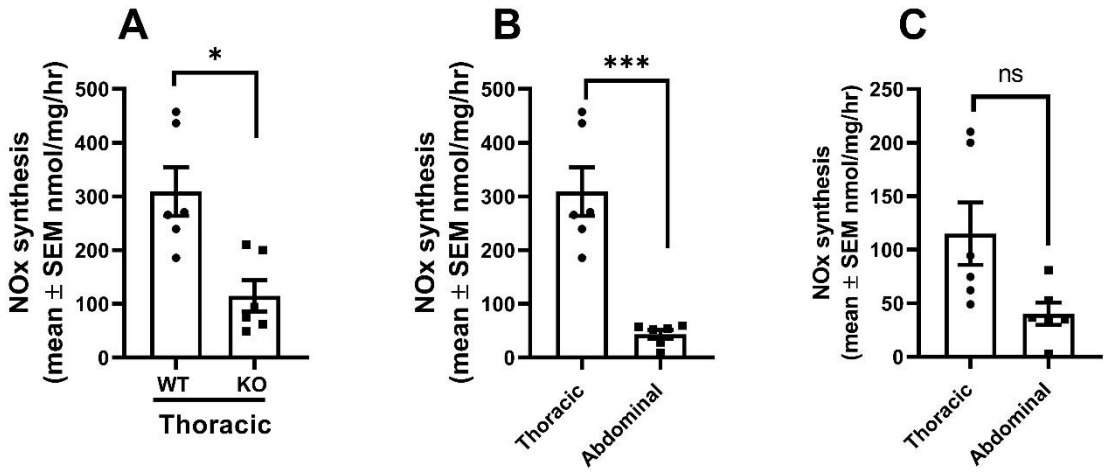

Figure 3-2: NOx production by thoracic and abdominal aortic PVAT in WT and KO mice

PVAT from thoracic or abdominal aortae were isolated from WT or KO mice. Conditioned media was generated for 30 min and assayed for NO_x content using a Sievers 280 NO analyser. Data shown represent the mean ± SEM nmol NOx synthesis/mg protein/h from 6 independent experiments (A) Comparison of WT and KO thoracic PVAT. (B) Comparison of thoracic and abdominal PVAT in WT mice. (C) Comparison of thoracic and abdominal PVAT in KO mice. *p<0.05, ***p<0.001. Statistical significance was determined by two-way ANOVA analysis (with Tukey's test).

3.4.4 eNOS, iNOS and nNOS levels in WT and AMPKα1$^{-/-}$ abdominal and thoracic aortic PVAT

Nitric oxide has been suggested to be a potential mediator of the anti-contractile action of PVAT on the underlying blood vessel, and so to assess if changes in NOS levels could account for the differences in NO production between PVAT depots or genotypes, lysates from PVAT were immunoblotted for NOS isoforms. Expression levels of eNOS were not different between thoracic and abdominal PVAT nor were they altered between genotypes (Figure 3-3 A&B). In addition, neither nNOS nor iNOS could be detected in PVAT lysates from either depot or genotype (Figure 3-3 C&D).

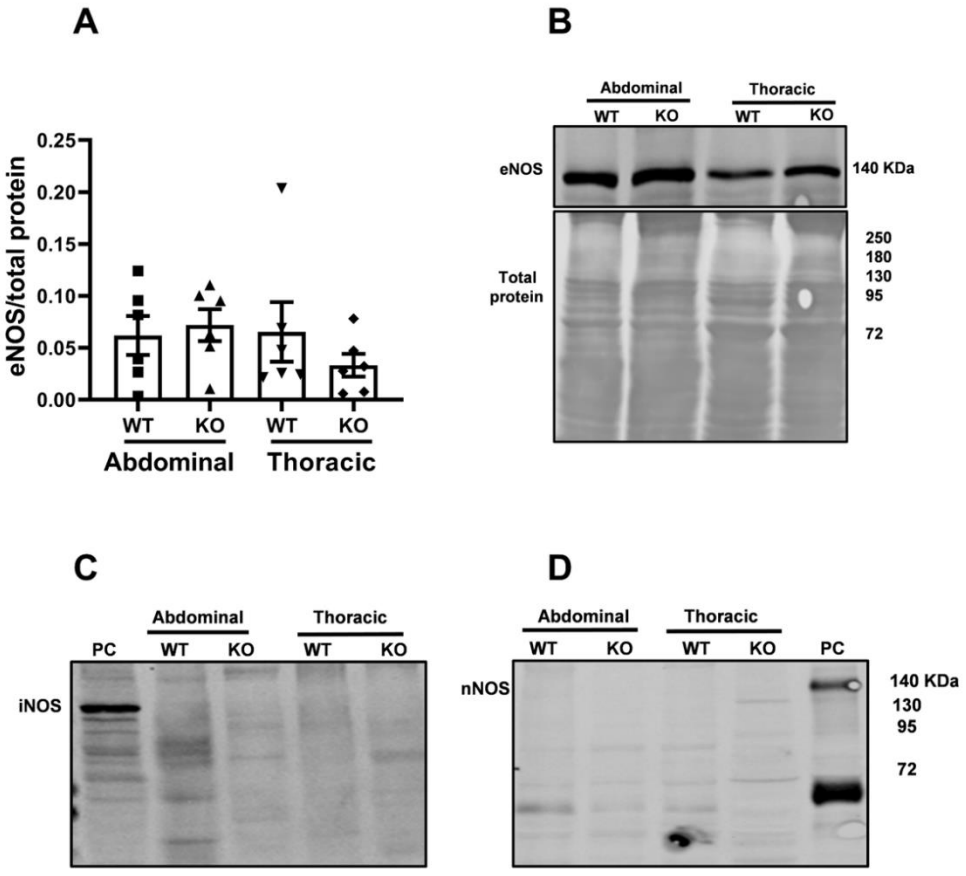

Figure 3-3: eNOS, iNOS and nNOS expression and activity in PVAT (WT and KO mice)

Thoracic and abdominal aortic PVAT tissues from WT and KO mice were lysed and 30 µg of protein was resolved by SDS-PAGE and immunoblotted with (A, B) anti-eNOS (C) anti-iNOS or (D) anti-nNOS antibodies. (A) Quantification of the level of eNOS relative to total lysate protein was assessed with REVERT total protein stain. Data shown represent the mean ± SEM of six independent experiments. (B, C, D) Representative B) anti-eNOS (C) anti-iNOS or (D) anti-nNOS immunoblots of (B) six and (C, D) four independent experiments.

3.4.5 eNOS activity in PVAT of WT and AMPKα1$^{-/-}$ mice

To assess whether the differences in NO production between WT and KO PVAT could be due to a difference in eNOS activity, this was assessed by measuring the rate of conversion of [^{14}C]-L-arginine to [^{14}C]-L-citrulline (Ladurner *et al.*, 2012) using an eNOS activity kit. WT thoracic PVAT had significantly increased eNOS activity (around 40%) compared to KO PVAT (Figure 3-4) p=0.0040. In addition, eNOS activity in WT abdominal PVAT was significantly decreased when compared to WT thoracic PVAT, p=0.0292, suggesting that changes in eNOS activity could account for the difference in NO production.

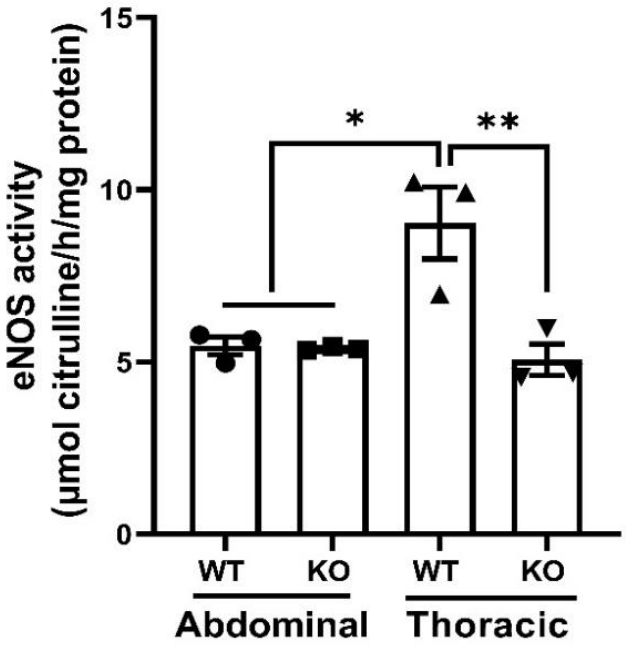

Figure 3-4: eNOS activity in PVAT of WT and KO mice

Thoracic and abdominal aortic PVAT tissue from WT and KO mice was lysed and eNOS activity was assessed by measuring [^{14}C]-L-arginine to [^{14}C]-L-citrulline conversion rate using a NOS activity assay kit. Data shown represent the mean ± SEM of three independent experiments. *p<0.05, ** p<0.01. Statistical significance was determined by two-way ANOVA analysis (with Tukey's test).

3.4.6 eNOS phosphorylation in abdominal and thoracic aortic PVAT of WT and AMPKα1$^{-/-}$ mice

To further investigate whether the reduced NO production in KO mice and in abdominal PVAT is associated with an altered level of eNOS phosphorylation at different sites, lysates from WT and KO PVAT samples were prepared and immunoblotted with phosphorylation site-specific antibodies (anti-phospho-Ser^{1177}, Ser^{615} or Thr^{495}). There were no differences in eNOS phosphorylation at Ser^{1177} relative to total eNOS between thoracic and abdominal PVAT in WT and KO mice (Figure 3-5 A). As shown in (Figure 3-5 B), despite loading 45 µg protein per lane, no immunoreactivity was observed with the other two anti-phospho-eNOS antibodies (p-eNOS Ser^{615} and p-eNOS Thr^{495}) in PVAT lysates from either depot or genotype, suggesting undetectable levels of phosphorylated eNOS at these specific sites. To validate the anti-phospho-eNOS antibodies that were used, human endothelial cell lysate (10 µg) was immunoblotted with each anti-phospho-eNOS antibody.

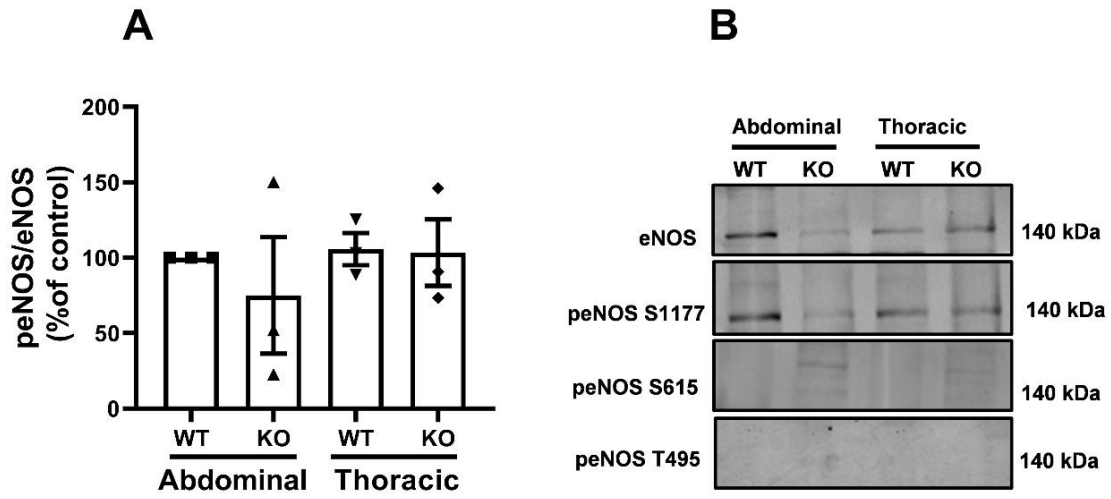

Figure 3-5: Levels of phospho-eNOS (Ser^{1177}, Ser^{615} or Thr^{495}) in thoracic and abdominal PVAT from WT and KO mice

Thoracic and abdominal aortic PVAT tissue from WT and KO mice were lysed and 45 µg protein was resolved by SDS-PAGE and immunoblotted with the anti-phospho-eNOS antibodies indicated. (A) Quantification of the level of phospho-eNOS (peNOS) relative to total eNOS is shown. Data shown represent the mean ± SEM from 3 independent experiments. (B) Representative immunoblots are shown.

3.4.7 UCP-1 levels in abdominal and thoracic aortic PVAT in WT and AMPKα1$^{-/-}$ mice

Thoracic PVAT exhibits BAT-like morphology with a smaller adipocyte size than WAT and has high expression of BAT markers including uncoupling protein-1 (UCP-1). Here the levels of the browning marker UCP-1 were investigated to identify the phenotype of the PVAT in each genotype. As shown in (Figure 3-6), there was a noticeable increase in the basal level of the UCP-1 in thoracic PVAT compared with abdominal PVAT from WT and KO mice.

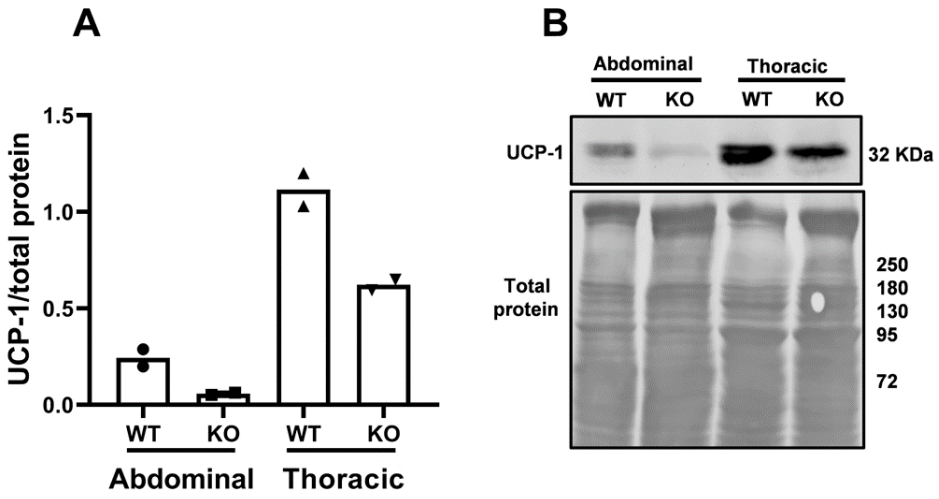

Figure 3-6: UCP-1 expression in PVAT from WT and KO mice

Thoracic and abdominal aortic PVAT tissue from WT and KO mice were lysed and 30 µg protein was resolved by SDS-PAGE and immunoblotted with anti-UCP-1 antibodies. (A) Quantification of the level of UCP-1 relative to total lysate protein, assessed with REVERT total protein stain. Data shown represent the mean ± SEM UCP-1 levels of 2 independent experiments. (B) Representative immunoblots.

3.4.8 UCP-1 expression in other fat depots of WT and AMPKα1$^{-/-}$ mice

To assess the phenotype of other fat depots, the levels of UCP-1 were assessed in mesenteric PVAT, subcutaneous (SC) and intrascapular adipose tissues (BAT) from WT and KO mice. The levels of UCP-1 in intrascapular adipose tissue in both WT and KO mice was higher compared with mesenteric PVAT and SC adipose (Figure 3-7).

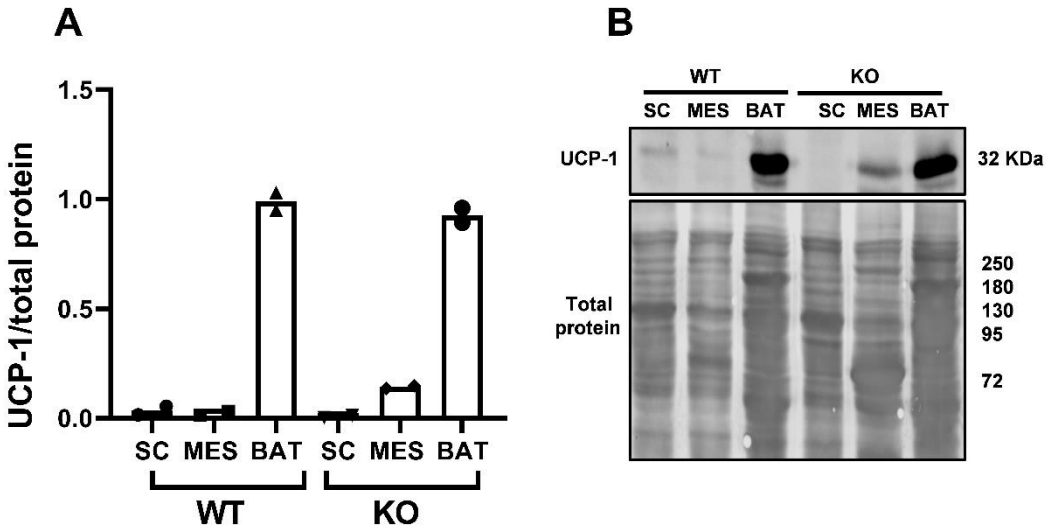

Figure 3-7: UCP-1 levels in other fat depots (WT and KO mice)

Mesenteric PVAT, SC and intrascapular fat tissues from WT and KO mice were lysed and 30 µg protein was resolved by SDS-PAGE and immunoblotted with anti-UCP-1 antibodies. (A) Quantification of the level of UCP-1 relative to total lysate protein was assessed with REVERT total protein stain. Data shown represent the mean ± SEM UCP-1 relative to WT BAT from 2 independent experiments, Representative immunoblots.

3.4.9 Nitric oxide synthesis is decreased in BAT and WAT depots from AMPKα1$^{-/-}$ mice

As shown in (Figure 3-3), thoracic aortic PVAT produces significantly more NO than abdominal PVAT in WT mice, but not in KO mice. Here the difference in NO production by other fat depots was measured in samples from WT and KO mice using a Sievers 280 NO analyser. Intrascapular BAT from WT mice produced significantly more NO compared with KO mice, p=0.0014. Surprisingly, comparing NO production between mesenteric PVAT in WT and KO mice revealed that significantly more NO was produced by WT mesenteric PVAT compared to KO mice, (Figure 3-8), p=0.0014.

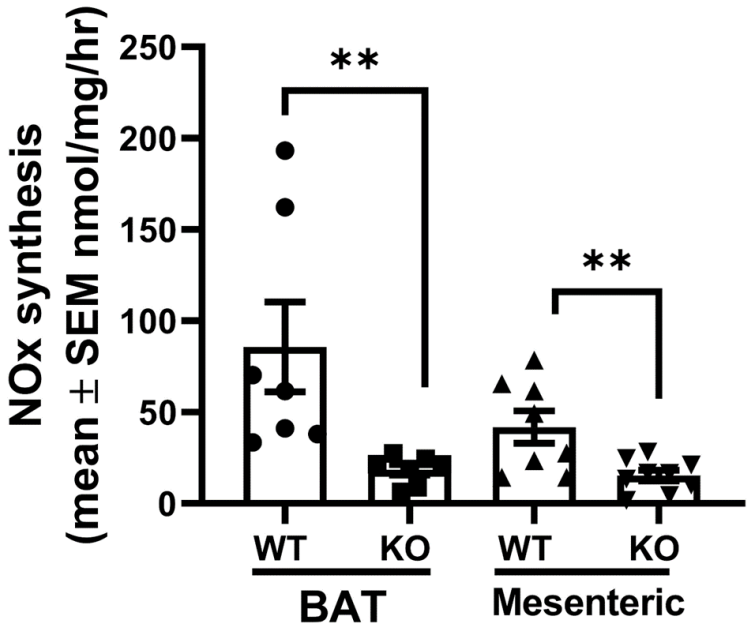

Figure 3-8: NO production is decreased in BAT and WAT depots from KO mice

Conditioned media was generated from BAT and mesenteric PVAT from WT and KO mice in a myograph chamber and assayed for NOx content using a Sievers 280 NO analyser. Data shown represent the mean ± SEM nmol NOx synthesis/mg protein/h from 7-8 independent experiments. ** $p < 0.01$. Statistical significance was determined by two-way ANOVA analysis (with Tukey's test).

3.4.10 Wild type abdominal PVAT releases less H_2O_2 compared with WT thoracic PVAT

PVAT induces an anticontractile effect via secretion of vasodilator substances that include NO and hydrogen peroxide (H_2O_2) (Gao *et al.*, 2007). Cai *et al* 2001 demonstrated that H_2O_2 positively regulates eNOS activity via protecting the Ca^{2+}/CaM binding site that is mediated by a JAK2 and CaM kinase II-dependent pathway, thereby increasing the level of NO production. Therefore, it was of interest to determine if there was a difference in H_2O_2 production between abdominal and thoracic PVAT and whether that could account for the difference in NO production between fat depots. H_2O_2 levels in thoracic and abdominal PVAT lysates from WT and KO mice were quantified using the Amplex Red Assay. In WT mice, H_2O_2 levels were elevated in thoracic PVAT relative to abdominal PVAT although there was no statistically significant difference between H_2O_2 production in thoracic and abdominal PVAT from KO mice, p=0.0090. H_2O_2 synthesis in KO mice was also unchanged compared to WT mice (Figure 3-9 A).

Nitric oxide is rapidly sequestered by superoxide to form peroxynitrite which reduces NO bioavailability. Malondialdehyde (MDA) is a natural product of lipid peroxidation which can be used as an indirect measurement of systemic oxidative stress. To evaluate if the level of lipid peroxidation was altered in $AMPK^{-/-}$ mice compared with WT mice, lipid peroxidation was assayed using a Thiobarbituric Acid Reactive Substances (TBARS) assay kit. There were no differences in TBARS levels between PVAT depots or genotypes (Figure 3-9 B), as PVAT masses were different, data were adjusted by protein concentration.

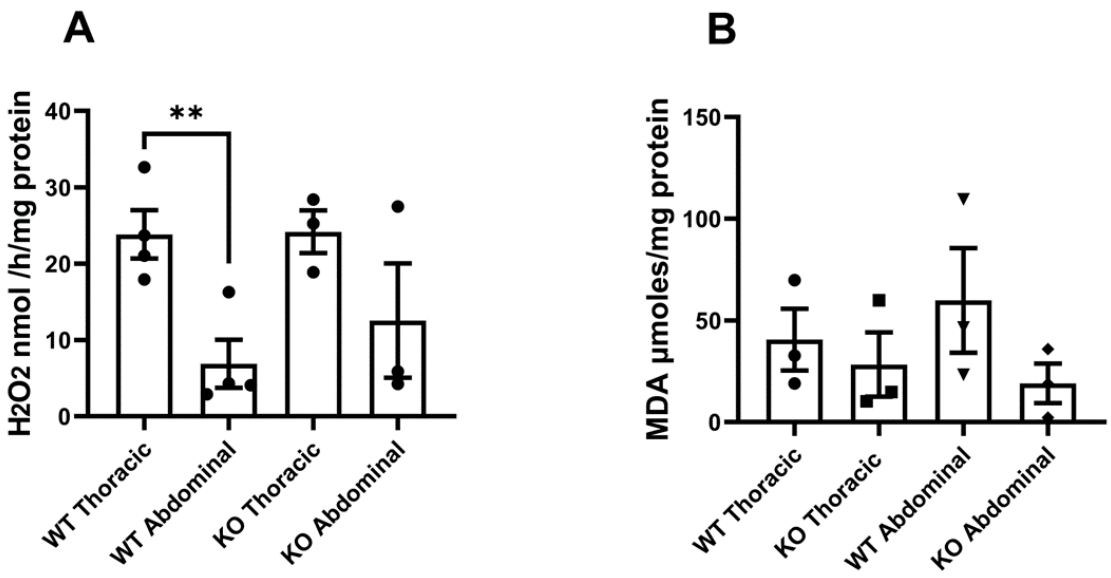

Figure 3-9: Abdominal PVAT exhibits reduced H_2O_2 levels

Lysates were prepared from thoracic and abdominal aortic PVAT of WT and KO mice. (A) H_2O_2 levels were determined using an Amplex Red kit, with data shown representing the mean ± SEM nmol H_2O_2 production/h/mg protein from four independent experiments. ** $p<0.01$. Statistical significance was determined by two-way ANOVA (with Tukey's test). (B) Lipid peroxidation levels in PVAT were determined using a TBARS kit. Data shown represent the mean ± SEM from three independent experiments.

3.4.11 Superoxide dismutase suppresses U46619-mediated contraction in thoracic aortic rings containing PVAT from both WT and AMPKα1$^{-/-}$ mice

To further examine what effect production of reactive oxygen species might have on vascular function, superoxide levels were manipulated using a cell-permeable superoxide dismutase mimetic (PEG-SOD) and the effect on vessel contractility in PVAT-containing aortic rings measured. Dose-response curves to the thromboxane-mimetic U46619 were constructed in WT and KO thoracic aortic rings preincubated in the presence or absence of 300IU/ml of PEG-SOD for 30 min. In WT vessels PEG-SOD significantly attenuated the maximal contraction to U46619 (E_{max} = 5.03 ± 1.23mN vs. 8.31 ± 2.01mN in control vessels; n=6; $p<0.05$). An attenuation of contraction was observed in response to PEG-SOD in KO thoracic aortic rings (E_{max}= 8.38 ± 2.57 mN vs. 12.98 ± 3.02 1mN in control vessels; n=6; $p<0.05$) (Figure 3-10).

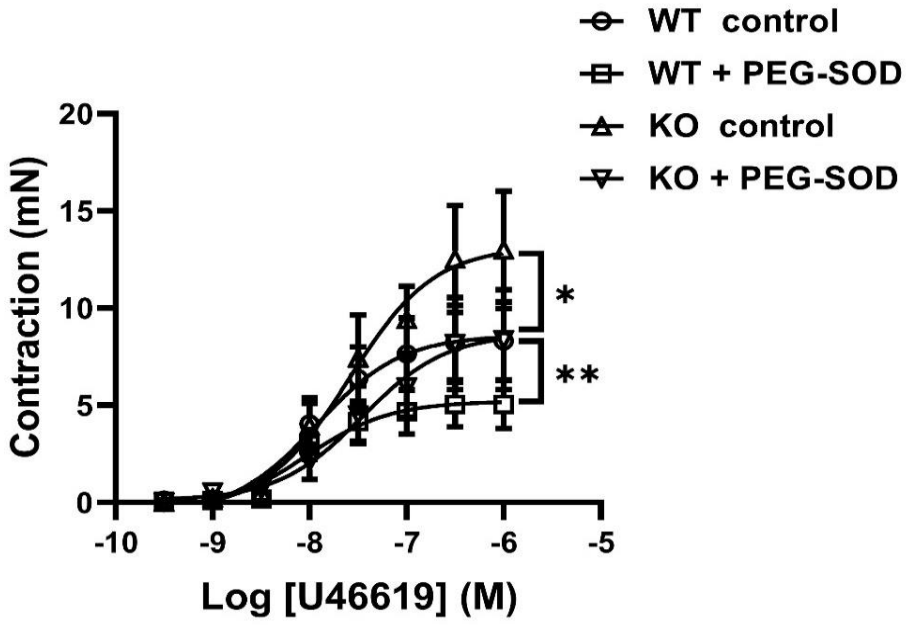

Figure 3-10: Superoxide dismutase (PEG-SOD) suppresses U46619-mediated contraction in thoracic aortic rings with PVAT from both WT and KO mice

PVAT-intact and endothelium-denuded thoracic rings from WT and AMPKα1$^{-/-}$ mice were incubated with 300 IU/ml PEG-SOD for 30 min and dose-response curves to U46619 were produced using wire myography. * $p < 0.05$, ** $p < 0.01$ vs. vehicle control for each genotype, n = 6-5 per group. Statistical significance was determined by two-way ANOVA (with Tukey's test).

3.4.12 Lower levels of caveolin-1 are associated with eNOS in thoracic PVAT relative to abdominal PVAT and are increased in thoracic PVAT from AMPKα1$^{-/-}$ mice

Caveolin-1 (Cav-1) binds to eNOS and that coupling occupies the Ca^{2+}/calmodulin binding site of eNOS, thereby reducing NO production (Razani *et al.*, 2002). The role of AMPK in the regulation of Cav-1/eNOS binding and NO production by PVAT has not been characterised. It was therefore of interest to investigate if the reduced NO production in AMKPα1 KO thoracic aortic PVAT could be due to increased levels of Cav-1 or increased association with eNOS. Interestingly, in abdominal PVAT, significantly more Cav-1 was detected in both WT and KO mice compared with thoracic PVAT (Figure 3-11 A). Furthermore, the level of Cav-1 associating with eNOS was assessed in PVAT from both depots and in both genotypes by immunoblotting of anti-eNOS immunoprecipitates. Cav-1 was detected in eNOS immunoprecipitates and levels of Cav-1/eNOS association were increased in abdominal PVAT relative to thoracic PVAT of WT mice (Figure 3-11 B), p=0.0094, also the total Cav-1 levels in abdominal PVAT lysates was increased. Intriguingly, Cav-1/eNOS association was markedly increased in thoracic PVAT from KO mice compared with WT thoracic PVAT, p=0.0079, which might account for the reduction in NO production in KO thoracic PVAT compared with WT.

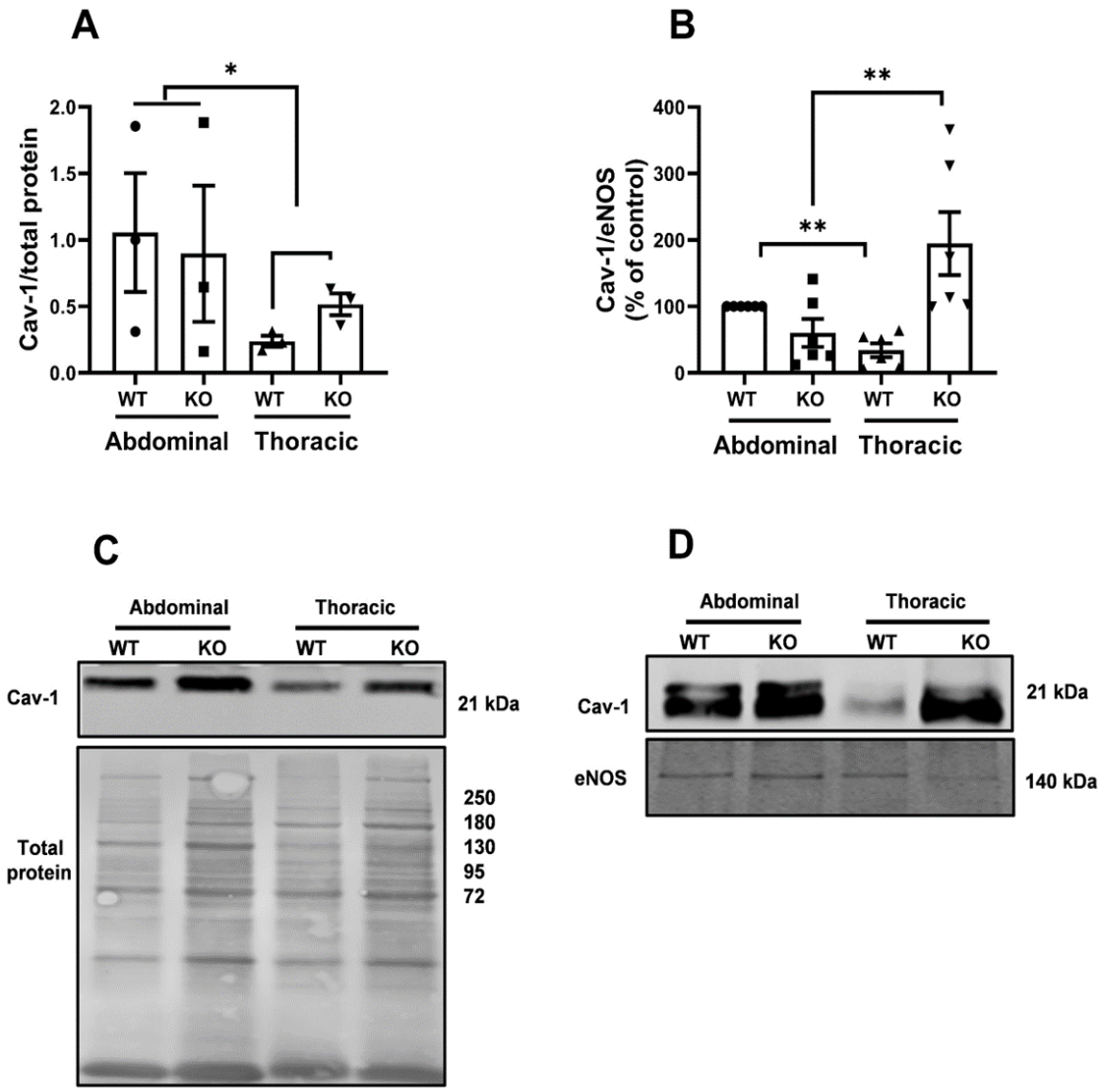

Figure 3-11: Lower levels of caveolin-1 are associated with eNOS in thoracic PVAT relative to abdominal PVAT and are increased in thoracic PVAT from KO mice compared with WT PVAT

Thoracic and abdominal aortic PVAT tissue from WT and KO mice was lysed and (A, C), 30 µg protein was resolved by SDS-PAGE and immunoblotted with an anti-caveolin-1 antibody. (A) Quantification of the level of Cav-1 relative to total lysate protein was assessed with REVERT total protein stain. Data shown represent the mean ± SEM Cav-1 levels from three independent experiments. (B, D) PVAT lysates (250 µg) were immunoprecipitated with 100 µl of Protein A-magnetic beads pre-bound to 10 µg of anti-eNOS antibodies. Immunoprecipitated proteins were resolved by SDS-PAGE and immunoblotted with anti-caveolin-1 antibodies. (B) Data shown represent the mean ± SEM %Cav-1 levels relative to eNOS normalised to WT abdominal PVAT from 6 independent experiments. (C, D) Representative immunoblots are shown, with the migration of molecular mass markers indicated on the right. Statistical significance was determined by two-way ANOVA (with Tukey's test). **p<0.01, *p<0.05.

3.4.13 Caveolin-1 gene (*Cav1*) is reduced in WT thoracic aortic PVAT compared with AMPKα1$^{-/-}$ mice

Cav1 gene expression levels were also assessed in thoracic PVAT from WT and KO mice. Consistent with total level of Cav-1 in KO thoracic PVAT, *Cav1* mRNA levels were increased in KO PVAT compared to WT PVAT (Figure 3-12).

The tables below (Table 3-2) display the cycle threshold (CT) values for the *Cav1* gene and the housekeeping gene *Tbp* in wild-type (WT) and knockout (KO) thoracic perivascular adipose tissue (PVAT). The CT values indicate the relative expression levels of these genes, with lower values representing higher gene expression. The data reveals that the housekeeping gene *Tbp* exhibits stable expression in the WT and KO thoracic PVAT, indicating its suitability as a reliable reference gene for normalizing gene expression levels. This finding ensures the accuracy and robustness of gene expression analysis in the context of WT thoracic PVAT studies.

Table 3-2: CT values for Cav1 and Tbp gene expression in WT and KO thoracic PVAT, statistical analysis was performed by t-test.

Genotype	**WT Thoracic**	KO Thoracic
CT *Cav1 (*± SEM)	0.1895	0.0984
	0.0130	0.1295
	0.0260	0.0747
	0.1167	0.1334
	0.0939	0.1437
CT *Tbp (*± SEM)	0.1310	0.0984
	0.072	0.1295
	0.0738	0.0747
	0.0728	0.1334
	0.0294	0.1437

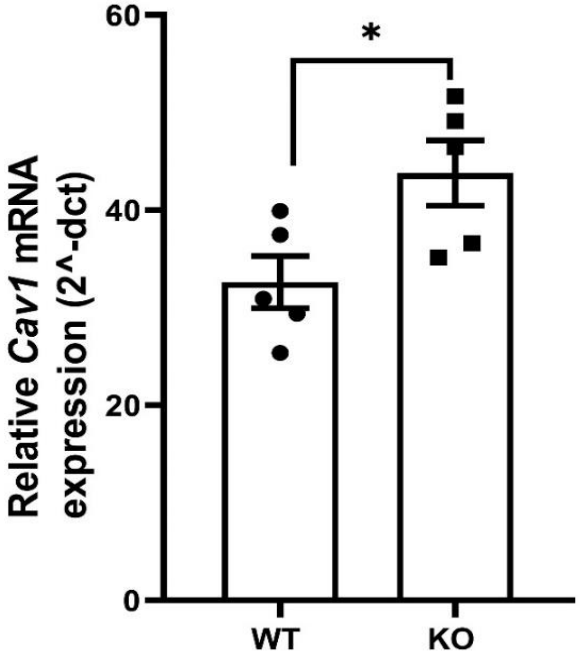

Figure 3-12: Cav1 mRNA in thoracic PVAT from WT and KO mice

Expression of *Cav1* mRNA in thoracic PVAT from WT and KO mice was assessed by real time PCR. Data shown represent the mean ± SEM fold change in *Cav1* mRNA expression relative to the TATA-Box Binding Protein (*Tbp)*, n=5 mice per group. * $p<0.05$ Statistical significance was determined by unpaired student t-test.

3.4.14 Lower levels of Hsp-90 are associated with eNOS in thoracic PVAT relative to abdominal PVAT and are increased in thoracic PVAT from AMPKα1$^{-/-}$ mice

Heat shock protein 90 (Hsp-90) regulates eNOS activity by recruiting kinases such as AMPK and Akt to phosphorylate eNOS at multiple sites, thereby increasing NO synthesis (Fulton *et al.*, 2004). Hsp-90 has also been reported to promote conformational changes in eNOS which stabilises the haem moiety (Czekay *et al.*, 2011). In these experiments the potential interactions between eNOS and Hsp-90 were examined in PVAT. Hsp-90 levels were assessed in total lysates from thoracic and abdominal aortic PVAT. Significantly more Hsp-90 was detected in abdominal PVAT compared with thoracic PVAT in both genotypes (Figure 3-13 A), p=0.0097. Similar to Cav-1, the role of AMPK in the regulation of Hsp-90/eNOS binding and NO production by PVAT has not been characterised. To assess Hsp-90/eNOS binding, eNOS was immunoprecipitated in thoracic and abdominal PVAT from WT and KO mice and levels of co-immunoprecipitation with Hsp-90 assessed (Figure 3-13 B). There was no difference in the levels of Hsp-90 bound to eNOS in PVAT from either depot or genotype.

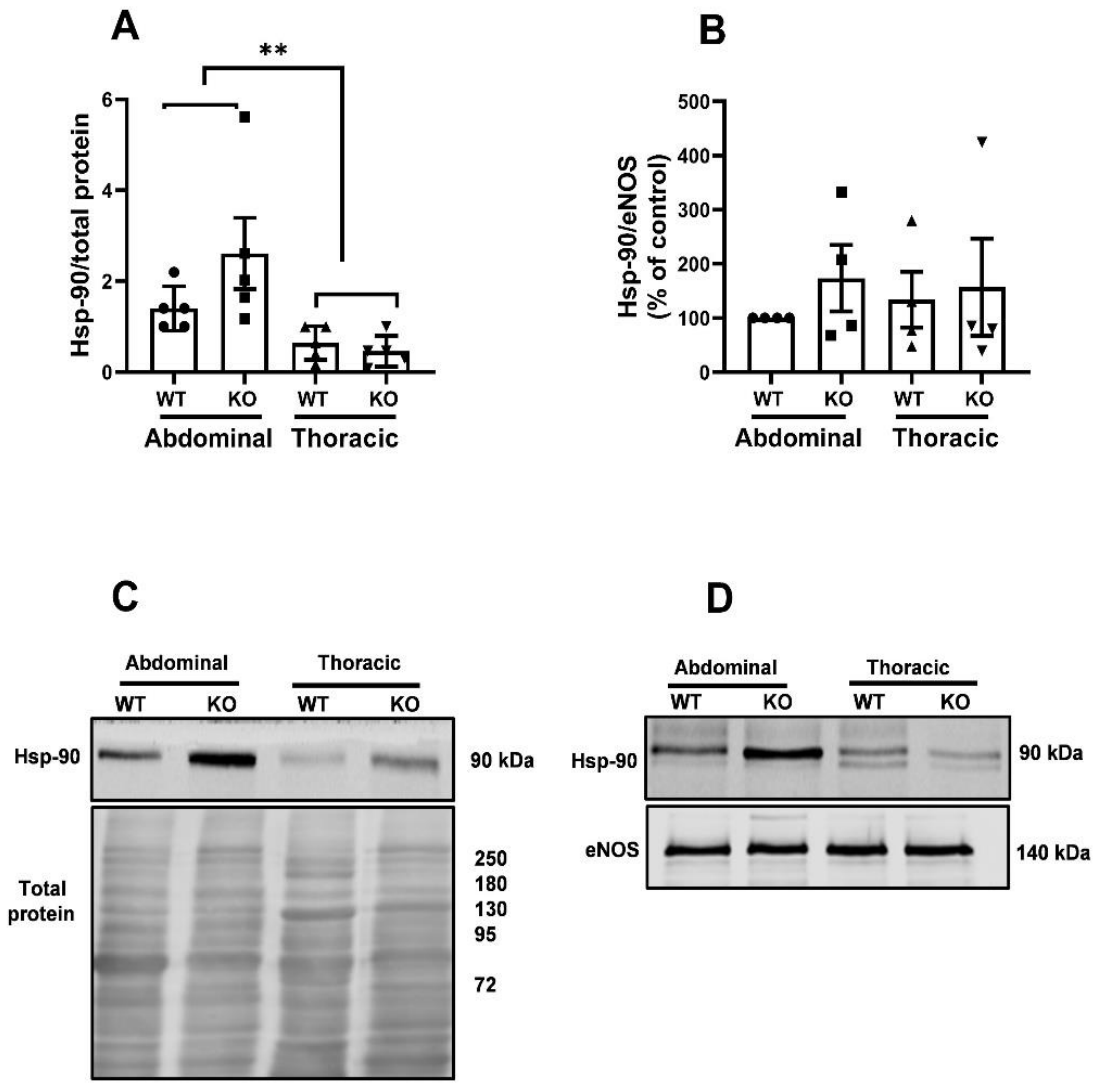

Figure 3-13: Higher levels of Hsp-90 are associated with eNOS in abdominal PVAT relative to thoracic PVAT

Thoracic and abdominal aortic PVAT tissue from WT and KO mice was lysed and (A, C), 30 µg protein was resolved by SDS-PAGE and immunoblotted with an anti-Hsp-90 antibodies. (A) Quantification of the level of Hsp-90 relative to total lysate protein was assessed with REVERT total protein stain. Data shown represent the mean ± SEM Hsp-90 levels from 5 independent experiments. (B, D) PVAT lysates (250 µg) were immunoprecipitated with 100 µl of Protein A-magnetic beads pre-bound to 10 µg of anti-eNOS antibodies. Immunoprecipitated proteins were resolved by SDS-PAGE and immunoblotted with anti- Hsp-90 antibodies. (B) Data shown represent the mean ± SEM % Hsp-90 levels relative to eNOS normalised to WT abdominal PVAT from 4 independent experiments. (C, D) Representative immunoblots are shown, with the migration of molecular mass markers indicated on the right. Statistical significance was determined by two-way ANOVA (with Tukey's test). **p<0.01, *p<0.05.

3.5 Discussion

Previous data from our laboratory demonstrated that the presence of PVAT enhances vascular relaxation to cromakalim in endothelium-intact thoracic aortic rings from wild type, but not AMPKα1$^{-/-}$ KO mice (Almabrouk *et al.*, 2017). These data suggest that PVAT has a direct vasodilatory influence on the aorta. In addition, an earlier study showed that the male offspring of female rats fed a high fat diet (HFD) during pregnancy and lactation showed dysfunctional mesenteric PVAT which could be associated with a reduction in AMPK activity and reduced NO bioavailability (Zaborska *et al.*, 2016). Unlike many previous studies which focus on the role of AMPK in regulation of NO release from the endothelium (Zhao *et al.*, 2020), the data presented in this chapter attempted to investigate the molecular pathways by which AMPK regulates NO production by PVAT.

Incubation of WT thoracic aortic rings with a non-selective NOS inhibitor (L-NAME) (Talarek *et al.*, 2011) significantly augmented the contraction to U46619 without affecting the maximal contraction and a similar effect was seen in KO thoracic aortic rings. In WT and KO abdominal aortic rings there was no significant effect of L-NAME on contraction to U46619; this is likely due to differences in NO production between the PVAT along the length of the aorta. Consistent with data presented here, a previous study demonstrated that inhibition of eNOS with L-NAME enhanced phenylephrine-induced contraction in endothelial-denuded rings with PVAT from thoracic but not abdominal aorta (Victorio *et al.*, 2016). Given that in all vessels the endothelium was denuded, this suggests that the effect of L-NAME was likely to be via inhibition of eNOS in PVAT and that the NO was likely produced by PVAT. These findings suggest that the lack of effect of L-NAME on abdominal rings with intact PVAT could be due to the different type of fat or, as was also demonstrated, the reduced formation of NO by abdominal PVAT compared to thoracic PVAT.

The results also showed that there was a significant decrease in NO production in conditioned media derived from thoracic PVAT from KO mice compared to WT mice; an effect not seen in abdominal PVAT (Figure 3-2 A). These data support and add to the plethora of evidence that PVAT releases NO and has an anticontractile effect in different vascular beds including human subcutaneous vessels and internal mammary artery (Gao *et al.*, 2005).

What is yet unclear is what causes the differences in NO formation and how AMPK is involved. However, changes in NOS expression could not account for the differences in NO production as levels of eNOS were not different between thoracic and abdominal PVAT and nor were they altered between genotypes (Figure 3-3 A&B).

Apart from its role in regulation of cerebral blood flow, published evidence shows that nNOS has a physiologically relevant role in the control of cardiovascular haemostasis (Costa *et al.*, 2016). Another study demonstrated that the presence of functional nNOS in vascular cell lysates and the same study showed that stimulation of vascular endothelial cells (HUVECs) with physiological concentrations of estrogen rapidly increased activating phosphorylation of nNOS and nNOS-dependent NO production (Lekontseva *et al.*, 2011). Furthermore, inhibition of iNOS with 1400 W (a selective iNOS inhibitor) attenuated PVAT-mediated hypo-contractility during sepsis (Awata *et al.*, 2019). In the current study neither nNOS nor iNOS could be detected in PVAT lysates from either depot or genotype (Figure 3-3 C&D). This is unlikely to be due to a technical issue since no iNOS or nNOS was detected even when the concentration of the protein loaded was increased up to 60 ug per lane. Furthermore, it should be noted that to verify the immunoreactivity of the iNOS and nNOS in our experiments, we used mouse brain lysate as a positive control for nNOS and 3T3-L1 adipocyte lysate treated with proinflammatory cytokines IL-1ß as a positive control for iNOS. Given that, PVAT-derived NO is therefore likely to be synthesised by eNOS in mouse aorta.

WT thoracic PVAT exhibited significantly increased eNOS activity (around 40%) compared to KO PVAT (Figure 3-4) assessed by measuring the rate of conversion of [^{14}C]-L-arginine to [^{14}C]-L-citrulline (Ladurner *et al.*, 2012). In addition, eNOS activity in abdominal PVAT was significantly decreased when compared to WT thoracic PVAT suggesting that changes in eNOS activity rather than levels of eNOS could account for the difference in NO production between thoracic and abdominal PVAT.

Earlier evidence reported that eNOS is phosphorylated at multiple sites. While phosphorylation of Ser^{615}, Ser^{635}, and Ser^{1177} results in the activation of eNOS, the phosphorylation of eNOS at Ser^{116} and Thr^{497} sites reduces eNOS activity (Fleming *et al.*, 2001, Kolluru *et al.*, 2010). The reduced NO production in KO mice and in

abdominal PVAT was not associated with altered levels of phosphorylated eNOS. Furthermore, it has been suggested that dephosphorylation of eNOS at Thr^{495} is implicated in the uncoupling of eNOS and the resulting enhanced production of superoxide (O_2^-) instead of NO, a process which is implicated in atherosclerotic lesion progression (Chen *et al.*, 2008). In bovine aortic endothelial cells, humoural factors like bradykinin stimulate NO synthesis by increasing phosphorylation of eNOS at multi-sites including eNOS-Ser^{633} and eNOS-Ser^{615} in a Ca^{2+}-dependent manner (Michell *et al.*, 2002). There were no differences in eNOS phosphorylation at Ser^{1177} relative to total eNOS (Figure 3-5 A). Furthermore, neither Ser^{615} nor Thr^{495} phosphorylation could be detected in PVAT lysates from either depot or genotype (Figure 3-5 B). Therefore, it is unlikely that altered eNOS phosphorylation at these sites underlies the increased NOS activity in WT thoracic PVAT.

We further aimed to study the effect of global AMPKα1 knockout on adipose tissue by looking at phenotypic markers in thoracic, abdominal, mesenteric PVAT and interscapular fat depots. This was performed by investigating the levels of UCP-1 (marker of BAT). Our results showed that thoracic PVAT and BAT have an elevated level of UCP-1 both in WT and KO mice compared to abdominal aortic and mesenteric PVAT which was composed mainly of WAT, as confirmed by low UCP-1 levels. The results suggest that deletion of AMPKα1 had no effect on phenotypic features of the PVAT regardless of the depot (Figure 3-6 and Figure 3-7). These results are consistent with earlier findings which reported that thoracic PVAT is composed mainly of a BAT-like phenotype and that PVAT surrounding the abdominal aorta consists mainly of WAT (Padilla *et al.*, 2013). This phenotypic characterization was done to investigate whether the difference in adipocyte type could account for the difference in NO production observed between thoracic and abdominal PVAT (Figure 3-2 and Figure 3-8).

Nevertheless, it is worth noting that previous studies demonstrate that PVAT can have characteristics of both BAT and WAT, but this largely depends on the animal strain, anatomical context, and the pathological state. In addition, investigating the factors responsible for the phenotypic difference in the thoracic and abdominal PVAT throughout the aorta and other arteries are an area of interest because phenotypic differences in PVAT depots may contribute to differences in

NO production and consequently the disease risk in blood vessels. A number of studies have demonstrated a relationship between elevated PVAT volume and the severity of coronary atherosclerosis, hypoadiponectinaemia, and other vascular disease (Greif *et al.*, 2009). However, in the current study there was no difference in the level of UCP-1 between wild type and AMPKα1 deficient mice. Indeed, earlier studies have proposed that mice with a global AMPKα1 knockout showed no observable alteration in activities associated with BAT such as cold-induced hyperphagia, chronic cold tolerance or acute non-shivering thermogenesis, and that a compensatory upregulation in AMPKα2 expression may explain this lack of effect (Bauwens *et al.*, 2011). As we had shown previously that thoracic aortic PVAT produces significantly more NO than abdominal PVAT in WT mice, but not in KO mice we went on to investigate if this effect was also seen in other adipose depots. NO production was reduced in BAT and mesenteric PVAT in KO mice compared with WT. This suggests that AMPKα1 positively regulates NO synthesis in several adipose tissue depots, including depots composed of predominantly WAT.

Many studies reported that increased ROS production is associated with endothelial dysfunction and further progression of vascular dysfunction. Increased ROS generation decreases bioavailability of endothelium-derived NO and promotes endothelial dysfunction which underlies the early stages of cardiovascular diseases (Fisslthaler and Fleming, 2009). Decreased bioavailability of NO is also linked with the generation of ROS in the vessel wall including peroxynitrite and $O_2^{\cdot-}$ that leads to development of endothelial dysfunction (Bouloumié *et al.*, 1997). The sources of these ROS are manifold but include eNOS uncoupling (Chen *et al.*, 2014), and peroxynitrite formation as a result of NO scavenging by superoxide (Cassuto *et al.*, 2014). Previous studies have demonstrated that AMPK has a protective role in the regulation of vascular redox balance, reducing the formation of ROS by NADPH oxidase and stimulating eNOS (Fisslthaler and Fleming, 2009). PVAT induces an anticontractile effect via secreting vasodilator substances that include not only NO but also H_2O_2 (Gao *et al.*, 2007). Earlier studies have reported that H_2O_2 can exert a positive regulatory effect on eNOS by protecting the Ca^{2+}/CaM binding site that is mediated by a JAK2 and CaM kinase II-dependent pathway (Cai *et al.*, 2001). H_2O_2 levels were elevated in thoracic PVAT relative to abdominal PVAT in WT mice while there was no statistically significant difference between H_2O_2

production in thoracic and abdominal PVAT from KO mice (Figure 3-9 A). The increased H_2O_2 levels in WT thoracic PVAT might therefore explain the increased NO production in thoracic PVAT by H_2O_2-mediated protection of the Ca^{2+}/CaM binding site in eNOS.

Under normal physiological conditions, the detrimental effects of ROS in PVAT are antagonized by several antioxidant enzymes such as CuZn-SOD, catalase, Mn-SOD and glutathione peroxidase (Awata *et al.*, 2019, Gao *et al.*, 2006). In the current study there were no differences in TBARS levels between PVAT depots or genotypes (Figure 3-9 B). In agreement, a previous study showed that although the relative expression levels of Mn-SOD and CuZn-SOD are different along the aorta, the lipid peroxidation levels appear to be similar between PVAT from the abdominal and thoracic aorta (Victorio *et al.*, 2016). These findings emphasize the specific regional roles of PVAT depots in the control of vascular function that can drive differences in the susceptibility of the aorta to vascular injury such as abdominal aortic aneurysm (AAA).

To examine whether the levels of reactive oxygen species, and in particular superoxide, were different between genotypes or PVAT depots and whether this might be involved in the modulatory action of PVAT on vascular function, we used PEG-SOD (Beckman *et al.*, 1988, Laurindo *et al.*, 2008). In WT vessels PEG-SOD significantly attenuated the maximal contraction to U46619 and a similar attenuation of contraction was observed in response to PEG-SOD in KO thoracic aortic rings (Figure 3-10). This partially agreed with a previous study showing that PEG-SOD exerted greater attenuation of electrical field stimulation-induced contraction in mesenteric vessel with intact PVAT (Gao *et al.*, 2006). Suggesting that PVAT from KO mice produce more superoxide compared with WT mice and explaining the reduced anticontractile effect of KO PVAT.

Cav-1 binding to eNOS occupies the Ca^{2+}/CaM binding site thereby reducing NO production via its scaffolding domain (amino acids 82–101), (Razani *et al.*, 2002). An earlier study using co-immunoprecipitation combined with enzymatic assays showed direct Cav-1/eNOS coupling followed by a reduction in NO production (Ju *et al.*, 1997). Previous reports have demonstrated that in endothelial cells the interaction between eNOS and Cav-1 is importantly regulated by Ca^{2+}/CaM, and calmodulin disrupts the heteromeric complex formed between eNOS and Cav-1 in

a Ca^{2+}-dependent fashion (Michel *et al.*, 1997). Another important question that was addressed in the present study was whether deletion of AMPKα1 affects the eNOS activity in PVAT via altering eNOS binding proteins such as Cav-1 and Hsp-90. The role of AMPK in regulation of Cav-1/ eNOS binding and NO production by PVAT has not been characterised previously. Our results showed that significantly more Cav-1 was detected in abdominal PVAT from WT and KO mice compared with thoracic PVAT (Figure 3-11 A), and that could explain the reduction in NO production in abdominal PVAT compared with thoracic PVAT given Cav-1 negatively regulates eNOS activity and NO production (Bernatchez *et al.*, 2011). Furthermore, Cav-1 was detected in eNOS immunoprecipitates and levels of Cav-1/ eNOS association were increased in abdominal PVAT relative to thoracic PVAT of WT mice (Figure 3-11 B), consistent with the increased total Cav-1 levels in abdominal PVAT lysates. Intriguingly, Cav-1/ eNOS association was markedly increased in thoracic PVAT from KO mice compared with WT mice, which might account for the reduction in NO production in KO thoracic PVAT compared with WT. In line with the differences in NO production between WT PVAT and KO PVAT and as we showed earlier that the elevated amount of Cav-1 in KO PVAT we also investigated the levels of *Cav1* gene expression in WT and KO mice, our result demonstrated that *Cav1* mRNA levels were increased in KO PVAT compared to WT PVAT and that consistent with increased total level of Cav-1 in KO thoracic PVAT (Figure 3-12).

Along with known eNOS interactors such as Cav-1, other proteins were associated with immunoprecipitated eNOS, including Hsp-90. Earlier experiments suggested that the Hsp-90/eNOS interaction facilitates Ca^{2+}/CaM displacement of Cav-1, leading to an increased NO production (Sessa, 2004). In contrast, binding of Hsp-90 to eNOS involves a complex system of protein-protein interactions: Hsp-70 coupling to Hsp-90 is essential to interact with eNOS; C-terminal Hsp-70-interacting protein (CHIP) is important in regulating Hsp-70 and Hsp-90 binding which reduces eNOS trafficking and downregulates NO production (Ramadoss *et al.*, 2013).

Hitherto, Hsp-90 coupling with eNOS in PVAT has not been investigated. Given that the role of Hsp-90 in regulation of eNOS activity and NO production is not well understood, we investigated and found that the level of Hsp-90 in abdominal

PVAT both in WT and KO mice is greater than that in thoracic PVAT even though less NO is produced by abdominal PVAT, while in eNOS immunoprecipitate we could not observe any differences in the level of Hsp-90 between thoracic and abdominal PVAT in both genotypes (Figure 3-13). Suggesting that Hsp-90 has less effect on eNOS activity, and NO production compared with Cav-1.

Overall, these data are the first to specifically study the signalling function of AMPK in regulating Cav-1 /eNOS binding in thoracic and abdominal PVAT in mice. We have shown that thoracic PVAT synthesises more NO, likely due to increased eNOS activity rather than levels of total eNOS, and possibly due to reduced association with Cav-1 and/or H_2O_2-mediated protection of eNOS. The functional data in mice aortic rings suggest that NO produced by PVAT is functionally important in regulating vascular contractility. Collectively, these data raise the possibility of studying the inhibitory influence of Cav-1 on eNOS without interfering with the other actions of endogenous Cav-1. Knowing that aortic atherosclerotic lesions and aneurysms are predominant in abdominal rather than thoracic segment of the aorta, these findings highlight a new specific regional role of PVAT depots in the control of vascular function that may drive differences in susceptibility to vascular injury between these two parts of the aorta.

Chapter 4 - Characterisation of nitric oxide synthesis and Cav-1 /eNOS coupling in 3T3-L1 adipocyte.

4.1 Introduction

As demonstrated in Chapter 3, PVAT-derived NO is greater in thoracic aorta compared with the abdominal aorta, an effect that was reduced in AMPKα1 KO mice. Furthermore, this altered NO synthesis was associated with a different adipocyte phenotype with altered Cav-1 levels and Cav1/eNOS association. This implies that NO synthesis is altered during adipogenesis into different adipocyte phenotypes and is regulated by AMPK and/or Cav-1.

Many cardiovascular diseases are associated with a reduction in NO bioavailability including hypercholesterolaemia, hypertension and diabetes (Naseem, 2005). There are many risk factors for cardiovascular diseases but one which is of particular concern due to its widespread and increasing incidence is obesity. Obesity is strongly linked to various health problems, including type 2 diabetes, coronary artery disease, stroke and hypertension (Després *et al.*, 2008). Evidence linking obesity with NO production is widespread, with many studies suggesting that the reduction in NO production in obesity is due to a reduction in endothelial nitric oxide synthase (eNOS) activity (Ren *et al.*, 2022). Brown adipose tissue is distinguished by multilocular lipid droplets and high mitochondrial content, which facilitate fat oxidation and heat generation. It is well known that increasing brown fat content is correlated with increases in the metabolic rate and reductions in metabolic disorders (Poher *et al.*, 2015).

Furthermore, in 2012 a new type of brown-like adipocyte which is characterised by transformation of white adipocytes to brown adipocyte-like cells ("beiging") was identified both mice and humans (Enerbäck, 2013). Nisoli *et al.* (1998) showed that NO may play a significant role in proliferation and differentiation of rat brown adipocytes in a culture medium and so could positively influence the phenotype of adipose tissue. 3T3-L1 is an adipocytic cell line which is widely used to study the adipogenesis process of white adipocytes (Vigilanza *et al.*, 2011). 3T3-L1 differentiation is a convenient way to generate adipocyte-like cells and to investigate adipogenic transcription factors, key molecular markers and the multiple interactions required for adipogenesis. Therefore, in the context of this thesis, it is of importance to understand the molecular mechanism underlying how NO regulates adipose tissue under normal and oxidative stress conditions, the latter of which contribute to metabolic dysregulation associated with obesity.

Adipogenesis is accomplished using a hormonal differentiation cocktail (HDC) of isobutylmethylxanthine (IBMX), insulin, troglitazone and dexamethasone. Adding this cocktail triggers the preadipocytes to undergo growth arrest in the G1 phase after which the cells undergo mitotic clonal expansion (MCE) (Tang *et al.*, 2003). In Iin this period, early adipogenic transcription factors, including C/EBP-δ, Kruppel-like factor (KLF) 4, KLF5 and CCAAT/enhancer-binding protein (C/EBP)-ß, are gradually expressed (Wu and Wang, 2013), *C/EBP-ß* and *C/EBP-δ* stimulate expression of adipocyte-specific transcription factors, such as *C/EBP-a* and peroxisome proliferator-activated receptor (*PPAR*)-γ. These factors play an essential role in the control of adipocyte differentiation by controlling downstream gene expression, including fatty acid synthase (FAS), perilipin, adipocyte fatty acid binding protein 2 (aP2) and mainly acetyl-CoA carboxylase (ACC), which subsequently promote lipid droplet formation in a mature adipocyte (Rosen *et al.*, 2000, Rosen and MacDougald, 2006).

Some studies have investigated the role of NO in adipogenesis and, interestingly, in 3T3-L1 cells treated with an NO donor, the NO inhibits the activity of the adipogenic transcription factor PPARγ, which leads to a reduction in adipogenesis (Kawachi *et al.*, 2007). However, the mechanisms underlying this effect and the role of eNOS during adipogenesis remain elusive.

Caveolin-1 (Cav-1) is a membrane protein associated with cholesterol distribution, extracellular matrix organisation and endocytosis, cell migration and signalling. (Nwosu *et al.*, 2016). Most cell types contain caveolae but they are particularly abundant in adipocytes, where they account for 30% of the plasma membrane surface area (Fan *et al.*, 1983). In adipocytes, Cav-1 is the isoform which is responsible for caveolae formation (Scherer *et al.*, 1994). It has been shown that Cav-1 is an fundamental part of adipocytes caveolae which facilitates insulin sensitivity during adipogenesis by binding the beta subunit of the insulin receptor (IR) to the caveolae and therefore Cav-1 is an important mediator of the insulin signalling pathway (Palacios-Ortega *et al.*, 2014). In addition. caveolae have been traditionally associated with trafficking of cholesterol and lipid, endocytosis and exocytosis cycles, integration, compartmentalization of signal transduction intermediates in adipocyte (Parton and Simons, 2007) but they also have an important role in eNOS function.

The role of Cav-1 in regulating eNOS function in adipocytes

Prior to this study, very little was known about eNOS and NO production and the role of Cav-1 in regulating eNOS function in adipocytes. It has been reported that TNF-α is able to slow down the pace of 3T3-L1 adipocyte differentiation in a mechanism involving a reduction in total and phosphorylated Cav-1 and reduction of insulin sensitivity to promote glucose uptake in these cells (Palacios-Ortega *et al.*, 2015). Furthermore, Cav-1 depletion accelerated insulin receptor and glucose transporter-4 (Glut-4) degradation in 3T3-L1 adipocytes (Cohen *et al.*, 2003); (Gonzalez-Munoz *et al.*, 2009). Even though Cav-1 deletion does not completely block Glut-4 translocation to the plasma membrane (Yuan *et al.*, 2007).

Additional studies have revealed that eNOS activity increases via interaction of eNOS with heat shock protein-90 (Hsp-90) (Gupta *et al.*, 2017), which promotes conformational changes in eNOS and stabilises the haem moiety in NOS (Czekay *et al.*, 2011). Furthermore, Hsp-90 has been reported to interact and regulate eNOS activity by recruiting kinases such as AMPK and Akt to phosphorylate eNOS at multiple sites (Ser^{1177}, Ser^{615}, Ser^{633}) and promote a dramatic increase in NO synthesis (Fulton *et al.*, 2004). However, to our knowledge, the current study is the first to investigate the effect of Cav-1 in regulation of NO and eNOS activity in adipocytes.

4.2 Aims of the study

The purpose of this study was to characterise NO production in adipocytes in 3T3-L1 cells. Also, we sought to investigate the influence of AMPK activity on NO production in 3T3-L1 adipocytes.

4.3 Methods

4.3.1 Analysis of NO synthesis by 3T3-L1 preadipocytes and adipocytes

In this study, nitric oxide (NO) synthesis by 3T3-L1 preadipocytes and adipocytes was investigated. 3T3-L1 adipocytes were washed with and incubated for 2 h in serum-free DMEM. The medium was removed and replaced with serum-free DMEM containing test substances or vehicle for the indicated times. Aliquots of the medium were collected after various incubation times, 4 volumes (1:4) of methanol added and samples were then centrifuged. Supernatant was collected and assayed for NOx content using a Sievers 280 NO Analyser.

4.3.2 3T3-L1 adipocyte culture

Preadipocytes were cultured in Corning T75 flasks in Dulbecco's modified Eagles medium (DMEM) supplemented with 10% (v/v) new-born calf serum (NCS) and 100 U/ml (w/v) penicillin and streptomycin. The cells were maintained at 37ºC in a humidified atmosphere, and the media was replenished every 48 hours.

Differentiation of 3T3-L1 Preadipocytes:

To induce differentiation, preadipocytes were grown to 100% confluence in DMEM containing 10% (v/v) NCS. Post-confluence, the medium was replaced with differentiation medium consisting of DMEM, fetal calf serum, 3-isobutyl-1-methylxanthine, dexamethasone, troglitazone, and insulin. After three days in this medium, it was replaced with DMEM supplemented with 10% (v/v) FCS alone. Adipocytes were ready for experimentation 8–12 days after induction of differentiation.

Preparation of 3T3-L1 Cell Lysates:

Cells in 6-well plates were washed, incubated in serum-free DMEM, followed by Krebs-Ringer Phosphate (KRP) buffer. Afterward, cell lysis buffer was added, and the cell extract was collected, incubated, and centrifuged. The supernatants were stored at -20^{0}C for further use.

4.3.3 Confocal microscopy and staining

3T3-L-1 preadipocytes and adipocytes were cultured on 6-well plates with sterilized 13 mm diameter glass coverslips and treated with MβCD for 6 hours. Following treatment, cells were fixed using paraformaldehyde. Triton was used to permeabilize cells. Cells were then incubated overnight with primary antibodies (anti-eNOS and anti-Cav-1) prepared in IF buffer. Then incubated with secondary antibodies for 1 hour in the dark. Then, coverslips were mounted on glass slides using VECTASHIELD and stored overnight in the dark to dry. Immunolabeled samples were analyzed using a Zeiss LSM 5 exciter laser scanning microscope. Co-localization of eNOS with other proteins was assessed using ImageJ with the BIOP/JACoP plug-in, calculating Pearson's correlation coefficient.

4.4 Results

4.4.1 Characterization of NOS levels and NO production during 3T3-L1 cell adipogenesis

As observed in chapter 3, there was a significant reduction in NO in abdominal PVAT (WAT) compared with thoracic PVAT. This finding suggests that adipocyte phenotype could have an influence on eNOS function and activity. To further investigate this, NOS levels were studied by immunoblotting during 3T3-L1 adipogenesis from 3T3-L1 preadipocytes as described in the methodology chapter (2.2.4.4). There was a significant reduction in the level of eNOS during 3T3-L1 adipogenesis (Figure 4-1 A), which correlated with a significant reduction in NO production between day 0 and day 10 (Figure 4-1 B). The source of NO is likely to be eNOS in 3T3-L1 preadipocytes as no immunoreactivity was observed throughout adipogenesis using anti-iNOS and anti-nNOS antibodies (Figure 4-1 D).

It is obvious that further evaluation and analysis of the mechanisms underlying this dramatic downregulation of eNOS protein expression are necessary. The data indicates an absence of eNOS protein at day 3, despite the presence of detectable NO production, suggesting the existence of small amounts of active NOS (eNOS, nNOS or iNOS) could account for the NO production at this time point, or it may just be that the antibodies are not sufficiently avid to detect very small levels of protein.

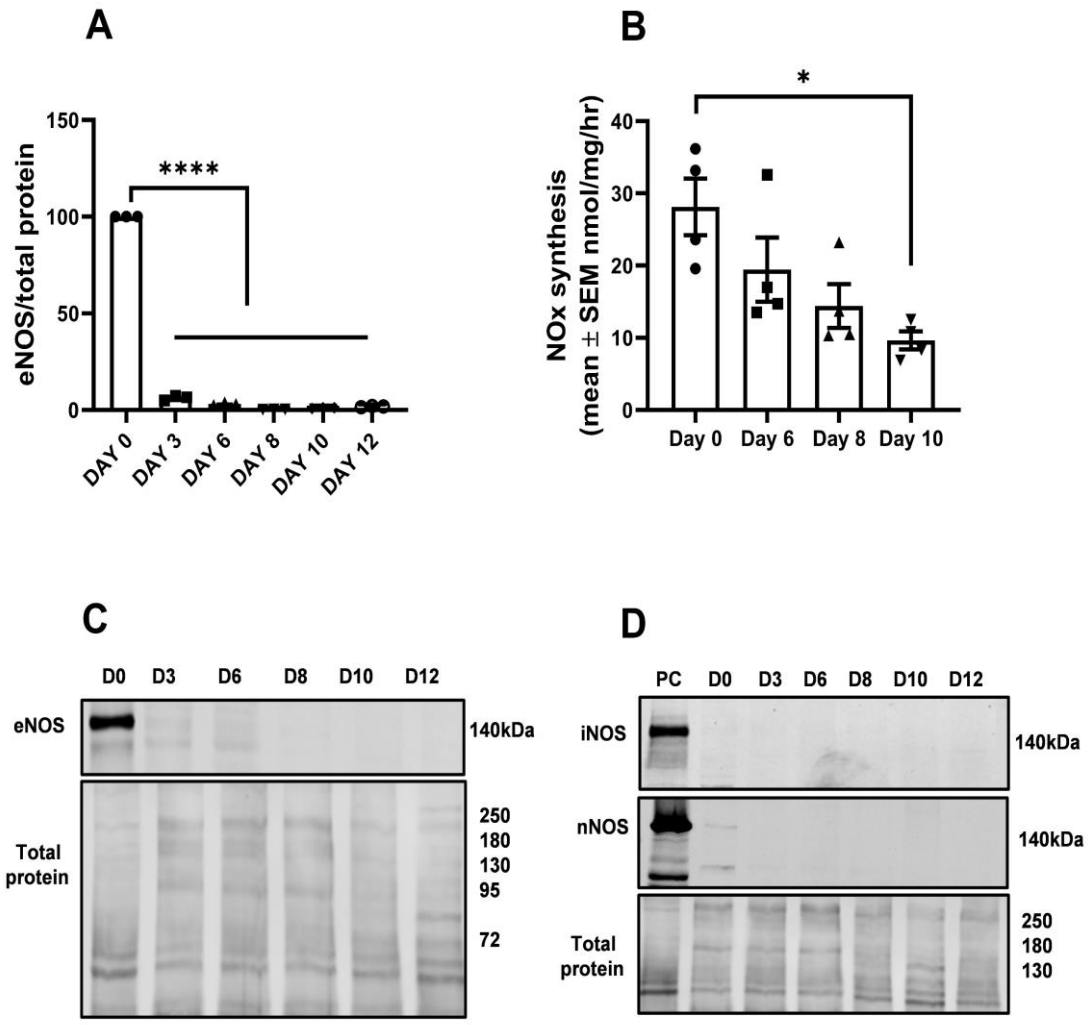

Figure 4-1: Levels of NOS isoforms and NO production during 3T3-L1 adipogenesis

3T3-L1 preadipocytes were differentiated into adipocytes and (A, C, D) lysates prepared at the indicated days during adipogenesis. Lysates (20 µg) were resolved by SDS-PAGE and subjected to immunoblotting with (A, C) anti-eNOS antibodies or (D) anti-iNOS and anti-nNOS antibodies. (A) Quantification of the level of eNOS relative to total lysate protein was assessed with REVERT total protein stain. Data shown is the mean ± SEM % day 0 eNOS levels from 3 independent experiments. (B) Conditioned media from 3T3-L1 cells was collected for 1 h at the indicated times during adipogenesis and assayed for NO + NO_2^- (NOx) content using a Sievers 280 NO analyser. Data shown represent the mean ± SEM nmol NOx synthesis/mg protein/h from 4 independent experiments. (C, D) Representative western blots and REVERT-stained blots. PC= positive control (for iNOS 3T3-L1 adipocyte cells incubated with IL-1β while for nNOS mouse brain lysate were used as a positive control). ****p<0.0001, *p<0.05, Statistical significance was determined by one-way ANOVA (with Tukey's test).

4.4.2 Effect of IL-1β and TNF- α on NO production in 3T3-L1 preadipocytes and adipocytes

To examine whether iNOS-generated NO could be induced in 3T3-L1 preadipocytes and adipocytes with proinflammatory cytokines, cells were incubated with proinflammatory cytokines IL-1ß or TNF-α and NO generated in conditioned media was measured. Incubation of preadipocytes with 10 ng/ml of IL-1ß for 24h did not alter NO production, whereas 24h incubation with TNF-α significantly increased NO production compared with control (Figure 4-1 A). In contrast, incubation of 3T3-L1 adipocytes with either cytokine for 24 h significantly stimulated NO production (Figure 4-2 B).

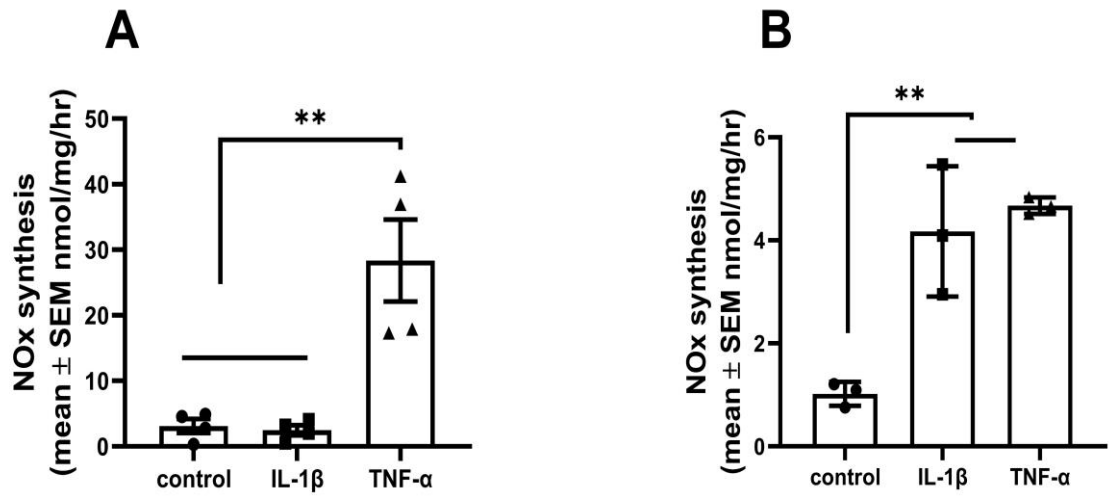

Figure 4-2: Effect of IL-1β or TNF-α on NOx production in 3T3-L1 preadipocytes and adipocytes

3T3-L1 (A) preadipocytes or (B) adipocytes were incubated with IL-1β or TNF-α (10 ng/ml) for 24 h, and conditioned medium was collected. Medium was assayed for NO + NO_2^- (NOx) content using a Sievers 280 NO analyser. Data shown represent the mean ± SEM nmol NOx synthesis/mg protein/h from three to four independent experiments. **p<0.01, Statistical significance was determined by one-way ANOVA (with Tukey's test).

4.4.3 Effect of IL-1β and TNF- α on iNOS levels in 3T3-L1 preadipocytes and adipocytes

To determine whether the increased NO synthesis by 3T3-L1 adipocytes in response to proinflammatory cytokines (Figure 4-2) was associated with altered iNOS levels, 3T3-L1 preadipocytes and adipocytes were incubated in the presence or absence of 10 ng/ml of IL-1ß or TNF-α for 24 h. Cell lysates were collected and subjected to SDS-PAGE prior to measurement of the iNOS protein levels by immunoblotting. As shown in (Figure 4-3 A), incubation of preadipocytes with TNF-α, but not IL-1ß caused a significant increase in iNOS levels. In adipocytes, IL-1ß caused a significant increase in iNOS levels after 24h but no effect was observed in response to TNF-α (Figure 4-3 B).

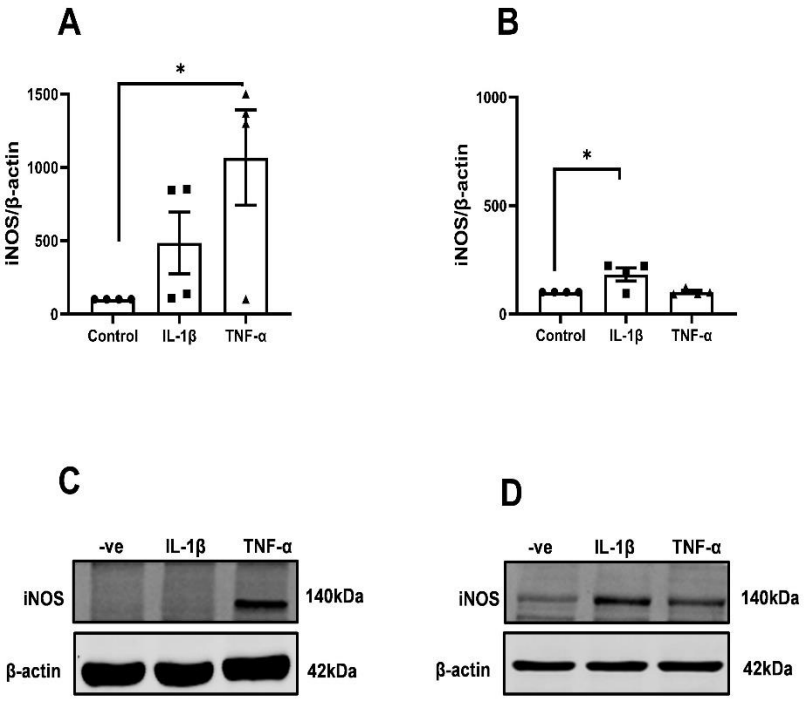

Figure 4-3: Effect of IL-1β or TNF-α on iNOS levels in 3T3-L1 preadipocytes and adipocytes

(A) 3T3-L1 preadipocytes or (B) adipocytes were incubated in the presence or absence of IL-1β or TNF-α (10 ng/ml) for 24 h and lysates prepared. Lysates (20 µg) were resolved by SDS-PAGE and subjected to immunoblotting with anti-iNOS antibodies. (A, B) Quantification of iNOS levels. Data shown represent the mean ± SEM % control iNOS levels relative to the housekeeping protein β-actin from four independent experiments. (C, D) Representative western blots. *p<0.05, Statistical significance was determined by one-way ANOVA (with Tukey's test).

4.4.4 Disruption of caveolae in 3T3-L1 preadipocytes and adipocytes using Methyl-β-cyclodextrin

Despite eNOS levels declining during 3T3-L1 adipogenesis, measurable levels of NO are still synthesised by 3T3-L1 adipocytes. Caveolin-1 (Cav-1) is the main coat protein of caveolae that has been demonstrated to associate with and downregulate eNOS (Razani *et al.*, 2001). To further assess the role of caveolin-1 in regulating eNOS activity and NO bioavailability in adipocytes, we studied the effect of depletion of caveolae with methyl-ß-cyclodextrin (MßCD) (Lee *et al.*, 2015). To investigate the extent of Cav-1/eNOS interaction in preadipocytes and adipocytes, colocalization was studied by immunofluorescence confocal microscopy. 3T3-L1 preadipocytes or adipocytes were cultured on glass coverslips and exposed to (1 mM) MßCD for 6 h. There was a significant reduction in Cav-1/eNOS colocalization in cells incubated with MßCD in both preadipocytes (Figure 4-4) and adipocytes (Figure 4-5).

The endothelial nitric oxide synthase (eNOS) remains inactive due to its direct interaction with Cav-1 via the caveolin scaffolding domain (CSD). Consistent with previous reports reduced Cav-1 expression in cells increases the activity of eNOS and NO production, this implies Cav-1 plays a role as a fundamental regulator of eNOS activity. The relative scarcity of Cav-1 in contrast to the abundant expression of eNOS presents an intriguing aspect about their interactions within caveolae. However, it's essential to differentiate between eNOS protein levels and its functional activity. While reduced Cav-1 levels might influence eNOS activity, this difference doesn't directly account for the eNOS activity this discrepancy implies the involvement of additional regulatory mechanisms or factors influencing eNOS stability or pathways of degradation. Various factors, such as post-translational modifications, proteolytic processes, or alterations in cellular signalling cascades, could contribute to this observed difference. Furthermore, the dynamic nature of caveolae and their structural proteins suggests the regulatory mechanisms that affect eNOS protein turnover and functionality (Harding *et al.*, 2018, Chen *et al.*, 2018).

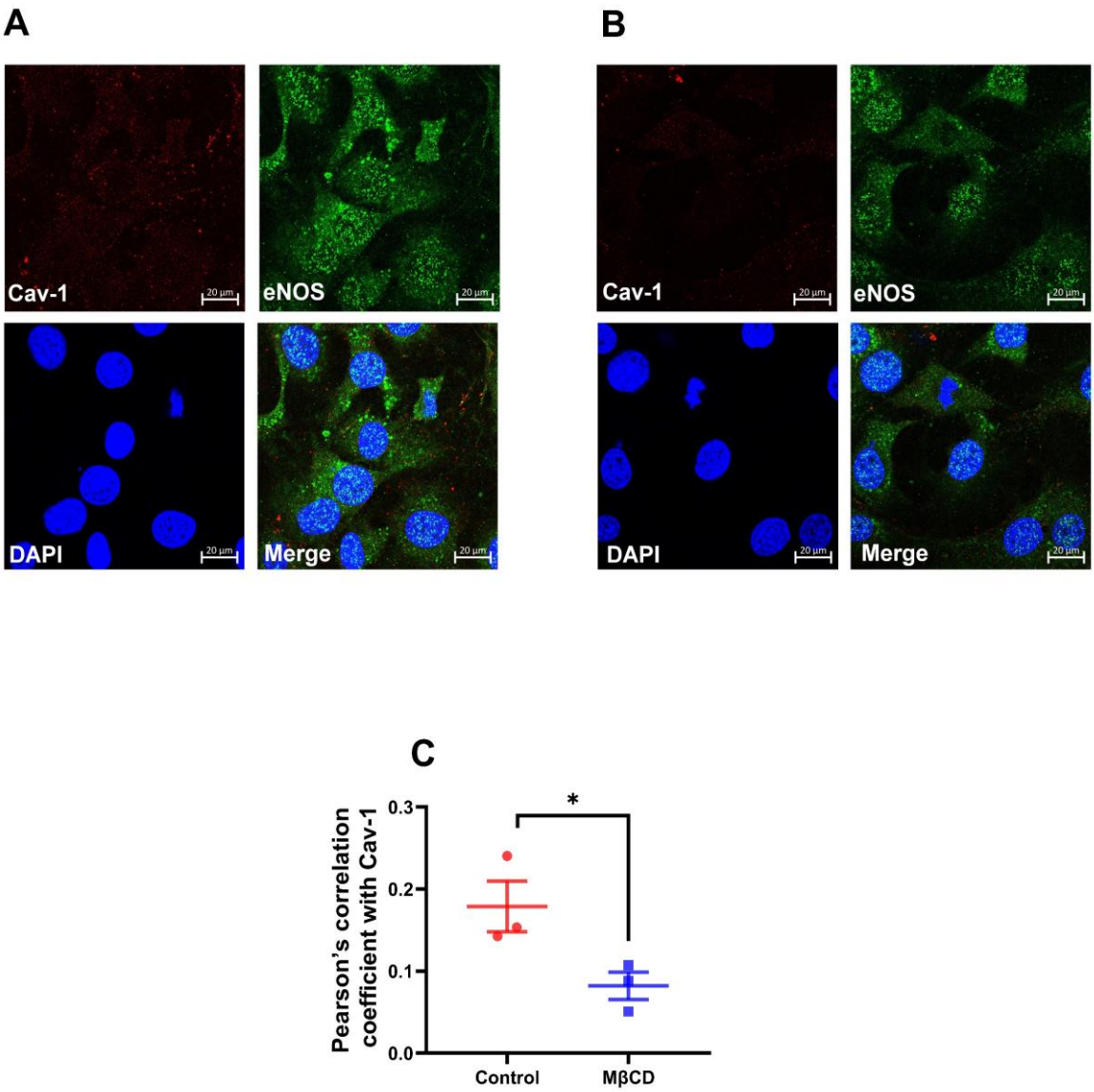

Figure 4-4: Methyl-β-cyclodextrin reduces Cav-1/ eNOS co-localisation in 3T3-L1 preadipocytes

3T3-L1 preadipocytes were incubated in the presence or absence of MβCD (1 mM) for 6 h. Coverslips of 3T3-L1 cells were incubated with anti-Cav-1 and anti-eNOS antibodies and analysed by immunofluorescence confocal microscopy. Representative micrographs from (A) control and (B) MβCD-treated cells. DAPI was used to stain cell nuclei. Scale bar = 20 µm. (C) Quantification using Pearson's correlation coefficient from three biological replicates with 50 cells per group. * $p<0.05$, Statistical significance was determined by Student's t-test (unpaired).

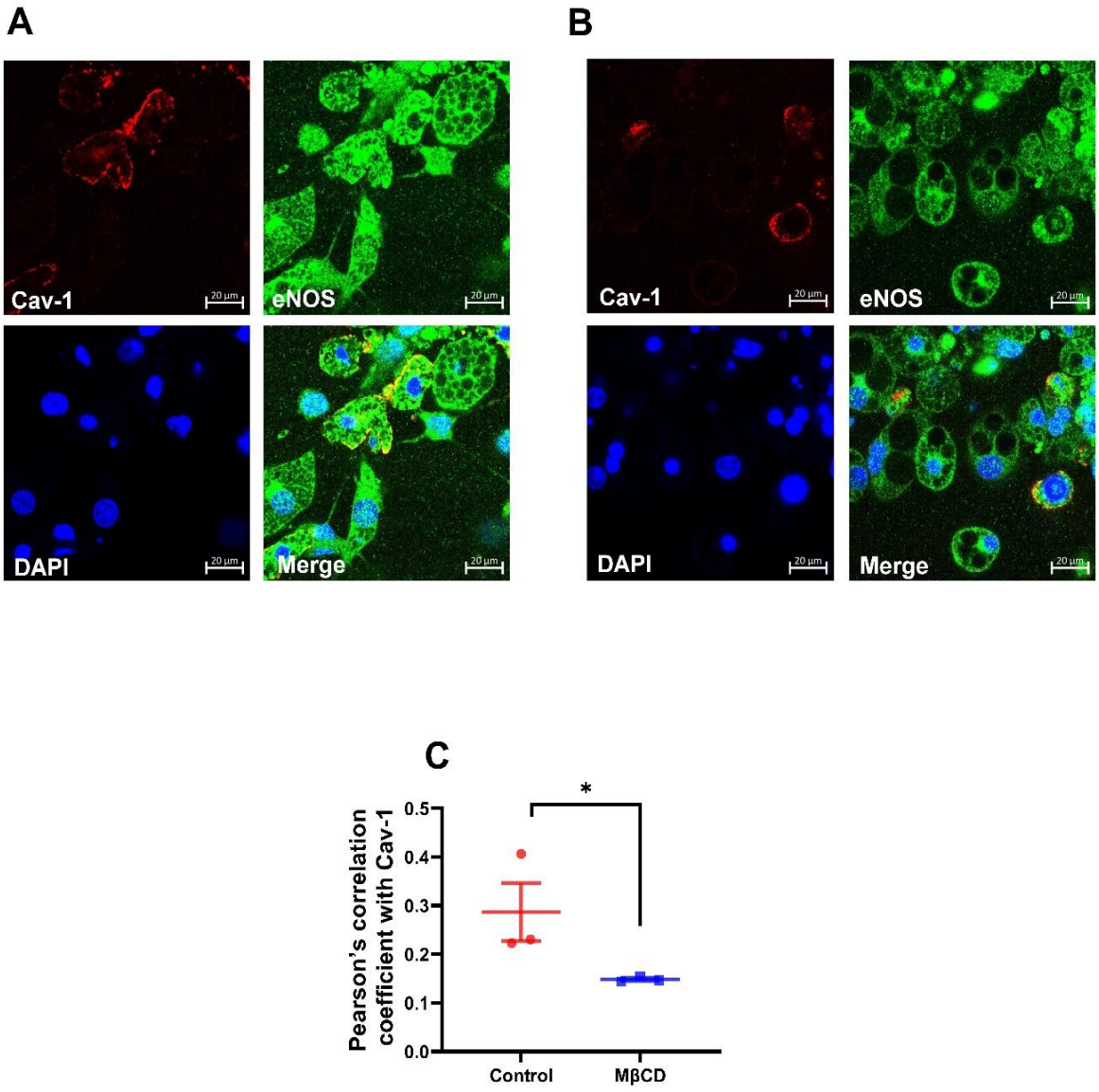

Figure 4-5: Methyl-β-cyclodextrin reduces Cav-1/ eNOS co-localisation in 3T3-L1 adipocytes

3T3-L1 adipocytes were incubated in the presence or absence of MβCD (1 mM) for 6 h. Coverslips of 3T3-L1 cells were incubated with anti-Cav-1 and anti-eNOS antibodies and analysed by immunofluorescence confocal microscopy. Representative micrographs from (A) control and (B) MβCD-treated cells. DAPI was used to stain cell nuclei. Scale bar = 20 µm. (C) Quantification using Pearson's correlation coefficient from three biological replicates with 50 cells per group. * $p<0.05$ compared to control. Statistical significance was determined by Student's t-test (unpaired).

4.4.5 Methyl-β-cyclodextrin increases NO synthesis in 3T3-L1 preadipocytes and adipocytes

As MβCD disrupted Cav-1 co-localisation with eNOS, the effect of MβCD on NO production in preadipocytes and adipocytes was examined. To determine the most suitable conditions for this experiment, the cells were incubated with a series of concentrations of MβCD between (0.1 mM to 5 mM) and different time points (2 h, to 24 h). The results from these optimization experiments guided the selection of the concentration and incubation time used in these experiments. Incubation of 3T3-L1 preadipocytes or adipocytes with MβCD (1 mM) for 6 h was associated with significant increases in NO production both in preadipocytes and adipocytes (Figure 4-6 A&B), without altering total cellular Cav-1 levels (Figure 4-6 C&D). Therefore, these data suggest that any NO synthesised is likely to be generated by eNOS in 3T3-L1 adipocytes as MβCD did not increase iNOS levels (Figure 4-6 E&F).

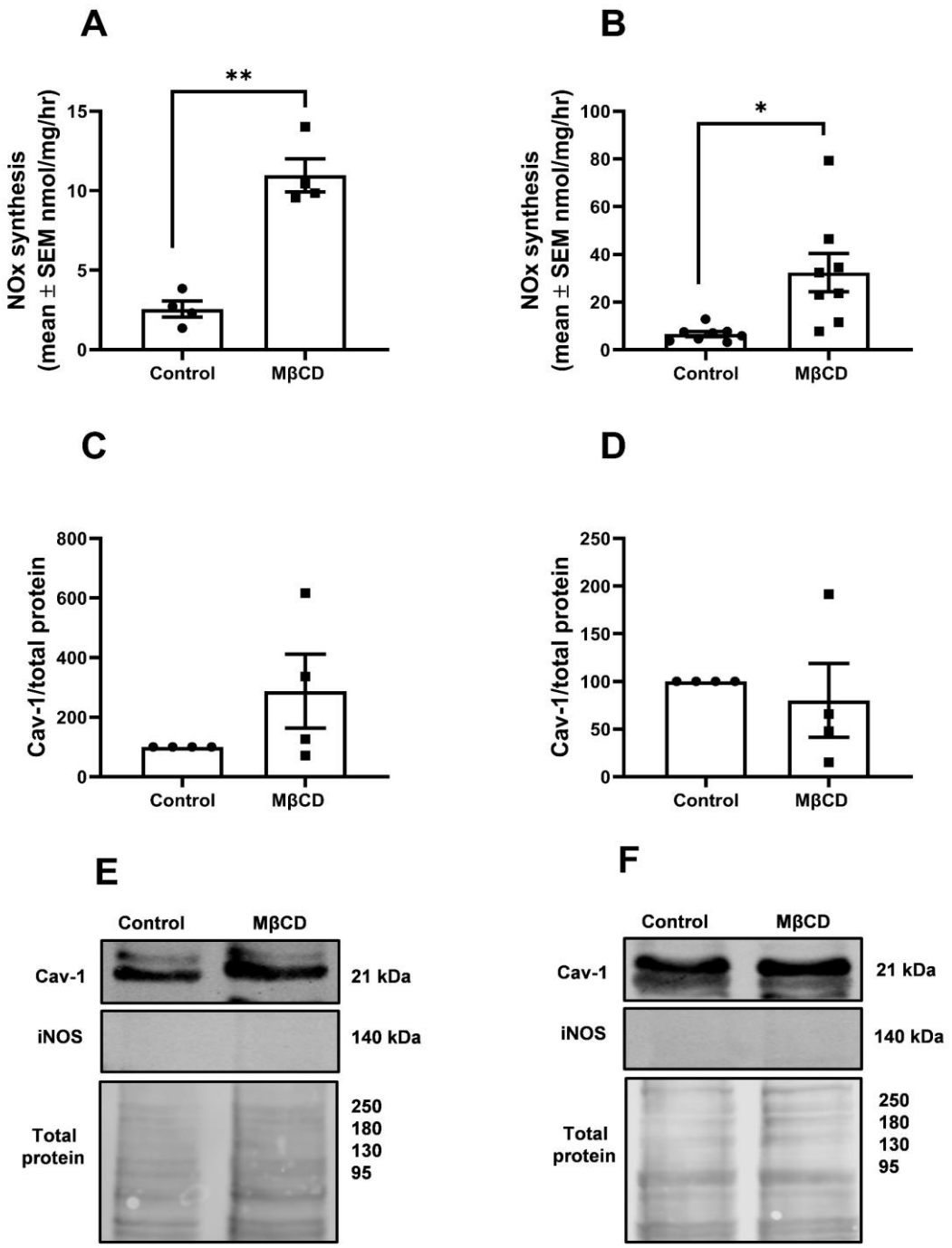

Figure 4-6: Disruption of caveolae with methyl-β-cyclodextrin increases NO synthesis by preadipocytes and adipocytes

3T3-L1 preadipocytes (A, C, E) or adipocytes (B, D, F) were incubated in the presence or absence of MβCD (1 mM) for 6 h, and (A, B) conditioned medium was collected. Medium was assayed for NO + NO_2^- (NOx) content using a Sievers 280 NO analyser. Data shown represent the mean ± SEM nmol NOx synthesis/mg protein/h from (A) 4 or (B) 8 independent experiments. Lysates from preadipocytes (C & E) or adipocytes (D & F), (20 µg) were resolved by SDS-PAGE and immunoblotted with anti-caveolin-1 (Cav-1) antibodies. (C, D) Quantification of mean ± SEM % control Cav-1 relative to total lysate protein assessed with REVERT total protein stain. (E & F) Representative images from 4 independent experiments. *p<0.05, **p<0.01, Statistical significance was determined by Student's t-test (unpaired).

4.4.6 Effect of geldanamycin on NO production in both preadipocytes and adipocytes

It has been demonstrated that Hsp-90 plays an important role in the maintenance of dimer structure and activity of eNOS (Chen *et al.*, 2014). Given that, it was of interest to investigate the role of Hsp-90 in the regulation of NO production in 3T3-L1 preadipocytes and adipocytes using the Hsp-90 inhibitor geldanamycin (Miyata, 2005). 3T3-L1 preadipocytes and adipocytes were incubated with geldanamycin (10 μM) for 6h and NO generated in conditioned media was measured. Geldanamycin had no effect on NO synthesis in either cell type (Figure 4-7 A&B).

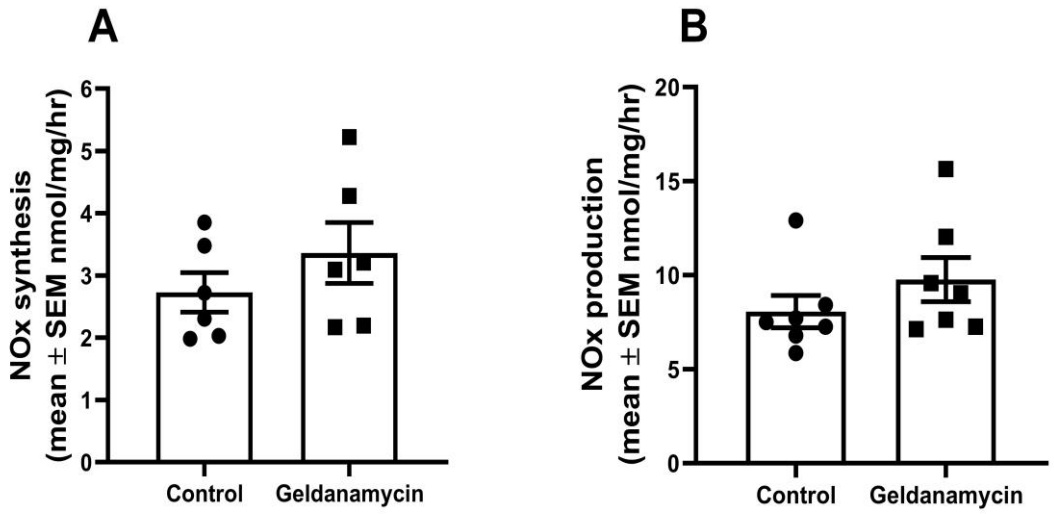

Figure 4-7: Effect of geldanamycin on NOx production in 3T3-L1 preadipocytes and adipocytes

3T3-L1 (A) preadipocytes (B) adipocytes were incubated in the presence or absence of geldanamycin (10 μM) for 6 h and conditioned medium was collected. Medium was assayed for NO + NO_2^- (NOx) content using a Sievers 280 NO analyser. Data shown represent the mean ± SEM nmol NOx synthesis/mg protein/h from 6-7 independent experiments.

4.4.7 Effect of AMPK activation by compound 991 on NO production in 3T3-L1 preadipocytes and adipocytes

In chapter 3, PVAT from AMPK KO mice produced less NO compared with PVAT from WT mice. AMPK activation has been previously reported to increase NO synthesis in several cell types, yet it is unknown whether AMPK activation increases NO synthesis in 3T3-L1 preadipocytes and adipocytes. The selective, direct allosteric AMPK activator, compound 991 (Willows *et al.*, 2017a) was therefore used to activate AMPK in 3T3-L1 cells. 3T3-L1 preadipocytes and adipocytes were incubated with (5 μM) compound 991 for 6 h, and NO generated in conditioned media was measured. To assess AMPK activation, the phosphorylation of the AMPK substrate, acetyl CoA carboxylase (ACC) at Ser^{79} was determined by western blotting. There was a significant increase in phosphorylation of ACC following compound 991 treatment compared with control both in preadipocytes and adipocytes (Figure 4-8 A&B). Compound 991 increased NO production in preadipocytes, but the effect did not achieve statistical significance, while it had no effect on NO production in adipocytes (Figure 4-9 E&F).

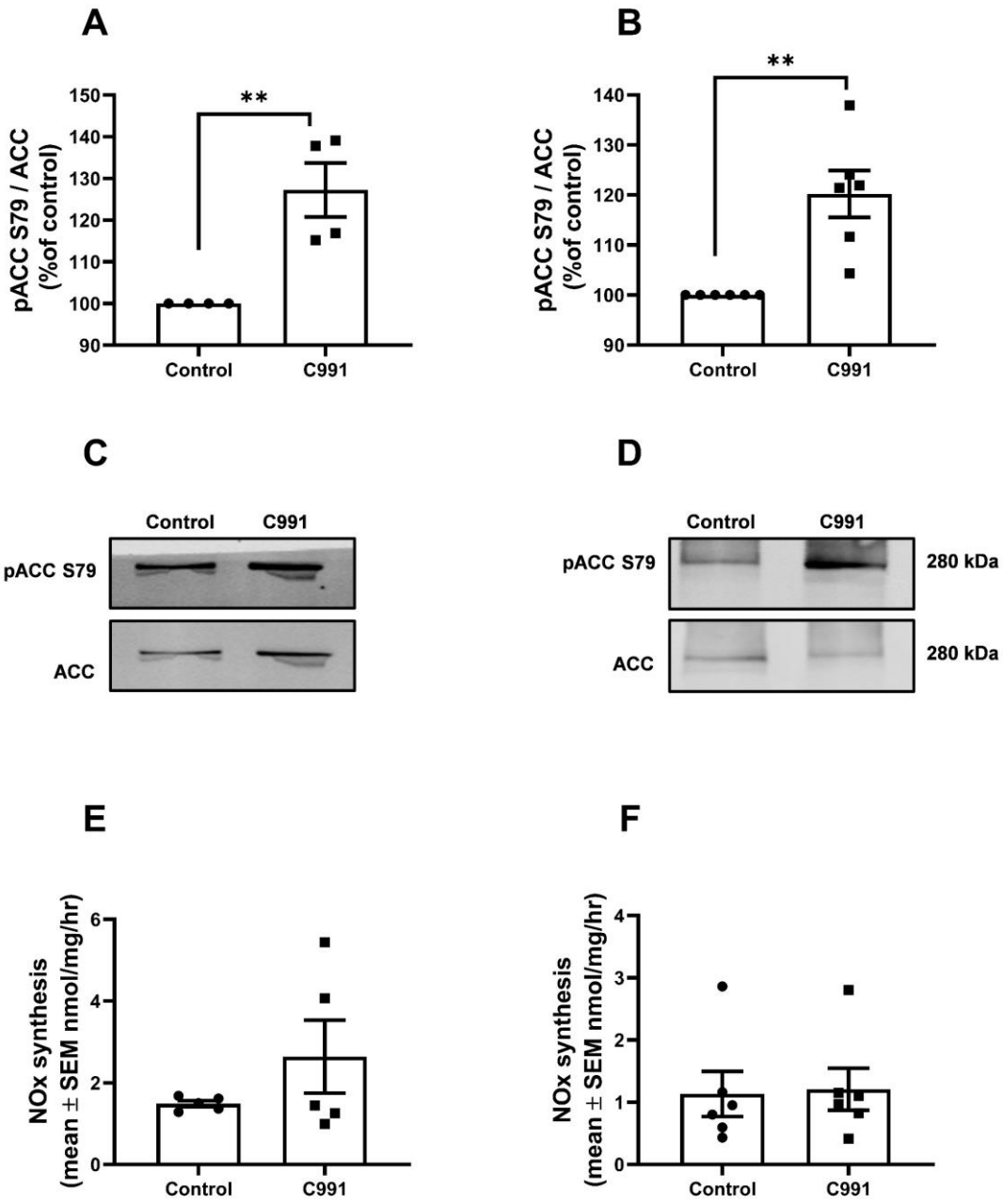

Figure 4-8: Effect of Compound 991 on ACC phosphorylation and NOx production in 3T3-L1 preadipocytes and adipocytes

3T3-L1 preadipocytes (A & C) or adipocytes (B & D) were incubated with compound 991 (5 µM) for 6h and lysates prepared. Lysates (20µg) were resolved by SDS-PAGE and subjected to immunoblotting with the indicated antibodies. (A, B) Quantification of phospho-ACC S79 (pACC S^{79}) normalized to total ACC levels. Graphs show mean ± SEM % control phosphorylation from four to six independent experiments. (C& D) Representative western blots. Conditioned medium was collected from (E) preadipocytes and (F) adipocytes and assayed for NO + NO_2^- (NOx) content after stimulation in the presence or absence of 5 µM compound 991 for 6h using a Sievers 280 NO analyser. Data shown represent the mean ± SEM nmol NOx synthesis/mg protein/h from five to six independent experiments. **p<0.01, Statistical significance was determined by Student's t-test (unpaired).

4.4.8 Effect of AICAR and A769662 on NO production in 3T3-L1 preadipocytes and adipocytes

Compound 991 has previously been demonstrated to have higher potency for AMPK complexes containing the β1 regulatory subunit (Ngoei *et al.*, 2018), yet studies in our laboratory have indicated that 3T3-L1 adipocytes have substantial AMPK activity due to complexes containing the β2 regulatory subunit (Katwan *et al.*, 2019). To further study the potential effect of AMPK on NO production in 3T3-L1 cells, 5-aminoimidazole-4-carboxamide ribonucleoside (AICAR) and A769662 were also used. AICAR is an adenosine analogue which enters cells via adenosine transporters and is phosphorylated to the nucleotide ZMP, which mimics the effect of AMP on AMPK, thereby activating AMPK complexes containing both β1 and β2 regulatory subunits. A769662 is similar to compound 991, a direct allosteric activator of AMPK that is selective for complexes containing the β2 regulatory subunit (Strembitska *et al.*, 2018). Cultured 3T3-L1 cells were pre-incubated with either AICAR (2 mM) for 6 h or A769662 (300 μM) for 6 h. AICAR significantly increased ACC phosphorylation both in preadipocytes and adipocytes compared with control, whereas A769662 caused a trend towards increased phosphorylation which was not significant (Figure 4-9 A &B). AICAR stimulated NO production in preadipocytes and adipocytes, but this did not achieve statistical significance, while A769662 had no effect on NO production in preadipocytes and adipocytes (Figure 4-9 E &F).

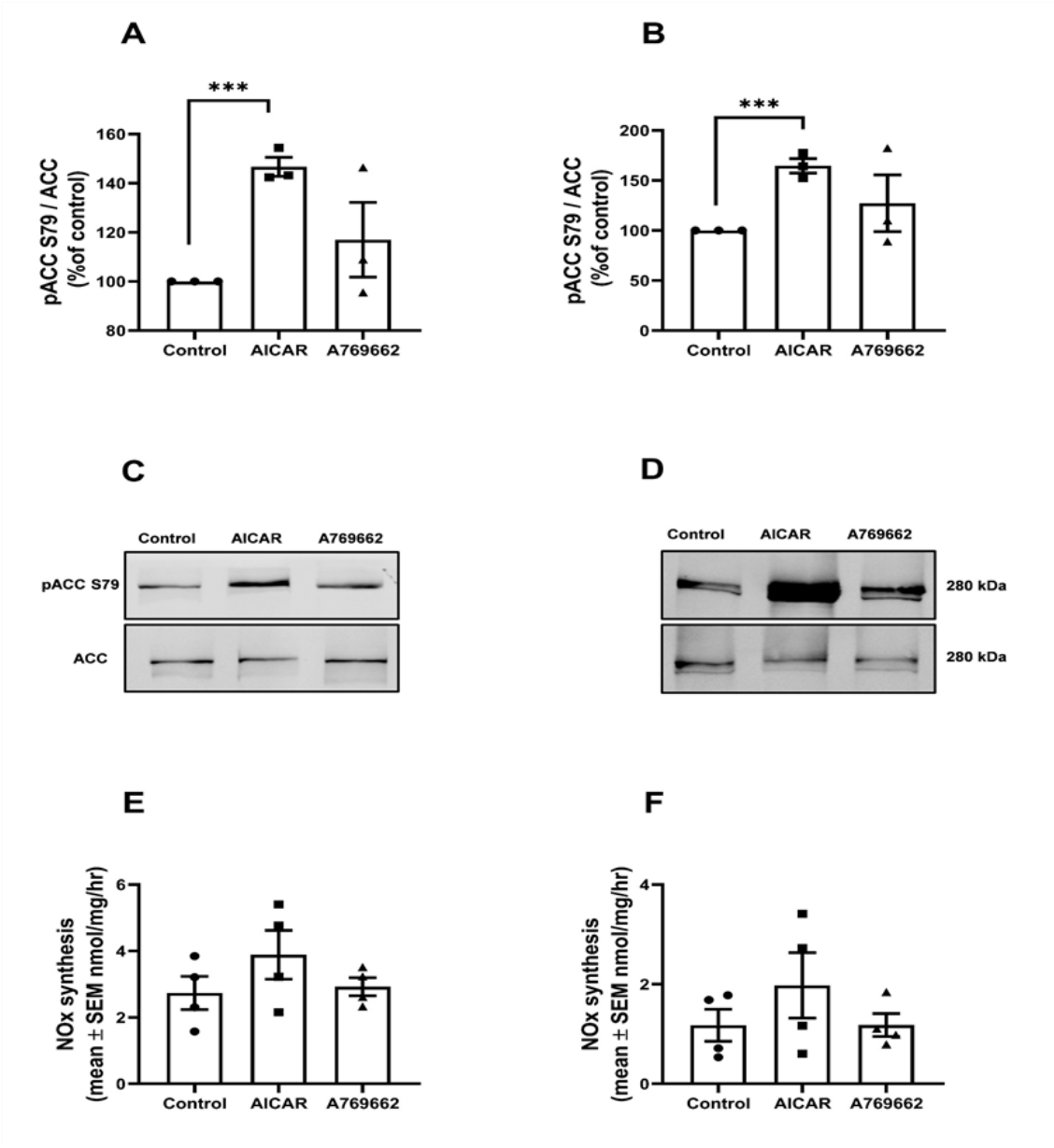

Figure 4-9: Effect of AICAR and A769662 on ACC phosphorylation and NO production in 3T3-L1 preadipocytes and adipocytes

3T3-L1 preadipocytes (A & C) or adipocytes (B & D) were incubated with AICAR or A769662 for 6 h, and lysates prepared. Lysates (20µg) were resolved by SDS-PAGE and subjected to immunoblotting with the indicated antibodies. (A, B) Quantification of phospho-ACC S79 (pACC S^{79}) normalized to total ACC levels. Graphs show mean ± SEM % control phosphorylation from four independent experiments. (C & D) Representative western blots. (A & B) Phosphorylation of ACC S79 (pACC S^{79}) was analysed by western blot of whole lysates normalized to total ACC levels. All graphs show mean ± SEM of AICAR and A769662-stimulated phosphorylation from four independent experiments. Conditioned medium was collected from (E) preadipocytes and (F) adipocytes and assayed for NO + NO_2^- (NOx) content after stimulation in the presence or absence of for AICAR (2 mM) or A769662 (300 µM) for 6h using a Sievers 280 NO analyser. Data shown represent the mean ± SEM nmol NOx synthesis/mg protein/h from six independent experiments. **p<0.01, ***p<0.001. Statistical significance was determined by two-way ANOVA (with Tukey's test).

4.4.9 Effect of compound C on NO production in 3T3-L1 preadipocytes and adipocytes

Compound C (CC) is an AMPK inhibitor and has been widely used as an experimental tool to block the effects of AMPK activators such as AICAR (Zhou *et al.*, 2001). Here we sought to investigate the effect of CC-related AMPK inhibition on the extent of NO production by 3T3-L1 preadipocytes and adipocytes. CC (60 μM) for 6 h significantly reduced ACC phosphorylation in adipocytes; however, it had no effect in preadipocytes (Figure 4-10 A&B). Furthermore, CC had no effect on NO production in 3T3-L1 preadipocytes or adipocytes (Figure 4-10 E & F).

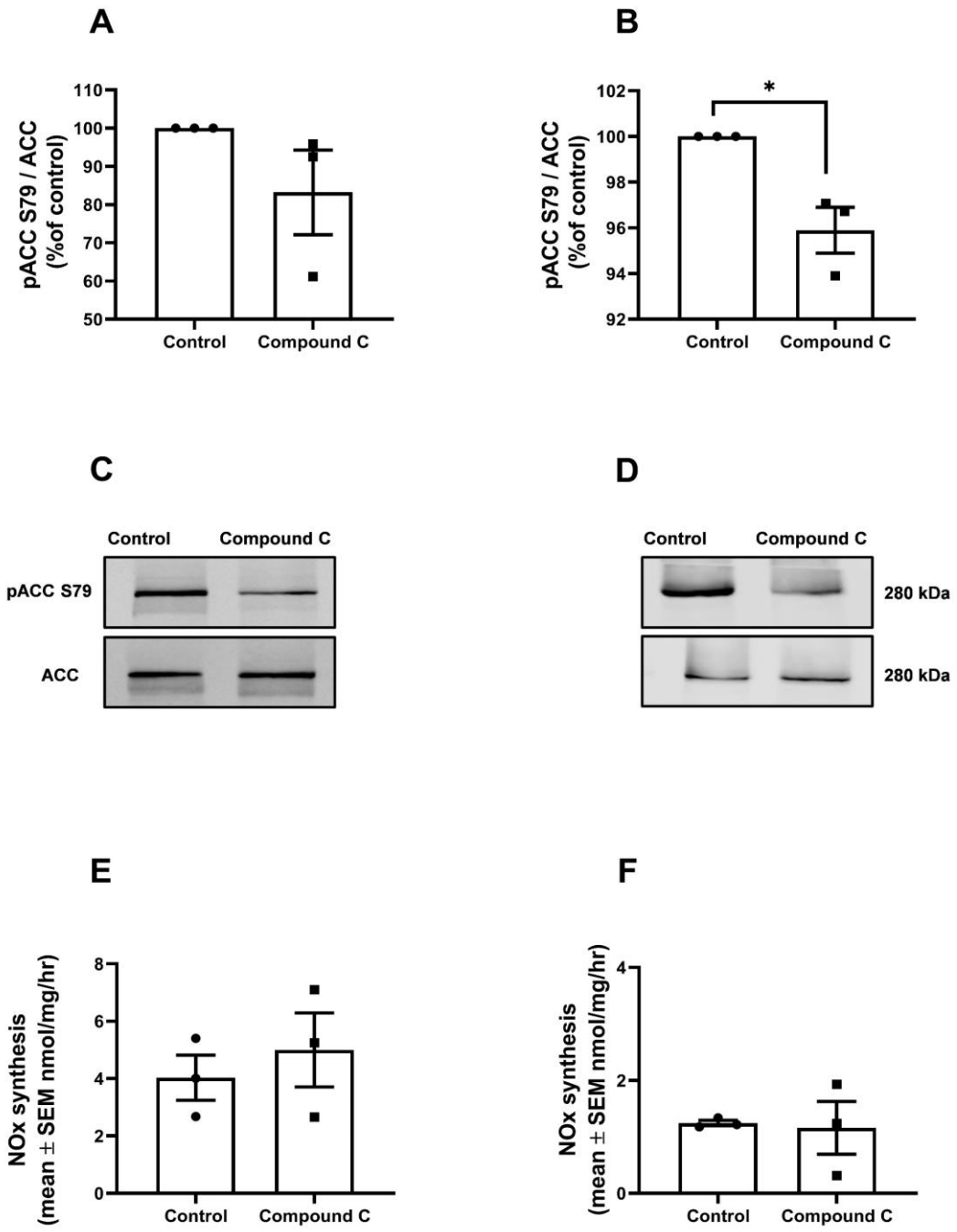

Figure 4-10: Effect of compound C on ACC phosphorylation and NO production in 3T3-L1 preadipocytes and adipocytes

3T3-L1 preadipocytes (A & C) adipocytes (B & D) were incubated with (60µM) compound C for 6 h and lysates prepared. Lysates (20µg) were resolved by SDS-PAGE and subjected to immunoblotting with the indicated antibodies. (A, B) Quantification of phospho-ACC S^{79} (pACC S^{79}) normalized to total ACC levels. Graphs show mean ± SEM % control phosphorylation from three independent experiments. (C & D) Representative western blots. Conditioned medium was collected from (E) preadipocytes and (F) adipocytes and assayed for NO + NO_2^- (NOx) content after stimulation in the presence or absence of (60) µM compound C for 6h, using a Sievers 280 NO analyser. Data shown represent the mean ± SEM nmol NOx synthesis/mg protein/h from three independent experiments. *p<0.05. Statistical significance was determined by Student's t-test (unpaired).

4.5 Discussion

This study investigated NOS levels, in particular eNOS, and NO production during adipogenesis in 3T3 adipocytes. In addition, the role of AMPK in NO production was studied using AMPK activators A769662, AICAR, and compound 991 as well as compound C as an AMPK inhibitor. To investigate the regulation of NO formation by Cav-1 and its co-localisation with eNOS in 3T3-L1 preadipocytes and adipocytes, the cell membrane cholesterol disrupter compound MβCD and Hsp-90 inhibitor geldanamycin were used. The principal findings in this chapter are that eNOS levels were markedly reduced during adipogenesis after day 3 and consistent with that, the level of NO production was reduced during adipogenesis. NO production can be attributed largely to eNOS activity as no immunoreactivity was observed throughout adipogenesis for other NOS isoforms (iNOS and nNOS). However, iNOS could be induced by incubating both preadipocytes and adipocytes with IL-1β or TNF-α and this resulted in increased NO production. Incubation of 3T3-L1 preadipocytes or adipocytes with MβCD was associated with a noticeable reduction in Cav-1/eNOS colocalization and a significant increase in NO production both in preadipocytes and adipocytes compared with non-treated cells. Finally, stimulation of AMPK with compound 991 and AICAR increased ACC phosphorylation without altering the levels of NO production in 3T3-L1 adipocytes, whereas compound C inhibited AMPK activity without altering NO production.

Initial studies were undertaken to measure the levels of eNOS and NO production during adipogenesis. This study showed that there was a significant reduction in the level of eNOS during 3T3-L1 adipogenesis, this was consistent with a significant reduction in NO production during adipogenesis (Figure 4-1 A). During adipogenesis the levels of eNOS were reduced and became undetectable by immunoblotting. Interestingly, since NO was still measurable after day 6, despite blots showing undetectable eNOS expression, there must still be small amounts of active eNOS in the cells at this time point. In addition, any NO synthesised is likely to be generated by eNOS in 3T3-L1 adipocytes as no immunoreactivity was observed throughout adipogenesis using anti-iNOS and anti-nNOS antibodies (Figure 4-1 D). This is consistent with a previous study showing that neither iNOS nor nNOS was detected in either 3T3-L1 preadipocytes or differentiating adipocytes (Yamada *et al.*, 2015).

In previous studies it has been demonstrated that lipopolysaccharide (LPS) and several proinflammatory cytokines induce iNOS in 3T3-L1 adipocytes which mediates downregulation of leptin induced by an IFN-γ–LPS mixture (Unno *et al.*, 2006). The data demonstrated that NO derived from iNOS mediates downregulation of the inflammatory response to external stimuli, indicates the important role of NO in adipocyte function. It was therefore of importance to confirm whether stimulation of iNOS upregulation by either IL-1ß or TNF-α in 3T3 cells leads to the release of a measurable amount of NO into the culture medium.

In this study, we have shown that incubation of preadipocytes with IL-1ß has no effect on NO production and does not alter iNOS levels. This could be due to a lack of IL-1ß signalling in preadipocytes, presumably upstream of transforming growth factor beta activated kinase-1 (TAK1) and I-kappa B kinase complex (IKK), which are used by both IL-1ß and TNF-α in proinflammatory signalling. In contrast, an earlier study demonstrated that human preadipocytes are highly sensitive to IL-1ß after 24 h of treatment (Alomar *et al.*, 2016), whereas TNF-α significantly increased NO production (Figure 4-2 A &B) consistent with the increase in iNOS levels in preadipocytes compared with untreated cells (Figure 4-3 A). In adipocytes, incubation with IL-1ß significantly increases NO (Figure 4-2 B) and iNOS levels (Figure 4-3 B), compared to the basal level, after 24h of treatment.

These data are partially inconsistent with a recent study which showed that IL-1ß induces high iNOS expression in 3T3-L1 preadipocytes, which largely depends on the activities of PKCs, JAKs/STATs and Src kinase (Park *et al.*, 2021). However, the ability of the proinflammatory cytokines studied here to induce iNOS expression in mature 3T3-L1 adipocytes and human preadipocytes remains elusive. Other cytokines have been studied and another group demonstrated a 12-fold increase in NO production by incubation of adipocytes with IFN-γ and a 10-fold increase in NO production in cells preincubated with LPS (Kapur *et al.*, 1999).

Caveolin-1 is the main coat protein of caveolae. The effect of depletion of caveolae from the cell membrane with MßCD has been previously demonstrated to down-regulate Cav-1 in human dermal fibroblasts (Lee *et al.*, 2015). In addition, It has been shown that eNOS localisation influences the enzyme's activity and NO production in endothelial cells (Chakraborty and Ain, 2017). Given that, eNOS translocation to the plasma membrane leads to its association with Cav-1 which

contributes to reduced enzymatic activity and consequently reduced NO production (Wang *et al.*, 2009). It is well known that under normal conditions eNOS undergoes a dynamic spatio-temporal subcellular translocation from cell membrane to Golgi apparatus and consequently, eNOS localised within the cell membrane also undergo internalisation from the plasma membrane to the cytoplasm after activation. Therefore, trafficking and localisation of eNOS may be essential for its activity (Ortiz and Garvin, 2003, Dudzinski *et al.*, 2006). In addition, another group showed that intracellular localisation of eNOS in the cytoplasm regulates its activity (Fulton *et al.*, 2004). To date, it appears that very little has been done to investigate the subcellular colocalization of Cav-1 and eNOS in adipocytes, therefore it is an important area for further investigation.

In the present study 3T3-L1 preadipocytes and adipocytes had a significant reduction in Cav-1/eNOS colocalization in cells incubated with MβCD compared with control (Figure 4-4 and Figure 4-5), indicating that cholesterol depletion with MβCD may disrupt the Cav-1/eNOS coupling leading to a reduction in the colocalization. In addition, incubation of either 3T3-L1 preadipocytes or adipocytes with MβCD was associated with a significant increase in NO production (Figure 4-6 A&B) but without any alteration in the total cellular Cav-1 levels (Figure 4-6 C&D). To rule out the possibility that the increase in NO production was generated by isoforms other than eNOS, the level of iNOS and nNOS was assessed and neither of them could be detected in 3T3-L1 lysates incubated with MβCD (Figure 4-6 E&F). This strongly suggests that the NO produced is most likely due to the eNOS activity.

Hsp-90 is one of a number of abundant molecular chaperones involved in various cellular processes including: post-translational modification, protein folding and cellular differentiation (Hu *et al.*, 2020). Although the role of Hsp-90 in regulating eNOS activity in endothelial cells has been partially studied, its role in regulation of eNOS activity in adipocytes remains elusive. It was demonstrated in chapter 3 that abdominal PVAT expresses more Hsp-90 in an eNOS immunoprecipitate compared with thoracic PVAT, so the question raised here was whether the reduction in NO production in abdominal PVAT is linked with the elevated levels of Hsp-90. In addition, it was found that geldanamycin had no effect on NO

production both in 3T3-L1 preadipocytes and adipocytes compared with control (Figure 4-7 A&B). These data suggest that Hsp-90 has either little or negligible effect on eNOS function in adipocytes.

Previous studies have shown that AICAR stimulates an increase in AMPK activation in rat primary and human adipocytes and reduces isoproterenol-stimulated lipolysis (Daval *et al.*, 2005, Bourron *et al.*, 2010). While in 3T3-L1 adipocytes AICAR and A769662 do not inhibit glucose uptake in an AMPK-independent manner (Kopietz *et al.*, 2021). In addition, Stimulation of 3T3-L1 adipocytes with either AICAR or A769662 significantly stimulated AMPK activity (Salt *et al.*, 2000, Mancini *et al.*, 2017). In our study we used A769662 which is a thienopyridone compound has been widely used as an AMPK activator (Cool *et al.*, 2006), It activates AMPK reversibly in an allosteric manner and only activates AMPK heterotrimers containing the ß1 subunit and to some extent by protecting AMPK from Thr^{172} dephosphorylation (Göransson *et al.*, 2007, Scott *et al.*, 2008). However, to date the effect of AICAR and A769662 on eNOS activity and NO production in adipocytes has not been investigated. The current study found that AICAR significantly increased ACC Ser^{79} phosphorylation both in preadipocytes and adipocytes compared with control, while A769662 increase the ACC phosphorylation in both cells, albeit not significantly (Figure 4-9 A &B). It is probable that a high degree of basal AMPK activation or the difference between preadipocytes and adipocytes could account for the modest effect of AICAR and A769662 in this experiment; alternatively, A769662 may not be particularly effective in preadipocytes.

Most of the previous studies which have attempted to determine the role of AMPK in regulating NO function have been conducted in endothelial cells rather than adipocytes. However, in endothelial cells there are many lines of evidence to suggest that AICAR-stimulated NO production is mediated by AMPK via increased phosphorylation at Ser^{1177} and activation of eNOS (Morrow *et al.*, 2003). Other studies have demonstrated that AMPK activation by AICAR restores impaired relaxation in mesenteric arteries from a rat model of type 2 diabetes via reduced oxidative stress, increased expression of cyclooxygenase-2 protein but without altering eNOS expression (Fisslthaler and Fleming, 2009). Here we have demonstrated that AICAR increases NO production in preadipocytes compared with

control but not to a statistically significant level, while A769662 had no effect on the NO production in preadipocytes or adipocytes (Figure 4-9 E&F).

Recently, compound 991, a benzimidazole derivative AMPK activator with greater potency, has been developed, it has a mode of action similar to that of A769662 (Xiao *et al.*, 2013). Although A769662 only activates AMPK β1 complexes, compound 991 stimulates β1- and β2-containing complexes but with a preference toward β1, at least in vitro (Xiao *et al.*, 2013, Lai *et al.*, 2014). Our data found that both in preadipocytes and adipocytes there was a significant increase in phosphorylation of ACC following compound 991 treatment compared with control (Figure 4-8 A&B), also compound 991 increased NO production in preadipocytes, but the effect did not achieve statistical significance, while it had no effect on NO production in adipocytes (Figure 4-9 E&F).

Compound C is a widely used AMPK inhibitor, although it is not an AMPK specific inhibitor and also inhibits other protein kinases including phosphorylase kinase (PHK), MAPK interacting-kinase 1 (MNK1), ERK 8 and sarcoma kinase (Src) (Bain *et al.*, 2007). Previous studies have investigated the effect of compound C on adipogenesis (Nam *et al.*, 2008), however, our study is the first to examine the effect of compound C on NO production in preadipocytes and adipocytes. It was found that although compound C significantly reduced ACC phosphorylation in adipocytes, but it had no effect on ACC phosphorylation in preadipocytes (Figure 4-10 A&B). Also, NO production was not altered in either preadipocytes and adipocytes (Figure 4-10 E&F), and that could be due the lack of activity or poorly selective nature of this compound for AMPK (Bain *et al.*, 2007).

In summary, this chapter demonstrated that there was a significant reduction in the level of eNOS during 3T3-L1 adipogenesis and this correlated with a significant reduction in NO production during adipogenesis. In addition, incubation of 3T3-L1 preadipocytes or adipocytes with MβCD was associated with a significant increase in NO production both in preadipocytes and adipocytes via a mechanism likely to be due to disrupting the binding between Cav-1 and eNOS, a conclusion backed-up by the data from the colocalization studies. Taken together, the evidence suggests that manipulating Cav-1/eNOS binding in adipocytes may have beneficial effects in restoration of NO production under conditions or diseases associated with impaired NO bioavailability.

Chapter 5 - Investigating the role of caveolin-1 in the regulation of nitric oxide synthesis by PVAT

5.1 Introduction

In Chapters 3 and 4, it was observed that PVAT generated NO and that this is reduced in AMPKα1 KO mice compared to WT mice. These changes were associated with altered regulation of vessel tone by PVAT, suggesting that PVAT-derived NO is capable of meaningfully regulating vascular tone. In addition, as shown in chapter 4, incubation of 3T3-L1 preadipocytes or adipocytes with MβCD was associated with a noticeable reduction in Cav-1/eNOS colocalization compared with non-treated cells and this was associated with a significant increase in NOx production both in preadipocytes and adipocytes. eNOS is regulated via multiple processes at various levels including protein–protein interactions and posttranslational modifications such as phosphorylation (Garcia *et al.*, 2020b). The regulation of NO and eNOS within PVAT is, however, much less well characterised. As discussed previously, eNOS function is negatively regulated via Cav-1 binding to plasmalemmal anchored eNOS (Hashimoto *et al.*, 2016). Other intracellular proteins have also been shown to regulate eNOS such as Hsp-90, which positively regulates eNOS activity (Gupta *et al.*, 2017), by promoting conformational changes and stabilising the haem moiety in eNOS (Czekay *et al.*, 2011). Furthermore, Hsp-90 has been reported to interact and regulate eNOS activity by recruiting kinases such as AMPK and Akt to phosphorylate eNOS at multiple sites (Ser^{1177}, Ser^{615}, Ser^{633}) and promote an increase in NO synthesis (Fulton *et al.*, 2004).

Given that little is known concerning the potential role of Cav-1 in regulating eNOS activity and NO production in adipocytes and PVAT. Therefore, it is of interest to study whether AMPK regulates Cav-1/eNOS binding as well as the role of Cav-1 in regulating eNOS function in PVAT tissue from WT and $AMPK^{-/-}$ KO mice.

5.2 Aims of the study

1- To assess whether AMPK regulates Cav-1/eNOS binding in PVAT.

2- To assess whether disruption of the Cav-1/eNOS binding in PVAT using a mutant peptide Cav-1 scaffolding peptide (CAV-AP) alters the anticontractile action of PVAT and whether any effect observed is affected by AMPKα1$^{-/-}$ knockout.

5.3 Methods

5.3.1 Analysis of NO synthesis by PVAT and other adipose tissue depots

In this study, adipose tissue from WT and KO mice was collected and incubated in an oxygenated physiological buffer solution to assess the production of nitric oxide (NO) by the perivascular adipose tissue (PVAT). Conditioned media from the incubation were collected and assayed for NO + $NO2^-$ content using a NO analyser. The NO analyser calculated the amount of NO produced by measuring the presence of NO2- in the conditioned medium. To validate the $NO2^-$ reduction, a reducing agent was added to the purge vessel, and the NO analyser measured the resulting chemiluminescence signal converted into an electrical potential.

5.3.2 Functional studies (wire myography)

In functional studies using wire myography, thoracic and abdominal aortae from WT and KO mice were dissected and mounted in a four-channel small vessel wire myograph. The vessels were pre-sensitized and constricted with U46619, followed by the creation of cumulative dose-response curves. The effect of the CAV-AP mutant peptide on vascular reactivity was also studied.

5.3.3 Immunoprecipitation

Immunoprecipitation was carried out using Protein A-conjugated magnetic beads and specific antibodies. Magnetic beads were suspended in PBS, and 100 µL (1 mg) was transferred to 1.5 mL tubes. After magnetization, the supernatant was discarded, and the beads were washed three times. Subsequently, 1 µg of anti-eNOS antibody was added to each 1 mg of beads, and the mixture was incubated

for 1 hour at room temperature. Following incubation, beads were washed three times with IP buffer. Cell lysate was introduced to the beads/antibodies complex and incubated overnight at 4^{0}C. After magnetization, supernatants (immunodepletes) were collected. Beads washes with IP buffer. The elution step involved the addition of 40 µL sample buffer, followed by a 10-minute incubation at 70^{0}C. The eluted samples were then resolved by SDS-PAGE to detect the target proteins.

5.3.4 Confocal microscopy and staining

Confocal microscopy and staining techniques were employed to examine the cellular localization and co-localization of target proteins.3T3-L-1 preadipocytes and adipocytes were cultured on 6-well plates with sterilized 13 mm diameter glass coverslips and treated with either CAV-AP for 6 hours. Following treatment, cells were fixed using paraformaldehyde. Triton was used to permeabilize cells. Cells were then incubated overnight with primary antibodies (anti-eNOS and anti-Cav-1) prepared in IF buffer. Then incubated with secondary antibodies for 1 hour in the dark. Then, coverslips were mounted on glass slides using VECTASHIELD and stored overnight in the dark to dry. Immunolabeled samples were analyzed using a Zeiss LSM 5 exciter laser scanning microscope. Co-localization of eNOS with other proteins was assessed using ImageJ with the BIOP/JACoP plug-in, calculating Pearson’s correlation coefficient.

5.4 Results

5.4.1 Effect of compound C and SBI-0206965 on the level of phospho-Acetyl-CoA Carboxylase

It has been previously demonstrated in chapter 3 that Cav-1/eNOS association was markedly increased in thoracic aortic PVAT from KO mice compared to WT mice, an effect that corresponded with reduced NO production in PVAT from KO mice. Therefore, to investigate the mechanism of the reduced NO production, it was of interest to first determine whether AMPK inhibition alters Cav-1/eNOS binding in thoracic and abdominal PVAT from WT mice. Compound C (dorsomorphin) is an AMPK inhibitor widely used in cell-based, biochemical and *in vivo* assays to study cellular function of AMPK (Liu *et al.*, 2014), although it is poorly selective for AMPK, inhibiting many other kinases more potently (Bain *et al.*, 2007). More recently the Unc-51-like kinase (ULK1) inhibitor SBI-0206965 has been reported to show greater selectivity for AMPK than compound C, inhibiting AMPK and ULK1 at similar concentrations (Dite *et al.*, 2018). To examine whether AMPK was inhibited by compound C or SBI-0206965 in PVAT, thoracic and abdominal PVAT were incubated with compound C (60 μM) or SBI-0206965 (30 μM) for 1h and the phosphorylation of the AMPK substrate, acetyl CoA carboxylase (ACC) at Ser^{79} determined by western blotting. There was an approximate two-fold reduction in phosphorylation of ACC following incubation with either compound C or SBI-0206965 both in thoracic and abdominal PVAT (Figure 5-1 A).

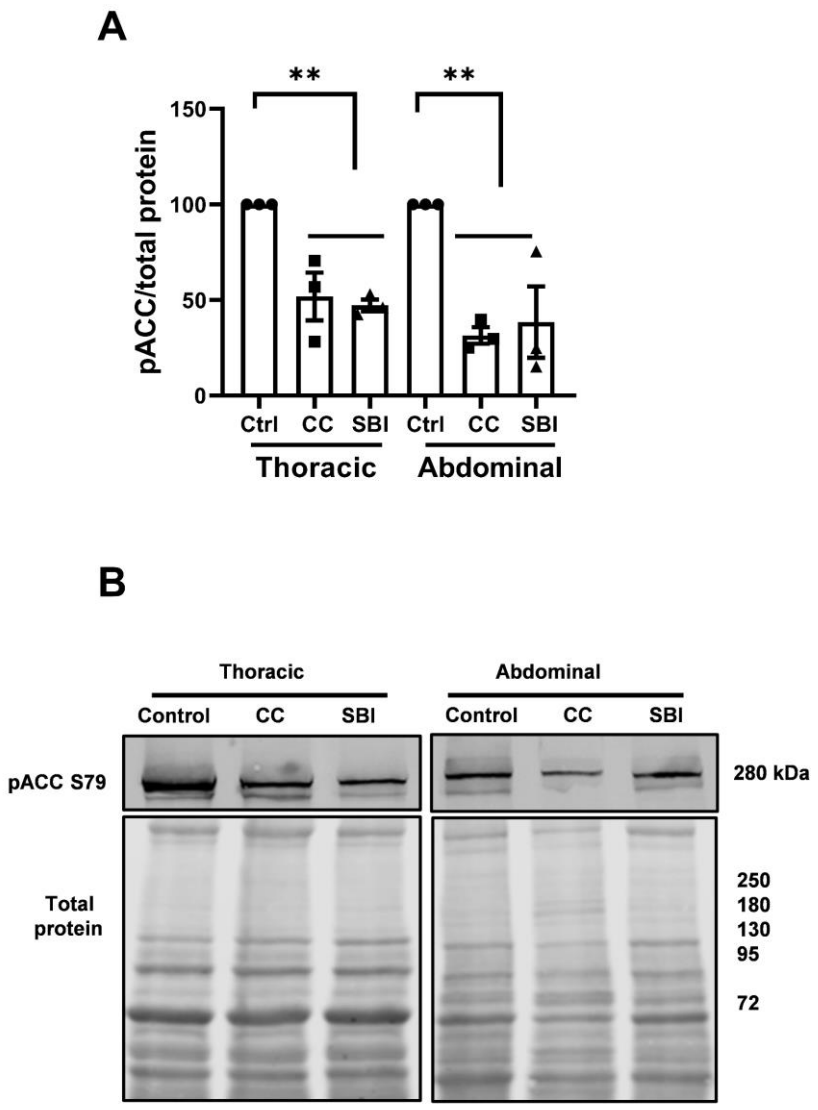

Figure 5-1: Effect of compound C and SBI-0206965 on ACC phosphorylation in thoracic and abdominal PVAT

Thoracic and abdominal aortic PVAT was incubated with (60 µM) compound C (CC) or (30 µM) SBI-0206965 (SBI) for 1 hr and lysates prepared. Lysates containing 20µg of protein were resolved by SDS-PAGE and immunoblotted with antibodies to phospho-Ser^{79} ACC (pACC). (A) Quantification of ACC -Ser^{79} phosphorylation relative to total lysate protein was assessed with REVERT total protein stain (mean ± SEM % relative to control ACC phosphorylation) from three independent experiments. (** $p < 0.01$). Statistical significance was determined by one-way ANOVA (with Tukey's test). (B) Representative immunoblots and total protein-stained blots are shown, with the molecular masses of marker proteins shown (kDa).

5.4.2 Effect of compound C and SBI-0206965 on Cav-1/eNOS and Hsp-90/eNOS binding in thoracic and abdominal PVAT

To further investigate the effect of AMPK inhibition on the level of Cav-1 and Hsp-90 binding to eNOS, PVAT was incubated in the presence or absence of compound C or SBI-0206965 as described in (section 5.3.1). The levels of Cav-1 and Hsp-90 associating with eNOS was assessed by immunoblotting of anti-eNOS immunoprecipitates. Cav-1 and Hsp-90 were both detected in anti-eNOS immunoprecipitates, but the extent of Cav-1/eNOS association was not significantly altered in abdominal and thoracic PVAT incubated with compound C or SBI-0206965 (Figure 5-2 A&B). Similarly, neither compound C nor SBI-0206965 altered Hsp-90/eNOS binding in thoracic and abdominal PVAT (Figure 5-2 C&D).

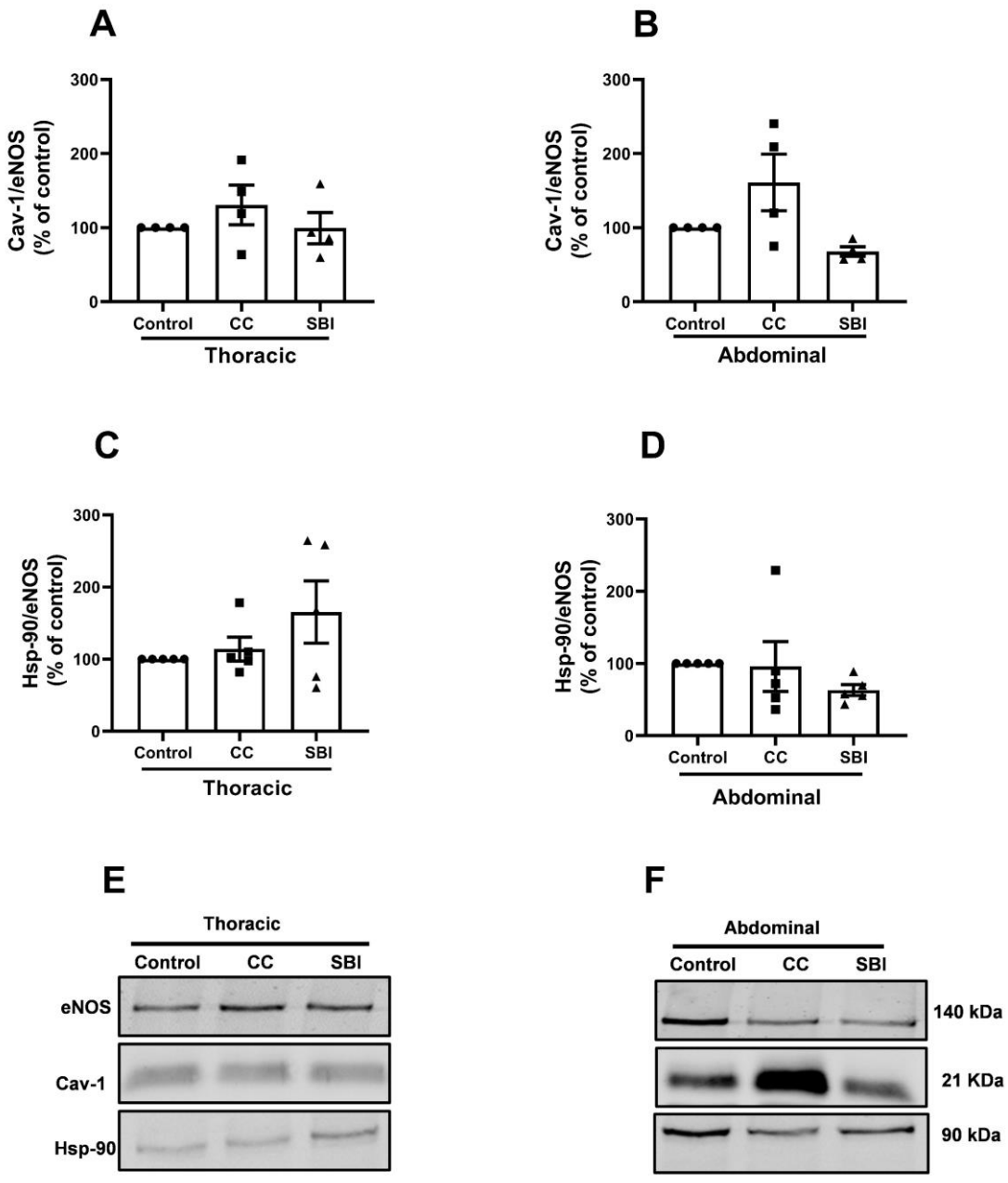

Figure 5-2: Effect of compound C or SBI-0206965 on Cav-1 and Hsp-90 binding to eNOS in thoracic and abdominal PVAT

Thoracic (A) and abdominal (B) aortic PVAT was incubated with (60 µM) compound C or (30 µM) SBI-0206965 for 1 hr and lysates prepared. PVAT lysates (250 µg) were immunoprecipitated with anti-eNOS antibodies. Immunoprecipitated proteins were resolved by SDS-PAGE and immunoblotted with the indicated antibodies. Graphs shown represent the mean ± SEM of (A&B) Cav-1 and (C&D) Hsp-90 levels relative to eNOS from 4-5 independent experiments. (E&F) Representative immunoblots, with the molecular masses of marker proteins shown (kDa).

5.4.3 Effect of compound 991 on Cav-1 and Hsp-90 /eNOS binding in thoracic and abdominal PVAT

To further determine whether AMPK activity influenced Cav-1 and Hsp-90/eNOS binding, thoracic and abdominal PVAT from WT mice was incubated with the AMPK activator compound 991 (10 μM) for 1 h. As with previous experiments with AMPK inhibitors, phosphorylation of ACC at Ser^{79} was determined by western blotting to assess effectiveness of activation. Compound 991 had no statistically significant effect on ACC phosphorylation (Figure 5-3 A&B). To examine whether compound 991 altered levels of Cav-1 or Hsp-90 associated with eNOS, eNOS was immunoprecipitated from thoracic and abdominal PVAT lysates. The data reported that No difference was found in the level of Cav-1 or Hsp-90 binding to eNOS after incubation with compound 991 (Figure 5-3).

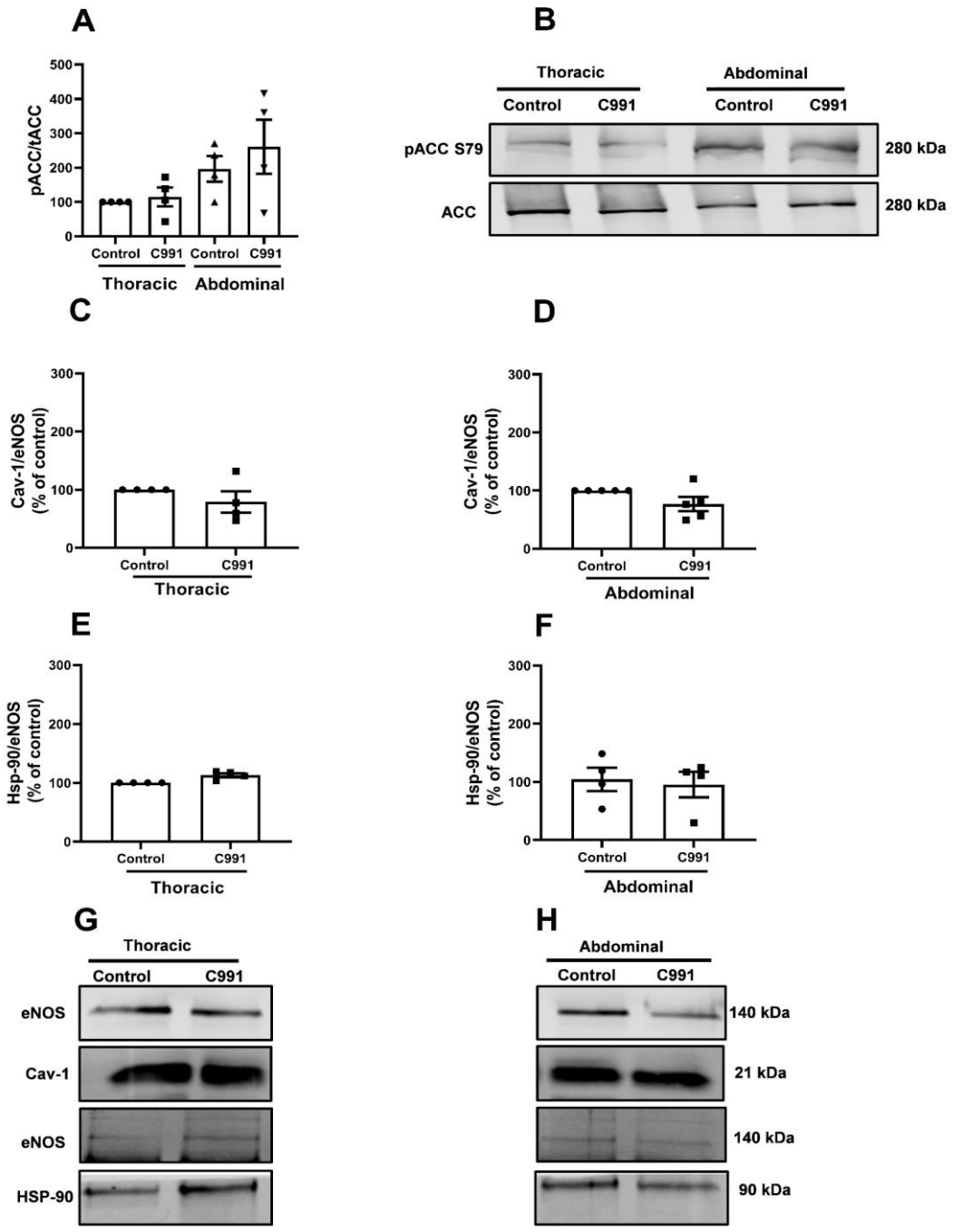

Figure 5-3: Effect of compound 991 on ACC phosphorylation and association of Cav-1 or Hsp-90 with eNOS in thoracic and abdominal PVAT

Thoracic and abdominal aortic PVAT tissues were incubated with (10 µM) compound 991 for 1 hr and lysates prepared. (A&B) Lysates were resolved by SDS-PAGE and immunoblotted with anti-phospho ACC Ser^{79} or anti-ACC antibodies. (A) Quantification of phospho-ACC S79 (pACC Ser^{79}) normalized to total ACC levels, mean ± SEM % thoracic control from four independent experiments. (B-F) PVAT lysates (250 µg) were immunoprecipitated with anti-eNOS antibodies. Immunoprecipitated proteins were resolved by SDS-PAGE and immunoblotted with the indicated antibodies. (C) Cav-1 and (D) Hsp-90 levels relative to the eNOS from 4-5 independent experiments (mean ± SEM % thoracic control). (G&H) Representative immunoblots, with the molecular masses of marker proteins shown (kDa).

5.4.4 CAV-AP peptide increases NO synthesis in thoracic PVAT from AMPKα1$^{-/-}$ mice but not in WT mice

A cell permeable mutant scaffolding domain peptide of Cav-1 has previously been reported to disrupt the inhibitory action of Cav-1 on eNOS, thereby alleviating inhibition of NO production (Bernatchez *et al.*, 2011). To examine whether disruption of Cav-1 binding to eNOS could rescue the impaired NO synthesis in thoracic PVAT from KO mice, PVAT from WT and KO mice was incubated with the mutant cell-permeable scaffolding domain peptide of Cav-1 (CAV-AP, 10 μM for 6h) or an antennapedia control peptide and NO production measured in conditioned media. CAV-AP increased NO release by thoracic PVAT from KO mice but not WT mice but did not have any effect in abdominal aortic PVAT from either WT or KO mice (Figure 5-4 A&B).

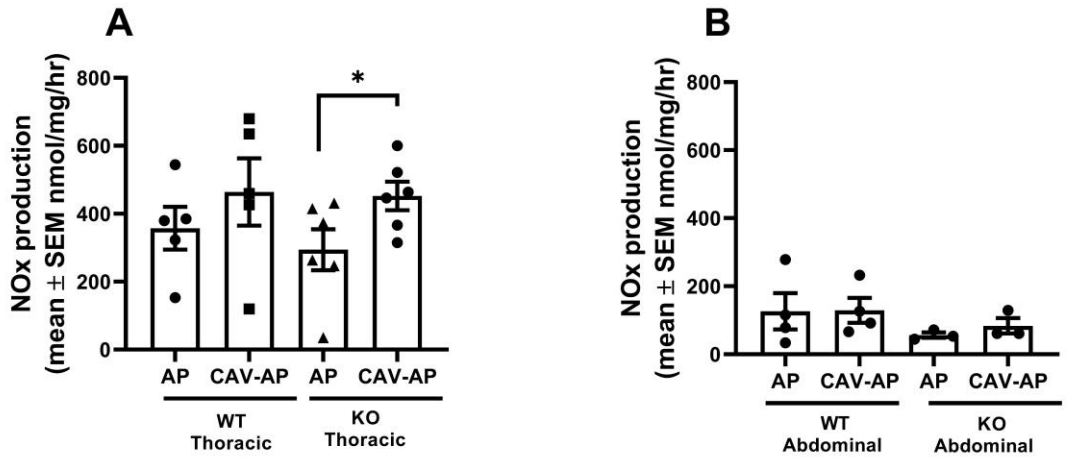

Figure 5-4: CAV-AP peptide increases NO synthesis by thoracic PVAT from AMPKα1$^{-/-}$ mice but not WT mice

Conditioned media was generated from (A) thoracic and (B) abdominal PVAT of WT and KO mice incubated with CAV-AP or antennapedia (AP) control peptide (10 Mm) for 6 h and assayed for NO_x content using a Sievers 280 NO analyser. Data shown represent the mean ± SEM nmol NOx synthesis/mg protein/h from (A) 6-7 or (B) 3-4 independent experiments, * $p < 0.05$. Statistical significance was determined by two-way ANOVA (with Tukey's test).

5.4.5 CAV-AP suppresses phenylephrine-stimulated contraction of thoracic aortic rings from AMPKα1$^{-/-}$ mice

To assess if disruption of the Cav-1/eNOS association in PVAT can influence vascular function, abdominal and thoracic aortic rings with intact PVAT from WT or KO mice were incubated with antennapedia as a control peptide or CAV-AP as a disruptive peptide for Cav-1/eNOS binding and vascular contractile responses to phenylephrine (PE) were examined. In order to rule out effects of NO produced by the endothelium, all rings in these experiments were denuded before being mounted in the myograph. As seen in (Figure 5-5 A), CAV-AP reduced PE-induced tension development in both WT (EC_{50} = 439± 147 nM vs. 212 ± 60 nM in control vessels; n=6; *p<0.05), and KO (EC_{50} = 302 ± 74 nM vs. 184 ± 36 nM in control vessels; n=6; *p<0.05) thoracic aortic rings. However, in abdominal aortic rings, CAV-AP had no effect in either WT (EC_{50} = 263 ± 73 nM vs. 234 ± 45 nM in control vessels; n=6) or KO (EC_{50} = 321 ± 99 nM vs. 340 ± 145 nM in control vessels; n=6) (Figure 5-5 B). These data are consistent with CAV-AP disruption of Cav-1/eNOS binding in PVAT, allowing greater generation of NO to oppose vessel constriction. Greater association of Cav-1 with eNOS in KO PVAT could underlie lower NO generation by KO thoracic PVAT.

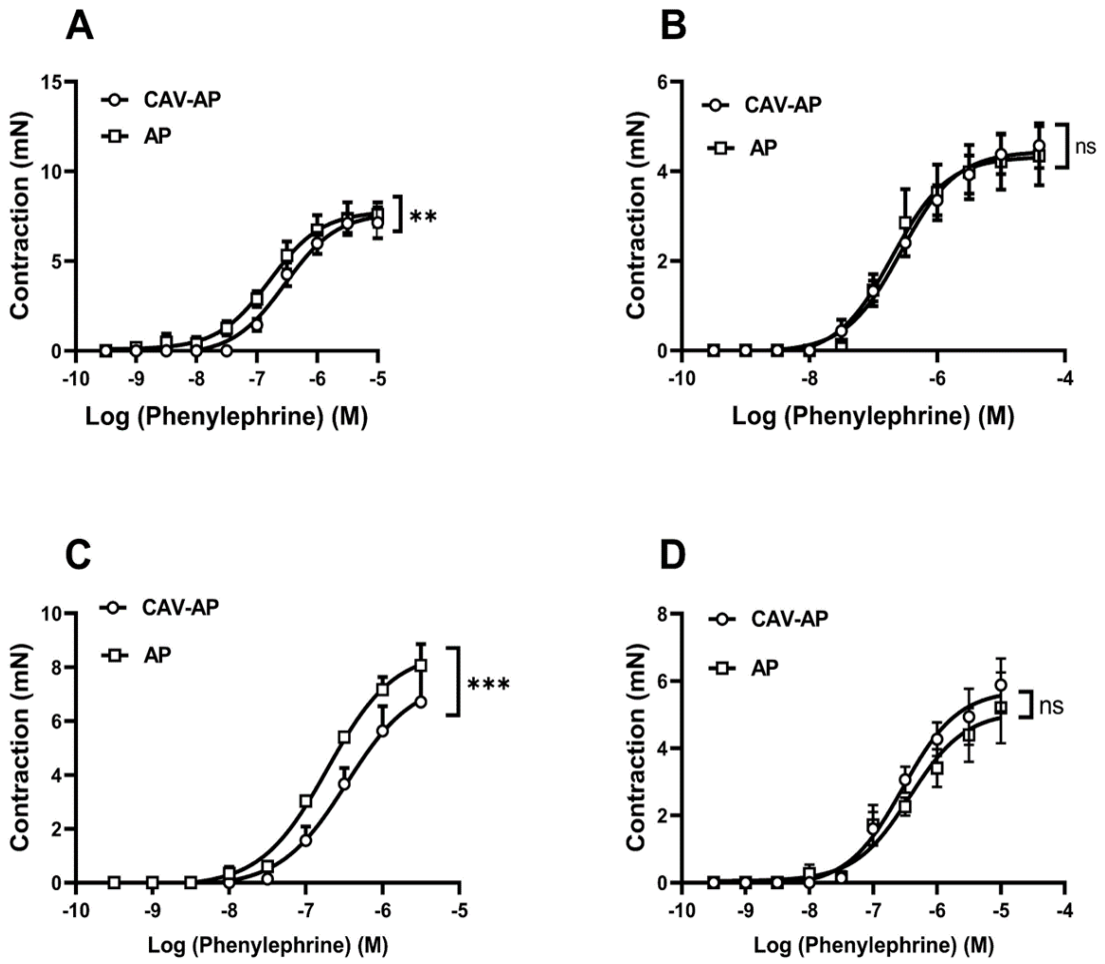

Figure 5-5: CAV-AP suppresses phenylephrine-stimulated contraction of thoracic aortic rings

(A) Thoracic or (B) abdominal rings from WT mice and (C) thoracic or (D) abdominal rings from KO mice with denuded endothelium and intact PVAT were incubated with (10 µM) CAV-AP or antennapedia (AP) control peptide for 6h. Dose-response curves to phenylephrine were generated in rings mounted under tension in a wire myograph. Data shown represent the mean ± SEM contraction from six independent experiments *** $p<0.001$, ** $p<0.01$ comparison of EC_{50}. Statistical significance was determined by two-way ANOVA (with Tukey's test).

5.4.6 Effect of CAV-AP on Cav-1/eNOS colocalization and nitric oxide production in 3T3-L1 preadipocytes and adipocytes

As shown in chapter 4, chemical disruption of caveolae with MβCD significantly reduces Cav-1/eNOS colocalization in 3T3-L1 preadipocytes and adipocytes, and this was associated with an increase in NO production. Therefore, it was of interest to further investigate the role of Cav-1/eNOS interaction in adipocyte cells using CAV-AP. Cav-1/eNOS colocalization was studied by immunofluorescence confocal microscopy. 3T3-L1 preadipocytes and adipocytes were cultured on glass coverslips and exposed to CAV-AP or antennapedia for 6 h as described in (section 2.2.8). There was no significant reduction in Cav-1/eNOS colocalization in 3T3-L1 preadipocytes incubated with CAV-AP and no alteration in NO production in conditioned media (Figure 5-6 C&D). In contrast, preincubation of 3T3-L1 adipocytes with CAV-AP was associated with a significant reduction in Cav-1/eNOS colocalization (Figure 5-7 C) but this had no significant effect on NO production in conditioned media (Figure 5-7 D).

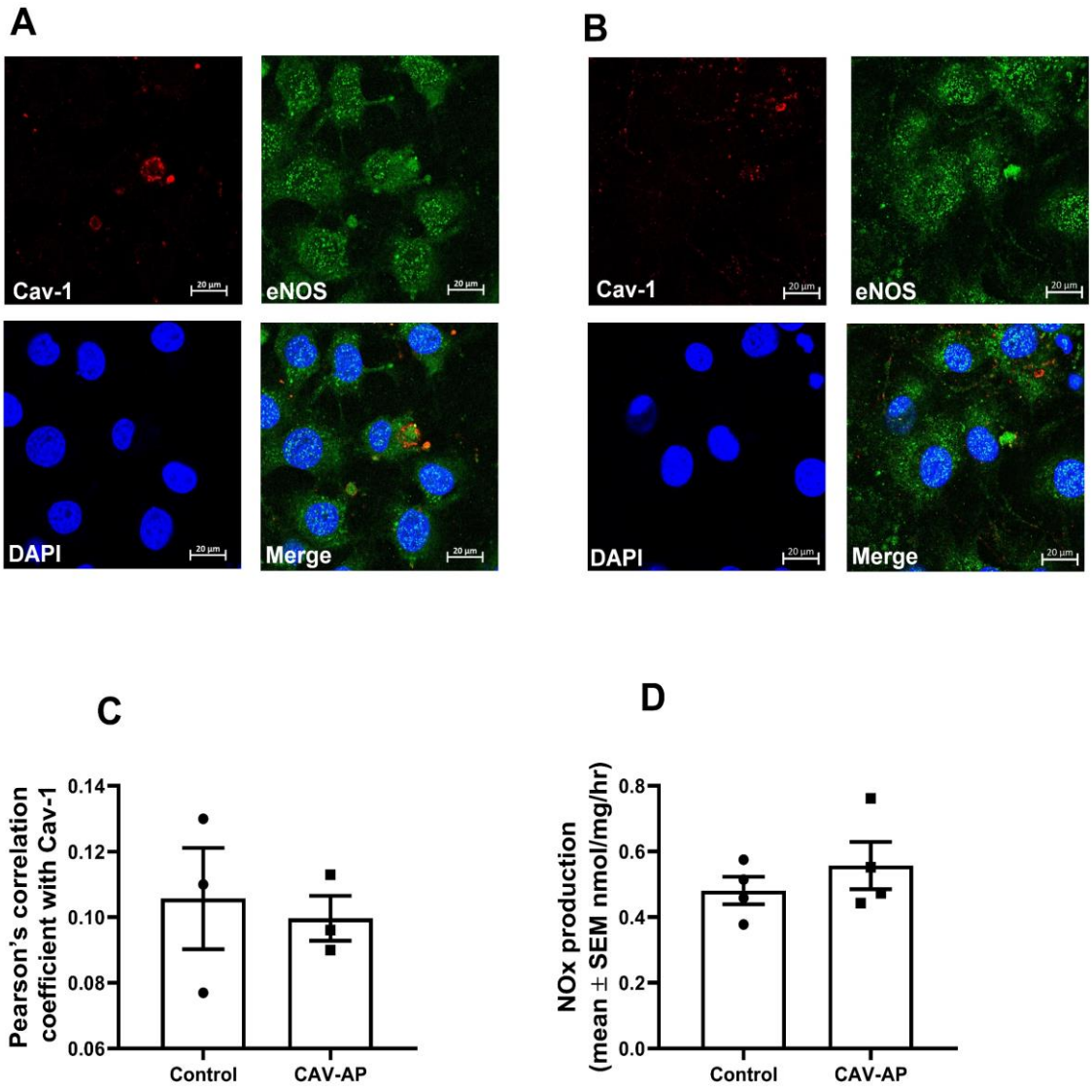

Figure 5-6: Effect of CAV-AP on Cav-1/eNOS colocalization and NO synthesis in 3T3-L1 preadipocytes

3T3-L1 preadipocytes were incubated in the presence or absence of (A) antennapedia control or (B) CAV-AP (10 µM) for 6 h. Coverslips of 3T3-L1 preadipocytes were incubated with anti-Cav-1 (red) and anti-eNOS (green) antibodies and analysed by immunofluorescence confocal microscopy. DAPI was used to stain cell nuclei. (C) Quantification using Pearson's correlation coefficient from three biological replicates with 50 cells per group. Scale bar = 20 µm. (D) Conditioned media was generated from 3T3-L1 preadipocytes incubated with CAV-AP or antennapedia control peptide (10 µM, 6 h) and assayed for NO_x content using a Sievers 280 NO analyser. Data shown represent the mean ± SEM NO_x production from 3-4 independent experiments.

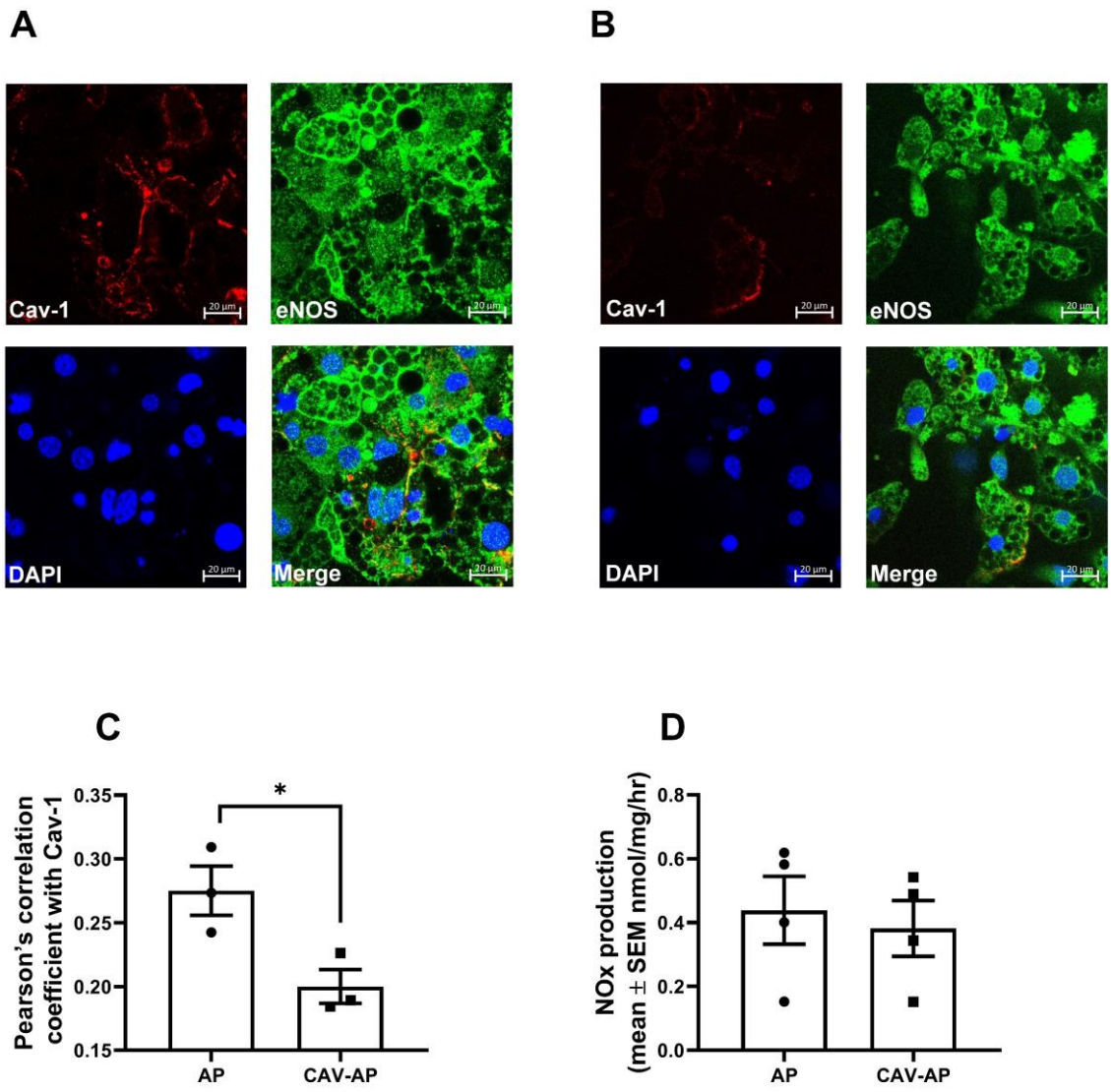

Figure 5-7: CAV-AP reduces Cav-1/eNOS co-localisation in 3T3-L1 adipocytes without altering NO synthesis.

3T3-L1 adipocytes incubated in the presence or absence of (A) antennapedia control (AP) or (B) CAV-AP (10 µM) for 6 h. Coverslips of 3T3-L1 adipocytes were incubated with anti-Cav-1 and anti-eNOS antibodies and analysed by immunofluorescence confocal microscopy. DAPI was used to stain cell nuclei. (C) Quantification using Pearson's correlation coefficient from three biological replicates with 50 cells per group. * $p<0.05$ compared to control (Student's t-test). Scale bar = 20 µm. (D) Conditioned media was generated from adipocytes incubated with CAV-AP or AP (10 µM, 6 h) and assayed for NO_x content using a Sievers 280 NO analyser. Data shown represent the mean ± SEM NO_x production from four independent experiments.

5.5 Discussion

As demonstrated in Chapter 4, in 3T3-L1 cells the eNOS levels were markedly reduced during adipogenesis after day 3 and consistent with that, the level of NO production was reduced during adipogenesis. Incubation of 3T3-L1 preadipocytes or adipocytes with MβCD was linked with a significant decrease in Cav-1/eNOS colocalization and a significant increase in NO production both in preadipocytes and adipocytes compared to control. The key findings of this chapter are that there was a reduction in Cav-1/eNOS colocalization in 3T3-L1 adipocytes incubated with a mutant cell–permeable scaffolding domain peptide of Cav-1 (CAV-AP) compared with control. To address whether these findings in cultured cells are also seen in arterial PVAT, the experiments were repeated in aortic tissue from WT and KO mice. Here, CAV-AP increased NO release by thoracic PVAT from KO mice but not WT mice but there was no change in NO production by abdominal PVAT from WT or KO mice in response to CAV-AP. In addition, our data showed that CAV-AP reduced PE-induced tension development both in WT and KO thoracic vessels with intact PVAT but lacking endothelium while it had no effect in abdominal vessels.

Even though the endothelium was intentionally denuded there is a possibility that some endothelial cells may remain, and these could release NO. Therefore, further experiments in the presence and absence of L-NAME, a nitric oxide synthase inhibitor would help to elucidate whether the actions of CAV-AP are indeed mediated by increased nitric oxide (NO) production. By comparing the vascular responses in the presence and absence of L-NAME, the role of NO in CAV-AP-induced effects can be better understood and substantiated.

First, experiments were undertaken to investigate the effect of AMPK in regulation of Cav-1/eNOS interaction. Two AMPK inhibitors, compound C and SBI-0206965 significantly reduced ACC phosphorylation in abdominal or thoracic PVAT, indicating that AMPK is effectively inhibited by both compounds (Figure 5-1). In line with a role for AMPK in the anticontractile action of PVAT, a recent study demonstrated that in thoracic aortic rings with intact PVAT from high fat diet-fed mice incubated with compound C, there was a reduced protective effect of the hypoglycaemic drug liraglutide on the anti-contractile capability of PVAT. The

authors concluded that the mechanism involved regulating a cAMP-independent PKA-AMPK pathway which suggests that AMPK might have a role in regulating the effect of liraglutide on PVAT in obese mice (Han *et al.*, 2019). However, in the current study, despite inhibiting basal AMPK activity, neither compound C nor SBI-0206965 (Dite *et al.*, 2018) had any effect on Cav-1/eNOS interaction (Figure 5-2 B). There is a possibility that the lack of effect of the inhibitors is due to the poorly selectivity of compound C and SBI-0206965 for AMPK as they inhibit multiple other kinases (Bain *et al.*, 2007).

In endothelial cells Hsp-90 has been found to positively regulate eNOS activity and this association between Hsp-90 and eNOS retains the enzyme in a coupled state which enhances eNOS activity, increasing NO production whilst limiting superoxide anion formation (Amour *et al.*, 2009). Paradoxically, in chapter 3 it was found that the level of Hsp-90 in abdominal PVAT both in WT and KO mice is greater than that in thoracic PVAT when normalised to total cellular protein, even though less NO is produced by abdominal PVAT. However, whether AMPK regulates Hsp-90-eNOS interaction has not been assessed. Previous studies have shown that in vascular endothelial cells, globular adiponectin increased eNOS binding with Hsp-90 and Akt as well as eNOS phosphorylation, leading to dose-dependent increases in NO production, an effect that was inhibited by geldanamycin. This implies that inhibition of Hsp-90 can suppress phosphorylation and activation of eNOS, possibly via Akt (Xi *et al.*, 2005). As shown in (Figure 5-2 C&D) Hsp-90 immunoreactivity was observed in immunoprecipitated eNOS from abdominal and thoracic PVAT incubated with compound C and SBI-0206965, however, neither AMPK inhibitor significantly altered Cav-1/eNOS or Hsp-90/eNOS binding.

Previous studies have shown that in rat adipocytes compound 991 allosterically activates AMPK and increases LKB1-mediated phosphorylation of Thr^{172} and suppresses dephosphorylation of Thr^{172}, thereby activating the kinase (Kopietz *et al.*, 2018, Gwinn, 2008). The current study demonstrated that compound 991 increased ACC phosphorylation, yet the increase was not statistically significant. A possible explanation is that AMPK activity was increased by compound 991 but that activity had returned to basal levels by 60 mins and that could be due to the fact that C991 prefers complexes containing ß1 rather than α1 subunit (Figure 5-3)

to overcome such challenge in future it would be better to optimise the time of incubation.

To further substantiate these findings and investigate the dynamics of AMPK activity and ACC phosphorylation, follow-up experiments could be conducted. For example, time course analysis, by expanding the incubation time points beyond 60 minutes, that could examine the temporal pattern of ACC phosphorylation in response to compound 991. This would establish the duration of the observed effect and whether the phosphorylation levels return to baseline or stabilize at a different level. The other approach could be by performing experiments with different AMPK activators that have distinct kinetics and preferential subunit binding profiles; this would help determine if the transient effect observed with compound 991 is specific to its mechanism of action or a general characteristic of AMPK activation.

Interestingly, stimulation of PVAT with compound 991 did tend to reduce Cav-1 immunoreactivity in eNOS immunoprecipitates from abdominal and thoracic PVAT and Hsp-90 association with eNOS in thoracic PVAT, which might suggest that AMPK activation can have a positive regulatory effect on eNOS activity through its association with Cav-1 and Hsp-90. We speculate that since the ß2 subunit of AMPK is the predominant subunit in adipocytes, this might underly why C991 did not activate AMPK in PVAT as it is selectively stimulates AMPK activity of ß1 containing complexes (Bultot *et al.*, 2016).

Cav-1 is the main coat protein of caveolae. Structure-function analysis of Cav-1 has shown that phenylalanine 92 (F92) is important for the inhibitory actions of Cav-1 towards eNOS and regulation of NO production. A cell-permeable mutant scaffolding domain peptide of Cav-1 (similar to CAV-AP in this study) has previously been reported to disrupt the inhibitory action of Cav-1 on eNOS, thereby alleviating inhibition of NO production (Bernatchez *et al.*, 2011). Another earlier study using co-immunoprecipitations combined with enzymatic assays showed direct Cav-1/eNOS coupling which was associated with a reduction in NO production (Ju *et al.*, 1997). It has been previously reported that Cav-1 negatively regulates the small GTPase Rac1 (Kinsella *et al.*, 1991, Burridge and Wennerberg, 2004) which in turn modifies the PI3K/Akt/eNOS pathway in endothelial cells (Gonzalez *et al.*, 2004, Gonzalez *et al.*, 2006). Another study reported that siRNA-

mediated caveolin-1 knockdown in Bovine Aorta Endothelial Cells (BAECs) enhances AMPK phosphorylation which in turn upregulates eNOS activity (Levine *et al.*, 2007).

Collectively, this prompted further investigation to examine whether interfering with Cav-1/eNOS binding might enhance eNOS activity and rescue the NO production in PVAT from mice lacking AMPKα1. Our data reported that, CAV-AP increased NO release by thoracic PVAT from KO mice and there was no change in NO production by abdominal PVAT from WT or KO mice in response to CAV-AP (Figure 5-4 A). These results therefore support the previous study which demonstrated that CAV-AP influences NO release by the endothelium (Bernatchez *et al.*, 2011) and demonstrate that the actions of CAV-AP are not limited to the endothelium. Bernatchez and colleagues also reported that overexpression of the F92A–Cav-1 scaffolding mutant peptide can reduce vessel tone *ex vivo* and also decrease blood pressure in a hypertensive mouse model in a Cav-1 and eNOS-dependent manner (Bernatchez *et al.*, 2011). In this study, CAV-AP reduced PE-induced tension development both in WT and KO thoracic vessels but had no effect in WT and KO abdominal vessels (Figure 5-5). These data suggest that CAV-AP disrupts Cav-1/eNOS binding in thoracic but not abdominal PVAT or perhaps the peptide was unable to overcome the greater inhibitory influence on eNOS in the abdominal PVAT. Therefore, that allowing greater generation of NO to oppose vessel constriction, and greater association of Cav-1 with eNOS in KO PVAT could underlie lower NO generation by KO thoracic PVAT.

To our knowledge, these data are the first to demonstrate the role of AMPK in regulating the Cav-1/eNOS interaction in PVAT. Similarly, a mutant peptide of the Cav-1 scaffolding domain (Cavnoxin 4 mg/kg, IP) with similar amino acid sequence of that CAV-AP has been used *in vivo*, where it caused a decrease in mean BP in mice in a dose-dependent manner compared with control peptide. This effect was not observed in hypertensive eNOS KO mice, demonstrating that eNOS is necessary for the BP-lowering effect of the mutant peptide (Bernatchez *et al.*, 2011). Given that, further work might provide more insight about the effect of CAV-AP in lowering blood pressure such as using CAV-AP *in vivo* and comparing the effect of the peptide in reducing BP between WT and AMPK KO mice.

Under normal conditions eNOS undergoes a dynamic subcellular translocation from cell membrane to Golgi apparatus and that trafficking and localization of eNOS may be essential for its activity and to maintain the temporal and spatial distribution of NO signalling in different cell types (Ortiz and Garvin, 2003, Dudzinski *et al.*, 2006). In addition, it should be emphasized that intracellular localization of eNOS regulates its activity (Fulton *et al.*, 2004) and this has been demonstrated for NO production in endothelial cells (Chakraborty and Ain, 2017). Under resting conditions eNOS localises to caveolae and in such conditions eNOS activity is reduced in a reversible manner via its coupling with the Cav-1 scaffolding domain (Bernatchez *et al.*, 2005).

Cav-1 plays a significant role in assembly of caveolae in the plasma membrane. Previous studies showed that deletion of Cav-1 resulted in caveolae structural deformity and consequently leads to eNOS dysfunction, reduction in NO production, and structural changes in the cell membrane which could be involved in conditions such as pulmonary hypertension (Drab *et al.*, 2001, Razani *et al.*, 2001). The subcellular localization of eNOS is also perinuclear in the Golgi apparatus as well as at the plasma membrane and is regulated by post-translational fatty acylation, palmitoylation and N-terminal myristoylation of the glycine residue at position 2 (Sessa *et al.*, 1992). Most work associated with studying eNOS trafficking from the plasma membrane to Golgi apparatus has been done in cultured endothelial cells. To our knowledge the subcellular localization and potential protein interactions of eNOS in adipocytes has not been studied. Thus, we aimed to investigate the eNOS co-localization in 3T3-L1 cells using the Cav-1 disruptive peptide (CAV-AP) by immunofluorescence. eNOS colocalization with Cav-1 was reduced as measured by Pearson's correlation coefficient in cells incubated with CAV-AP compared with control (Figure 5-7 C) indicating that the mutant peptide was specifically targeting the Cav-1/eNOS binding.

However, evaluation of colocalization or proximity of proteins or cellular structures requires more robust visualisation techniques. Indeed, detecting the subcellular colocalization of two proteins does not essentially mean an interaction between them. As such, highly sophisticated microscopy techniques can be utilized, which monitor a physical proximity of tagged proteins (fluorophores), such as Förster resonance energy transfer (FRET) microscopy (Lutz *et al.*, 2017)

and this could be considered in future studies to assess the location of eNOS in PVAT and how eNOS activity and NO production is affected upon AMPKα1 deletion.

Despite the efforts that have been made to understand how eNOS is regulated to produce NO in endothelium, there is still a huge gap in our knowledge of the molecular mechanisms by which PVAT generates NO, how this process is regulated and if AMPK is involved in generation of NO by PVAT.

The following figure demonstrate the Cav-1/eNOS binding site and the CAV-AP Peptides (Figure 5-8).

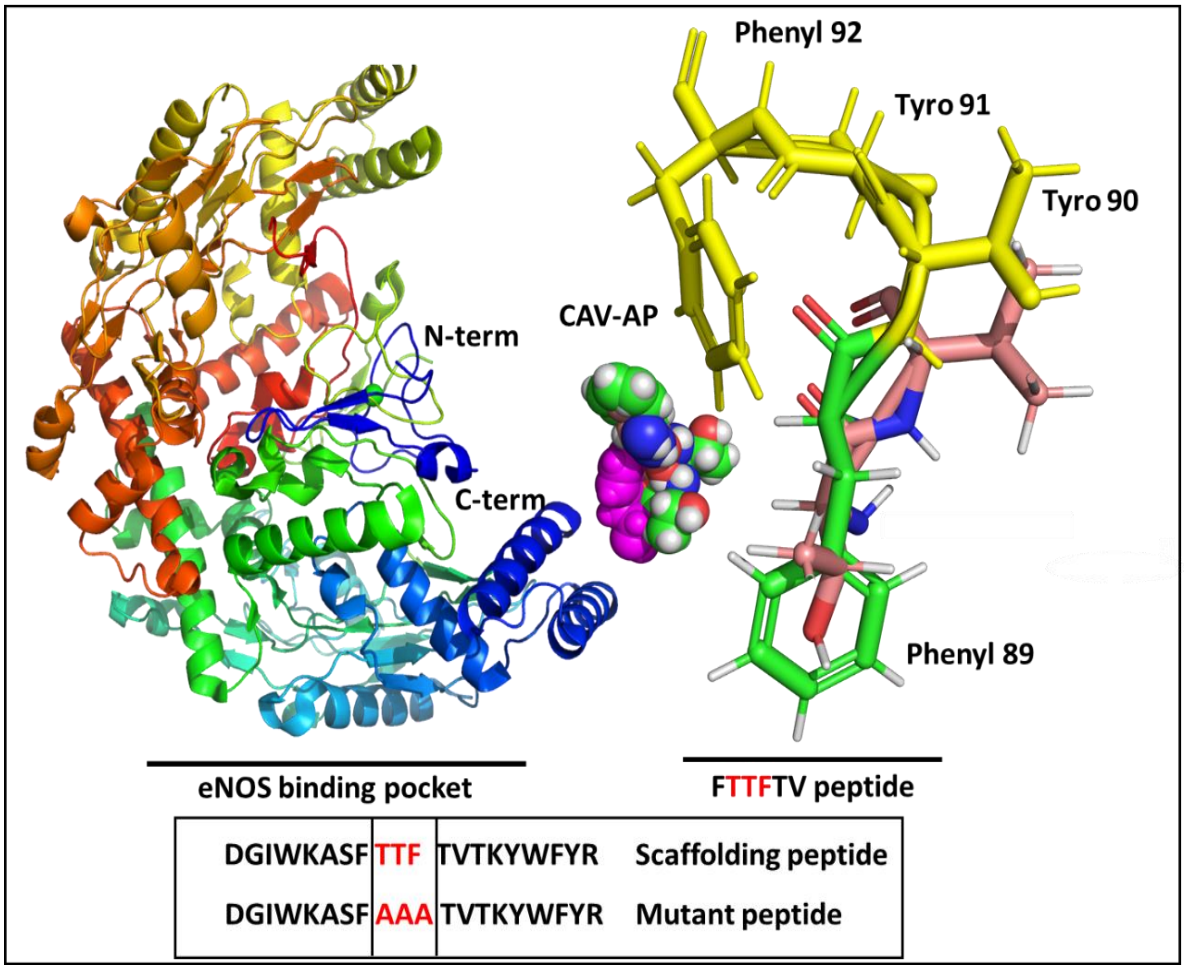

Figure 5-8: Depicted representation of Cav-1/eNOS binding site

CAV-AP targets the Cav-1/eNOS binding site. Left- the eNOS binding pocket. Right- the Cav-1 scaffolding domain and in particular subdomain B (FTTFTVT amino acids 98-95) and Ph 92 (mediating eNOS inhibition). CAV-AP Peptides, corresponding to Cav-1 scaffolding domain (amino acids 82-101) are fused to the C terminus of the Antennapedia (RQIKIWFQNRRMKWKKDGIWKASFAAATVTKWYFYR). Depicted figure generated by PyMOL Molecular Graphics System, Version 2.0 Schrödinger, LLC.

In conclusion, this study has demonstrated that disruption of Cav-1/eNOS binding using (CAV-AP) reduced PE-induced tension development both in WT, and KO thoracic vessels, but had no effect in WT and KO abdominal vessels. The anticontractile effect of CAV-AP was likely due to an increase in NO production via reduction of Cav-1/eNOS coupling. In addition, this study has also revealed that the Cav-1/eNOS interaction which is disrupted by CAV-AP is mediated by

amino acids 89–95 within the Cav-1 scaffolding domain and that F92 is crucial for such activity. Collectively, these data raise the possibility of studying the inhibitory influence of Cav-1 on eNOS without interfering with the other actions of endogenous Cav-1. These scaffolding mutant peptides may provide a useful approach for therapeutic application in regulating the eNOS/Cav-1 interaction in diseases characterized by decreased NO release and vascular leakage associated with inflammation or tumour growth. Data from this study revealed that AMPK might have a role in regulating Cav-1/eNOS binding.

Chapter 6 - Final discussion and future work

Perivascular adipose tissue (PVAT) surrounds blood vessels and releases a variety of bioactive molecules which modulate vascular function. In recent years PVAT has become an important new area for research in cardiovascular pathophysiology, as it provides potential new therapeutic approaches to alleviate cardiovascular disease (Grigoras *et al.*, 2019). Many clinical studies have revealed that a reduction of NO bioavailability has a significant role in the development of endothelial dysfunction and has been linked to eNOS uncoupling, and is a hallmark of many cardiovascular complications (Siragusa and Fleming, 2016). PVAT also has the ability to generate NO but there has been much less published work on how PVAT-derived NO might influence vascular function and how this is affected in the presence of cardiovascular disease. NO released by PVAT may contribute to the anticontractile effect of PVAT and indeed previous studies have demonstrated that PVAT can enhance vascular relaxation through release of other mediators such as adiponectin (Almabrouk *et al.*, 2017) (Figure 6-1).

6.1 Nitric oxide production by PVAT

The data presented in this thesis demonstrates that PVAT releases NO and that induces an anti-contractile effect on mouse thoracic aorta. This study also investigated the difference in NO production between PVAT from thoracic and abdominal aorta, and results show that thoracic PVAT produces more NO compared with abdominal PVAT, suggesting that differences exist between PVAT dependent on location. These results emphasize the specific regional roles of PVAT depots in control of vascular function and may drive differences in susceptibility to vascular pathologies such as abdominal aortic aneurysm (Ye *et al.*, 2021) . These data support previous findings showing that there is a significant increase in eNOS-derived NO production in PVAT from thoracic compared with abdominal aorta (Victorio *et al.*, 2016). Since we have shown that thoracic PVAT expresses higher levels of the BAT marker UCP-1 compared to abdominal PVAT it may be that PVAT phenotype is crucial in regulating NO production along the length of the aorta. In addition, Inflammation can also affect PVAT function, for example PVAT from obese mice has been found to release proinflammatory factors that induce inflammation, vasoconstriction and vascular stress (Stanek *et al.*, 2021). Interestingly, there may be differences in susceptibility of the thoracic and the abdominal PVAT to the inflammation, given that, an earlier study

demonstrated that an increased level of inflammatory markers in abdominal PVAT compared with thoracic PVAT in obese mice (Police *et al.*, 2009). It appears that the thoracic PVAT phenotype is less atherogenic and generates less pro-inflammatory cytokines compared with abdominal PVAT and this may explain the reason why the abdominal aorta is more susceptible to abdominal aortic aneurysm (AAA) compared with thoracic aorta (Police *et al.*, 2009, Fitzgibbons *et al.*, 2011, Padilla *et al.*, 2013). In addition, formation of atherosclerotic plaques within the abdominal aorta may be more prevalent for these same reasons (Padilla *et al.*, 2013), and one factor which could contribute to that greater risk to the abdominal aortic aneurysm is a reduction in NO production by abdominal PVAT. Since NO plays a key role in inhibiting platelet aggregation, leukocyte adhesion and accumulation of lipid streaks responsible for the initiation and progression of atherosclerosis, abdominal PVAT could be a potential pharmacological target to improve NO bioavailability in high-risk individuals with cardiovascular complications.

Even though the current study reinforces the concept that there are fundamental phenotypic differences between thoracic PVAT and abdominal PVAT, it is not yet known whether these distinctions are as a consequence of intrinsic cell factors or extrinsic anatomical factors (Tran *et al.*, 2018).

Some studies have investigated factors which could influence NO bioavailability in PVAT such as an oxidant stress. One such study showed that the anti-oxidant capacity changes along the aorta, where the relative expression levels of Mn-SOD were lower in PVAT from abdominal aorta compared with thoracic aorta, which correlated with detection of more oxidation stress in abdominal compared with thoracic aorta (Victorio *et al.*, 2016). Here, our results showed that there were no differences in lipid peroxidation between thoracic and abdominal PVAT. Taken together, these studies, though not conclusive, suggest that exposure of NO to oxidative stress might be not different between thoracic and abdominal PVAT in mouse and that do not underlie the different in NO production. Alternatively, it could be that antioxidant defences within the different depots of PVAT are equally effective at reducing the level of oxidant stress when lipid peroxidation is used as a marker.

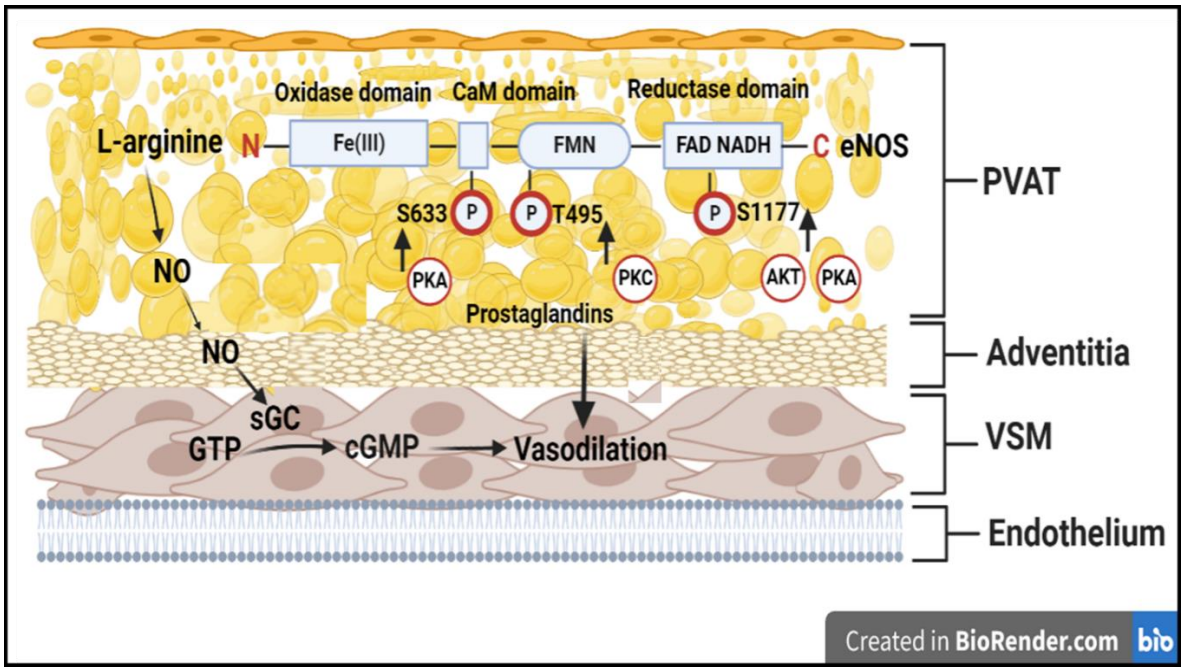

Figure 6-1: Vasorelaxation effect of PVAT

eNOS has oxidase, reductase, and CaM domains. eNOS activity is regulated through phosphorylation of the inhibitory site Thr^{495} and phosphorylation of activation sites Ser^{1177} and Ser^{633} by several upstream kinases including protein kinase A (PKA), protein kinase C (PKC) and protein kinase B (AKT). Also, prostaglandins play a role in vascular homeostasis. NO diffuses to the VSM, activating sGC which converts GTP to cGMP. Created with BioRender.com.

6.2 Role of AMPK in PVAT function

Previous data from our laboratory demonstrated that the presence of PVAT enhances vascular relaxation to cromakalim in endothelium-denuded thoracic aortic rings from wild type, but not AMPKα1 KO mice (Almabrouk *et al.*, 2017). In addition, an earlier study showed that the male offspring of female rats fed a HFD during pregnancy and lactation showed dysfunctional mesenteric PVAT which was associated with a reduction in AMPK activity and reduced NO bioavailability (Zaborska *et al.*, 2016). Unlike many previous studies which focussed on the role of AMPK in regulation of NO release from the endothelium (Zhao *et al.*, 2020), the current study addressed the role of AMPK in regulating NO production by PVAT which was achieved by measuring NO produced by PVAT in conditioned media from WT and AMPK KO mice.

These data revealed that thoracic PVAT from AMPK KO mice produces significantly less NO compared with thoracic PVAT from WT mice and regulated by AMPK.

These data support and add to the plethora of evidence that PVAT releases NO and that functionally this NO contributes to the anticontractile effect in different vascular beds including human subcutaneous vessels and internal mammary artery (Gao *et al.*, 2005).

Furthermore, we aimed to functionally assess the difference in NO between WT and AMPK KO mice via pharmacological inhibition of eNOS. Incubation of WT thoracic aortic rings denuded of endothelium with the eNOS inhibitor L-NAME (Talarek *et al.*, 2011), significantly augmented the contraction to U46619 without affecting the maximal contraction while a similar effect was seen in KO thoracic aortic rings. However, in abdominal aortic rings from WT and KO mice there was no significant effect of L-NAME on contraction to U46619; likely due to lower NO production in abdominal PVAT. Consistent with data presented here, a previous study demonstrated that inhibition of eNOS with L-NAME enhanced phenylephrine-induced contraction in endothelial-denuded rings from Wistar rats with intact PVAT from thoracic but not abdominal aorta (Victorio *et al.*, 2016).

It has been previously reported that PVAT releases a variety of bioactive molecules which act in a paracrine manner and regulate the vascular tone including adipokines (Maenhaut and Van de Voorde, 2011, Almabrouk *et al.*, 2014). One of these adipokines is adiponectin which is reported to facilitate vasodilation through AMPK- mediated eNOS phosphorylation (Chen *et al.*, 2003). Additionally, previous data from our laboratory demonstrated that PVAT from AMPK KO mice releases less adiponectin compared with PVAT from WT mice, and incubation with an adiponectin receptor blocker attenuated the relaxation induced by AICAR and cromakalim in intact aortic rings from WT but not AMPK KO aortic rings with intact PVAT, suggesting that adiponectin could be a potential vasodilator in a mechanism that involved AMPK activity (Almabrouk *et al.*, 2017). Furthermore, in AMPK KO aortic rings, addition of the AdipoR1 blocker to vessels without PVAT did not affect the relaxation induced by either AICAR or cromakalim, data from this study suggested that AMPK within the PVAT has an important regulatory role in production of anticontractile substances (Almabrouk *et al.*, 2017).

Linking the role of adiponectin in regulating the NO production by PVAT, an early study reported that an *ex vivo* experiments on human internal mammary arteries, adiponectin levels increase tetrahydrobiopterin (BH_4) bioavailability, in which BH_4

regulates PI3/Akt-mediated phosphorylation of eNOS and thus promoting eNOS coupling and increase NO bioavailability (Margaritis *et al.*, 2013). In summary, NO production and adiponectin from PVAT are important regulators of vascular function and play a critical role in maintaining cardiovascular health.

6.3 Role of AMPK in regulation of Cav-1 /eNOS binding in PVAT

Multiple lines of evidence indicate that dysregulation of eNOS is linked to many microvascular and macrovascular diseases. Cav-1 binding to eNOS occupies the Ca^{2+}/CaM binding site thereby reducing NO production via its scaffolding domain (Razani *et al.*, 2001). An earlier study in BAECs using co-immunoprecipitation combined with enzymatic assays showed direct Cav-1/eNOS coupling is associated with a reduction in NO production (Ju *et al.*, 1997). Data presented in this thesis demonstrated that significantly more Cav-1 was associated with eNOS in abdominal PVAT compared with thoracic PVAT which could account for the reduced NO production in abdominal PVAT compared with thoracic PVAT (Bernatchez *et al.*, 2011).

It has been shown that NO production by eNOS in endothelial caveolae has a key role in in regulating vascular tone, vascular smooth muscle cell proliferation, leukocyte adhesion, platelet aggregation, and vascular lesion formation (Dinerman *et al.*, 1993). Given its key role in vascular homeostasis, it is of great interest to investigate if the Cav-1/eNOS association in abdominal PVAT could contribute to the greater susceptibility of abdominal aorta to vascular injury and atherosclerosis compared with thoracic aorta (Liu *et al.*, 2020). The results presented here suggest that modulating the Cav-1/eNOS interaction in abdominal PVAT might restore NO bioavailability. In future, selectively targeting abdominal PVAT could be accomplished by phage display techniques which can be utilised to predict tissue-specific targeting peptides using random peptide-displaying phage libraries carried out using machine learning (Jung *et al.*, 2012, Andrieu *et al.*, 2019).

AMPK has been considered as a promising target to alleviate many metabolic disorders including TD2M and obesity (Heidary Moghaddam *et al.*, 2022). Indeed, activation of AMPK has been proposed as a therapeutic target for atherosclerosis

and other cardiovascular diseases associated with obesity and T2DM and one beneficial effect would be the positive regulation of eNOS activity via multiple mechanisms. These mechanisms include increases in BH_4 concentration via preventing degradation of GTP cyclohydrolase I (GTPCH-1), inhibiting NADPH oxidase (NOX) expression and activating superoxide dismutase-2 (SOD_2), leading to a reduction of superoxide synthesis reviewed in (Salt and Hardie, 2017).

To date, the role of AMPK in the regulation of Cav-1/eNOS binding and NO production by PVAT has not been investigated. Therefore, this study is the first to show that AMPK regulates eNOS activity in PVAT via altering eNOS binding to Cav-1. Our data reported that thoracic PVAT from AMPKα1 KO mice produced less NO compared with WT mice and that accompanied with increased levels of Cav-1 in thoracic PVAT from AMPK KO mice. This increased Cav-1/eNOS association could account for the reduction in NO production in AMPK KO thoracic PVAT compared with WT and that AMPK could be a potential therapeutic target to regulate Cav-1/eNOS binding in cardiometabolic disorders. A schematic overview outlining the potential of AMPK in regulating Cav-1/eNOS binding, is depicted in (Figure 6-2).

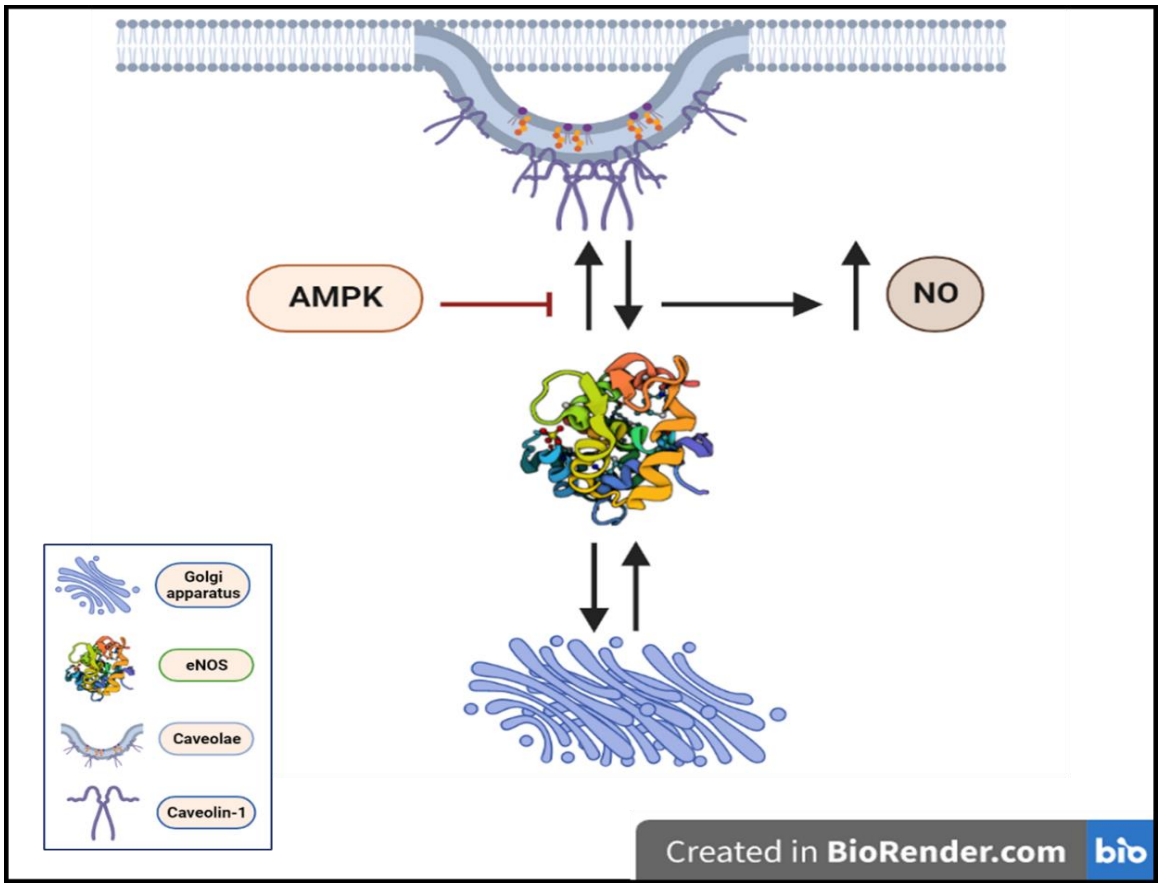

Figure 6-2: Regulation of NO production in PVAT mediated by AMPK signalling within adipocytes

Schematic diagram showing role of AMPK-mediated regulation of Cav-1/eNOS binding in PVAT. AMPK reduces Cav-1 binding to eNOS, which then allows increased eNOS activity and NO production. eNOS activity is regulated by localization of eNOS between the cytoplasmic face of Golgi apparatus and the caveolae in the plasma membrane. Created with BioRender.com.

To further investigate the role of AMPK in regulating Cav-1/eNOS binding, we used a cell permeable mutant peptide scaffolding domain of Cav-1 (CAV-AP). We demonstrated that NO production was noticeably increased in thoracic PVAT from AMPK KO mice treated with CAV-AP compared with thoracic PVAT from WT mice while there was no change in NO production by abdominal PVAT from WT or AMPK KO mice in response to CAV-AP. This suggests that inhibition of Cav-1 binding to eNOS in AMPK KO thoracic PVAT restores NO production. Furthermore, an *ex vivo* testing of CAV-AP on thoracic and abdominal aorta from both genotypes showed CAV-AP reduced phenylephrine-induced contraction both in WT and AMPK KO thoracic vessels but had no effect in WT and AMPK KO abdominal vessels. The absence of CAV-AP effect on abdominal vessels could be due the fact that

abdominal PVAT has more Cav-1 compared with thoracic PVAT, or perhaps the peptide cannot overcome the greater amount of Cav-1 in the abdominal PVAT, therefore the effect was not observed. These finding signify that CAV-AP disrupts Cav-1/eNOS binding (Figure 6-3), allowing greater generation of NO to oppose vessel constriction and may explain why greater association of Cav-1 with eNOS in PVAT of AMPK KO mice underlies lower NO generation by AMPK KO thoracic PVAT, it also indicates the importance of AMPK in regulation of eNOS/Cav-1 binding.

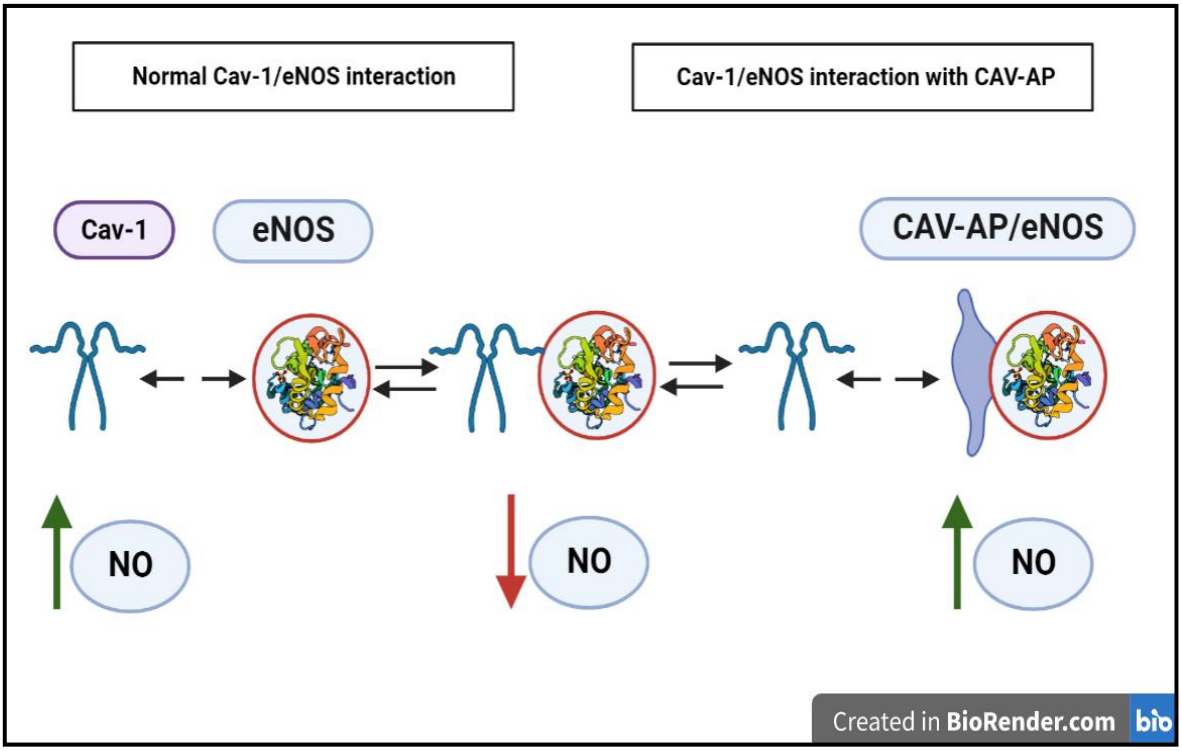

Figure 6-3: A proposed mechanism of increased eNOS- NO release by CAV-AP

eNOS is proposed to be in a dynamic state balanced between an active state (left) free of Cav-1 inhibitory domain and a less active state (middle) bound to endogenous Cav-1. CAV-AP (right) can bind eNOS and prevent its inhibition by endogenous Cav-1, allowing greater generation of NO. Created with BioRender.com.

6.4 Future work

The current study demonstrated that AMPK plays a regulatory role in Cav-1/eNOS binding in adipose tissue, however since PVAT consists of many types of cells including adipocytes, it is hard to determine whether the measured NO was produced by adipocytes or another cell type. However, further investigation on

other cell lines would be useful to extend our understanding of the molecular mechanisms by which AMPK regulates NO production in adipocytes. To address this, generation of 3T3-L1 preadipocytes in which the scaffolding domain of Cav-1 is mutated might be a suitable tool to better investigate the role of AMPK in regulating Cav-1/eNOS binding and NO production in adipocytes.

It has been over 20 years since the first Cav-1 KO mice model was generated (Drab *et al.*, 2001). In that mouse model the deletion of Cav-1 was not tissue specific which resulted in complete absence of caveolae in endothelial and epithelial cells including lung tissue. This was associated with diminished calcium signalling and NO production in the cardiovascular system, causing a reduction in endothelium-dependent relaxation and severe thickening of the alveolar septa of the lung. Given the dramatic effects of global knockout, generating a mouse model with specific ablation of Cav-1 in adipocytes (ad-cav1 knockout [KO] mouse) (Crewe *et al.*, 2022), would be a very useful tool to advance our knowledge in this area.

For example, an antisense-mediated down-regulation of Cav-1, gene targeting strategy, or genome CRISPR cas9 editing system technology that could be used to disrupt the *Cav-1* gene locus specifically in adipocytes without affecting other functions of Cav-1 in caveolar assembly in other tissues. This model could be used to better investigate the role of Cav-1 in eNOS activity and NO production in adipocytes and PVAT. On the other hand, instead of complete deletion of *Cav-1* gene and since the scaffolding domain (SD) plays an important role in Cav-1/eNOS binding, genetically mutating the scaffolding domain of Cav-1 in adipocytes would provide better understanding of its role in regulating eNOS activity and NO production.

The other method to investigate the role of Cav-1 in eNOS function would be via generating genetically engineered mouse models using the Cre-loxP system to specifically ablate Cav-1 in adipocytes using an adiponectin promoter-driven Cre, and Cav-1 flanked by *loxP* sites which are targets of recombination by the Cre recombinase. This methodology has been previously utilised to generate endothelial cell-specific Cav-1 null mice (EC-$Cav1^{-/-}$) by breeding of hemizygous Tie2-$Cre^{+/-}$ mice with homozygous $Cav1^{lox/lox}$ mice, in which the endothelial-specific Tie-2 promoter-driven Cre was used (Oliveira *et al.*, 2017, De Ieso *et al.*, 2020).

Furthermore, data in this study showed that CAV-AP increased NO release by thoracic PVAT from KO mice but not WT mice and there was no change in NO production by abdominal PVAT from WT or KO mice in response to CAV-AP. Given that, insight about the effect of CAV-AP in lowering blood pressure could be examined by administering CAV-AP *in vivo* and comparing the effect of the peptide in reducing blood pressure between WT and AMPK KO mice.

6.5 Chemical libraries for protein-protein interaction inhibitors

Utilising a chemical library to select proposed compound/s that might target specific pre-identified amino acid sequences is a useful tool to understand how protein-protein interaction can be targeted. Nowadays, identifying a robust and novel chemical compound is still one of the major challenges in drug discovery and development. The main advantage of using target-led approaches is to reduce the time and the cost of selecting nominated target compounds among thousands of potential compounds. In drug discovery, applying structure-activity relationships is a powerful tool for drug screening, drug repurposing, cell stimulation and identification of drug mechanism of action(s). Many cellular processes are regulated and/or mediated by protein-protein interactions (PPIs), therefore, protein-protein interaction inhibitors (iPPIs) have become a significant new class of compounds for investigating this interaction and additionally they may have therapeutic potential. Indeed, several PPI inhibitors (iPPIs) have been studied in pre-clinical and clinical trials and an increasing number of validated (iPPIs) have been approved (Li *et al.*, 2017, Donev, 2018, Bosc *et al.*, 2020).

A more advanced technique has been developed to reduce the number of expected compounds and specifically to identify inhibitors based on molecular descriptors and machine learning methods. High-throughput screening (HTS) is one of the most common techniques for discovering (iPPIs), particularly when no chemical structural compound is available for the particular protein-protein interaction being investigated. Many databases are available as a screening tool including iPPI-DB (Labbé *et al.*, 2016) and TIMBAL (database containing small molecules that inhibit protein–protein interactions) (Higueruelo *et al.*, 2013), which have been developed during the last decade to screen chemical compounds and to validate different (iPPIs) and define their physicochemical properties (Bosc *et al.*, 2020).

However, in this research we demonstrated that eNOS is less active in abdominal PVAT, associated with more Cav-1 coupling, and less NO production compared with thoracic PVAT. Therefore, utilising such high-throughput (HTP) libraries to identify a reversible and specific chemical compound that target Cav-1/eNOS binding without interfering with other physiological functions of Cav-1 would provide a good starting point to develop pharmacological compounds that alleviate cardiovascular and metabolic diseases associated with a reduction of NO bioavailability such as T2DM and obesity.

It has been reported that AMPK activation using (AICAR), salicylate, metformin all increase phosphorylation of PVAT eNOS and improve PVAT functions in different studies (Man *et al.*, 2022). To our knowledge not too much has been done to identify the role of AMPK in regulating Cav-1 /eNOS binding and NO production in PVAT. In thoracic PVAT from AMPKα1 KO model, there was more Cav-1 bound to eNOS compared to thoracic PVAT from WT mice, and in line with that there was a noticeable reduction in NO production. It is well defined that in many cardiovascular diseases most of the blood vessel layers are affected including endothelial cells, VSMCs and PVAT, therefore, modulating Cav-1/eNOS binding in diseases associated with dysfunctional PVAT would afford a novel approach in alleviating diseases associated with a reduction in NO. The challenging side of dissecting Cav-1/eNOS binding is how to specifically target this interaction without interfering with the endogenous function of Cav-1 in caveolae assembly. Together, these approaches suggest the possibility of investigating the inhibitory effect of Cav-1 on eNOS activity and NO production without interfering with other endogenous functions of Cav-1 via developing specific PPi inhibitors.

While the study included various aspects of vascular function and considered multiple layers, such as endothelium-intact and endothelium-denuded vessels and PVAT, it is essential to recognize that a comprehensive understanding of vascular function should also include the contribution of VSMCs and their role in mediating vasodilation and vasoconstriction is a critical aspect of vascular physiology and pharmacology. To address this limitation, future studies should consider including experiments specifically targeting VSMCs. This could involve assessing VSMC contractility or studying the effect of the compounds on VSMC-specific signaling pathways, gene expression or developing a specific adipose or PVAT KO mouse so

that AMPK function in the VSMCs is preserved. By including VSMC-focused experiments, a more complete picture of the pharmacological actions can be obtained, providing deeper insights into the mechanisms and potential therapeutic applications.

Finally, it is important to acknowledge the limitation of not including VSMC-specific experiments in the study. By recognizing this gap, future investigations can address this aspect to provide a more comprehensive understanding of the pharmacological effects on different vascular layers.

6.6 Conclusion

The data presented in this study is the first to demonstrate that AMPK plays an important role in the regulation of NO production by PVAT in a mechanism that involves altered Cav-1/eNOS coupling. Thoracic PVAT from AMPKα1 KO mice produced considerably less NO compared with WT thus exhibit less vasoconstrictor tolerance. Furthermore, disruption of Cav-1/eNOS binding using a disruptive peptide (CAV-AP), increased the anticontractile of PVAT in thoracic aorta, and that was likely due to increase NO production via reduction of Cav-1/eNOS coupling. Therefore, considering the findings of this study, and further elucidate of the molecular mechanism/s by which AMPK regulates Cav-1/eNOS binding in adipocytes could offer a novel therapeutic approach for targeting the AMPK-Cav-1/eNOS pathway to ameliorate the clinical signs associated with vascular dysfunction caused by a reduction in NO bioavailability.

6.7 Appendices

Levels of eNOS expression and activity in PVAT (WT and KO mice)

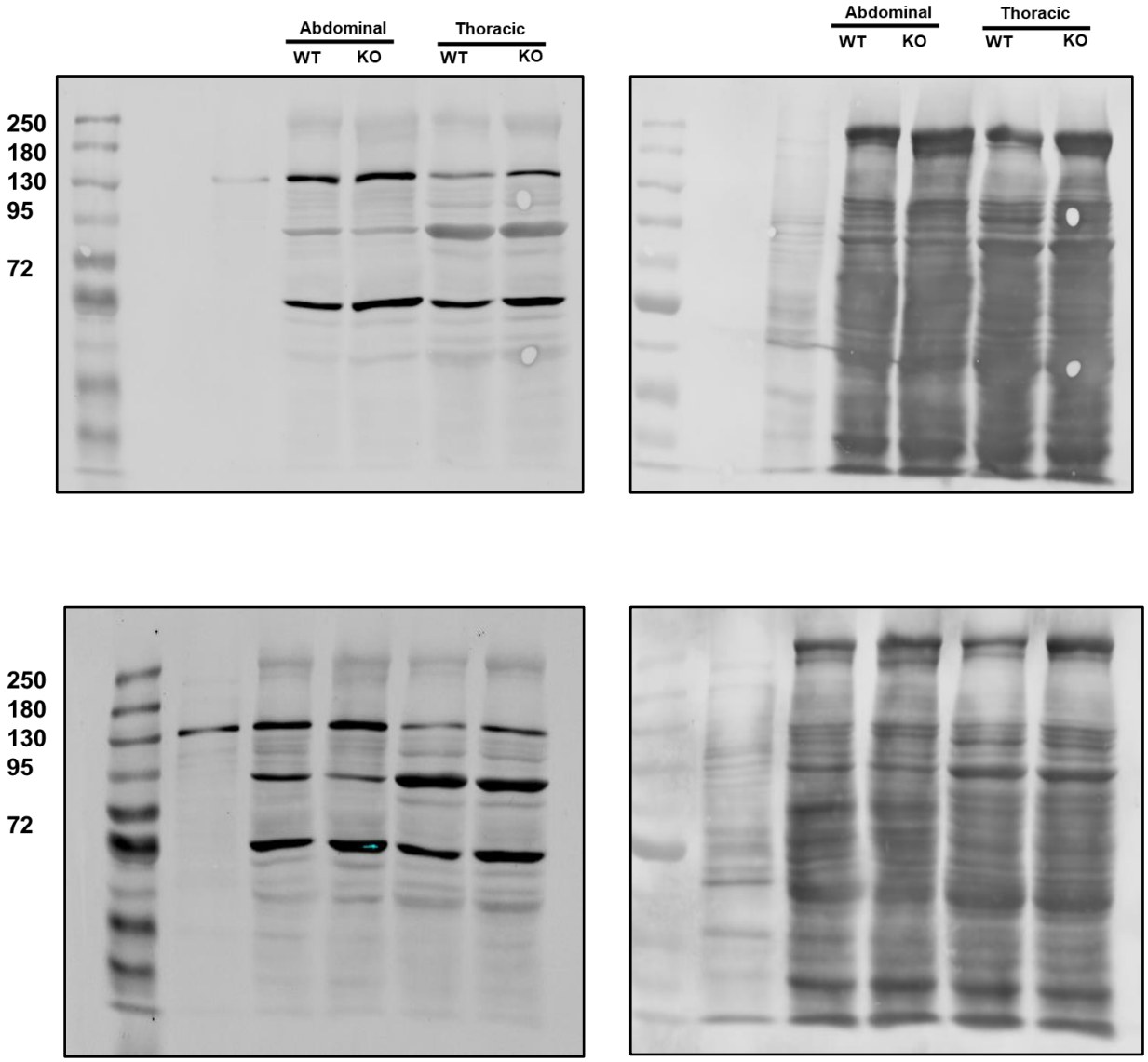

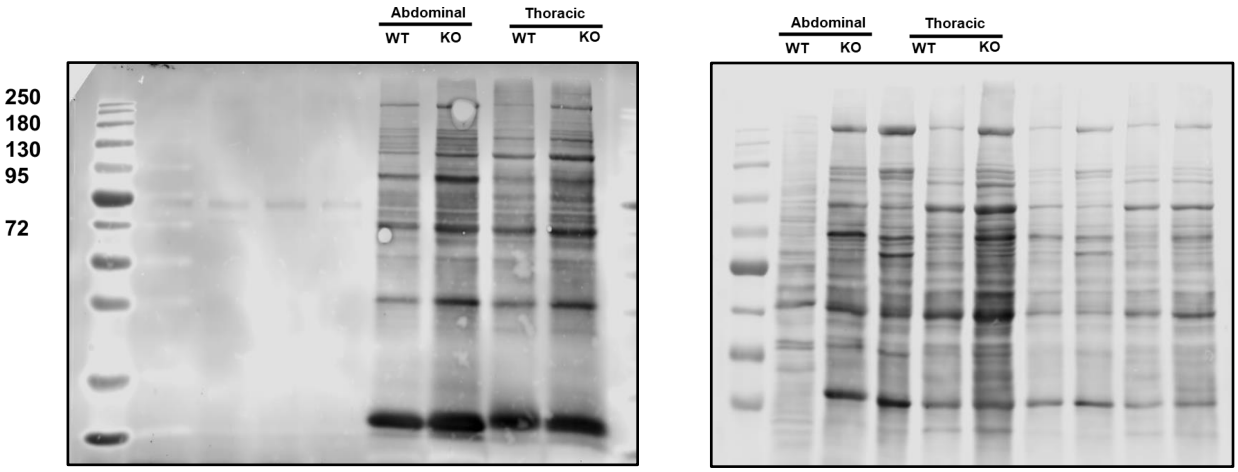
Abdominal
Thoracic
WT
KO
WT
KO
250
180
130
95
72
Abdominal
Thoracic
WT
KO
WT
KO

Levels of iNOS and nNOS expression and activity in PVAT (WT and KO mice)

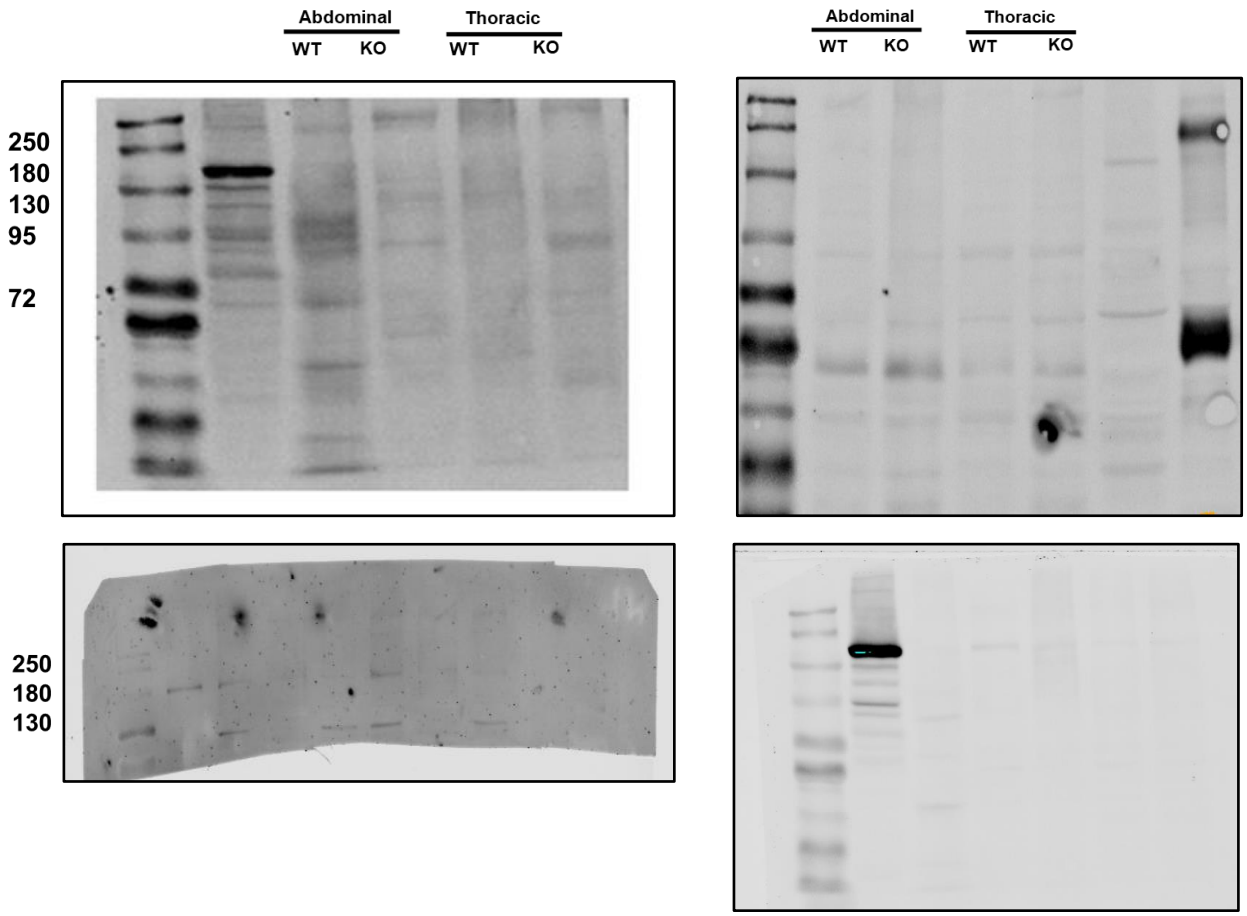

Levels of phospho-eNOS in thoracic and abdominal PVAT from WT and KO mice.

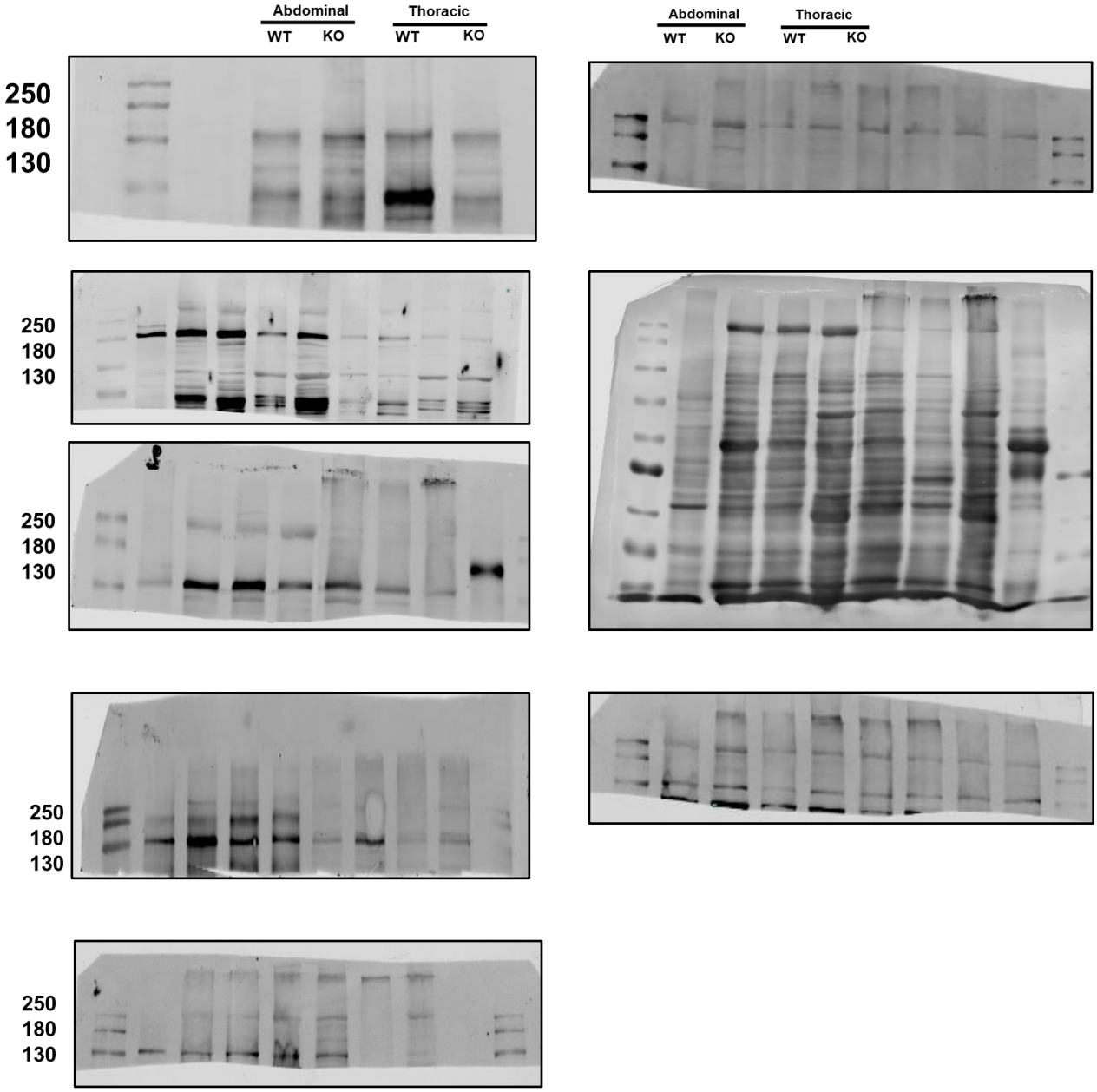

Chapter 6

Levels of peNOS 615

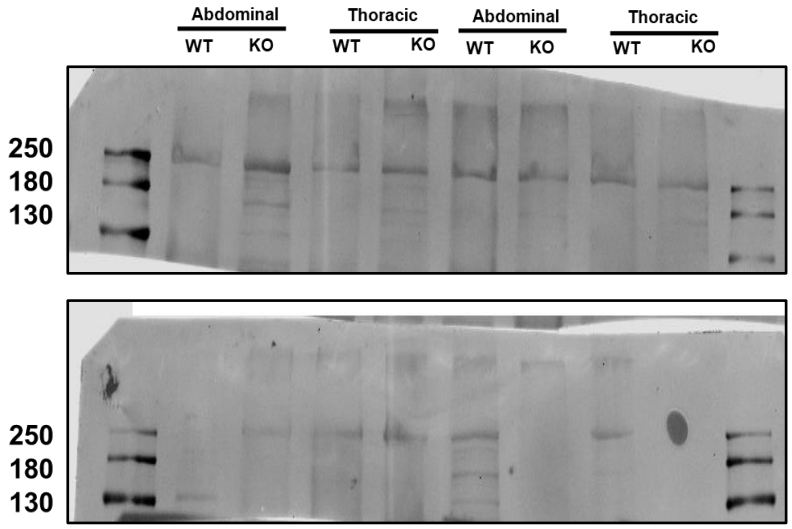

Levels UCP-1 expression in PVAT/fat depots from WT and KO mice

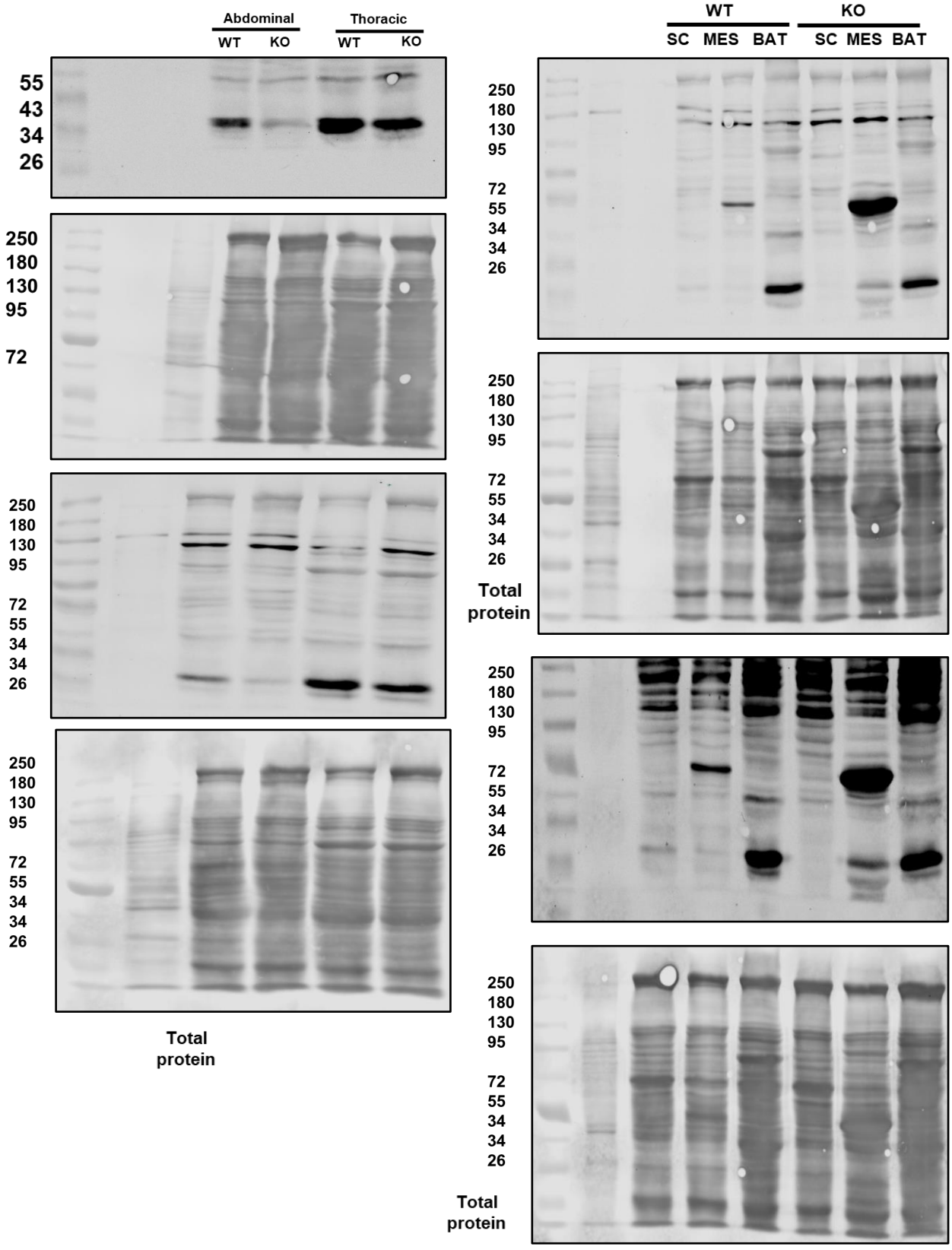

Levels of caveolin-1 /eNOS in thoracic PVAT and abdominal PVAT from WT and KO mice (total protein)

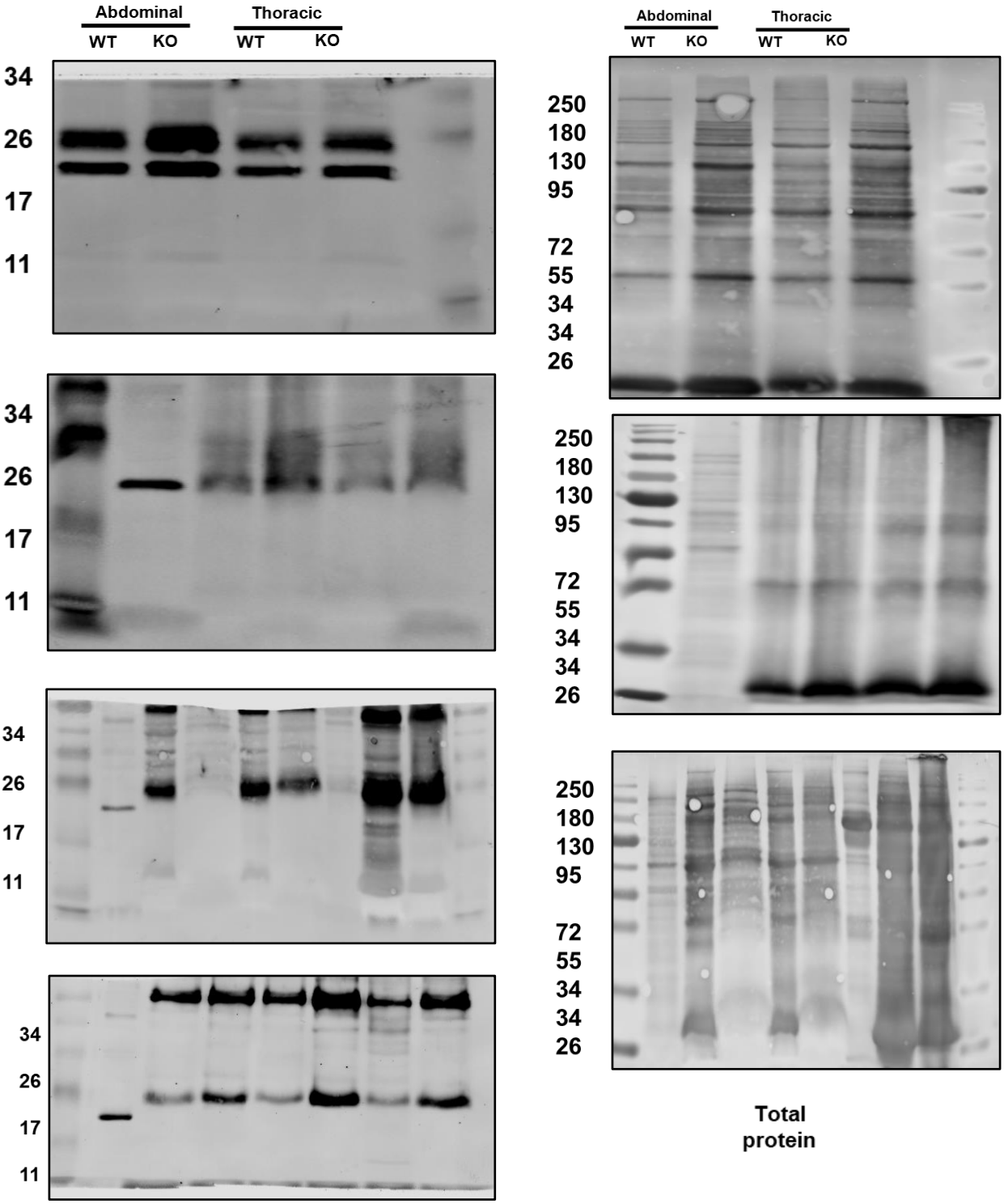

Levels of cav-1 /eNOS in abdominal PVAT relative to thoracic PVAT

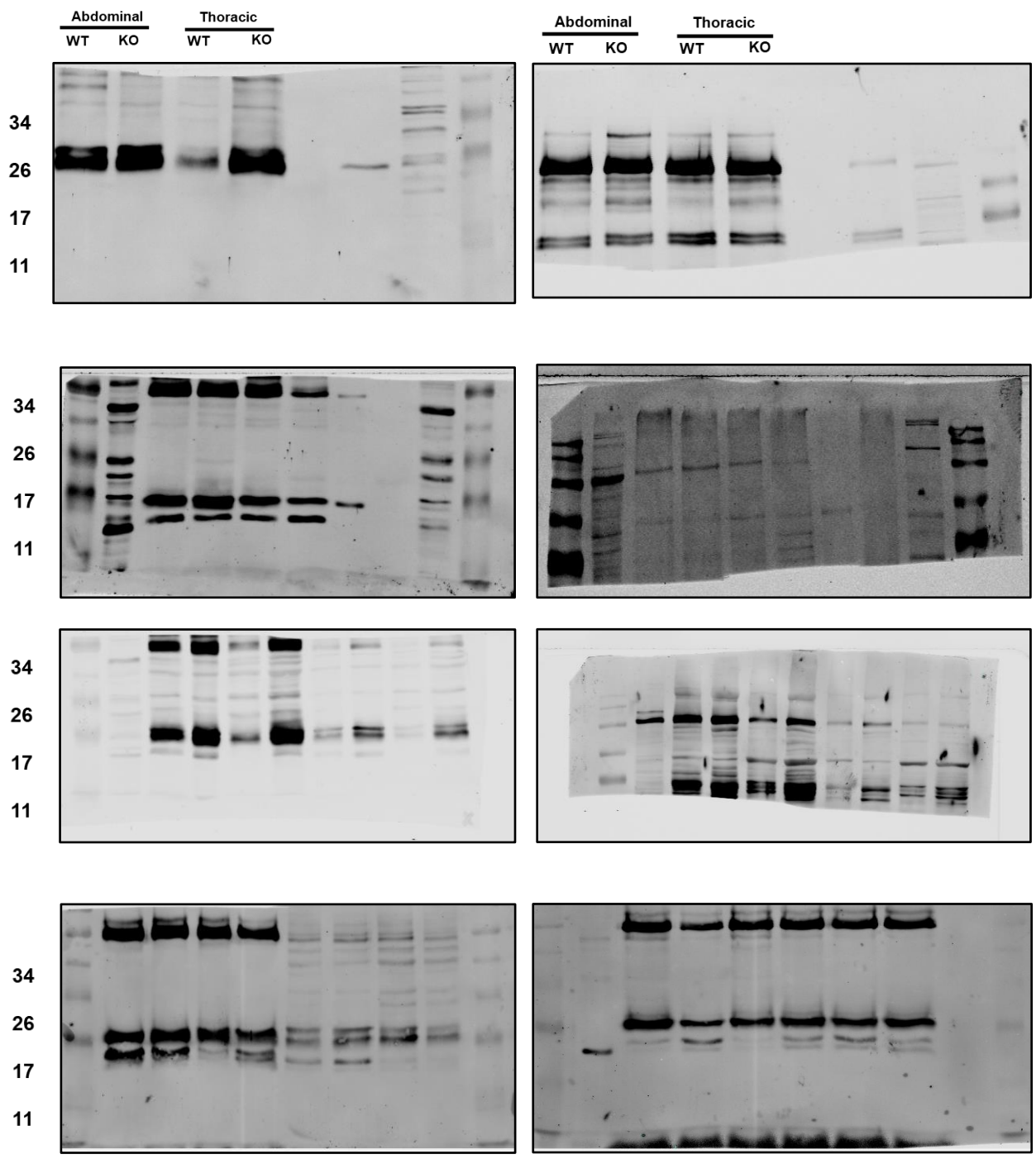

Levels of NOS isoforms and NO production during 3T3-L1 adipogenesis

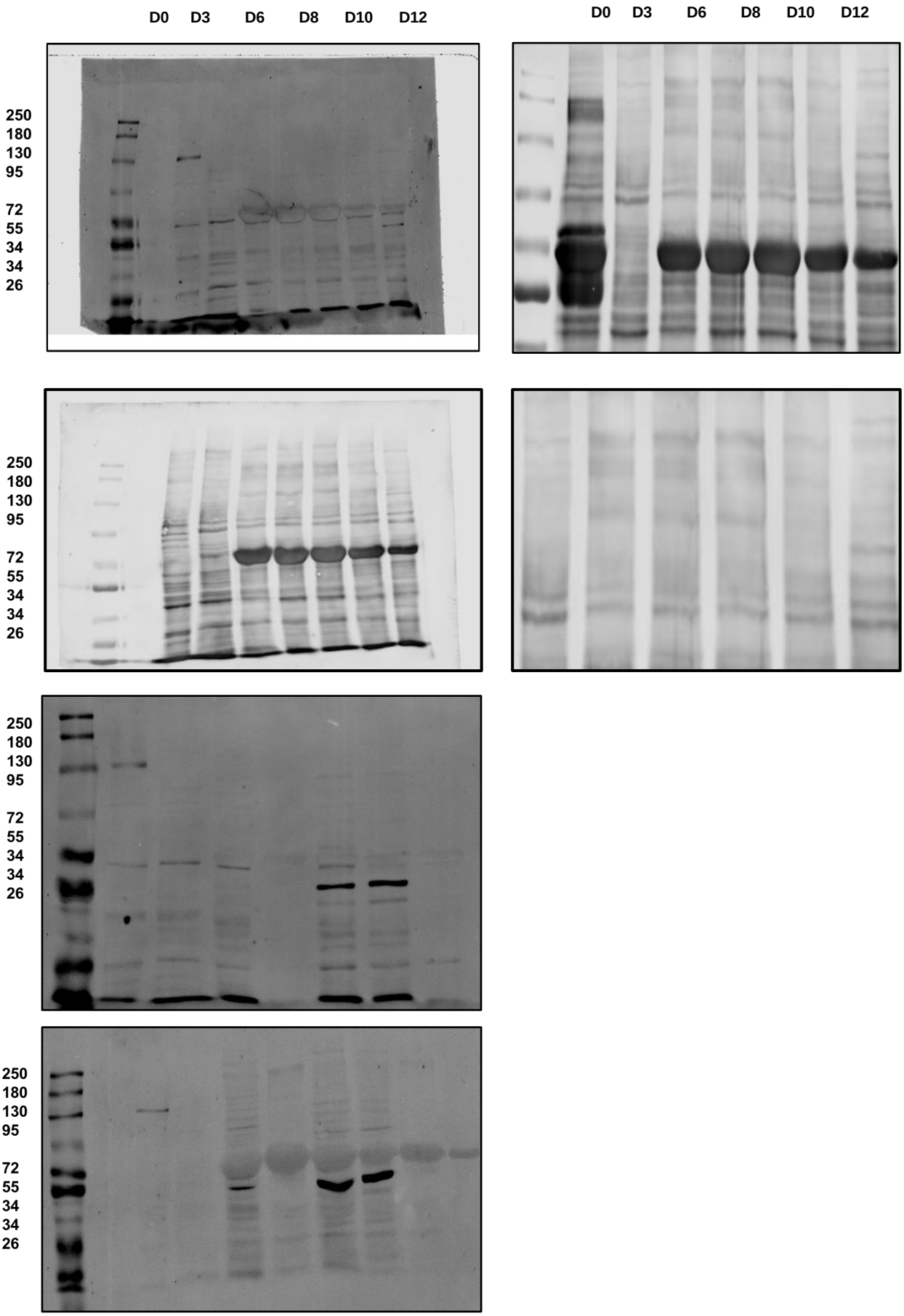

Levels of iNOS in methyl-ß-cyclodextrin 3T3-L1

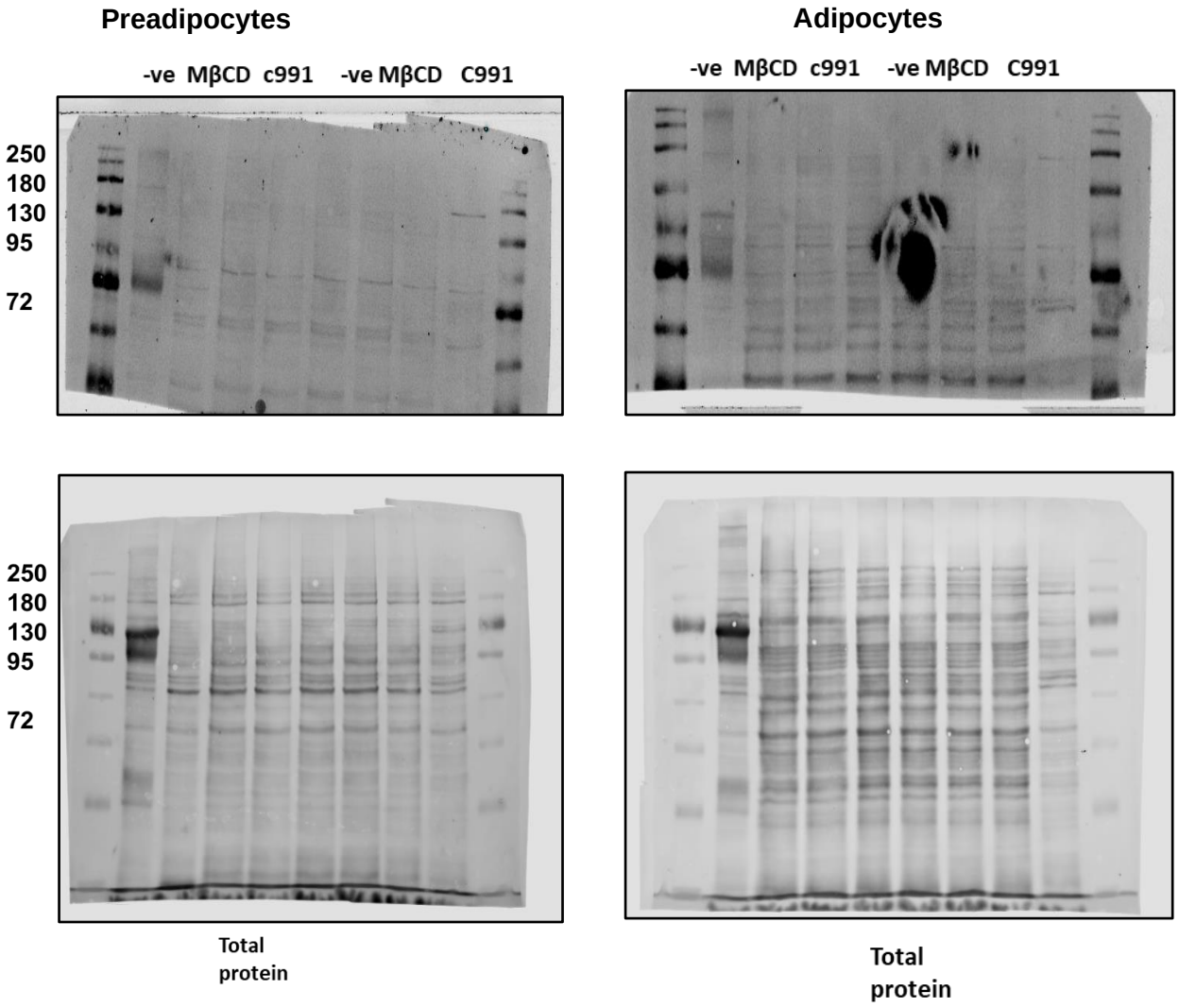

Levels of cav-1/eNOS in 3T3-L1 incubated with methyl-ß-cyclodextrin

preadipocytes **Adipocyte**

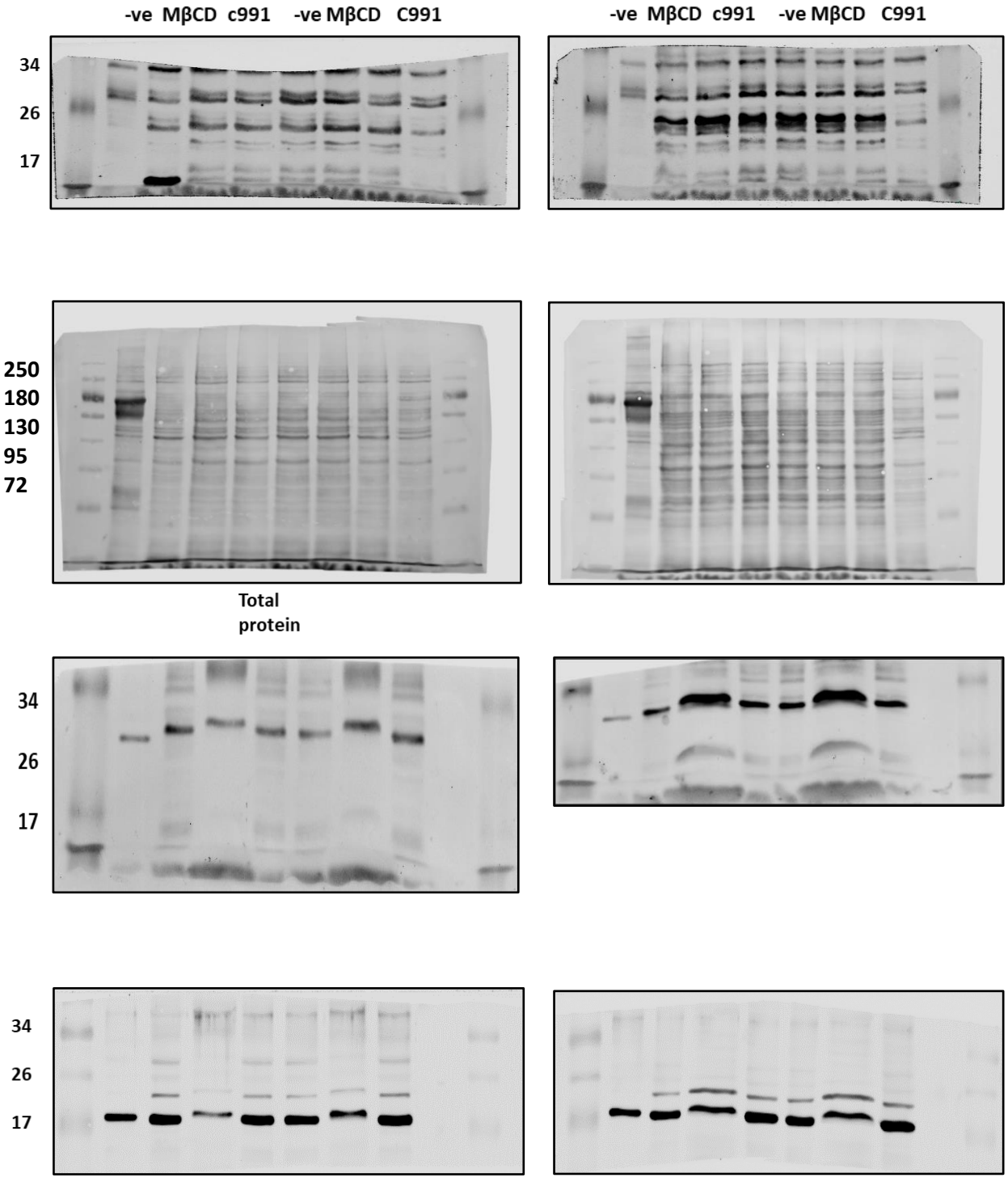

Effect of Compound 991 on ACC phosphorylation in 3T3-L1

Total ACC (Preadipocyte)

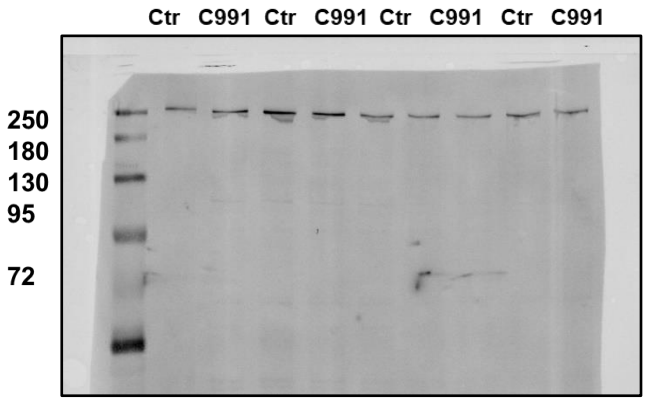

Total ACC (Adipocyte)

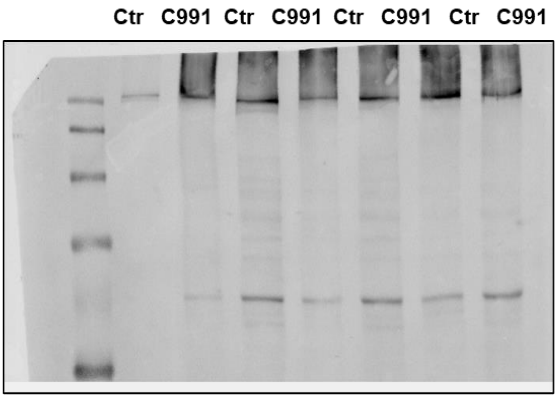

Pospho-ACC (Preadipocyte)

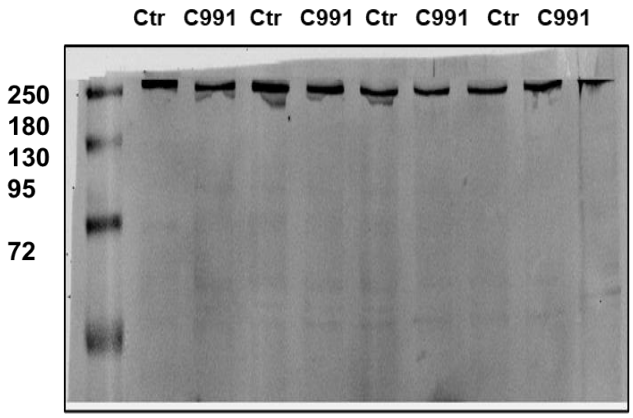

Pospho-ACC (adipocyte)

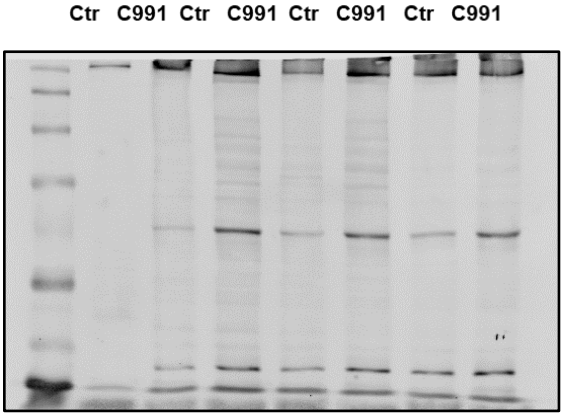

Effect of AICAR and A769662 on ACC phosphorylation in 3T3-L1

Total ACC (Preadipocyte)

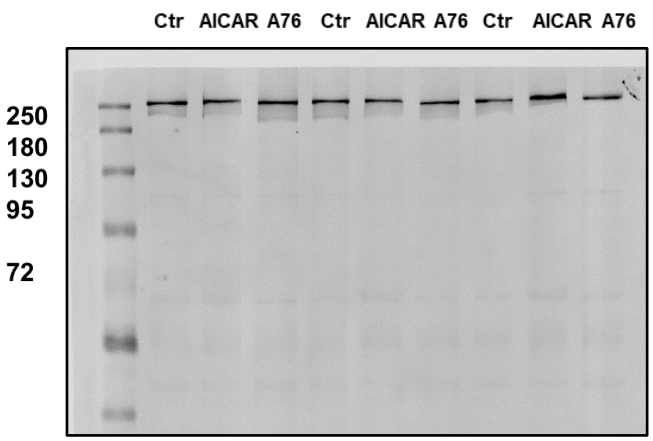

Total ACC (Adipocyte)

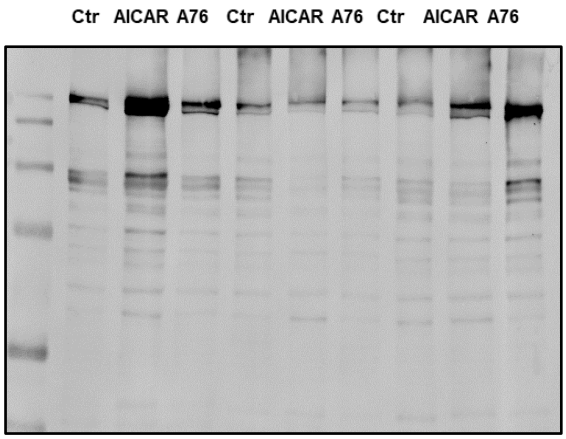

Pospho-ACC (Preadipocyte)

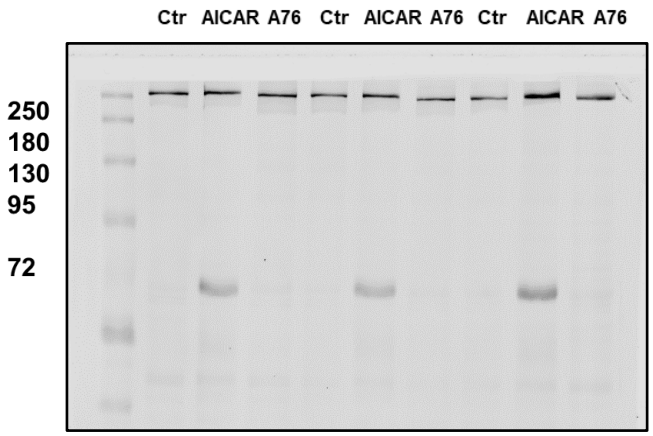

Pospho- ACC (Adipocyte)

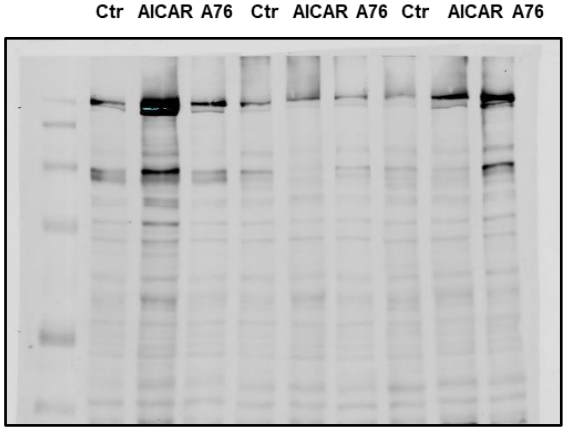

Chapter 7 - List of References

Aghamohammadzadeh, R., Withers, S., Lynch, F., Greenstein, A., Malik, R. & Heagerty, A. 2012. Perivascular adipose tissue from human systemic and coronary vessels: the emergence of a new pharmacotherapeutic target. *British journal of pharmacology,* 165**,** 670-682.

Ahmad, R., Hussain, A. & Ahsan, H. 2019. Peroxynitrite: cellular pathology and implications in autoimmunity. *Journal of Immunoassay and Immunochemistry,* 40**,** 123-138.

Ahwazi, D., Neopane, K., Markby, G. R., Kopietz, F., Ovens, A. J., Dall, M., Hassing, A. S., Gräsle, P., Alshuweishi, Y. & Treebak, J. T. 2021. Investigation of the specificity and mechanism of action of the ULK1/AMPK inhibitor SBI-0206965. *Biochemical Journal,* 478**,** 2977-2997.

Alderton, W. K., Cooper, C. E. & Knowles, R. G. 2001. Nitric oxide synthases: structure, function and inhibition. *Biochemical journal,* 357**,** 593-615.

Aledavood, E., Forte, A., Estarellas, C. & Javier Luque, F. 2021. Structural basis of the selective activation of enzyme isoforms: Allosteric response to activators of β1- and β2-containing AMPK complexes. *Computational and Structural Biotechnology Journal,* 19**,** 3394-3406.

Ali, A. T., Hochfeld, W. E., Myburgh, R. & Pepper, M. S. 2013. Adipocyte and adipogenesis. *European journal of cell biology,* 92**,** 229-236.

Almabrouk, T., Ewart, M., Salt, I. & Kennedy, S. 2014. Perivascular fat, AMP-activated protein kinase and vascular diseases. *British Journal of Pharmacology,* 171**,** 595-617.

Almabrouk, T. A., Ugusman, A. B., Katwan, O. J., Salt, I. P. & Kennedy, S. 2017. Deletion of AMPKα1 attenuates the anticontractile effect of perivascular adipose tissue (PVAT) and reduces adiponectin release. *British journal of pharmacology,* 174**,** 3398-3410.

Almabrouk, T. A., White, A. D., Ugusman, A. B., Skiba, D. S., Katwan, O. J., Alganga, H., Guzik, T. J., Touyz, R. M., Salt, I. P. & Kennedy, S. 2018. High fat diet attenuates the anticontractile activity of aortic PVAT via a mechanism involving AMPK and reduced adiponectin secretion. *Frontiers in physiology,* 9**,** 51.

Alomar, S. Y., Gentili, A., Zaibi, M. S., Kępczyńska, M. A. & Trayhurn, P. 2016. IL-1 ß (interleukin-1 ß) stimulates the production and release of multiple cytokines and chemokines by human preadipocytes. *Archives of physiology and biochemistry,* 122**,** 117-122.

Alpoim, P. N., Sousa, L. P. N., Mota, A. P. L., Rios, D. R. A. & Dusse, L. M. S. 2015. Asymmetric Dimethylarginine (ADMA) in cardiovascular and renal disease. *Clinica Chimica Acta,* 440**,** 36-39.

Altamish, M., Dahiya, R., Singh, A. K., Mishra, A., Aljabali, A. A., Satija, S., Mehta, M., Dureja, H., Prasher, P. & Negi, P. 2020. Role of the serine/threonine kinase 11 (STK11) or liver kinase B1 (LKB1) gene in

Peutz-Jeghers syndrome. *Critical Reviews™ in Eukaryotic Gene Expression,* 30.

Amour, J., Brzezinska, A. K., Weihrauch, D., Billstrom, A. R., Zielonka, J., Krolikowski, J. G., Bienengraeber, M. W., Warltier, D. C., Pratt, P. F. & Kersten, J. R. 2009. Role of heat shock protein 90 and endothelial nitric oxide synthase during early anesthetic and ischemic preconditioning. *The Journal of the American Society of Anesthesiologists,* 110**,** 317-325.

Andrieu, J., Re, F., Russo, L. & Nicotra, F. 2019. Phage-displayed peptides targeting specific tissues and organs. *Journal of drug targeting,* 27**,** 555-565.

Antoniades, C., Antonopoulos, A., Tousoulis, D. & Stefanadis, C. 2009. Adiponectin: from obesity to cardiovascular disease. *obesity reviews,* 10**,** 269-279.

Awata, W. M., Gonzaga, N. A., Borges, V. F., Silva, C. B., Tanus-Santos, J. E., Cunha, F. Q. & Tirapelli, C. R. 2019. Perivascular adipose tissue contributes to lethal sepsis-induced vasoplegia in rats. *European Journal of Pharmacology,* 863**,** 172706.

Bagatell, R. & Whitesell, L. 2004. Altered Hsp90 function in cancer: a unique therapeutic opportunity. *Molecular cancer therapeutics,* 3**,** 1021-1030.

Bain, J., Plater, L., Elliott, M., Shpiro, N., Hastie, C. J., Mclauchlan, H., Klevernic, I., Arthur, J. S. C., Alessi, D. R. & Cohen, P. 2007. The selectivity of protein kinase inhibitors: a further update. *Biochemical Journal,* 408**,** 297-315.

Banerjee, S., Buhrlage, S. J., Huang, H.-T., Deng, X., Zhou, W., Wang, J., Traynor, R., Prescott, A. R., Alessi, D. R. & Gray, N. S. 2014. Characterization of WZ4003 and HTH-01-015 as selective inhibitors of the LKB1-tumour-suppressor-activated NUAK kinases. *Biochemical Journal,* 457**,** 215-225.

Barp, C. G., Bonaventura, D. & Assreuy, J. 2021. NO, ROS, RAS, and PVAT: More than a soup of letters. *Frontiers in Physiology,* 12**,** 640021.

Bauer, P. M., Fulton, D., Boo, Y. C., Sorescu, G. P., Kemp, B. E., Jo, H. & Sessa, W. C. 2003. Compensatory phosphorylation and protein-protein interactions revealed by loss of function and gain of function mutants of multiple serine phosphorylation sites in endothelial nitric-oxide synthase. *Journal of biological chemistry,* 278**,** 14841-14849.

Bauwens, J. D., Schmuck, E. G., Lindholm, C. R., Ertel, R. L., Mulligan, J. D., Hovis, I., Viollet, B. & Saupe, K. W. 2011. Cold tolerance, cold-induced hyperphagia, and nonshivering thermogenesis are normal in α1-AMPK−/− mice. *American Journal of Physiology-Regulatory, Integrative and Comparative Physiology,* 301**,** R473-R483.

Beckman, J. S., Minor, R., White, C., Repine, J., Rosen, G. & Freeman, B. 1988. Superoxide dismutase and catalase conjugated to polyethylene glycol

increases endothelial enzyme activity and oxidant resistance. *Journal of Biological Chemistry,* 263**,** 6884-6892.

Beg, Z. H., Stonik, J. A. & Brewer Jr, H. B. 1978. 3-Hydroxy-3-methylglutaryl coenzyme A reductase: regulation of enzymatic activity by phosphorylation and dephosphorylation. *Proceedings of the National Academy of Sciences,* 75**,** 3678-3682.

Berbée, J. F., Boon, M. R., Khedoe, P., Bartelt, A., Schlein, C., Worthmann, A., Kooijman, S., Hoeke, G., Mol, I. M. & John, C. 2015. Brown fat activation reduces hypercholesterolaemia and protects from atherosclerosis development. *Nature communications,* 6**,** 1-11.

Bernatchez, P., Sharma, A., Bauer, P. M., Marin, E. & Sessa, W. C. 2011. A noninhibitory mutant of the caveolin-1 scaffolding domain enhances eNOS-derived NO synthesis and vasodilation in mice. *J Clin Invest,* 121**,** 3747-55.

Bernatchez, P. N., Bauer, P. M., Yu, J., Prendergast, J. S., He, P. & Sessa, W. C. 2005. Dissecting the molecular control of endothelial NO synthase by caveolin-1 using cell-permeable peptides. *Proceedings of the National Academy of Sciences,* 102**,** 761-766.

Bhattacharya, S., Patra, S. C., Roy, S. B., Kahn, N. & Sinha, A. K. 2001. Purification and properties of insulin-activated nitric oxide synthase from human erythrocyte membranes. *Archives of physiology and biochemistry,* 109**,** 441-449.

Boateng, S. Y., Olfert, I. M. & Chantler, P. D. 2021. Role of perivascular adipose tissue and exercise on arterial function with obesity. *Exercise and sport sciences reviews,* 49**,** 188.

Böger, R. H. 2003. Association of asymmetric dimethylarginine and endothelial dysfunction. *Clin Chem Lab Med,* 41**,** 1467-72.

Boo, Y. C., Sorescu, G., Boyd, N., Shiojima, I., Walsh, K., Du, J. & Jo, H. 2002. Shear stress stimulates phosphorylation of endothelial nitric-oxide synthase at Ser1179 by Akt-independent mechanisms: role of protein kinase A. *Journal of Biological Chemistry,* 277**,** 3388-3396.

Bosc, N., Muller, C., Hoffer, L., Lagorce, D., Bourg, S., Derviaux, C., Gourdel, M.-E., Rain, J.-C., Miller, T. W. & Villoutreix, B. O. 2020. Fr-PPIChem: An academic compound library dedicated to protein–protein interactions. *ACS chemical biology,* 15**,** 1566-1574.

Boudaba, N., Marion, A., Huet, C., Pierre, R., Viollet, B. & Foretz, M. 2018. AMPK re-activation suppresses hepatic steatosis but its downregulation does not promote fatty liver development. *EBioMedicine,* 28**,** 194-209.

Bouloumié, A., Bauersachs, J., Linz, W., Schölkens, B. A., Wiemer, G., Fleming, I. & Busse, R. 1997. Endothelial dysfunction coincides with an enhanced nitric oxide synthase expression and superoxide anion production. *Hypertension,* 30**,** 934-941.

Bourron, O., Daval, M., Hainault, I., Hajduch, E., Servant, J., Gautier, J., Ferre, P. & Foufelle, F. 2010. Biguanides and thiazolidinediones inhibit stimulated lipolysis in human adipocytes through activation of AMP-activated protein kinase. *Diabetologia,* 53**,** 768-778.

Boyle, J. G., Logan, P. J., Ewart, M.-A., Reihill, J. A., Ritchie, S. A., Connell, J. M., Cleland, S. J. & Salt, I. P. 2008. Rosiglitazone stimulates nitric oxide synthesis in human aortic endothelial cells via AMP-activated protein kinase. *Journal of Biological Chemistry,* 283**,** 11210-11217.

Bredt, D. 1990. Hwang PM, and Snyder SH. *Localization of nitric oxide synthase indicating a neural role for nitric oxide. Nature,* 347**,** 768-770.

Brown, N. K., Zhou, Z., Zhang, J., Zeng, R., Wu, J., Eitzman, D. T., Chen, Y. E. & Chang, L. 2014. Perivascular adipose tissue in vascular function and disease: a review of current research and animal models. *Arteriosclerosis, thrombosis, and vascular biology,* 34**,** 1621-1630.

Bultot, L., Jensen, T. E., Lai, Y.-C., Madsen, A. L., Collodet, C., Kviklyte, S., Deak, M., Yavari, A., Foretz, M. & Ghaffari, S. 2016. Benzimidazole derivative small-molecule 991 enhances AMPK activity and glucose uptake induced by AICAR or contraction in skeletal muscle. *American Journal of Physiology-Endocrinology and Metabolism,* 311**,** E706-E719.

Burridge, K. & Wennerberg, K. 2004. Rho and Rac take center stage. *Cell,* 116**,** 167-179.

Butt, E., Bernhardt, M., Smolenski, A., Kotsonis, P., Fröhlich, L. G., Sickmann, A., Meyer, H. E., Lohmann, S. M. & Schmidt, H. H. 2000. Endothelial nitric-oxide synthase (type III) is activated and becomes calcium independent upon phosphorylation by cyclic nucleotide-dependent protein kinases. *Journal of Biological Chemistry,* 275**,** 5179-5187.

Cai, H., Davis, M. E., Drummond, G. R. & Harrison, D. G. 2001. Induction of endothelial NO synthase by hydrogen peroxide via a Ca2+/calmodulin-dependent protein kinase II/janus kinase 2–dependent pathway. *Arteriosclerosis, thrombosis, and vascular biology,* 21**,** 1571-1576.

Campos, A., Burgos-Ravanal, R., González, M. F., Huilcaman, R., Lobos González, L. & Quest, A. F. G. 2019. Cell intrinsic and extrinsic mechanisms of caveolin-1-enhanced metastasis. *Biomolecules,* 9**,** 314.

Cannon, B. & Nedergaard, J. 2004. Brown adipose tissue: function and physiological significance. *Physiol Rev,* 84**,** 277-359.

Cao, G., Xuan, X., Hu, J., Zhang, R., Jin, H. & Dong, H. 2022. How vascular smooth muscle cell phenotype switching contributes to vascular disease. *Cell Communication and Signaling,* 20**,** 1-22.

Capettini, L., Cortes, S., Silva, J., Alvarez-Leite, J. & Lemos, V. 2011. Decreased production of neuronal NOS-derived hydrogen peroxide contributes to endothelial dysfunction in atherosclerosis. *British journal of pharmacology,* 164**,** 1738-1748.

Carling, D., Thornton, C., Woods, A. & Sanders, M. J. 2012. AMP-activated protein kinase: new regulation, new roles? *Biochemical Journal,* 445**,** 11-27.

Carling, D., Zammit, V. A. & Hardie, D. G. 1987. A common bicyclic protein kinase cascade inactivates the regulatory enzymes of fatty acid and cholesterol biosynthesis. *FEBS letters,* 223**,** 217-222.

Carlson, C. A. & Kim, K.-H. 1973. Regulation of hepatic acetyl coenzyme A carboxylase by phosphorylation and dephosphorylation. *Journal of Biological Chemistry,* 248**,** 378-380.

Cassuto, J., Dou, H., Czikora, I., Szabo, A., Patel, V. S., Kamath, V., Belin De Chantemele, E., Feher, A., Romero, M. J. & Bagi, Z. 2014. Peroxynitrite disrupts endothelial caveolae leading to eNOS uncoupling and diminished flow-mediated dilation in coronary arterioles of diabetic patients. *Diabetes,* 63**,** 1381-1393.

Chakraborty, S. & Ain, R. 2017. Nitric-oxide synthase trafficking inducer is a pleiotropic regulator of endothelial cell function and signaling. *Journal of Biological Chemistry,* 292**,** 6600-6620.

Chakravortty, D. & Hensel, M. 2003. Inducible nitric oxide synthase and control of intracellular bacterial pathogens. *Microbes and Infection,* 5**,** 621-627.

Chang, F., Flavahan, S. & Flavahan, N. A. 2019. Potential pitfalls in analyzing structural uncoupling of eNOS: aging is not associated with increased enzyme monomerization. *American Journal of Physiology-Heart and Circulatory Physiology,* 316**,** H80-H88.

Chang, L., Garcia-Barrio, M. T. & Chen, Y. E. 2020. Perivascular adipose tissue regulates vascular function by targeting vascular smooth muscle cells. *Arteriosclerosis, thrombosis, and vascular biology,* 40**,** 1094-1109.

Chang, L., Villacorta, L., Li, R., Hamblin, M., Xu, W., Dou, C., Zhang, J., Wu, J., Zeng, R. & Chen, Y. E. 2012. Loss of perivascular adipose tissue on peroxisome proliferator–activated receptor-γ deletion in smooth muscle cells impairs intravascular thermoregulation and enhances atherosclerosis. *Circulation,* 126**,** 1067-1078.

Chatterjee, B. K., Jayaraj, A., Kumar, V., Blagg, B., Davis, R. E., Jayaram, B., Deep, S. & Chaudhuri, T. K. 2019. Stimulation of heat shock protein 90 chaperone function through binding of a novobiocin analog KU-32. *Journal of Biological Chemistry,* 294**,** 6450-6467.

Chen, C.-A., Druhan, L. J., Varadharaj, S., Chen, Y.-R. & Zweier, J. L. 2008. Phosphorylation of endothelial nitric-oxide synthase regulates superoxide generation from the enzyme. *Journal of Biological Chemistry,* 283**,** 27038-27047.

Chen, F., Kumar, S., Yu, Y., Aggarwal, S., Gross, C., Wang, Y., Chakraborty, T., Verin, A. D., Catravas, J. D. & Lucas, R. 2014. PKC-dependent phosphorylation of eNOS at T495 regulates eNOS coupling and endothelial barrier function in response to G+-toxins. *PLoS One,* 9**,** e99823.

Chen, H., Montagnani, M., Funahashi, T., Shimomura, I. & Quon, M. J. 2003. Adiponectin stimulates production of nitric oxide in vascular endothelial cells. *Journal of Biological Chemistry,* 278**,** 45021-45026.

Chen, H., Vanhoutte, P. M. & Leung, S. W. 2019. Acute activation of endothelial AMPK surprisingly inhibits endothelium-dependent hyperpolarization-like relaxations in rat mesenteric arteries. *British Journal of Pharmacology,* 176**,** 2905-2921.

Chen, H., Vanhoutte, P. M. & Leung, S. W. S. 2020. Vascular adenosine monophosphate-activated protein kinase: Enhancer, brake or both? *Basic & clinical pharmacology & toxicology,* 127**,** 81-91.

Chen, L. & Liu, L. 2016. The regulation of adipogenesis from adipose-derived stem/stromal cells. *The Biology and Therapeutic Application of Mesenchymal Cells***,** 114-130.

Chen, Z.-P., Mitchelhill, K. I., Michell, B. J., Stapleton, D., Rodriguez-Crespo, I., Witters, L. A., Power, D. A., De Montellano, P. R. O. & Kemp, B. E. 1999. AMP-activated protein kinase phosphorylation of endothelial NO synthase. *FEBS letters,* 443**,** 285-289.

Chen, Z., Ds Oliveira, S., Zimnicka, A. M., Jiang, Y., Sharma, T., Chen, S., Lazarov, O., Bonini, M. G., Haus, J. M. & Minshall, R. D. 2018. Reciprocal regulation of eNOS and caveolin-1 functions in endothelial cells. *Molecular Biology of the Cell,* 29**,** 1190-1202.

Chen, Z., Peng, I.-C., Sun, W., Su, M.-I., Hsu, P.-H., Fu, Y., Zhu, Y., Defea, K., Pan, S. & Tsai, M.-D. 2009. AMP-activated protein kinase functionally phosphorylates endothelial nitric oxide synthase Ser633. *Circulation research,* 104**,** 496-505.

Choe, S. S., Huh, J. Y., Hwang, I. J., Kim, J. I. & Kim, J. B. 2016. Adipose tissue remodeling: its role in energy metabolism and metabolic disorders. *Frontiers in endocrinology,* 7**,** 30.

Chrissobolis, S., Miller, A. A., Drummond, G. R., Kemp-Harper, B. K. & Sobey, C. G. 2011. Oxidative stress and endothelial dysfunction in cerebrovascular disease. *Frontiers in Bioscience-Landmark,* 16**,** 1733-1745.

Cinelli, M. A., Do, H. T., Miley, G. P. & Silverman, R. B. 2020. Inducible nitric oxide synthase: Regulation, structure, and inhibition. *Medicinal research reviews,* 40**,** 158-189.

Cinti, S. 2011. Between brown and white: novel aspects of adipocyte differentiation. *Annals of medicine,* 43**,** 104-115.

Cohen, A. W., Razani, B., Wang, X. B., Combs, T. P., Williams, T. M., Scherer, P. E. & Lisanti, M. P. 2003. Caveolin-1-deficient mice show insulin resistance and defective insulin receptor protein expression in adipose tissue. *American Journal of Physiology-Cell Physiology,* 285**,** C222-C235.

Cooke, J. P. 2010. DDAH: a target for vascular therapy? *Vasc Med,* 15**,** 235-8.

Cool, B., Zinker, B., Chiou, W., Kifle, L., Cao, N., Perham, M., Dickinson, R., Adler, A., Gagne, G. & Iyengar, R. 2006. Identification and characterization of a small molecule AMPK activator that treats key components of type 2 diabetes and the metabolic syndrome. *Cell metabolism,* 3**,** 403-416.

Cortese-Krott, M. M. & Kelm, M. 2014. Endothelial nitric oxide synthase in red blood cells: key to a new erythrocrine function? *Redox biology,* 2**,** 251-258.

Cortese-Krott, M. M., Rodriguez-Mateos, A., Sansone, R., Kuhnle, G. G., Thasian-Sivarajah, S., Krenz, T., Horn, P., Krisp, C., Wolters, D. & Heiß, C. 2012. Human red blood cells at work: identification and visualization of erythrocytic eNOS activity in health and disease. *Blood, The Journal of the American Society of Hematology,* 120**,** 4229-4237.

Costa, E. D., Rezende, B. A., Cortes, S. F. & Lemos, V. S. 2016. Neuronal nitric oxide synthase in vascular physiology and diseases. *Frontiers in Physiology,* 7**,** 206.

Costa, R. M., Neves, K. B., Tostes, R. C. & Lobato, N. S. 2018. Perivascular adipose tissue as a relevant fat depot for cardiovascular risk in obesity. *Frontiers in physiology,* 9**,** 253.

Crewe, C., Chen, S., Bu, D., Gliniak, C. M., Wernstedt Asterholm, I., Yu, X. X., Joffin, N., De Souza, C. O., Funcke, J. B., Oh, D. Y., Varlamov, O., Robino, J. J., Gordillo, R. & Scherer, P. E. 2022. Deficient Caveolin-1 Synthesis in Adipocytes Stimulates Systemic Insulin-Independent Glucose Uptake via Extracellular Vesicles. *Diabetes,* 71**,** 2496-2512.

Crute, B. E., Seefeld, K., Gamble, J., Kemp, B. E. & Witters, L. A. 1998. Functional domains of the α1 catalytic subunit of the AMP-activated protein kinase. *Journal of Biological Chemistry,* 273**,** 35347-35354.

Csiszar, A., Labinskyy, N., Pinto, J. T., Ballabh, P., Zhang, H., Losonczy, G., Pearson, K., De Cabo, R., Pacher, P. & Zhang, C. 2009. Resveratrol induces mitochondrial biogenesis in endothelial cells. *American Journal of Physiology-Heart and Circulatory Physiology,* 297**,** H13-H20.

Czekay, R.-P., Wilkins-Port, C. E., Higgins, S. P., Freytag, J., Overstreet, J. M., Klein, R. M., Higgins, C. E., Samarakoon, R. & Higgins, P. J. 2011. PAI-1: an integrator of cell signaling and migration. *International journal of cell biology,* 2011.

Daiber, A., Xia, N., Steven, S., Oelze, M., Hanf, A., Kröller-Schön, S., Münzel, T. & Li, H. 2019. New therapeutic implications of endothelial nitric oxide synthase (eNOS) function/dysfunction in cardiovascular disease. *International journal of molecular sciences,* 20**,** 187.

Daly, C. J. 2019. Examining vascular structure and function using confocal microscopy and 3d imaging techniques. *Biomedical Visualisation: Volume 1,* 97-106.

Daval, M., Diot-Dupuy, F., Bazin, R., Hainault, I., Viollet, B., Vaulont, S., Hajduch, E., Ferré, P. & Foufelle, F. 2005. Anti-lipolytic action of AMP-activated protein kinase in rodent adipocytes. *Journal of Biological Chemistry,* 280**,** 25250-25257.

Davis, B. J., Xie, Z., Viollet, B. & Zou, M.-H. 2006. Activation of the AMP-activated kinase by antidiabetes drug metformin stimulates nitric oxide synthesis in vivo by promoting the association of heat shock protein 90 and endothelial nitric oxide synthase. *Diabetes,* 55**,** 496-505.

De Ieso, M. L., Gurley, J. M., Mcclellan, M. E., Gu, X., Navarro, I., Li, G., Gomez-Caraballo, M., Enyong, E., Stamer, W. D. & Elliott, M. H. 2020. Physiologic consequences of caveolin-1 ablation in conventional outflow endothelia. *Investigative Ophthalmology & Visual Science,* 61**,** 32-32.

Deanfield, J. E., Halcox, J. P. & Rabelink, T. J. 2007. Endothelial function and dysfunction: testing and clinical relevance. *Circulation,* 115**,** 1285-1295.

Després, J.-P., Lemieux, I., Bergeron, J., Pibarot, P., Mathieu, P., Larose, E., Rodés-Cabau, J., Bertrand, O. F. & Poirier, P. 2008. Abdominal obesity and the metabolic syndrome: contribution to global cardiometabolic risk. *Arteriosclerosis, thrombosis, and vascular biology,* 28**,** 1039-1049.

Dimmeler, S., Fleming, I., Fisslthaler, B., Hermann, C., Busse, R. & Zeiher, A. M. 1999. Activation of nitric oxide synthase in endothelial cells by Akt-dependent phosphorylation. *Nature,* 399**,** 601-605.

Dinerman, J. L., Lowenstein, C. J. & Snyder, S. 1993. Molecular mechanisms of nitric oxide regulation. Potential relevance to cardiovascular disease. *Circulation Research,* 73**,** 217-222.

Dite, T. A., Langendorf, C. G., Hoque, A., Galic, S., Rebello, R. J., Ovens, A. J., Lindqvist, L. M., Ngoei, K. R., Ling, N. X. & Furic, L. 2018. AMP-activated protein kinase selectively inhibited by the type II inhibitor SBI-0206965. *Journal of Biological Chemistry,* 293**,** 8874-8885.

Dix, M. 2017. Everything you should know about oxidative stress. *Medically reviewed by Timothy J. Legg https://www. sciencedirect. com/science/article/pii/0278691594900116.*

Donev, R. 2018. *Therapeutic proteins and peptides,* Cambridge, MA, Academic Press is an imprint of Elsevier.

Douglas, G., Hale, A. B., Patel, J., Chuaiphichai, S., Al Haj Zen, A., Rashbrook, V. S., Trelfa, L., Crabtree, M. J., Mcneill, E. & Channon, K. M. 2018. Roles for endothelial cell and macrophage Gch1 and tetrahydrobiopterin in atherosclerosis progression. *Cardiovascular Research,* 114**,** 1385-1399.

Drab, M., Verkade, P., Elger, M., Kasper, M., Lohn, M., Lauterbach, B., Menne, J., Lindschau, C., Mende, F. & Luft, F. C. 2001. Loss of caveolae, vascular dysfunction, and pulmonary defects in caveolin-1 gene-disrupted mice. *science,* 293**,** 2449-2452.

Dubrovska, G., Verlohren, S., Luft, F. C. & Gollasch, M. 2004. Mechanisms of ADRF release from rat aortic adventitial adipose tissue. *American Journal of Physiology-Heart and Circulatory Physiology,* 286**,** H1107-H1113.

Dudzinski, D. M., Igarashi, J., Greif, D. & Michel, T. 2006. The regulation and pharmacology of endothelial nitric oxide synthase. *Annual review of pharmacology and toxicology,* 46**,** 235-276.

Duplain, H., Burcelin, R. M., Sartori, C., Cook, S. P., Egli, M., Lepori, M., Vollenweider, P., Pedrazzini, T., Nicod, P. & Thorens, B. 2001. Insulin resistance, hyperlipidemia, and hypertension in mice lacking endothelial nitric oxide synthase. *Circulation,* 104**,** 342-345.

Edgar, K. S., Galvin, O. M., Collins, A., Katusic, Z. S. & Mcdonald, D. M. 2017. BH4-mediated enhancement of endothelial nitric oxide synthase activity reduces hyperoxia-induced endothelial damage and preserves vascular integrity in the neonate. *Investigative ophthalmology & visual science,* 58**,** 230-241.

Egan, D. F., Shackelford, D. B., Mihaylova, M. M., Gelino, S., Kohnz, R. A., Mair, W., Vasquez, D. S., Joshi, A., Gwinn, D. M. & Taylor, R. 2011. Phosphorylation of ULK1 (hATG1) by AMP-activated protein kinase connects energy sensing to mitophagy. *Science,* 331**,** 456-461.

Enerbäck, S. 2013. Adipose tissue plasticity and new therapeutic targets. *Nature Reviews Endocrinology,* 9**,** 69-70.

Ewart, M.-A. & Kennedy, S. 2011. AMPK and vasculoprotection. *Pharmacology & therapeutics,* 131**,** 242-253.

Fadó, R., Rodríguez-Rodríguez, R. & Casals, N. 2021. The return of malonyl-CoA to the brain: Cognition and other stories. *Progress in lipid research,* 81**,** 101071.

Fan, J. Y., Carpentier, J., Van Obberghen, E., Grunfeld, C., Gorden, P. & Orci, L. 1983. Morphological changes of the 3T3-L1 fibroblast plasma membrane upon differentiation to the adipocyte form. *Journal of cell science,* 61**,** 219-230.

Fernández-Hernando, C., Fukata, M., Bernatchez, P. N., Fukata, Y., Lin, M. I., Bredt, D. S. & Sessa, W. C. 2006. Identification of Golgi-localized acyl transferases that palmitoylate and regulate endothelial nitric oxide synthase. *The Journal of cell biology,* 174**,** 369-377.

Fésüs, G., Dubrovska, G., Gorzelniak, K., Kluge, R., Huang, Y., Luft, F. C. & Gollasch, M. 2007. Adiponectin is a novel humoral vasodilator. *Cardiovascular research,* 75**,** 719-727.

Fisslthaler, B. & Fleming, I. 2009. Activation and signaling by the AMP-activated protein kinase in endothelial cells. *Circulation research,* 105**,** 114-127.

Fitzgibbons, T. P., Kogan, S., Aouadi, M., Hendricks, G. M., Straubhaar, J. & Czech, M. P. 2011. Similarity of mouse perivascular and brown adipose tissues and their resistance to diet-induced inflammation. *American*

Journal of Physiology-Heart and Circulatory Physiology, 301**,** H1425-H1437.

Fleming, I. & Busse, R. 2003. Molecular mechanisms involved in the regulation of the endothelial nitric oxide synthase. *American Journal of Physiology-Regulatory, Integrative and Comparative Physiology,* 284**,** R1-R12.

Fleming, I., Fisslthaler, B., Dimmeler, S., Kemp, B. E. & Busse, R. 2001. Phosphorylation of Thr495 regulates Ca2+/calmodulin-dependent endothelial nitric oxide synthase activity. *Circulation research,* 88**,** e68-e75.

Fogarty, S., Hawley, S. A., Green, K. A., Saner, N., Mustard, K. J. & Hardie, D. G. 2010. Calmodulin-dependent protein kinase kinase-β activates AMPK without forming a stable complex: synergistic effects of Ca2+ and AMP. *Biochemical Journal,* 426**,** 109-118.

Förstermann, U., Closs, E. I., Pollock, J. S., Nakane, M., Schwarz, P., Gath, I. & Kleinert, H. 1994. Nitric oxide synthase isozymes. Characterization, purification, molecular cloning, and functions. *Hypertension,* 23**,** 1121-1131.

Förstermann, U. & Li, H. 2011. Therapeutic effect of enhancing endothelial nitric oxide synthase (eNOS) expression and preventing eNOS uncoupling. *British journal of pharmacology,* 164**,** 213-223.

Förstermann, U. & Sessa, W. C. 2012. Nitric oxide synthases: regulation and function. *European heart journal,* 33**,** 829-837.

Förstermann, U., Xia, N. & Li, H. 2017. Roles of vascular oxidative stress and nitric oxide in the pathogenesis of atherosclerosis. *Circulation research,* 120**,** 713-735.

Freedman, J. E., Sauter, R., Battinelli, E. M., Ault, K., Knowles, C., Huang, P. L. & Loscalzo, J. 1999. Deficient platelet-derived nitric oxide and enhanced hemostasis in mice lacking the NOSIII gene. *Circulation research,* 84**,** 1416-1421.

Fridolfsson, H. N., Roth, D. M., Insel, P. A. & Patel, H. H. 2014. Regulation of intracellular signaling and function by caveolin. *The FASEB Journal,* 28**,** 3823-3831.

Frontini, A., Vitali, A., Perugini, J., Murano, I., Romiti, C., Ricquier, D., Guerrieri, M. & Cinti, S. 2013. White-to-brown transdifferentiation of omental adipocytes in patients affected by pheochromocytoma. *Biochimica et Biophysica Acta (BBA)-Molecular and Cell Biology of Lipids,* 1831**,** 950-959.

Fryer, L. G., Parbu-Patel, A. & Carling, D. 2002. The anti-diabetic drugs rosiglitazone and metformin stimulate AMP-activated protein kinase through distinct signaling pathways. *Journal of Biological Chemistry,* 277**,** 25226-25232.

Fulton, D., Babbitt, R., Zoellner, S., Fontana, J., Acevedo, L., Mccabe, T. J., Iwakiri, Y. & Sessa, W. C. 2004. Targeting of endothelial nitric-oxide synthase to the cytoplasmic face of the Golgi complex or plasma membrane regulates Akt-versus calcium-dependent mechanisms for nitric oxide release. *Journal of Biological Chemistry,* 279**,** 30349-30357.

Gallis, B., Corthals, G. L., Goodlett, D. R., Ueba, H., Kim, F., Presnell, S. R., Figeys, D., Harrison, D. G., Berk, B. C. & Aebersold, R. 1999. Identification of flow-dependent endothelial nitric-oxide synthase phosphorylation sites by mass spectrometry and regulation of phosphorylation and nitric oxide production by the phosphatidylinositol 3-kinase inhibitor LY294002. *Journal of Biological Chemistry,* 274**,** 30101-30108.

Gao, J., Xiong, R., Xiong, D., Zhao, W., Zhang, S., Yin, T., Zhang, X., Jiang, G. & Yin, Z. 2018. The Adenosine Monophosphate (AMP) Analog, 5-Aminoimidazole-4-Carboxamide Ribonucleotide (AICAR) Inhibits Hepatosteatosis and Liver Tumorigenesis in a High-Fat Diet Murine Model Treated with Diethylnitrosamine (DEN). *Med Sci Monit,* 24**,** 8533-8543.

Gao, Y.-J. 2007. Dual modulation of vascular function by perivascular adipose tissue and its potential correlation with adiposity/lipoatrophy-related vascular dysfunction. *Current pharmaceutical design,* 13**,** 2185-2192.

Gao, Y.-J., Takemori, K., Su, L.-Y., An, W.-S., Lu, C., Sharma, A. M. & Lee, R. M. 2006. Perivascular adipose tissue promotes vasoconstriction: the role of superoxide anion. *Cardiovascular research,* 71**,** 363-373.

Gao, Y.-J., Zeng, Z.-H., Teoh, K., Sharma, A. M., Abouzahr, L., Cybulsky, I., Lamy, A., Semelhago, L. & Lee, R. M. 2005. Perivascular adipose tissue modulates vascular function in the human internal thoracic artery. *The Journal of thoracic and cardiovascular surgery,* 130**,** 1130-1136.

Gao, Y. J., Lu, C., Su, L. Y., Sharma, A. & Lee, R. 2007. Modulation of vascular function by perivascular adipose tissue: the role of endothelium and hydrogen peroxide. *British journal of pharmacology,* 151**,** 323-331.

Garcia-Cardena, G., Martasek, P. & Masters, S. 1997. PM, Couet, J., Li, S., Lisanti, M. P., & Sessa, WC Dissecting the interaction between nitric oxide synthase (NOS) and caveolin. Functional significance of the noscaveolin binding domain in vivo. *J Biol Chem,* 272**,** 25437-25440.

Garcia, D., Mihaylova, M. M. & Shaw, R. J. 2020a. AMPK: central Regulator of glucose and lipid metabolism and target of type 2 diabetes therapeutics. *The Liver: Biology and Pathobiology***,** 472-484.

Garcia, D. & Shaw, R. J. 2017. AMPK: mechanisms of cellular energy sensing and restoration of metabolic balance. *Molecular cell,* 66**,** 789-800.

Garcia, V., Park, E. J., Siragusa, M., Frohlich, F., Mahfuzul Haque, M., Pascale, J. V., Heberlein, K. R., Isakson, B. E., Stuehr, D. J. & Sessa, W. C. 2020b. Unbiased proteomics identifies plasminogen activator inhibitor-1 as a negative regulator of endothelial nitric oxide synthase. *Proceedings of the National Academy of Sciences,* 117**,** 9497-9507.

Garcia, V. & Sessa, W. C. 2019. Endothelial NOS: perspective and recent developments. *British Journal of Pharmacology,* 176**,** 189-196.

Garg, U. C. & Hassid, A. 1989. Nitric oxide-generating vasodilators and 8-bromo-cyclic guanosine monophosphate inhibit mitogenesis and proliferation of cultured rat vascular smooth muscle cells. *The Journal of clinical investigation,* 83**,** 1774-1777.

Gaynullina, D. K., Tarasova, O. S., Shvetsova, A. A., Borzykh, A. A. & Schubert, R. 2022. The effects of acidosis on eNOS in the systemic vasculature: a focus on early postnatal ontogenesis. *International Journal of Molecular Sciences,* 23**,** 5987.

Ghosh, S., Wolan, D., Adak, S., Crane, B. R., Kwon, N. S., Tainer, J. A., Getzoff, E. D. & Stuehr, D. J. 1999. Mutational analysis of the tetrahydrobiopterin-binding site in inducible nitric-oxide synthase. *Journal of Biological Chemistry,* 274**,** 24100-24112.

Gil-Ortega, M., Somoza, B., Huang, Y., Gollasch, M. & Fernández-Alfonso, M. S. 2015. Regional differences in perivascular adipose tissue impacting vascular homeostasis. *Trends in Endocrinology & Metabolism,* 26**,** 367-375.

Giri, S., Rattan, R., Haq, E., Khan, M., Yasmin, R., Won, J.-S., Key, L., Singh, A. K. & Singh, I. 2006. AICAR inhibits adipocyte differentiation in 3T3L1 and restores metabolic alterations in diet-induced obesity mice model. *Nutrition & metabolism,* 3**,** 1-20.

Gonzalez-Munoz, E., Lopez-Iglesias, C., Calvo, M., Palacín, M., Zorzano, A. & Camps, M. 2009. Caveolin-1 loss of function accelerates glucose transporter 4 and insulin receptor degradation in 3T3-L1 adipocytes. *Endocrinology,* 150**,** 3493-3502.

Gonzalez, E., Kou, R., Lin, A. J., Golan, D. E. & Michel, T. 2002. Subcellular targeting and agonist-induced site-specific phosphorylation of endothelial nitric-oxide synthase. *Journal of Biological Chemistry,* 277**,** 39554-39560.

Gonzalez, E., Kou, R. & Michel, T. 2006. Rac1 modulates sphingosine 1-phosphate-mediated activation of phosphoinositide 3-kinase/Akt signaling pathways in vascular endothelial cells. *Journal of Biological Chemistry,* 281**,** 3210-3216.

Gonzalez, E., Nagiel, A., Lin, A. J., Golan, D. E. & Michel, T. 2004. Small interfering RNA-mediated down-regulation of caveolin-1 differentially modulates signaling pathways in endothelial cells. *Journal of Biological Chemistry,* 279**,** 40659-40669.

GöRansson, O., Mcbride, A., Hawley, S. A., Ross, F. A., Shpiro, N., Foretz, M., Viollet, B., Hardie, D. G. & Sakamoto, K. 2007. Mechanism of action of A-769662, a valuable tool for activation of AMP-activated protein kinase. *Journal of Biological Chemistry,* 282**,** 32549-32560.

Gowans, G. J. & Hardie, D. G. 2014. AMPK: a cellular energy sensor primarily regulated by AMP. *Biochem Soc Trans,* 42**,** 71-5.

Gratton, J.-P., Fontana, J., O'connor, D. S., García-Cardeña, G., Mccabe, T. J. & Sessa, W. C. 2000. Reconstitution of an endothelial nitric-oxide synthase (eNOS), hsp90, and caveolin-1 complex in vitro: evidence that hsp90 facilitates calmodulin stimulated displacement of eNOS from caveolin-1. *Journal of Biological Chemistry,* 275**,** 22268-22272.

Greenstein, A. S., Khavandi, K., Withers, S. B., Sonoyama, K., Clancy, O., Jeziorska, M., Laing, I., Yates, A. P., Pemberton, P. W. & Malik, R. A. 2009. Local inflammation and hypoxia abolish the protective anticontractile properties of perivascular fat in obese patients. *Circulation,* 119**,** 1661-1670.

Greif, M., Becker, A., Von Ziegler, F., Lebherz, C., Lehrke, M., Broedl, U. C., Tittus, J., Parhofer, K., Becker, C. & Reiser, M. 2009. Pericardial adipose tissue determined by dual source CT is a risk factor for coronary atherosclerosis. *Arteriosclerosis, thrombosis, and vascular biology,* 29**,** 781-786.

Griendling, K. K., Touyz, R. M., Zweier, J. L., Dikalov, S., Chilian, W., Chen, Y.-R., Harrison, D. G. & Bhatnagar, A. 2016. Measurement of reactive oxygen species, reactive nitrogen species, and redox-dependent signaling in the cardiovascular system: a scientific statement from the American Heart Association. *Circulation research,* 119**,** e39-e75.

Grigoras, A., Amalinei, C., Balan, R. A., Giusca, S. E. & Caruntu, I. D. 2019. Perivascular adipose tissue in cardiovascular diseases-an update. *Anatolian Journal of Cardiology,* 22**,** 219.

Gupta, K. K., Donahue, D. L., Sandoval-Cooper, M. J., Castellino, F. J. & Ploplis, V. A. 2017. Plasminogen activator inhibitor-1 protects mice against cardiac fibrosis by inhibiting urokinase-type plasminogen activator-mediated plasminogen activation. *Scientific reports,* 7**,** 1-11.

Gwinn, D. 2008. Shackelford DB, Egan DF, Mihaylova MM, Mery A, Vasquez DS, Turk BE, Shaw RJ. *AMPK phosphorylation of raptor mediates a metabolic checkpoint. Mol Cell,* 30**,** 214-226.

Han, F., Hou, N., Liu, Y., Huang, N., Pan, R., Zhang, X., Mao, E. & Sun, X. 2019. Liraglutide improves vascular dysfunction by regulating a cAMP-independent PKA-AMPK pathway in perivascular adipose tissue in obese mice. *Biomedicine & Pharmacotherapy,* 120**,** 109537.

Hanafy, K. A., Krumenacker, J. S. & Murad, F. 2001. NO, nitrotyrosine, and cyclic GMP in signal transduction. *Med Sci Monit,* 7**,** 801-19.

Hardie, D. G. 2011. AMP-activated protein kinase—an energy sensor that regulates all aspects of cell function. *Genes & development,* 25**,** 1895-1908.

Hardie, D. G. 2022. AMP-activated protein kinase—a journey from 1 to 100 downstream targets. *Biochemical Journal,* 479**,** 2327-2343.

Hardie, D. G. & Lin, S. C. 2017. AMP-activated protein kinase - not just an energy sensor. *F1000Res,* 6**,** 1724.

Hardie, D. G., Ross, F. A. & Hawley, S. A. 2012. AMPK: a nutrient and energy sensor that maintains energy homeostasis. *Nature reviews Molecular cell biology,* 13**,** 251-262.

Harding, I. C., Mitra, R., Mensah, S. A., Herman, I. M. & Ebong, E. E. 2018. Pro-atherosclerotic disturbed flow disrupts caveolin-1 expression, localization, and function via glycocalyx degradation. *Journal of Translational Medicine,* 16**,** 1-20.

Hasanvand, A. 2022. The role of AMPK-dependent pathways in cellular and molecular mechanisms of metformin: a new perspective for treatment and prevention of diseases. *Inflammopharmacology,* 30**,** 775-788.

Hashimoto, T., Tsuneki, M., Foster, T. R., Santana, J. M., Bai, H., Wang, M., Hu, H., Hanisch, J. J. & Dardik, A. 2016. Membrane-mediated regulation of vascular identity. *Birth Defects Research Part C: Embryo Today: Reviews,* 108**,** 65-84.

Hawley, S. A., Boudeau, J., Reid, J. L., Mustard, K. J., Udd, L., Mäkelä, T. P., Alessi, D. R. & Hardie, D. G. 2003. Complexes between the LKB1 tumor suppressor, STRADα/β and MO25α/β are upstream kinases in the AMP-activated protein kinase cascade. *Journal of biology,* 2**,** 1-16.

Hawley, S. A., Davison, M., Woods, A., Davies, S. P., Beri, R. K., Carling, D. & Hardie, D. G. 1996. Characterization of the AMP-activated protein kinase kinase from rat liver and identification of threonine 172 as the major site at which it phosphorylates AMP-activated protein kinase. *Journal of Biological Chemistry,* 271**,** 27879-27887.

Hawley, S. A., Fullerton, M. D., Ross, F. A., Schertzer, J. D., Chevtzoff, C., Walker, K. J., Peggie, M. W., Zibrova, D., Green, K. A. & Mustard, K. J. 2012. The ancient drug salicylate directly activates AMP-activated protein kinase. *Science,* 336**,** 918-922.

Hawley, S. A., Pan, D. A., Mustard, K. J., Ross, L., Bain, J., Edelman, A. M., Frenguelli, B. G. & Hardie, D. G. 2005. Calmodulin-dependent protein kinase kinase-β is an alternative upstream kinase for AMP-activated protein kinase. *Cell metabolism,* 2**,** 9-19.

Hawley, S. A., Ross, F. A., Chevtzoff, C., Green, K. A., Evans, A., Fogarty, S., Towler, M. C., Brown, L. J., Ogunbayo, O. A. & Evans, A. M. 2010. Use of cells expressing γ subunit variants to identify diverse mechanisms of AMPK activation. *Cell metabolism,* 11**,** 554-565.

Hayer, A., Stoeber, M., Ritz, D., Engel, S., Meyer, H. H. & Helenius, A. 2010. Caveolin-1 is ubiquitinated and targeted to intralumenal vesicles in endolysosomes for degradation. *Journal of Cell Biology,* 191**,** 615-629.

He, A., Hu, S., Pi, Q., Guo, Y., Long, Y., Luo, S. & Xia, Y. 2020. Regulation of O-GlcNAcylation on endothelial nitric oxide synthase by glucose deprivation and identification of its O-GlcNAcylation sites. *Scientific Reports,* 10**,** 1-14.

He, C., Li, H., Viollet, B., Zou, M.-H. & Xie, Z. 2015. AMPK suppresses vascular inflammation in vivo by inhibiting signal transducer and activator of transcription-1. *Diabetes,* 64**,** 4285-4297.

He, Y., Li, Y., Zhao, T., Wang, Y. & Sun, C. 2013. Ursolic acid inhibits adipogenesis in 3T3-L1 adipocytes through LKB1/AMPK pathway. *PloS one,* 8**,** e70135.

Heidary Moghaddam, R., Samimi, Z., Asgary, S., Mohammadi, P., Hozeifi, S., Hoseinzadeh-Chahkandak, F., Xu, S. & Farzaei, M. H. 2022. Natural AMPK activators in cardiovascular disease prevention. *Frontiers in Pharmacology***,** 3323.

Heiss, E. & Dirsch, V. 2014a. Regulation of eNOS enzyme activity by posttranslational modification. *Current pharmaceutical design,* 20**,** 3503-3513.

Heiss, E. H. & Dirsch, V. M. 2014b. Regulation of eNOS enzyme activity by posttranslational modification. *Curr Pharm Des,* 20**,** 3503-13.

Hemminki, A., Markie, D., Tomlinson, I., Avizienyte, E., Roth, S., Loukola, A., Bignell, G., Warren, W., Aminoff, M. & Höglund, P. 1998. A serine/threonine kinase gene defective in Peutz–Jeghers syndrome. *Nature,* 391**,** 184-187.

Higueruelo, A. P., Jubb, H. & Blundell, T. L. 2013. TIMBAL v2: update of a database holding small molecules modulating protein–protein interactions. *Database,* 2013.

Hildebrand, S., Stümer, J. & Pfeifer, A. 2018. PVAT and its relation to brown, beige, and white adipose tissue in development and function. *Frontiers in Physiology,* 9**,** 70.

Horman, S., Morel, N., Vertommen, D., Hussain, N., Neumann, D., Beauloye, C., El Najjar, N., Forcet, C., Viollet, B. & Walsh, M. P. 2008. AMP-activated Protein Kinase Phosphorylates and Desensitizes Smooth Muscle Myosin Light Chain Kinase*♦. *Journal of Biological Chemistry,* 283**,** 18505-18512.

Hsu, C. P., Zhao, J. F., Lin, S. J., Shyue, S. K., Guo, B. C., Lu, T. M. & Lee, T. S. 2016. Asymmetric dimethylarginine limits the efficacy of simvastatin activating endothelial nitric oxide synthase. *Journal of the American Heart Association,* 5**,** e003327.

Hsu, W.-H., Chen, T.-H., Lee, B.-H., Hsu, Y.-W. & Pan, T.-M. 2014. Monascin and ankaflavin act as natural AMPK activators with PPARα agonist activity to down-regulate nonalcoholic steatohepatitis in high-fat diet-fed C57BL/6 mice. *Food and Chemical Toxicology,* 64**,** 94-103.

Hu, D., Yin, C., Luo, S., Habenicht, A. J. & Mohanta, S. K. 2019. Vascular smooth muscle cells contribute to atherosclerosis immunity. *Frontiers in immunology,* 10**,** 1101.

Hu, L., Zhao, R., Liu, Q. & Li, Q. 2020. New insights into heat shock protein 90 in the pathogenesis of pulmonary arterial hypertension. *Frontiers in Physiology,* 11**,** 1081.

Hulin, J.-A., Gubareva, E. A., Jarzebska, N., Rodionov, R. N., Mangoni, A. A. & Tommasi, S. 2020. Inhibition of dimethylarginine dimethylaminohydrolase (DDAH) enzymes as an emerging therapeutic strategy to target angiogenesis and vasculogenic mimicry in cancer. *Frontiers in Oncology,* 9**,** 1455.

Ignoul, S. & Eggermont, J. 2005. CBS domains: structure, function, and pathology in human proteins. *American Journal of Physiology-Cell Physiology,* 289**,** C1369-C1378.

Iseli, T. J., Walter, M., Van Denderen, B. J., Katsis, F., Witters, L. A., Kemp, B. E., Michell, B. J. & Stapleton, D. 2005. AMP-activated protein kinase β subunit tethers α and γ subunits via its C-terminal sequence (186–270). *Journal of Biological Chemistry,* 280**,** 13395-13400.

Isoda, K., Young, J. L., Zirlik, A., Macfarlane, L. A., Tsuboi, N., Gerdes, N., Schonbeck, U. & Libby, P. 2006. Metformin inhibits proinflammatory responses and nuclear factor-κB in human vascular wall cells. *Arteriosclerosis, thrombosis, and vascular biology,* 26**,** 611-617.

Jackson, W. F. 2017. Boosting the signal: Endothelial inward rectifier K(+) channels. *Microcirculation,* 24.

Johanns, M., Hue, L. & Rider, M. H. 2023. AMPK inhibits liver gluconeogenesis: fact or fiction? *Biochemical Journal,* 480**,** 105-125.

Jørgensen, S. B., Viollet, B., Andreelli, F., Frøsig, C., Birk, J. B., Schjerling, P., Vaulont, S., Richter, E. A. & Wojtaszewski, J. F. 2004. Knockout of the α2 but not α1 5′-AMP-activated protein kinase isoform abolishes 5-aminoimidazole-4-carboxamide-1-β-4-ribofuranosidebut not contraction-induced glucose uptake in skeletal muscle. *Journal of Biological Chemistry,* 279**,** 1070-1079.

Ju, H., Zou, R., Venema, V. J. & Venema, R. C. 1997. Direct interaction of endothelial nitric-oxide synthase and caveolin-1 inhibits synthase activity. *Journal of Biological Chemistry,* 272**,** 18522-18525.

Jung, E., Lee, N. K., Kang, S.-K., Choi, S.-H., Kim, D., Park, K., Choi, K., Choi, Y.-J. & Jung, D. H. 2012. Identification of tissue-specific targeting peptide. *Journal of computer-aided molecular design,* 26**,** 1267-1275.

Kahn, B. B., Alquier, T., Carling, D. & Hardie, D. G. 2005. AMP-activated protein kinase: ancient energy gauge provides clues to modern understanding of metabolism. *Cell metabolism,* 1**,** 15-25.

Kang, L. S., Nurkiewicz, T. R., Wu, G. & Boegehold, M. A. 2012. Changes in eNOS phosphorylation contribute to increased arteriolar NO release during juvenile growth. *American Journal of Physiology-Heart and Circulatory Physiology,* 302**,** H560-H566.

Kapur, S., Marcotte, B. & Marette, A. 1999. Mechanism of adipose tissue iNOS induction in endotoxemia. *American Journal of Physiology-Endocrinology And Metabolism,* 276**,** E635-E641.

Karabiyik, C. 2021. *A study on non-canonical autophagy signalling.* University of Cambridge.

Katwan, O. J., Alghamdi, F., Almabrouk, T. A., Mancini, S. J., Kennedy, S., Oakhill, J. S., Scott, J. W. & Salt, I. P. 2019. AMP-activated protein kinase complexes containing the ß2 regulatory subunit are up-regulated during and contribute to adipogenesis. *Biochemical Journal,* 476**,** 1725-1740.

Kawabe, J.-I., Grant, B. S., Yamamoto, M., Schwencke, C., Okumura, S. & Ishikawa, Y. 2001. Changes in caveolin subtype protein expression in aging rat organs. *Molecular and cellular endocrinology,* 176**,** 91-95.

Kawachi, H., Moriya, N. H., Korai, T., Tanaka, S.-Y., Watanabe, M., Matsui, T., Kawada, T. & Yano, H. 2007. Nitric oxide suppresses preadipocyte differentiation in 3T3-L1 culture. *Molecular and cellular biochemistry,* 300**,** 61-67.

Khalil, R. A. Regulation of vascular smooth muscle function. Colloquium Series on Integrated Systems Physiology: From Molecule to Function, 2010. Morgan & Claypool Life Sciences, 1-62.

Kim, J., Kim, Y. C., Fang, C., Russell, R. C., Kim, J. H., Fan, W., Liu, R., Zhong, Q. & Guan, K.-L. 2013. Differential regulation of distinct Vps34 complexes by AMPK in nutrient stress and autophagy. *Cell,* 152**,** 290-303.

Kim, J., Kundu, M., Viollet, B. & Guan, K.-L. 2011. AMPK and mTOR regulate autophagy through direct phosphorylation of Ulk1. *Nature cell biology,* 13**,** 132-141.

Kim, S. A. & Choi, H. C. 2012. Metformin inhibits inflammatory response via AMPK–PTEN pathway in vascular smooth muscle cells. *Biochemical and biophysical research communications,* 425**,** 866-872.

Kinsella, B. T., Erdman, R. & Maltese, W. 1991. Carboxyl-terminal isoprenylation of ras-related GTP-binding proteins encoded by rac1, rac2, and ralA. *Journal of Biological Chemistry,* 266**,** 9786-9794.

Kitaura, H., Uozumi, N., Tohmi, M., Yamazaki, M., Sakimura, K., Kudoh, M., Shimizu, T. & Shibuki, K. 2007. Roles of nitric oxide as a vasodilator in neurovascular coupling of mouse somatosensory cortex. *Neuroscience research,* 59**,** 160-171.

Kleinbongard, P., Schulz, R., Rassaf, T., Lauer, T., Dejam, A., Jax, T., Kumara, I., Gharini, P., Kabanova, S. & ÖZüYaman, B. 2006. Red blood cells express a functional endothelial nitric oxide synthase. *Blood,* 107**,** 2943-2951.

Knowles, R. G. & Moncada, S. 1994. Nitric oxide synthases in mammals. *Biochemical Journal,* 298**,** 249.

Kolluru, G. K., Siamwala, J. H. & Chatterjee, S. 2010. eNOS phosphorylation in health and disease. *Biochimie,* 92**,** 1186-1198.

Kong, L.-R., Zhou, Y.-P., Chen, D.-R., Ruan, C.-C. & Gao, P.-J. 2018. Decrease of perivascular adipose tissue browning is associated with vascular dysfunction in spontaneous hypertensive rats during aging. *Frontiers in Physiology,* 9**,** 400.

Konukoglu, D. & Uzun, H. 2017. Endothelial dysfunction and hypertension. *Hypertension: from basic research to clinical practice***,** 511-540.

Kopietz, F., Alshuweishi, Y., Bijland, S., Alghamdi, F., Degerman, E., Sakamoto, K., Salt, I. P. & Göransson, O. 2021. A-769662 inhibits adipocyte glucose uptake in an AMPK-independent manner. *Biochemical Journal,* 478**,** 633-646.

Kopietz, F., Berggreen, C., Larsson, S., Säll, J., Ekelund, M., Sakamoto, K., Degerman, E., Holm, C. & Göransson, O. 2018. AMPK activation by A-769662 and 991 does not affect catecholamine-induced lipolysis in human adipocytes. *American journal of physiology-endocrinology and metabolism,* 315**,** E1075-E1085.

Krishna, A. & Sengupta, D. 2019. Interplay between membrane curvature and cholesterol: Role of palmitoylated caveolin-1. *Biophysical journal,* 116**,** 69-78.

Król, M. & Kepinska, M. 2020. Human nitric oxide Synthase—Its functions, polymorphisms, and inhibitors in the context of inflammation, diabetes and cardiovascular diseases. *International Journal of Molecular Sciences,* 22**,** 56.

Kuhn, V., Diederich, L., Keller Iv, T. S., Kramer, C. M., Lückstädt, W., Panknin, C., Suvorava, T., Isakson, B. E., Kelm, M. & Cortese-Krott, M. M. 2017. Red blood cell function and dysfunction: redox regulation, nitric oxide metabolism, anemia. *Antioxidants & redox signaling,* 26**,** 718-742.

Kuzkaya, N., Weissmann, N., Harrison, D. G. & Dikalov, S. 2003. Interactions of peroxynitrite, tetrahydrobiopterin, ascorbic acid, and thiols: implications for uncoupling endothelial nitric-oxide synthase. *Journal of Biological Chemistry,* 278**,** 22546-22554.

Labbé, C. M., Kuenemann, M. A., Zarzycka, B., Vriend, G., Nicolaes, G. A., Lagorce, D., Miteva, M. A., Villoutreix, B. O. & Sperandio, O. 2016. iPPI-DB: an online database of modulators of protein–protein interactions. *Nucleic acids research,* 44**,** D542-D547.

Ladurner, A., Atanasov, A. G., Heiss, E. H., Baumgartner, L., Schwaiger, S., Rollinger, J. M., Stuppner, H. & Dirsch, V. M. 2012. 2-(2, 4-dihydroxyphenyl)-5-(E)-propenylbenzofuran promotes endothelial nitric oxide synthase activity in human endothelial cells. *Biochemical Pharmacology,* 84**,** 804-812.

Laher, I. 2014. *Systems biology of free radicals and antioxidants,* Heidelberg, Springer.

Lai, Y.-C., Kviklyte, S., Vertommen, D., Lantier, L., Foretz, M., Viollet, B., Hallén, S. & Rider, M. H. 2014. A small-molecule benzimidazole derivative that potently activates AMPK to increase glucose transport in skeletal muscle: comparison with effects of contraction and other AMPK activators. *Biochemical Journal,* 460**,** 363-375.

Lasar, D., Julius, A., Fromme, T. & Klingenspor, M. 2013. Browning attenuates murine white adipose tissue expansion during postnatal development. *Biochimica et Biophysica Acta (BBA)-Molecular and Cell Biology of Lipids,* 1831**,** 960-968.

Laurindo, F. R., Fernandes, D. C. & Santos, C. X. 2008. Assessment of superoxide production and NADPH oxidase activity by HPLC analysis of dihydroethidium oxidation products. *Methods in enzymology,* 441**,** 237-260.

Lebrasseur, N. K., Kelly, M., Tsao, T.-S., Farmer, S. R., Saha, A. K., Ruderman, N. B. & Tomas, E. 2006. Thiazolidinediones can rapidly activate AMP-activated protein kinase in mammalian tissues. *American Journal of Physiology-Endocrinology and Metabolism,* 291**,** E175-E181.

Lee, J.-A., Choi, D.-I., Choi, J.-Y., Kim, S.-O., Cho, K.-A., Lee, J.-B., Yun, S.-J. & Lee, S.-C. 2015. Methyl-ß-cyclodextrin up-regulates collagen I expression in chronologically-aged skin via its anti-caveolin-1 activity. *Oncotarget,* 6**,** 1942.

Lee, R. M., Lu, C., Su, L.-Y. & Gao, Y.-J. 2009. Endothelium-dependent relaxation factor released by perivascular adipose tissue. *Journal of hypertension,* 27**,** 782-790.

Lefer, D. J., Jones, S. P., Girod, W. G., Baines, A., Grisham, M. B., Cockrell, A. S., Huang, P. L. & Scalia, R. 1999. Leukocyte-endothelial cell interactions in nitric oxide synthase-deficient mice. *American Journal of Physiology-Heart and Circulatory Physiology,* 276**,** H1943-H1950.

Lekontseva, O., Chakrabarti, S., Jiang, Y., Cheung, C. C. & Davidge, S. T. 2011. Role of neuronal nitric-oxide synthase in estrogen-induced relaxation in rat resistance arteries. *Journal of Pharmacology and Experimental Therapeutics,* 339**,** 367-375.

Lerman, A. & Zeiher, A. M. 2005. Endothelial function: cardiac events. *Circulation,* 111**,** 363-368.

Levine, Y. C., Li, G. K. & Michel, T. 2007. Agonist-modulated regulation of AMP-activated protein kinase (AMPK) in endothelial cells: evidence for an AMPK→ Rac1→ Akt→ endothelial nitric-oxide synthase pathway. *Journal of Biological Chemistry,* 282**,** 20351-20364.

Li, S., Couet, J. & Lisanti, M. P. 1996. Src tyrosine kinases, Gα subunits, and H-Ras share a common membrane-anchored scaffolding protein, caveolin: caveolin binding negatively regulates the auto-activation of Src tyrosine kinases. *Journal of Biological Chemistry,* 271**,** 29182-29190.

Li, Y. & Chen, Y. 2019. AMPK and autophagy. *Autophagy: Biology and Diseases*, 85-108.

Li, Z., Ivanov, A. A., Su, R., Gonzalez-Pecchi, V., Qi, Q., Liu, S., Webber, P., Mcmillan, E., Rusnak, L. & Pham, C. 2017. Corrigendum: the OncoPPi network of cancer-focused protein–protein interactions to inform biological insights and therapeutic strategies. *Nature communications,* 8.

Lin, Y., Feng, M., Lu, C.-W., Lei, Y.-P., He, Z.-M. & Xiong, Y. 2017. Preservation of vascular DDAH activity contributes to the protection of captopril against endothelial dysfunction in hyperlipidemic rabbits. *European Journal of Pharmacology,* 798, 43-48.

Liu, V. W. & Huang, P. L. 2008. Cardiovascular roles of nitric oxide: a review of insights from nitric oxide synthase gene disrupted mice. *Cardiovascular research,* 77, 19-29.

Liu, X., Chhipa, R. R., Nakano, I. & Dasgupta, B. 2014. The AMPK Inhibitor Compound C Is a Potent AMPK-Independent Antiglioma AgentAntiglioma Actions of Compound C. *Molecular cancer therapeutics,* 13, 596-605.

Liu, X., Miller, M. J., Joshi, M. S., Thomas, D. D. & Lancaster Jr, J. R. 1998. Accelerated reaction of nitric oxide with O2 within the hydrophobic interior of biological membranes. *Proceedings of the National Academy of Sciences,* 95, 2175-2179.

Liu, Y., Sun, Y., Hu, C., Liu, J., Gao, A., Han, H., Chai, M., Zhang, J., Zhou, Y. & Zhao, Y. 2020. Perivascular adipose tissue as an indication, contributor to, and therapeutic target for atherosclerosis. *Frontiers in Physiology,* 11, 615503.

Löhn, M., Dubrovska, G., Lauterbach, B., Luft, F. C., Gollasch, M. & Sharma, A. M. 2002. Periadventitial fat releases a vascular relaxing factor. *The FASEB Journal,* 16, 1057-1063.

Loot, A. E., Schreiber, J. G., Fisslthaler, B. & Fleming, I. 2009. Angiotensin II impairs endothelial function via tyrosine phosphorylation of the endothelial nitric oxide synthase. *Journal of Experimental Medicine,* 206, 2889-2896.

Lührs, H. 2002. Papadopoulos HH, Schmidt HW, and Menzel T. *Type I nitric oxide synthase in the human lung is predominantly expressed in capillary endothelial cells. Respir Physiol,* 129, 367-374.

Lutz, M. I., Schwaiger, C., Hochreiter, B., Kovacs, G. G. & Schmid, J. A. 2017. Novel approach for accurate tissue-based protein colocalization and proximity microscopy. *Scientific reports,* 7, 1-10.

Lynch, F. M., Withers, S. B., Yao, Z., Werner, M. E., Edwards, G., Weston, A. H. & Heagerty, A. M. 2013. Perivascular adipose tissue-derived adiponectin activates BKCa channels to induce anticontractile responses. *American Journal of Physiology-Heart and Circulatory Physiology,* 304, H786-H795.

Machado, S. A., Pasquarelli-Do-Nascimento, G., Da Silva, D. S., Farias, G. R., De Oliveira Santos, I., Baptista, L. B. & Magalhães, K. G. 2022. Browning of the white adipose tissue regulation: New insights into nutritional and metabolic relevance in health and diseases. *Nutrition & Metabolism,* 19**,** 1-27.

Mack, H. I., Zheng, B., Asara, J. M. & Thomas, S. M. 2012. AMPK-dependent phosphorylation of ULK1 regulates ATG9 localization. *Autophagy,* 8**,** 1197-1214.

Maenhaut, N. & Van De Voorde, J. 2011. Regulation of vascular tone by adipocytes. *BMC medicine,* 9**,** 1-12.

Maiuolo, J., Gliozzi, M., Musolino, V., Carresi, C., Nucera, S., Macrì, R., Scicchitano, M., Bosco, F., Scarano, F. & Ruga, S. 2019. The role of endothelial dysfunction in peripheral blood nerve barrier: molecular mechanisms and pathophysiological implications. *International journal of molecular sciences,* 20**,** 3022.

Malinowski, M., Deja, M. A., Gołba, K. S., Roleder, T., Biernat, J. & Woś, S. 2008. Perivascular tissue of internal thoracic artery releases potent nitric oxide and prostacyclin-independent anticontractile factor. *European journal of cardio-thoracic surgery,* 33**,** 225-231.

Man, A. W., Zhou, Y., Xia, N. & Li, H. 2020. Perivascular adipose tissue as a target for antioxidant therapy for cardiovascular complications. *Antioxidants,* 9**,** 574.

Man, A. W., Zhou, Y., Xia, N. & Li, H. 2022. Endothelial Nitric Oxide Synthase in the Perivascular Adipose Tissue. *Biomedicines,* 10**,** 1754.

Mancini, S. J., Boyd, D., Katwan, O. J., Strembitska, A., Almabrouk, T. A., Kennedy, S., Palmer, T. M. & Salt, I. P. 2018. Canagliflozin inhibits interleukin-1ß-stimulated cytokine and chemokine secretion in vascular endothelial cells by AMP-activated protein kinase-dependent and-independent mechanisms. *Scientific reports,* 8**,** 1-14.

Mancini, S. J., White, A. D., Bijland, S., Rutherford, C., Graham, D., Richter, E. A., Viollet, B., Touyz, R. M., Palmer, T. M. & Salt, I. P. 2017. Activation of AMP-activated protein kinase rapidly suppresses multiple pro-inflammatory pathways in adipocytes including IL-1 receptor-associated kinase-4 phosphorylation. *Molecular and cellular endocrinology,* 440**,** 44-56.

Margaritis, M., Antonopoulos, A. S., Digby, J., Lee, R., Reilly, S., Coutinho, P., Shirodaria, C., Sayeed, R., Petrou, M. & De Silva, R. 2013. Interactions between vascular wall and perivascular adipose tissue reveal novel roles for adiponectin in the regulation of endothelial nitric oxide synthase function in human vessels. *Circulation,* 127**,** 2209-2221.

Matienzo, D. & Bordoni, B. 2023. Anatomy, Blood Flow. *StatPearls*. Treasure Island (FL): StatPearls Publishing Copyright © 2023, StatPearls Publishing LLC.

Mazrouei, S., Sharifpanah, F., Caldwell, R. W., Franz, M., Shatanawi, A., Muessig, J., Fritzenwanger, M., Schulze, P. C. & Jung, C. 2019. Regulation of MAP kinase-mediated endothelial dysfunction in hyperglycemia via arginase I and eNOS dysregulation. *Biochimica et Biophysica Acta (BBA)-Molecular Cell Research,* 1866**,** 1398-1411.

Mcbride, A., Ghilagaber, S., Nikolaev, A. & Hardie, D. G. 2009. The glycogen-binding domain on the AMPK ß subunit allows the kinase to act as a glycogen sensor. *Cell metabolism,* 9**,** 23-34.

Mcgarry, J. 1995. The mitochondrial carnitine palmitoyltransferase system: its broadening role in fuel homoeostasis and new insights into its molecular features. *Biochemical Society Transactions,* 23**,** 321-324.

Merrill, G. F., Kurth, E. J., Hardie, D. & Winder, W. 1997. AICA riboside increases AMP-activated protein kinase, fatty acid oxidation, and glucose uptake in rat muscle. *American Journal of Physiology-Endocrinology And Metabolism,* 273**,** E1107-E1112.

Meyer, M. R., Fredette, N. C., Barton, M. & Prossnitz, E. R. 2013. Regulation of vascular smooth muscle tone by adipose-derived contracting factor. *PloS one,* 8**,** e79245.

Meza, C. A., La Favor, J. D., Kim, D.-H. & Hickner, R. C. 2019. Endothelial dysfunction: is there a hyperglycemia-induced imbalance of NOX and NOS? *International journal of molecular sciences,* 20**,** 3775.

Michel, J. B., Feron, O., Sacks, D. & Michel, T. 1997. Reciprocal regulation of endothelial nitric-oxide synthase by Ca2+-calmodulin and caveolin. *Journal of Biological Chemistry,* 272**,** 15583-15586.

Michell, B., Griffiths, J., Mitchelhill, K., Rodriguez-Crespo, I., Tiganis, T., Bozinovski, S., De Montellano, P. O., Kemp, B. & Pearson, R. 1999. The Akt kinase signals directly to endothelial nitric oxide synthase. *Current biology,* 9**,** 845-S1.

Michell, B. J., Harris, M. B., Chen, Z.-P., Ju, H., Venema, V. J., Blackstone, M. A., Huang, W., Venema, R. C. & Kemp, B. E. 2002. Identification of regulatory sites of phosphorylation of the bovine endothelial nitric-oxide synthase at serine 617 and serine 635. *Journal of Biological Chemistry,* 277**,** 42344-42351.

Mihaylova, M. M. & Shaw, R. J. 2011. The AMPK signalling pathway coordinates cell growth, autophagy and metabolism. *Nature cell biology,* 13**,** 1016-1023.

Miyata, Y. 2005. Hsp90 inhibitor geldanamycin and its derivatives as novel cancer chemotherapeutic agents. *Current pharmaceutical design,* 11**,** 1131-1138.

Mohseni, R., Teimouri, M., Safaei, M. & Arab Sadeghabadi, Z. 2023. AMP-activated protein kinase is a key regulator of obesity-associated factors. *Cell Biochemistry and Function,* 41**,** 20-32.

Moreno-Navarrete, J. M., Ortega, F. J., Rodríguez-Hermosa, J.-I., Sabater, M., Pardo, G., Ricart, W. & Fernández-Real, J. M. 2011. OCT1 expression in adipocytes could contribute to increased metformin action in obese subjects. *Diabetes,* 60**,** 168-176.

Morrow, V. A., Foufelle, F., Connell, J. M., Petrie, J. R., Gould, G. W. & Salt, I. P. 2003. Direct activation of AMP-activated protein kinase stimulates nitric-oxide synthesis in human aortic endothelial cells. *Journal of Biological Chemistry,* 278**,** 31629-31639.

Moseti, D., Regassa, A. & Kim, W.-K. 2016. Molecular regulation of adipogenesis and potential anti-adipogenic bioactive molecules. *International journal of molecular sciences,* 17**,** 124.

Munday, M. R., Campbell, D. G., Carling, D. & Hardie, D. G. 1988. Identification by amino acid sequencing of three major regulatory phosphorylation sites on rat acetyl-CoA carboxylase. *European journal of biochemistry,* 175**,** 331-338.

Münzel, T. & Daiber, A. 2018. Role of endothelial and macrophage tetrahydrobiopterin in development and progression of atherosclerosis: BH4 puzzle solved? *Cardiovascular Research,* 114**,** 1310-1312.

Münzel, T., Gori, T., Bruno, R. M. & Taddei, S. 2010. Is oxidative stress a therapeutic target in cardiovascular disease? *European heart journal,* 31**,** 2741-2748.

Musicki, B., Kramer, M. F., Becker, R. E. & Burnett, A. L. 2005. Inactivation of phosphorylated endothelial nitric oxide synthase (Ser-1177) by O-GlcNAc in diabetes-associated erectile dysfunction. *Proceedings of the National Academy of Sciences,* 102**,** 11870-11875.

Musicki, B., Liu, T., Strong, T. D., Lagoda, G. A., Bivalacqua, T. J. & Burnett, A. L. 2010. Post-translational regulation of endothelial nitric oxide synthase (eNOS) by estrogens in the rat vagina. *The journal of sexual medicine,* 7**,** 1768-1777.

Nakagawa, K., Higashi, Y., Sasaki, S., Ohshima, T., Matsuura, H. & Kajiyama, G. 2000. Leptin Causes Vasodilation in Humans. *Hypertension (Dallas, Tex. 1979),* 36**,** 725-725.

Nam, M., Lee, W. H., Bae, E. J. & Kim, S. G. 2008. Compound C inhibits clonal expansion of preadipocytes by increasing p21 level irrespectively of AMPK inhibition. *Archives of biochemistry and biophysics,* 479**,** 74-81.

Naseem, K. M. 2005. The role of nitric oxide in cardiovascular diseases. *Molecular aspects of medicine,* 26**,** 33-65.

Ngoei, K. R., Langendorf, C. G., Ling, N. X., Hoque, A., Varghese, S., Camerino, M. A., Walker, S. R., Bozikis, Y. E., Dite, T. A. & Ovens, A. J. 2018. Structural determinants for small-molecule activation of skeletal muscle AMPK α2β2γ1 by the glucose importagog SC4. *Cell chemical biology,* 25**,** 728-737. e9.

Ning, J. & Clemmons, D. R. 2010. AMP-activated protein kinase inhibits IGF-I signaling and protein synthesis in vascular smooth muscle cells via stimulation of insulin receptor substrate 1 S794 and tuberous sclerosis 2 S1345 phosphorylation. *Molecular endocrinology,* 24**,** 1218-1229.

Nisoli, E., Clementi, E., Tonello, C., Sciorati, C., Briscini, L. & Carruba, M. O. 1998. Effects of nitric oxide on proliferation and differentiation of rat brown adipocytes in primary cultures. *British journal of pharmacology,* 125**,** 888-894.

Nisoli, E., Tonello, C., Cardile, A., Cozzi, V., Bracale, R., Tedesco, L., Falcone, S., Valerio, A., Cantoni, O. & Clementi, E. 2005. Calorie restriction promotes mitochondrial biogenesis by inducing the expression of eNOS. *Science,* 310**,** 314-317.

Noor, H. B., Mou, N. A., Salem, L., Shimul, M. F., Biswas, S., Akther, R., Khan, S., Raihan, S., Mohib, M. M. & Sagor, M. A. 2020. Anti-inflammatory property of AMP-activated protein kinase. *Anti-Inflammatory & Anti-Allergy Agents in Medicinal Chemistry (Formerly Current Medicinal Chemistry-Anti-Inflammatory and Anti-Allergy Agents),* 19**,** 2-41.

Nwosu, Z. C., Ebert, M. P., Dooley, S. & Meyer, C. 2016. Caveolin-1 in the regulation of cell metabolism: a cancer perspective. *Molecular cancer,* 15**,** 1-12.

Oakhill, J. S., Steel, R., Chen, Z.-P., Scott, J. W., Ling, N., Tam, S. & Kemp, B. E. 2011. AMPK is a direct adenylate charge-regulated protein kinase. *Science,* 332**,** 1433-1435.

Oliveira-Paula, G. H., Lacchini, R. & Tanus-Santos, J. E. 2017. Clinical and pharmacogenetic impact of endothelial nitric oxide synthase polymorphisms on cardiovascular diseases. *Nitric Oxide,* 63**,** 39-51.

Oliveira, S. D., Castellon, M., Chen, J., Bonini, M. G., Gu, X., Elliott, M. H., Machado, R. F. & Minshall, R. D. 2017. Inflammation-induced caveolin-1 and BMPRII depletion promotes endothelial dysfunction and TGF-β-driven pulmonary vascular remodeling. *American Journal of Physiology-Lung Cellular and Molecular Physiology,* 312**,** L760-L771.

Oriowo, M. A. 2015. Perivascular adipose tissue, vascular reactivity and hypertension. *Medical Principles and Practice,* 24**,** 29-37.

Orshal, J. M. & Khalil, R. A. 2004. Interleukin-6 impairs endothelium-dependent NO-cGMP-mediated relaxation and enhances contraction in systemic vessels of pregnant rats. *American Journal of Physiology-Regulatory, Integrative and Comparative Physiology,* 286**,** R1013-R1023.

Ortiz, P. & Garvin, J. 2003. Trafficking and activation of eNOS in epithelial cells. *Acta physiologica scandinavica,* 179**,** 107-114.

Ovens, A. J., Scott, J. W., Langendorf, C. G., Kemp, B. E., Oakhill, J. S. & Smiles, W. J. 2021. Post-translational modifications of the energy guardian AMP-activated protein kinase. *International journal of molecular sciences,* 22**,** 1229.

Owens, G. K., Kumar, M. S. & Wamhoff, B. R. 2004. Molecular regulation of vascular smooth muscle cell differentiation in development and disease. *Physiological reviews,* 84**,** 767-801.

Packer, M. 2020. Role of deranged energy deprivation signaling in the pathogenesis of cardiac and renal disease in states of perceived nutrient overabundance. *Circulation,* 141**,** 2095-2105.

Padilla, J., Jenkins, N. T., Vieira-Potter, V. J. & Laughlin, M. H. 2013. Divergent phenotype of rat thoracic and abdominal perivascular adipose tissues. *American Journal of Physiology-Regulatory, Integrative and Comparative Physiology,* 304**,** R543-R552.

Palacios-Ortega, S., Varela-Guruceaga, M., Algarabel, M., Milagro, F. I., Martínez, J. A. & De Miguel, C. 2015. Effect of tnf-alpha on caveolin-1 expression and insulin signaling during adipocyte differentiation and in mature adipocytes. *Cellular Physiology and Biochemistry,* 36**,** 1499-1516.

Palacios-Ortega, S., Varela-Guruceaga, M., Milagro, F. I., Martínez, J. A. & De Miguel, C. 2014. Expression of Caveolin 1 is enhanced by DNA demethylation during adipocyte differentiation. status of insulin signaling. *PloS one,* 9**,** e95100.

Pang, T., Xiong, B., Li, J.-Y., Qiu, B.-Y., Jin, G.-Z., Shen, J.-K. & Li, J. 2007. Conserved α-helix acts as autoinhibitory sequence in AMP-activated protein kinase α subunits. *Journal of Biological Chemistry,* 282**,** 495-506.

Park, A., Kim, W. K. & Bae, K.-H. 2014. Distinction of white, beige and brown adipocytes derived from mesenchymal stem cells. *World journal of stem cells,* 6**,** 33.

Park, Y.-K., Wang, S. & Jang, B.-C. 2021. Interleukin 1β Up-Regulates mRNA Expression of Inducible Nitric Oxide Synthase in 3T3-L1 Preadipocytes: Role of JAKs/STATs, PKCs, and Src. *Keimyung Medical Journal,* 40**,** 1-8.

Parton, R. G. & Simons, K. 2007. The multiple faces of caveolae. *Nature reviews Molecular cell biology,* 8**,** 185-194.

Pautz, A., Art, J., Hahn, S., Nowag, S., Voss, C. & Kleinert, H. 2010. Regulation of the expression of inducible nitric oxide synthase. *Nitric oxide,* 23**,** 75-93.

Phalitakul, S., Okada, M., Hara, Y. & Yamawaki, H. 2012. A novel adipocytokine, vaspin inhibits platelet-derived growth factor-BB-induced migration of vascular smooth muscle cells. *Biochemical and biophysical research communications,* 423**,** 844-849.

Pi, X., Xie, L. & Patterson, C. 2018. Emerging roles of vascular endothelium in metabolic homeostasis. *Circulation Research,* 123**,** 477-494.

Poher, A.-L., Altirriba, J., Veyrat-Durebex, C. & Rohner-Jeanrenaud, F. 2015. Brown adipose tissue activity as a target for the treatment of obesity/insulin resistance. *Frontiers in physiology*, 4.

Police, S. B., Thatcher, S. E., Charnigo, R., Daugherty, A. & Cassis, L. A. 2009. Obesity promotes inflammation in periaortic adipose tissue and angiotensin II-induced abdominal aortic aneurysm formation. *Arteriosclerosis, thrombosis, and vascular biology,* 29**,** 1458-1464.

Qi, D. & Young, L. H. 2015. AMPK: energy sensor and survival mechanism in the ischemic heart. *Trends in Endocrinology & Metabolism,* 26**,** 422-429.

Quesada, I., Cejas, J., García, R., Cannizzo, B., Redondo, A. & Castro, C. 2018. Vascular dysfunction elicited by a cross talk between periaortic adipose tissue and the vascular wall is reversed by pioglitazone. *Cardiovascular therapeutics,* 36**,** e12322.

Rabelo, L. A., Cortes, S. F., Alvarez-Leite, J. I. & Lemos, V. S. 2003. Endothelium dysfunction in LDL receptor knockout mice: a role for H2O2. *British journal of pharmacology,* 138**,** 1215-1220.

Rafikov, R., Fonseca, F. V., Kumar, S., Pardo, D., Darragh, C., Elms, S., Fulton, D. & Black, S. M. 2011. eNOS activation and NO function: structural motifs responsible for the posttranslational control of endothelial nitric oxide synthase activity. *The Journal of endocrinology,* 210**,** 271.

Ramadoss, J., Pastore, M. B. & Magness, R. R. 2013. Endothelial caveolar subcellular domain regulation of endothelial nitric oxide synthase. *Clinical and Experimental Pharmacology and Physiology,* 40**,** 753-764.

Ramirez, J., O'malley, E. & Ho, W. 2017. Pro-contractile effects of perivascular fat in health and disease. *British Journal of Pharmacology,* 174**,** 3482-3495.

Razani, B., Engelman, J. A., Wang, X. B., Schubert, W., Zhang, X. L., Marks, C. B., Macaluso, F., Russell, R. G., Li, M. & Pestell, R. G. 2001. Caveolin-1 null mice are viable but show evidence of hyperproliferative and vascular abnormalities. *Journal of Biological Chemistry,* 276**,** 38121-38138.

Razani, B., Woodman, S. E. & Lisanti, M. P. 2002. Caveolae: from cell biology to animal physiology. *Pharmacological reviews,* 54**,** 431-467.

Ren, G., Hwang, P. T. J., Millican, R., Shin, J., Brott, B. C., Van Groen, T., Powell, C. M., Bhatnagar, S., Young, M. E. & Jun, H.-W. 2022. Subcutaneous Administration of a Nitric Oxide-Releasing Nanomatrix Gel Ameliorates Obesity and Insulin Resistance in High-Fat Diet-Induced Obese Mice. *ACS Applied Materials & Interfaces,* 14**,** 19104-19115.

Rena, G., Hardie, D. G. & Pearson, E. R. 2017. The mechanisms of action of metformin. *Diabetologia,* 60**,** 1577-1585.

Richard, A. J., White, U., Elks, C. M. & Stephens, J. M. 2020. Adipose tissue: physiology to metabolic dysfunction. *Endotext [Internet] South Dartmouth (MA): MDText.com, Inc.; 2000-. Available from:* https://www.ncbi.nlm.nih.gov/books/NBK555602/.

Ritchie, S. A., Kohlhaas, C. F., Boyd, A. R., Yalla, K. C., Walsh, K., Connell, J. M. & Salt, I. P. 2010. Insulin-stimulated phosphorylation of endothelial

nitric oxide synthase at serine-615 contributes to nitric oxide synthesis. *Biochemical Journal,* 426**,** 85-90.

Rodríguez, C., Muñoz, M., Contreras, C. & Prieto, D. 2021. AMPK, metabolism, and vascular function. *The FEBS Journal,* 288**,** 3746-3771.

Root, K. T., Plucinsky, S. M. & Glover, K. J. 2015. Recent progress in the topology, structure, and oligomerization of caveolin: a building block of caveolae. *Curr Top Membr,* 75**,** 305-36.

Rosen, E. D. & Macdougald, O. A. 2006. Adipocyte differentiation from the inside out. *Nature reviews Molecular cell biology,* 7**,** 885-896.

Rosen, E. D., Walkey, C. J., Puigserver, P. & Spiegelman, B. M. 2000. Transcriptional regulation of adipogenesis. *Genes & development,* 14**,** 1293-1307.

Rubin, L. J., Magliola, L., Feng, X., Jones, A. W. & Hale, C. C. 2005. Metabolic activation of AMP kinase in vascular smooth muscle. *Journal of applied physiology,* 98**,** 296-306.

Rui, H., Root, K. T., Lee, J., Glover, K. J. & Im, W. 2014. Probing the U-shaped conformation of caveolin-1 in a bilayer. *Biophysical journal,* 106**,** 1371-1380.

Ruiz-Ojeda, F. J., Rupérez, A. I., Gomez-Llorente, C., Gil, A. & Aguilera, C. M. 2016. Cell models and their application for studying adipogenic differentiation in relation to obesity: a review. *International journal of molecular sciences,* 17**,** 1040.

Rutherford, C., Speirs, C., Williams, J. J., Ewart, M.-A., Mancini, S. J., Hawley, S. A., Delles, C., Viollet, B., Costa-Pereira, A. P. & Baillie, G. S. 2016. Phosphorylation of Janus kinase 1 (JAK1) by AMP-activated protein kinase (AMPK) links energy sensing to anti-inflammatory signaling. *Science signaling,* 9**,** ra109-ra109.

Sag, D., Carling, D., Stout, R. D. & Suttles, J. 2008. Adenosine 5′-monophosphate-activated protein kinase promotes macrophage polarization to an anti-inflammatory functional phenotype. *The Journal of Immunology,* 181**,** 8633-8641.

Şahin, A. S. & Bariskaner, H. 2007. The mechanisms of vasorelaxant effect of leptin on isolated rabbit aorta. *Fundamental & clinical pharmacology,* 21**,** 595-600.

Salt, I., Celler, J. W., Hawley, S. A., Prescott, A., Woods, A., Carling, D. & Hardie, D. G. 1998. AMP-activated protein kinase: greater AMP dependence, and preferential nuclear localization, of complexes containing the α2 isoform. *Biochemical Journal,* 334**,** 177-187.

Salt, I. P., Connell, J. & Gould, G. W. 2000. 5-aminoimidazole-4-carboxamide ribonucleoside (AICAR) inhibits insulin-stimulated glucose transport in 3T3-L1 adipocytes. *Diabetes,* 49**,** 1649-1656.

Salt, I. P. & Hardie, D. G. 2017. AMP-activated protein kinase: an ubiquitous signaling pathway with key roles in the cardiovascular system. *Circulation research,* 120**,** 1825-1841.

Scherer, P. E., Lisanti, M. P., Baldini, G., Sargiacomo, M., Mastick, C. C. & Lodish, H. F. 1994. Induction of caveolin during adipogenesis and association of GLUT4 with caveolin-rich vesicles. *The Journal of cell biology,* 127**,** 1233-1243.

Schieber, M. & Chandel, N. S. 2014. ROS function in redox signaling and oxidative stress. *Current biology,* 24**,** R453-R462.

Schiffrin, E. L. 2008. Oxidative Stress, Nitric Oxide Synthase, and Superoxide Dismutase: A Matter of Imbalance Underlies Endothelial Dysfunction in the Human Coronary Circulation. *Hypertension (Dallas, Tex. 1979),* 51**,** 31-32.

Schneider, H., Schubert, K. M., Blodow, S., Kreutz, C.-P., Erdogmus, S., Wiedenmann, M., Qiu, J., Fey, T., Ruth, P. & Lubomirov, L. T. 2015. AMPK dilates resistance arteries via activation of SERCA and BKCa channels in smooth muscle. *Hypertension,* 66**,** 108-116.

Schulz, E., Wenzel, P., Münzel, T. & Daiber, A. 2014. Mitochondrial redox signaling: interaction of mitochondrial reactive oxygen species with other sources of oxidative stress. *Antioxidants & redox signaling,* 20**,** 308-324.

Schwarz, P. M., Kleinert, H. & FöRstermann, U. 1999. Potential functional significance of brain-type and muscle-type nitric oxide synthase I expressed in adventitia and media of rat aorta. *Arteriosclerosis, thrombosis, and vascular biology,* 19**,** 2584-2590.

Scott, J. W., Van Denderen, B. J., Jorgensen, S. B., Honeyman, J. E., Steinberg, G. R., Oakhill, J. S., Iseli, T. J., Koay, A., Gooley, P. R. & Stapleton, D. 2008. Thienopyridone drugs are selective activators of AMP-activated protein kinase ß1-containing complexes. *Chemistry & biology,* 15**,** 1220-1230.

Seddon, M., Melikian, N., Dworakowski, R., Shabeeh, H., Jiang, B., Byrne, J., Casadei, B., Chowienczyk, P. & Shah, A. M. 2009. Effects of neuronal nitric oxide synthase on human coronary artery diameter and blood flow in vivo. *Circulation,* 119**,** 2656-2662.

Sessa, W., Harrison, J., Barber, C., Zeng, D., Durieux, M., D'angelo, D., Lynch, K. & Peach, M. 1992. Molecular cloning and expression of a cDNA encoding endothelial cell nitric oxide synthase. *Journal of biological chemistry,* 267**,** 15274-15276.

Sessa, W. C. 2004. eNOS at a glance. *Journal of cell science,* 117**,** 2427-2429.

Siragusa, M. & Fleming, I. 2016. The eNOS signalosome and its link to endothelial dysfunction. *Pflügers Archiv-European Journal of Physiology,* 468**,** 1125-1137.

Soccio, R. E., Chen, E. R. & Lazar, M. A. 2014. Thiazolidinediones and the promise of insulin sensitization in type 2 diabetes. *Cell metabolism,* 20**,** 573-591.

Soltis, E. E. & Cassis, L. A. 1991. Influence of perivascular adipose tissue on rat aortic smooth muscle responsiveness. *Clinical and Experimental Hypertension. Part A: Theory and Practice,* 13**,** 277-296.

Spiers, J. G., Chen, H.-J. C., Bourgognon, J.-M. & Steinert, J. R. 2019. Dysregulation of stress systems and nitric oxide signaling underlies neuronal dysfunction in Alzheimer's disease. *Free Radical Biology and Medicine,* 134**,** 468-483.

Sproston, N. R., El Mohtadi, M., Slevin, M., Gilmore, W. & Ashworth, J. J. 2018. The effect of C-reactive protein isoforms on nitric oxide production by U937 monocytes/macrophages. *Frontiers in immunology,* 9**,** 1500.

Stanek, A., Brożyna-Tkaczyk, K. & Myśliński, W. 2021. The role of obesity-induced perivascular adipose tissue (PVAT) dysfunction in vascular homeostasis. *Nutrients,* 13**,** 3843.

Stastny, J., Bienertova-Vasku, J. & Vasku, A. 2012. Visfatin and its role in obesity development. *Diabetes & Metabolic Syndrome: Clinical Research & Reviews,* 6**,** 120-124.

Steinberg, G. R. & Carling, D. 2019. AMP-activated protein kinase: the current landscape for drug development. *Nature reviews Drug discovery,* 18**,** 527-551.

Strembitska, A., Mancini, S. J., Gamwell, J. M., Palmer, T. M., Baillie, G. S. & Salt, I. P. 2018. A769662 inhibits insulin-stimulated Akt activation in human macrovascular endothelial cells independent of AMP-activated protein kinase. *International journal of molecular sciences,* 19**,** 3886.

Sun, Y., Li, J., Xiao, N., Wang, M., Kou, J., Qi, L., Huang, F., Liu, B. & Liu, K. 2014. Pharmacological activation of AMPK ameliorates perivascular adipose/endothelial dysfunction in a manner interdependent on AMPK and SIRT1. *Pharmacological Research,* 89**,** 19-28.

Suvorava, T., Metry, S., Pick, S. & Kojda, G. 2022. Alterations in endothelial nitric oxide synthase activity and their relevance to blood pressure. *Biochemical Pharmacology*, 115256.

Szasz, P. L., Szentagotai, A. & Hofmann, S. G. 2012. Effects of emotion regulation strategies on smoking craving, attentional bias, and task persistence. *Behaviour research and therapy,* 50**,** 333-340.

Szasz, T. & Webb, R. C. 2012. Perivascular adipose tissue: more than just structural support. *Clinical science,* 122**,** 1-12.

Taipale, M., Jarosz, D. F. & Lindquist, S. 2010. HSP90 at the hub of protein homeostasis: emerging mechanistic insights. *Nature reviews Molecular cell biology,* 11**,** 515-528.

Takahashi, S. & Mendelsohn, M. E. 2003. Synergistic activation of endothelial nitric-oxide synthase (eNOS) by HSP90 and Akt: calcium-independent eNOS activation involves formation of an HSP90-Akt-CaM-bound eNOS complex. *Journal of Biological Chemistry,* 278**,** 30821-30827.

Talarek, S., Listos, J. & Fidecka, S. 2011. Effect of nitric oxide synthase inhibitors on benzodiazepine withdrawal in mice and rats. *Pharmacological Reports,* 63**,** 680-689.

Tang, Q.-Q., Otto, T. C. & Lane, M. D. 2003. Mitotic clonal expansion: a synchronous process required for adipogenesis. *Proceedings of the National Academy of Sciences,* 100**,** 44-49.

Taylor, E. B. 2021. The complex role of adipokines in obesity, inflammation, and autoimmunity. *Clinical Science,* 135**,** 731-752.

Tejero, J., Hunt, A. P., Santolini, J., Lehnert, N. & Stuehr, D. J. 2019a. Mechanism and regulation of ferrous heme-nitric oxide (NO) oxidation in NO synthases. *Journal of Biological Chemistry,* 294**,** 7904-7916.

Tejero, J., Shiva, S. & Gladwin, M. T. 2019b. Sources of vascular nitric oxide and reactive oxygen species and their regulation. *Physiological reviews,* 99**,** 311-379.

Thalmann, S. & Meier, C. A. 2007. Local adipose tissue depots as cardiovascular risk factors. *Cardiovascular research,* 75**,** 690-701.

Thomas, D. D. 2015. Breathing new life into nitric oxide signaling: a brief overview of the interplay between oxygen and nitric oxide. *Redox biology,* 5**,** 225-233.

Thomas, D. D., Liu, X., Kantrow, S. P. & Lancaster Jr, J. R. 2001. The biological lifetime of nitric oxide: implications for the perivascular dynamics of NO and O2. *Proceedings of the National Academy of Sciences,* 98**,** 355-360.

Tran, C. T., Leiper, J. M. & Vallance, P. 2003. The ddah/adma/nos pathway. *Atherosclerosis Supplements,* 4**,** 33-40.

Tran, K.-V., Fitzgibbons, T., Min, S. Y., Desouza, T. & Corvera, S. 2018. Distinct adipocyte progenitor cells are associated with regional phenotypes of perivascular aortic fat in mice. *Molecular metabolism,* 9**,** 199-206.

Tran, N., Garcia, T., Aniqa, M., Ali, S., Ally, A. & Nauli, S. M. 2022. Endothelial nitric oxide synthase (eNOS) and the cardiovascular system: In physiology and in disease states. *American journal of biomedical science & research,* 15**,** 153.

Tsutsui, M. 2004. Neuronal nitric oxide synthase as a novel anti-atherogenic factor. *Journal of atherosclerosis and thrombosis,* 11**,** 41-48.

Tzeng, E., Billiar, T. R., Robbins, P. D., Loftus, M. & Stuehr, D. J. 1995. Expression of human inducible nitric oxide synthase in a tetrahydrobiopterin (H4B)-deficient cell line: H4B promotes assembly of

enzyme subunits into an active dimer. *Proceedings of the National Academy of Sciences,* 92**,** 11771-11775.

Unno, Y., Akuta, T., Sakamoto, Y.-I., Horiuchi, S. & Akaike, T. 2006. Nitric oxide-induced downregulation of leptin production by 3T3-L1 adipocytes. *Nitric Oxide,* 15**,** 125-132.

Vallance, P., Leone, A., Calver, A., Collier, J. & Moncada, S. 1992. Endogenous dimethylarginine as an inhibitor of nitric oxide synthesis. *Journal of cardiovascular pharmacology,* 20**,** S60-2.

Vallianou, N. G., Mitesh, S., Gkogkou, A. & Geladari, E. 2019. Chronic kidney disease and cardiovascular disease: is there any relationship? *Current cardiology reviews,* 15**,** 55-63.

Verlohren, S., Dubrovska, G., Tsang, S.-Y., Essin, K., Luft, F. C., Huang, Y. & Gollasch, M. 2004. Visceral periadventitial adipose tissue regulates arterial tone of mesenteric arteries. *Hypertension,* 44**,** 271-276.

Victorio, J. A., Fontes, M. T., Rossoni, L. V. & Davel, A. P. 2016. Different anti-contractile function and nitric oxide production of thoracic and abdominal perivascular adipose tissues. *Frontiers in physiology,* 7**,** 295.

Vigilanza, P., Aquilano, K., Baldelli, S., Rotilio, G. & Ciriolo, M. R. 2011. Modulation of intracellular glutathione affects adipogenesis in 3T3-L1 cells. *Journal of cellular physiology,* 226**,** 2016-2024.

Villanueva, C. & Giulivi, C. 2010. Subcellular and cellular locations of nitric oxide synthase isoforms as determinants of health and disease. *Free Radical Biology and Medicine,* 49**,** 307-316.

Virdis, A., Duranti, E., Rossi, C., Dell'agnello, U., Santini, E., Anselmino, M., Chiarugi, M., Taddei, S. & Solini, A. 2015. Tumour necrosis factor-alpha participates on the endothelin-1/nitric oxide imbalance in small arteries from obese patients: role of perivascular adipose tissue. *European heart journal,* 36**,** 784-794.

Vita, J. A. & Keaney, J. J. F. 2002. Endothelial function: a barometer for cardiovascular risk? *Circulation (New York, N.Y.),* 106**,** 640-642.

Vitali, A., Murano, I., Zingaretti, M., Frontini, A., Ricquier, D. & Cinti, S. 2012. The adipose organ of obesity-prone C57BL/6J mice is composed of mixed white and brown adipocytes. *Journal of lipid research,* 53**,** 619-629.

Wang, H., Wang, A. X., Liu, Z., Chai, W. & Barrett, E. J. 2009. The trafficking/interaction of eNOS and caveolin-1 induced by insulin modulates endothelial nitric oxide production. *Molecular endocrinology,* 23**,** 1613-1623.

Wang, Q. A., Tao, C., Gupta, R. K. & Scherer, P. E. 2013. Tracking adipogenesis during white adipose tissue development, expansion and regeneration. *Nature medicine,* 19**,** 1338-1344.

Wang, S., Li, H., Yuan, M., Fan, H. & Cai, Z. 2022. Role of AMPK in autophagy. *Frontiers in Physiology,* 13**,** 2479.

Wang, S., Zhang, M., Liang, B., Xu, J., Xie, Z., Liu, C., Viollet, B., Yan, D. & Zou, M.-H. 2010. AMPKα2 deletion causes aberrant expression and activation of NAD (P) H oxidase and consequent endothelial dysfunction in vivo: role of 26S proteasomes. *Circulation research,* 106**,** 1117-1128.

Wang, Y., Branicky, R., Noë, A. & Hekimi, S. 2018. Superoxide dismutases: Dual roles in controlling ROS damage and regulating ROS signaling. *Journal of Cell Biology,* 217**,** 1915-1928.

Williams, T. M. & Lisanti, M. P. 2004. The caveolin proteins. *Genome biology,* 5**,** 1-8.

Willows, R., Sanders, M. J., Xiao, B., Patel, B. R., Martin, S. R., Read, J., Wilson, J. R., Hubbard, J., Gamblin, S. J. & Carling, D. 2017a. Phosphorylation of AMPK by upstream kinases is required for activity in mammalian cells. *Biochemical Journal,* 474**,** 3059-3073.

Willows, R., Sanders, M. J., Xiao, B., Patel, B. R., Martin, S. R., Read, J., Wilson, J. R., Hubbard, J., Gamblin, S. J. & Carling, D. 2017b. Phosphorylation of AMPK by upstream kinases is required for activity in mammalian cells. *Biochem J,* 474**,** 3059-3073.

Wood, K. C., Cortese-Krott, M. M., Kovacic, J. C., Noguchi, A., Liu, V. B., Wang, X., Raghavachari, N., Boehm, M., Kato, G. J. & Kelm, M. 2013. Circulating blood endothelial nitric oxide synthase contributes to the regulation of systemic blood pressure and nitrite homeostasis. *Arteriosclerosis, thrombosis, and vascular biology,* 33**,** 1861-1871.

Woods, A., Johnstone, S. R., Dickerson, K., Leiper, F. C., Fryer, L. G., Neumann, D., Schlattner, U., Wallimann, T., Carlson, M. & Carling, D. 2003. LKB1 is the upstream kinase in the AMP-activated protein kinase cascade. *Current biology,* 13**,** 2004-2008.

Wu, J., Boström, P., Sparks, L. M., Ye, L., Choi, J. H., Giang, A.-H., Khandekar, M., Virtanen, K. A., Nuutila, P. & Schaart, G. 2012. Beige adipocytes are a distinct type of thermogenic fat cell in mouse and human. *Cell,* 150**,** 366-376.

Wu, K. K.-L., Cheung, S. W.-M. & Cheng, K. K.-Y. 2020. NLRP3 Inflammasome Activation in Adipose Tissues and Its Implications on Metabolic Diseases. *International Journal of Molecular Sciences,* 21**,** 4184.

Wu, Z. & Wang, S. 2013. Role of kruppel-like transcription factors in adipogenesis. *Developmental biology,* 373**,** 235-243.

Xi, W., Satoh, H., Kase, H., Suzuki, K. & Hattori, Y. 2005. Stimulated HSP90 binding to eNOS and activation of the PI3–Akt pathway contribute to globular adiponectin-induced NO production: Vasorelaxation in response to globular adiponectin. *Biochemical and biophysical research communications,* 332**,** 200-205.

Xia, N., Förstermann, U. & Li, H. 2017. Effects of resveratrol on eNOS in the endothelium and the perivascular adipose tissue. *Annals of the New York Academy of Sciences,* 1403**,** 132-141.

Xiao, B., Heath, R., Saiu, P., Leiper, F. C., Leone, P., Jing, C., Walker, P. A., Haire, L., Eccleston, J. F. & Davis, C. T. 2007. Structural basis for AMP binding to mammalian AMP-activated protein kinase. *Nature,* 449**,** 496-500.

Xiao, B., Sanders, M. J., Carmena, D., Bright, N. J., Haire, L. F., Underwood, E., Patel, B. R., Heath, R. B., Walker, P. A. & Hallen, S. 2013. Structural basis of AMPK regulation by small molecule activators. *Nature communications,* 4**,** 1-10.

Xu, K. Y., Huso, D. L., Dawson, T. M., Bredt, D. S. & Becker, L. C. 1999. Nitric oxide synthase in cardiac sarcoplasmic reticulum. *Proceedings of the National Academy of Sciences,* 96**,** 657-662.

Yamada, Y., Eto, M., Ito, Y., Mochizuki, S., Son, B.-K., Ogawa, S., Iijima, K., Kaneki, M., Kozaki, K. & Toba, K. 2015. Suppressive role of PPARγ-regulated endothelial nitric oxide synthase in adipocyte lipolysis. *PloS one,* 10**,** e0136597.

Yamauchi, T., Kamon, J., Minokoshi, Y. A., Ito, Y., Waki, H., Uchida, S., Yamashita, S., Noda, M., Kita, S. & Ueki, K. 2002. Adiponectin stimulates glucose utilization and fatty-acid oxidation by activating AMP-activated protein kinase. *Nature medicine,* 8**,** 1288-1295.

Yamawaki, H., Kameshima, S., Usui, T., Okada, M. & Hara, Y. 2012. A novel adipocytokine, chemerin exerts anti-inflammatory roles in human vascular endothelial cells. *Biochemical and biophysical research communications,* 423**,** 152-157.

Yang, J., Gonon, A. T., Sjöquist, P.-O., Lundberg, J. O. & Pernow, J. 2013. Arginase regulates red blood cell nitric oxide synthase and export of cardioprotective nitric oxide bioactivity. *Proceedings of the National Academy of Sciences,* 110**,** 15049-15054.

Yang, Y.-M., Huang, A., Kaley, G. & Sun, D. 2009. eNOS uncoupling and endothelial dysfunction in aged vessels. *American Journal of Physiology-Heart and Circulatory Physiology,* 297**,** H1829-H1836.

Yang, Z., Yang, Y., Xiong, K., Li, X., Qi, P., Tu, Q., Jing, F., Weng, Y., Wang, J. & Huang, N. 2015. Nitric oxide producing coating mimicking endothelium function for multifunctional vascular stents. *Biomaterials,* 63**,** 80-92.

Ye, T., Zhang, G., Liu, H., Shi, J., Qiu, H., Liu, Y., Han, F. & Hou, N. 2021. Relationships Between Perivascular Adipose Tissue and Abdominal Aortic Aneurysms. *Front Endocrinol (Lausanne),* 12**,** 704845.

Yuan, T., Hong, S., Yao, Y. & Liao, K. 2007. Glut-4 is translocated to both caveolae and non-caveolar lipid rafts, but is partially internalized through caveolae in insulin-stimulated adipocytes. *Cell research,* 17**,** 772-782.

Zaborska, K., Wareing, M., Edwards, G. & Austin, C. 2016. Loss of anti-contractile effect of perivascular adipose tissue in offspring of obese rats. *International Journal of Obesity,* 40**,** 1205-1214.

Zavaritskaya, O., Zhuravleva, N., Schleifenbaum, J., Gloe, T., Devermann, L., Kluge, R., Mladenov, M., Frey, M., Gagov, H. & Fésüs, G. 2013. Role of KCNQ channels in skeletal muscle arteries and periadventitial vascular dysfunction. *Hypertension,* 61**,** 151-159.

Zhao, H., Wu, L., Yan, G., Chen, Y., Zhou, M., Wu, Y. & Li, Y. 2021. Inflammation and tumor progression: signaling pathways and targeted intervention. *Signal transduction and targeted therapy,* 6**,** 263.

Zhao, Y., Zhu, J., Liang, H., Yang, S., Zhang, Y., Han, W., Chen, C., Cao, N., Liang, P. & Du, X. 2020. Kang Le Xin reduces blood pressure through inducing endothelial-dependent vasodilation by activating the AMPK-eNOS pathway. *Frontiers in pharmacology,* 10**,** 1548.

Zhou, G., Myers, R., Li, Y., Chen, Y., Shen, X., Fenyk-Melody, J., Wu, M., Ventre, J., Doebber, T. & Fujii, N. 2001. Role of AMP-activated protein kinase in mechanism of metformin action. *The Journal of clinical investigation,* 108**,** 1167-1174.

Zhou, Y., Wang, D., Zhu, Q., Gao, X., Yang, S., Xu, A. & Wu, D. 2009. Inhibitory effects of A-769662, a novel activator of AMP-activated protein kinase, on 3T3-L1 adipogenesis. *Biological and Pharmaceutical Bulletin,* 32**,** 993-998.

Zhu, J., Song, W., Li, L. & Fan, X. 2016. Endothelial nitric oxide synthase: a potential therapeutic target for cerebrovascular diseases. *Molecular brain,* 9**,** 1-8.

Zhu, W., Cheng, K. K., Vanhoutte, P. M., Lam, K. S. & Xu, A. 2008. Vascular effects of adiponectin: molecular mechanisms and potential therapeutic intervention. *Clinical Science,* 114**,** 361-374.

Zipes, D. P., Jalife, J. Ǵ. & Stevenson, W. G. 2018. *Cardiac electrophysiology: from cell to bedside,* Philadelphia, PA, Elsevier.